NASA Contractor Report 198423, Vol. III

2 kWe Solar Dynamic Ground Test Demonstration Project

Volume III: Fabrication and Test Report

Dennis Alexander
AlliedSignal Aerospace
Tempe, Arizona

February 1997

Prepared for
Lewis Research Center
Under Contract NAS3–26605

National Aeronautics and
Space Administration

Trade names or manufacturers' names are used in this report for identification only. This usage does not constitute an official endorsement, either expressed or implied, by the National Aeronautics and Space Administration.

Rev	By	Approved	Date	Revision Summary
NC	MAB	D. Alexander	1-04-96	Initial issue.

Table of Contents

List of Figures

List of Tables

List of Appendices

Acronyms

ADD	AEROSPACE DESIGN & DEVELOPMENT INC
AES	AEROSPACE EQUIPMENT SYSTEMS (a unit of AlliedSignal Aerospace)
ATP	ACCEPTANCE TEST PROCEDURE
ATR	ALTERNATOR TEST RIG
BAP	BUILDUP ASSEMBLY PLATFORM
BIPS	BRAYTON ISOTOPE POWER SYSTEM
CDR	CRITICAL DESIGN REVIEW
CIT	COMPRESSOR INLET TEMPERATURE
CRC	CONTROL ROOM CONSOLE
CRES	CORROSION RESISTANT STAINLESS
DACS	DATA ACQUISTION AND CONTROL SUBSYSTEM
DDPC	DATA DISPLAY PERSONAL COMPUTER
ELS	ELECTRIC LOAD SIMULATOR
GPIB	GENERAL PURPOSE INTERFACE BUS
IC	INSTRUMENTATION CONSOLE
ICD	INTERFACE CONTROL DRAWING
ICPC	INSTRUMENTATION CONTROL PERSONAL COMPUTER
ID	INNER DIAMETER
kW	KILOWATT
LEO	LOW EARTH ORBIT
LeRC	LEWIS RESEARCH CENTER
LN2	LIQUID NITROGEN
LUP	LIQUID UTILITIES PALLET
LV	LORAL VOUGHT, INC
MSDS	MATERIAL SAFETY DATA SHEET
MLI	MULTI LAYER INSULATION
MS	MICROSOFT
NASA	NATIONAL AERONAUTICS & SPACE ADMINISTRATION
OCS	OPTICAL CONTROL SURFACE
OD	OUTER DIAMETER
PAL	PROGRAMMABLE ARRAY LOGIC
P&ID	PIPING AND INSTRUMENTATION DIAGRAM
PCCU	POWER CONDITIONING AND CONTROL UNIT
PCS	POWER CONVERSION SUBSYSTEM
PCM	PHASE CHANGE MATERIAL
PDR	PRELIMINARY DESIGN REVIEW
PGS	POWER GENERATION SUBSYSTEM (same as PCS)
PLR	PARASITIC LOAD RADIATOR (OR RESISTOR)
PROM	PROGRAMMABLE READ ONLY MEMORY
PVR	PHOTOVOLTAIC RADIATOR
PWM	PULSE WIDTH MODULATED
SCAD	SOLAR CONCENTRATOR ADVANCED DEVELOMENT

SDGTD	SOLAR DYNAMIC GROUND TEST DEMONSTRATION
SIPS	START INVERTER POWER SUPPLY
SKI	SOLAR KINETICS INC
SSF	SPACE STATION *FREEDOM*
TAC	TURBO-ALTERNATOR-COMPRESSOR
TCPC	TEST CONTROLLER PERSONAL COMPUTER
TID	TURBINE INLET DUCT
TIT	TURBINE INLET TEMPERATURE
UPS	UNINTERRUPTABLE POWER SUPPLY
WHR	WASTE HEAT RADIATOR

1. INTRODUCTION

The Solar Dynamic Ground Test Demonstration (SDGTD) project has successfully designed and fabricated a complete solar-powered closed Brayton electrical power generation system and tested it in a relevant thermal vacuum facility at NASA Lewis Research Center (LeRC). In addition to completing technical objectives, the project was completed 3 1/2 months early, and under budget.

The system which was designed and developed is shown schematically in Figure 1-1. In addition to development of the test unit significant design, fabrication and development of the thermal vacuum facility to incorporate a solar simulator was accomplished by NASA LeRC. The government/industry team which successfully accomplished this work, including their respective roles, is shown in Figure 1-2.

Significant milestones occurred as follows:

Contract Start	April 1, 1992
Contract Kickoff Meeting	May 20-21, 1992
System Requirements Review	July 13-15, 1992
Preliminary Design Review	Nov 17-19, 1992
Critical Design Reviews	
Radiator	Feb 26, 1993
Concentrator	April 13-14, 1993
Heat Exchangers	May 12-14, 1993
Electrical Equipment	May 25-27, 1993
TAC & System Integ	June 2-4, 1993
Radiator/Tank Integration Test	July 1994
Concentrator/Tank Integration Test	Nov 14-15, 1994
System Test Readiness Review	Dec 2, 1994
System Test	Dec 12, 1994 through Feb 17, 1995
Turnover to NASA	March 22, 1995

Figure 1-1. SDGTD Equipment in Tank 6

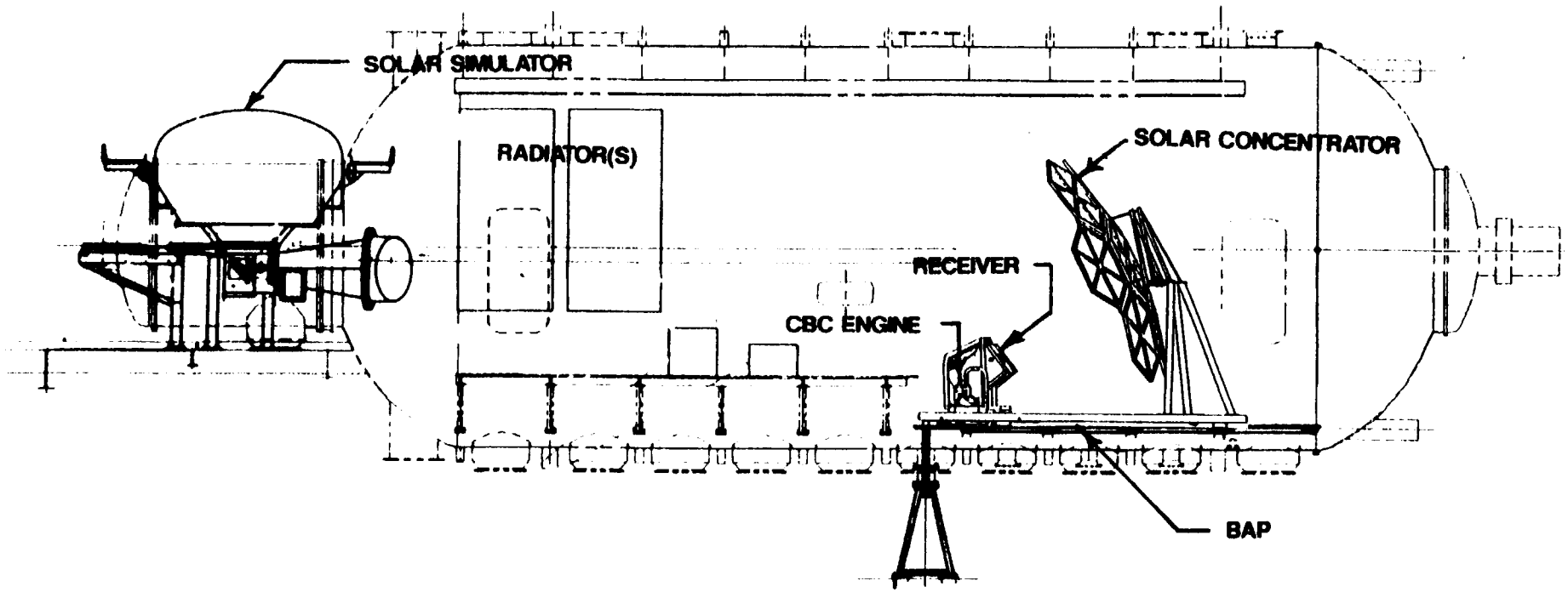

Figure 1-2. Government/Industry Team

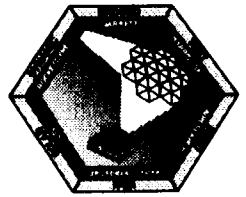

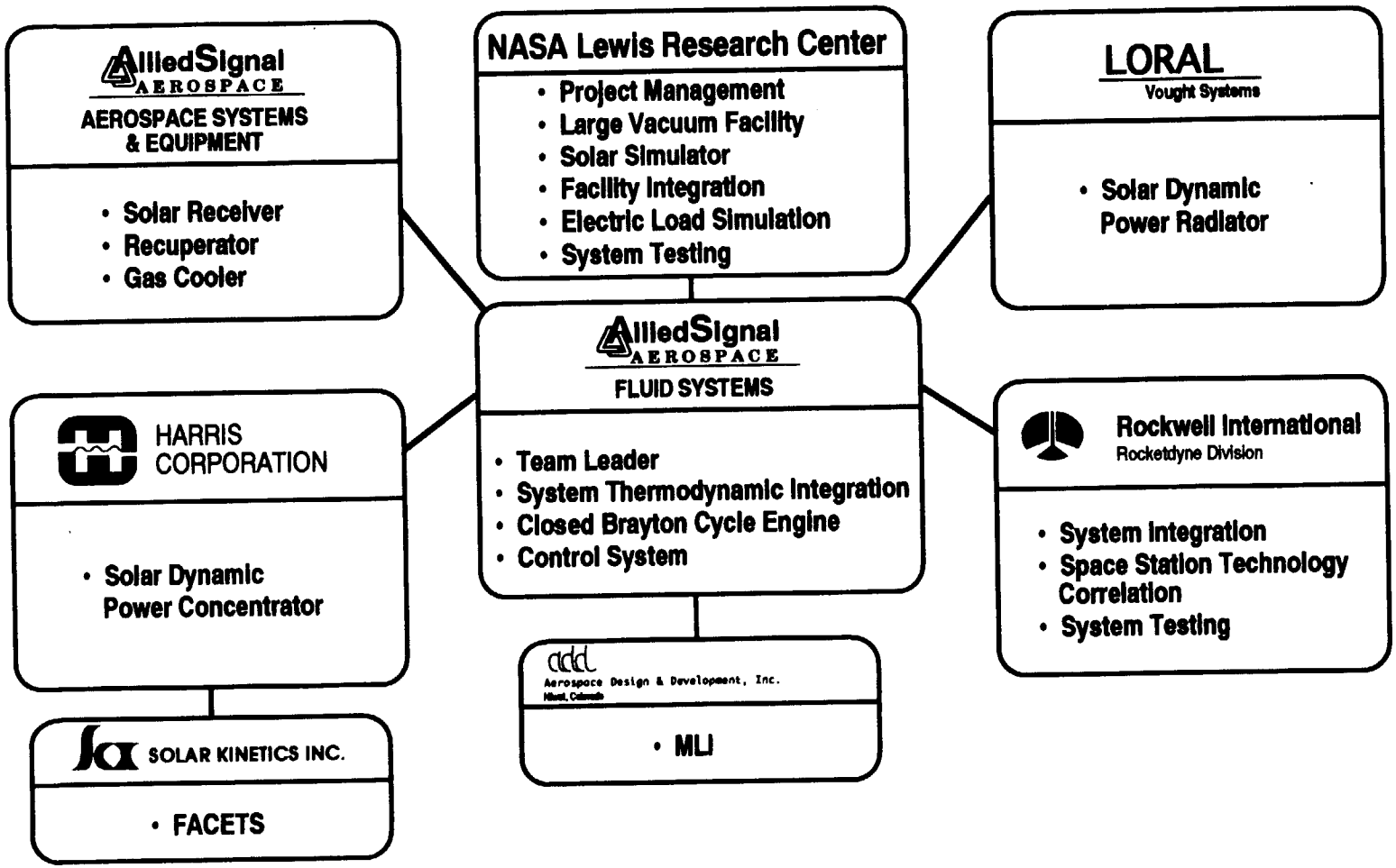

k:\ger\14056-3.doc

The technical objectives and accomplishments relative to those objectives were as follows:

Objectives	Accomplishments
Test a complete solar-powered closed Brayton electrical generation system in a relevant thermal vacuum facility.	A complete solar-powered closed Brayton system was assembled in NASA LeRC Tank 6 and tested in vacuum and thermal sink conditions consistent with Low Earth Orbit (LEO) operation. No laboratory support equipment, other than the thermal vacuum facility, was required by the test unit. Forty-eight hours of successful operation were demonstrated before the system was turned over to NASA LeRC for postturnkey continued operation.
Demonstrate 2.0 kWe alternator output AC power during a simulated orbit.	2.08 kWe was generated at alternator output terminals during continuous insolation operation. During simulated orbital operation, an average of 1.95 kWe was generated. Limitations in the amount of solar simulator output energy to the concentrator reduced the amount of electrical power generated. Only 8 of 9 lamps in the solar simulator were operable during this test. When lamp 9 is back on line, the average orbital power will be increased 1.95 to 2.0 kWe This will be demonstrated by NASA.
Demonstrate 15 percent end-to-end efficiency = usable kWe/intercepted light energy	Efficiency in the range of 14 to 17.4 percent was demonstrated. See Section 2 for detailed calculation.
Evaluate analytical codes used for the prediction of concentrator optical performance, receiver thermal, and Brayton engine performance.	Analytical codes provided excellent correlation to test data. Concentrator optical codes performed well. The engine code provided excellent orbital operation predictions when compared to the test data. The engine/receiver is operating in the latent salt range. Improvements to better predict cold start performance (sensible heat receiver) are required.
Evaluate approaches to accomplish the work quicker, better, faster.	The following methods were found to be very successful in completing the project early and under budget: • Common financial incentives (failure of one was failure by all). This resulted in "what's best for the program" attitudes rather than "what's best for my organization." • Open communication - discussions between any team member, including NASA to subcontractor expert were encouraged. • Encouragement of frank discussion. "Tell it like it is" even in the presence of NASA. Get the issues out in the open where

they can be dealt with effectively. Speaking up was required if you didn't agree with a position. Subcontractors attended all design reviews and actively participated.

- Elimination of paperwork and tasks which did not directly add to the success of the effort. "If we don't use it we don't need it."
- Generation of a trust relationship where each team member, including NASA, took care of their own tasks. Allowing mistakes without fear of repercussion.
- Team-building workshop conducted early to foster understanding and teaming skills.

Volume II of this final report provides a technical summary of the design activities through Critical Design Review. The remaining sections of this document will provide an overview of the activities from CDR through the completion of the system testing prior to the system being turned over to NASA. Each section will provide:

- A summary of major design changes, if any, after CDR
- A summary of lessons learned during the fabrication process
- A summary of the component testing and component performance during the system tests.
- Conclusions relative to that component.

Each of the following sections is written by the technical experts of the respective components and no attempt has been made to edit the contents for common style or grammar. In this manner each of the component experts speaks directly to the reader without editorial interference. Substantial technical documentation was generated, including analysis results, design documents, test plans, test procedures, and test reports. Appendix 1 contains a bibliography of technical papers, Appendix 2 a bibliography of the technical documents generated on this project.

2. SYSTEM INTEGRATION AND SYSTEM TEST

2.1 Summary and Conclusions

The system integration task was successfully conducted by the Rocketdyne division of Rockwell International. This task involved completion of the following elements:

- Development of the overall tank/test unit layout
- Development of the optical flow path and optical control surface
- Generation of top-level requirements and documents
- Allocation of top-level requirements to component levels including generation of specifications and interface control documents (ICSs)
- Generation of electrical and instrumentation schematics and control documents and lists
- Generation of system-level test plan and test procedure
- Identification of component installation sequencing
- Coordination of the safety program, including hazard reports and hazards analysis
- Coordination with all project technical organizations to resolve technical issues

The system components arrived at Tank 6 and were integrated and checked out as anticipated in the installation flow plan (213TI000005). Component-to-tank integration tests and system testing were successfully conducted in accordance with the test plan, 213TPS000002. All system test objectives were successfully accomplished in 48 hours of system testing prior to turning the system over to NASA Lewis for continued operation.

2.2 Design Changes after CDR

The following changes were made the system design and in the system installation methodology after the critical design review:

2.2.1 Planned Changes

1. The liquid loop plumbing was changed from flexible, wire-wrapped Teflon hose to metal tubing with AN flared fittings. This change was made because the Teflon hose would not pass the helium leak test required by safety prior to filling with n-heptane.
2. A wrap of aluminized Mylar was added to the liquid loop plumbing to ensure that the plumbing was isothermal to the maximum extent possible.
3. The inlet and outlet plumbing to Radiator Panel 2 was reversed to simplify system installation.
4. A stationary mirror (spare facet) was added behind the concentrator to allow viewing of the receiver aperture from outside the tank. Video recordings of the receiver interior were made during testing.
5. Cabling options were implemented to allow the PCCU/PLR to be operated outside the tank for initial checkout.
6. Cabling options were implemented to allow the PCCU to be operated with the Alternator Test Rig (ATR) when the PCCU was installed inside the tank. This required the incorporation of a series of

multiple contact switches to switch field wires and monopole signals between the ATR (located outside the tank) and the TAC (located inside the tank).

7. A GN2 purge to the drain system was added to the liquid loop.
8. The installation sequence was altered to allow earlier concentrator testing. The CDR plan was to install the receiver/power generation system (PGS) pallet inside the tank before the concentrator alignment and flux testing. After completion of this testing the receiver/PGS pallet would be switched with the flux test fixture pallet. When it became clear that the concentrator would be completed earlier than the receiver, the installation sequence was changed. The BAP was rolled outside the tank after completion of concentrator alignment and flux testing. The two pallets were switched outside the tank. This required a series of tests to verify that the optical alignment of the concentrator did not change during this operation. It also incorporated an optical test to verify that the facets were still focused on the aperture. This was done by placing a light bulb in the solar simulator window and observing the facet images on the plane of the aperture.

2.2.2 Changes Made During Installation

1. The as-built location of the solar simulator beam optical port was slightly different from that established by the ICD. The concentrator was aligned to the location of the Harris Flux Test Fixture using Harris procedures. The receiver and receiver aperture were placed in the same location as the flux test fixture aperture. Supplementary survey monuments were incorporated into the tank to record the actual location of the installed optical components.
2. During installation of the receiver/PGS to the pallet a misalignment was noted. Either the receiver/pallet interface or the PGS/pallet interface could be aligned but not simultaneously without distorting the interconnecting ducts. It was decided not to investigate the cause (probably interconnect duct installation). Instead, the receiver-to-pallet interface was correctly established. The PGS mounting pads were then tack welded to the pallet to keep them from migrating.
3. The IEEE-488 data exchange link between the solar simulator controller and the DACS was not established due to hardware/software difficulties within the solar simulator control computer. This did not cause any test difficulties. In fact, the DACS was unduly busy with IEEE-488 handshaking, and the elimination of another computer from that network was appreciated.

2.3 System Installation in Tank 6, NASA LeRC Building 301

System installation of the SDGTD was achieved through a series of subsystem build and test activities. These subsystem activities allowed separate checkout of the major components supplied by the hardware/software team members. NASA built and tested the solar simulator (see Section 4) at the test site. The primary documents controlling installation of the SDGTD were the system installation drawing 213000018 and the installation flow diagram 213T000005. Some changes from the planned flow were made to take advantage of component and test personnel availability. These changes were as follows:

1. The radiator testing was moved forward in time to take advantage of early delivery by Loral Vought of both radiator panels. AlliedSignal Fluid Systems provided the Liquid Utilities Pallet (LUP), which provided the pumps, heater, and instrumentation necessary to conduct the radiator test.

AlliedSignal shipped the LUP to NASA to coincide with the arrival of the radiator. This required that AlliedSignal conduct their subsystem testing in Tempe, Arizona, using other support equipment.

2. The concentrator test preceded the initial installation of the receiver/PCS pallet onto the BAP. Both the receiver and concentrator arrived at the test site early. The receiver then required several weeks for assembly, installation of multilayer insulation, and mating with the Power Conversion Subsystem (PCS). Rather than delay the concentrator testing until the receiver/PCS was ready for installation into the tank, concentrator testing was begun without the receiver/PCS in the tank as originally planned. Testing prior to conducting the concentrator alignment demonstrated that this alignment would not be affected by rolling the BAP out of the tank and then returning it to its original location.
3. The DACS testing which was to be conducted on the assembly floor was eliminated. The DACS was used to conduct Power Conversion Subsystem testing at AlliedSignal Fluid Systems, and control functions were satisfactorily demonstrated. Further, the DACS was used to conduct the radiator/tank integration test as well as the concentrator/tank integration tests.
4. Since the solar simulator "window" was located approximately 1 inch from the position defined by the optical ICD, it was not possible to place the receiver at an ICD location. The actual locations were unimportant, and only relative positions between the optical components were relevant. Therefore, the concentrator was aligned to the flux test fixture using Harris procedures discussed in Section 3.0. The receiver/PCS operates hotter than the flux test fixture, and a bias was added to account for the calculated difference in thermal expansion between the receiver aperture and the flux fixture aperture. This desired bias was 0.120 in. up, 0.090 in. west, and 0.020 in. north. The measured installed values were 0.123, 0.088, and 0.024 respectively. Movement of the pallet was accomplished using the jackscrews built into the pallet. The pitch of these jackscrews was 0.0625 in. per revolution.
5. The operational solar simulator was delivered 3 months early by NASA. This allowed subsystem testing to begin in October 1994.

Liquid interconnections between components was by field routing plumbing as defined in Piping and Instrumentation Diagram 213000002. Cabling was installed in accordance with the intercabling schematic 213000014. For some testing the PCCU and PLR were located outside the tank for convenience and required changes in the cabling interconnections. These changes were documented in Appendix E of 213TI000002 (system test planning instructions); in the AlliedSignal initial installation and checkout procedure, 41-1366; and in the subsequent pretest checkout procedure, 41-13511.

2.4 System Testing Summary

2.4.1 Test Chronology

The testing conducted during the contractor-controlled testing is summarized in Table 2-1.

Table 2-1. System Test Summary (Contractor Testing)

Date	Testing Accomplished	Test Results
12-12-94	Initial heating of receiver, including one brief period of TAC motoring. Aperture Q called for from solar simulator was 7.5 kW.	Slow thermal response; inadequate temperature achieved to allow engine operation.
12-13-94	Increased solar input to approximately 10.5 kW aperture. Limited operation to approximately 550 W output.	Again, slow thermal response. Unit is heating up much slower than expected. Found concentrator contaminated.
01-25-95 through 01-27-95	Heated receiver with solar simulator to bake out Nextel thread. Concentrator protected with clear Teflon film.	Receiver heated to 1850 R and held at temperature for 8 hours.
02-01-95	Low-power steady state and orbital operation at 48,000 rpm. 66 minute insolation, 28 minutes eclipse.	Approximately 1375 W ac achieved. Completed 3 orbits. Temperatures decayed during orbits, indicating energy shortfall. Performance lower than predicted for the indicated light energy.
02-02-95	Increased light intensity. Ran steady state at 52,000 rpm. Accomplished 5 orbits	Achieved design turbine inlet temperature (TIT) and generated 1830 volt amps ac power. During orbit ops temps were decaying. Decreased speed to 48,000 to achieve stable orbits. Engine performance was low for an achieved TIT. Analysis showed this to be a result of high receiver pressure loss.
02-17-95	Increased light intensity to maximum possible from 8 operating lamps. Removed MLI from radiator to lower compressor inlet temperature. Ran steady state at 52,000 rpm and then ran 3 orbit cycles.	Achieved 2120 volt amps ac (1960 W dc) by suppressing compressor inlet temp and increasing receiver outlet temp approximately 35 degrees. Eclipse time was reduced from 28 to 18 minutes to achieve balanced orbit. Net thermal energy is still low.

2.4.2 Discussion of Tests

2.4.2.1 12-12 and 12-13-94 Testing

On 12-12-94 the solar simulator was energized; light calculated to provide 7.5 kW into the aperture was selected.

14:30	Shutter opened.
14:58	Solar simulator went off.
15:05	Solar simulator back on line.
15:27	Solar simulator went off.
15:42	Motored the TAC to ascertain ability to self-sustain. Insufficient gas temperature out of the receiver. Stopped motoring.
15:44	Solar simulator back on line.
16:31	Solar simulator closed after being open for 1 hour 36 minutes. Average receiver canister temperature reached was 1170 R and increasing much slower than anticipated. Analysis had predicted that the receiver would be in the 1700 R range in less than one hour.

Discussion with the performance analyst disclosed that the thermal model only includes the receiver tubes, canisters and salt. It does not include the manifolds, inner liner, or outer shell, all of which get hot and absorb heat. These elements of the receiver are not predicted to participate in the thermal energy transfer during orbital operation because the temperature changes are only 30 or 40 degrees. However, initial heating will need to bring these items up to temperature.

On 12-13 we increased the solar simulator setting to provide a calculated 10.5 kW input to the receiver aperture. The following events occurred.

10:31	Shutter opened.
10:36	Solar simulator went off line.
10:44	Solar simulator back on line.
11:39	Motored TAC with shutdown valves open to ascertain receiver outlet temperature; system still not hot enough.
12:33	Motored TAC with shutdown valve open preparatory to attempting a start.
12:35	Accomplished a motoring start with shutdown valves closed. System took 11 minutes to self-sustain. If the receiver had been just a little cooler it would not have made it.
15:45	Closed shutter; system not coming up to temperature. Rate of temperature increase is only 30 or 40 degrees per hour instead of several hundred degrees. Something is significantly amiss.
16:07	Increased solar simulator power 10 percent and opened shutter.
16:27	Closed shutter.
17:24	TAC stopped.

Again, system is not storing energy at a rate consistent with the solar simulator setting. Engine operation during the period where the shutter is off (16:27 to 17:24) indicates that the engine and receiver are operating correctly. Decided to open tank and have a look at the hardware.

Examination of the hardware found the concentrator contaminated with a foreign substance. Measurement of concentrator specular reflectivity showed that the concentrator's performance had been significantly reduced. The substance was traced to outgassing from Nextel thread in the receiver.

2.4.2.2 1-25 to 1-27 95 Receiver Bakeout

Examination of the receiver heating rates from 12-12 and 12-13 indicated that the concentrator was contaminated early in the testing on 12-12. Chemical analysis of the Nextel fiber indicated that the volatile content would have been baked out during the 12-12 and 12-13 testing. To make sure, the receiver was heated to operating temperature to drive off any volatile contents. The concentrator was covered with a clear Teflon film, the solar simulator turned on at low power, and the receiver gradually brought to design temperature (1850 R) and held at this temperature for 8 hours. The solar simulator was turned off and the receiver cooled over a 2½ day period.

2.4.2.3 2-1-95 Testing

The solar simulator was turned on and set to provide 10.5 kW into the receiver aperture.

08:55	Shutter opened. TAC motored at same time to verify controls operation.
10:30	TAC motored with shutdown valves open to preheat turbine prior to attempting a start. Remembered from Hot Loop testing that the TAC compressor surges if the unit is started with a cold turbine. If the TAC is motored with shutdown valves open it keeps compressor out of surge and allows, for reasons unknown, some flow through the receiver to the turbine.
10:33	Conducted TAC motoring start with valves closed. Unit was self-sustaining in 10 minutes. Accelerated to 48,000 rpm.
13:28	Closed shutter when receiver temperature averaged approximately 1800 R. Initiated orbital operation 66 minutes sun on and 28 minutes sun off. Reduced solar simulator power to provide a calculated 9 kW into receiver aperture.
13:56	Opened shutter.
15:02	Closed shutter.
15:30	Opened shutter.
16:36	Closed shutter.
17:04	Opened shutter.
18:10	Closed shutter. Reduced solar simulator power to provide 7.5 kW aperture power.
18:14	Opened shutter to run steady state case.
19:09	Closed shutter reset solar simulator to provide 5.5 kW at the aperture.
19:40	Opened shutter.
20:04	Closed shutter.
21:40	TAC stopped.

This day's testing indicates that the receiver is not getting as hot as it should for the amount of light energy we are or should be providing. Measurements of energy delivered to gas and estimates of receiver losses based on temperature indicate that either solar input is low or receiver losses are high. Receiver cooldown following bakeout on 1-25-95 indicates that receiver losses are nominal.

2.4.2.4 2-2-95 Testing

Solar simulator was turned on and set to achieve approximately 11.5 kW through the aperture (solar simulator radiometer reading 1.5 kW/m^2). Unit was still warm from previous day's testing. Receiver temperature was still 1000 R.

08:02	Opened shutter.
08:53	Since unit was warm a turbine preheating spin up was not required. Attempted an auto start. TAC was accelerated to 36,000 rpm, the SIPS deenergized, and the TAC decelerated to 0.
08:54	Conducted a motoring start. Unit was self-sustaining in approximately 3 minutes.
11:19	Solar simulator had a fault and went off line just as we were approaching maximum temperature.
12:18	TAC shut down.
12:20	Performed an auto start successfully.
12:28	TAC shut down from 48,000 rpm to observe soakback at approximately 1400 R condition.
14:37	Shutter opened with seven lamps operating approximately 10.0 kW.
15:14	Solar simulator off line again.
15:37	Solar simulator back on line and lamp power set to deliver 12 kW.
16:04	TAC restarted and speed set to 52,000 rpm.
17:45	Reached design receiver outlet temperature and was making 1.83 KVA electric power at alternator. Power was low; receiver pressure drop very high.
18:13	Opened shutter after 28 minutes of eclipse.
19:56	Closed shutter after 103 minutes of insolation. It took this long to reheat to design receiver outlet temperature instead of the predicted 66 minutes. Energy available to heat receiver was down. Reduced speed to 48,000 rpm to decrease gas flow and energy demand to/from receiver. Began orbital cases at this speed.
20:24	Shutter opened.
21:30	Shutter closed.
21:58	Shutter opened.
23:04	Shutter closed.
23:32	Shutter opened.
00:38	Shutter closed.
01:06	Shutter opened.
01:13	Shutter closed.
02:11	TAC stopped at 1500 R.

This day's testing indicated that the Brayton cycle was down in power for a given set of temperatures and pressures compared to the predictions and that the receiver energy balance was off. Either less light was

being delivered than measured by radiometer or the receiver losses are higher than predicted. The TAC showed no appreciable soakback from shutting down at 1500 R.

2.4.2.5 2-17-95 Testing

Performance analysis of the test data of 2-2-95 showed that the primary loss of engine performance was the large receiver pressure drop (3.3 psid vs. the allowed 1.5). In order to operate the system at the goal of 2.0 kWe, the MLI was removed from Radiator Panel 2 to decrease sink temperature and compressor inlet temperature, and a small increase in cycle gas inventory was made. The cause of the noted receiver/solar simulator energy imbalance remains unresolved. The solar simulator was turned on with 8 of 9 lamps operating at the maximum power level.

08:32	Shutter open.
09:54	Conducted a motoring of TAC with shutdown valves open to preheat turbine in preparation for a cold system start.
09:59	Conducted a motoring start of TAC with receiver heated so that salt was melted back to the center of the receiver. This was a hot receiver start. Took 7-8 minutes to self-sustain. Accelerated to 48,000 rpm.
10:45	Accelerated TAC to 52,000.
11:40	Decelerated TAC to 48,000 to allow receiver to heat up faster.
12:52	Accelerated TAC to 52,000. At 13:00 unit was producing 2120 volt amps of ac power and was 35 degrees hotter than design.
13:00	Closed shutter to begin orbitals.
13:28	Opened shutter after 28 minutes and noted receiver outlet temperature was 1860 R.
14:34	Closed shutter receiver outlet temperature right near design value.
14:53	Opened shutter at receiver outlet temperature of 1860 R, which should allow the unit to reheat to design value in 66 minutes.
15:42	Lost one lamp. Continued operation.
15:59	Shutter closed. Receiver outlet temperature back to design value. Continued operation with 66/18 minute orbital cycle. Lamp which shut down at 15:42 brought back on line during eclipse period but operating at slightly reduced power.
16:18	Shutter opened one minute late.
17:24	Shutter closed. Three good orbits achieved.
19:30	TAC stopped.

Decreasing compressor inlet, raising turbine inlet temperature, and slightly increasing system gas inventory has resulted in the generation of 2080 W ac power, which rectified to 1960 W dc. Achieved balanced orbits in the salt melt range by reducing eclipse time. Energy imbalance can be estimated by ratioing orbit period. Actual orbit run was 66 plus 18 minutes; it should have been 66 plus 28 minutes. Therefore, the light energy delivered is approximately 84/94 of the required value. To operate at design power on a 94 minute orbit, analysis indicates that 11.6 kW is required. 84/94ths of 11.6 is 10.4 kW. NASA believes the solar simulator is putting out 12 kW. There is a discrepancy of approximately 1.6 kW.

Detailed performance analysis of the Brayton cycle test data is found in AlliedSignal Document 41-13692, "Solar Dynamic Ground Test Demonstrator Test Report - PCS/Tank 6 Testing." This document provides raw test data as well as detailed analysis. Copies of this document can be obtained by contacting

Dennis Alexander
AlliedSignal Aerospace
P.O. Box 22200
1300 W. Warner Rd.
Tempe, AZ. 85285-2200
(602) 893-4746

2.4.3 System Test Results

System testing was conducted to demonstrate the following objectives:

- That component operating characteristics were consistent with analytical predictions. Analytical codes for engine performance, heat receiver thermal performance, radiator thermal performance, and concentrator optical performance were of key significance.
- Overall efficiency of 15 percent. Previous closed Brayton cycle testing had involved the use of laboratory heat exchangers for cycle heat input and waste heat removal. SDGTD was established to demonstrate an integrated solar dynamic closed Brayton cycle with thermal storage in a relevant test environment.
- A system control method which would maintain satisfactory operation over the range of solar insolation and eclipse times encountered in low earth orbit.

The sections which follow, and the referenced documents which support them, discuss the components individually. Excellent correlation between test data and predicted component performance was achieved throughout the system.

2.4.3.1 Measured System Efficiency

The integrated test, conducted in the space environment provided by Tank 6 at NASA LeRC, satisfactorily accomplished the second system objective. Figure 2-1 provides a plot of electrical output dc power and receiver outlet gas temperature vs. time for the 2-2-95 testing. Figure 2-2 is an enlarge view of that data during the orbital period of the test. Figure 2-3 and Figure 2-4 provides the same information for the 2-17-95 testing. Figure 2-2 and Figure 2-4 show clearly that solar dynamic closed Brayton cycle systems, with integral thermal energy storage, provide continuous and uniform levels of power during both insolation and eclipse time periods.

Figure 2-1. Receiver Gas Outlet Temp. and DC Power vs. Time (2 Feb 95)

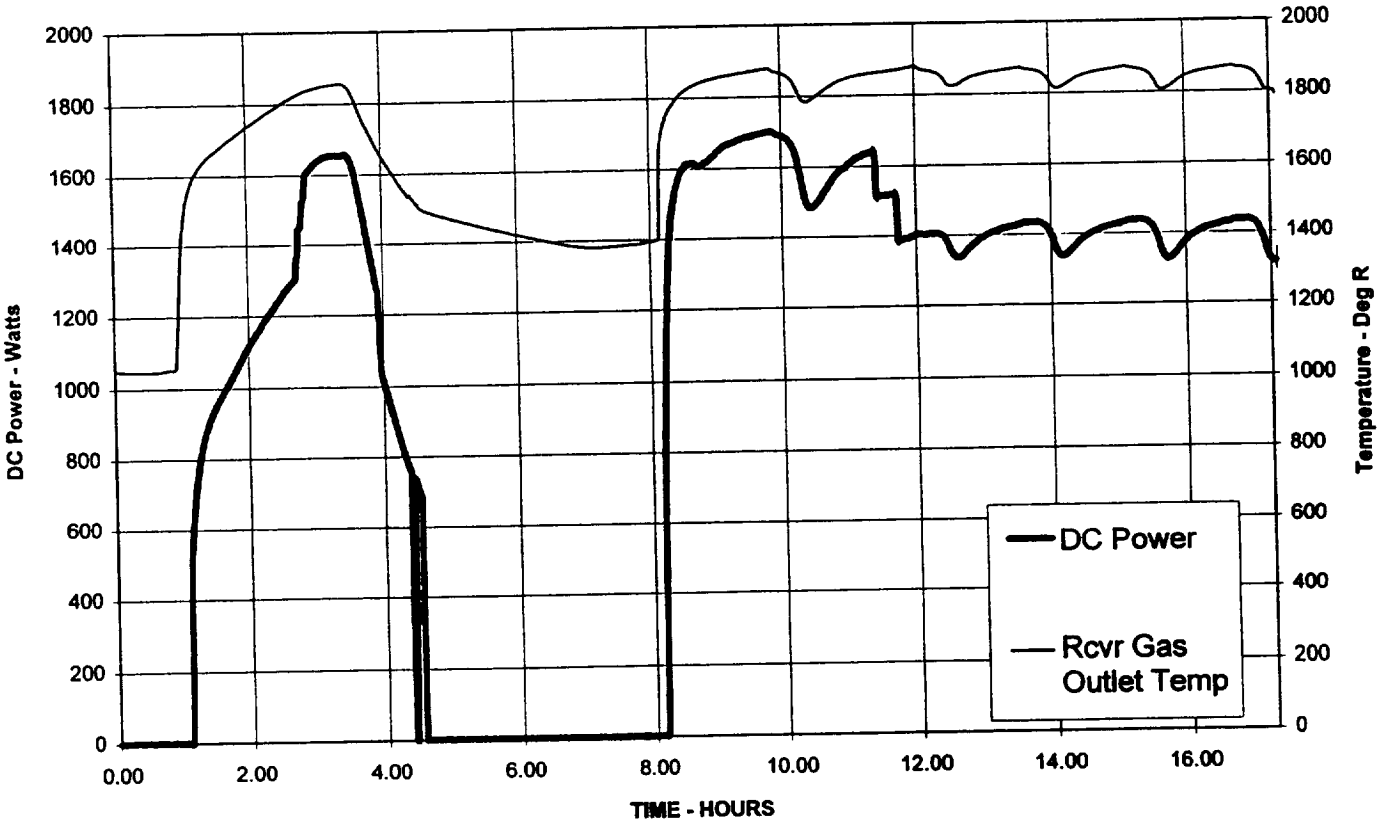

Figure 2-2. Receiver Gas Outlet Temp. and DC Power vs. Time (2 Feb 95; Orbital Cycles Only)

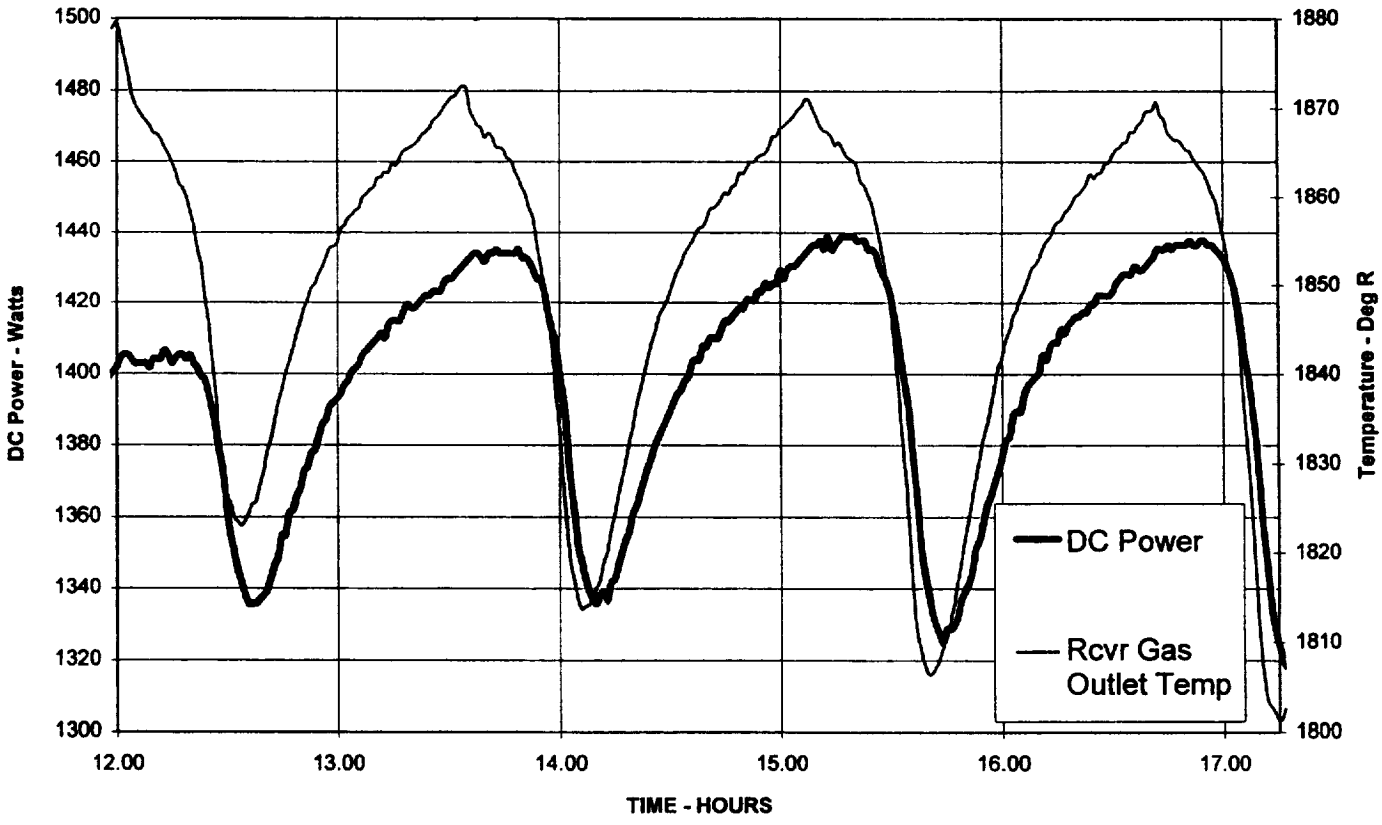

k:\gen\14056-3.doc

Figure 2-3. 17 Feb 95 Power and Temp. vs. Time

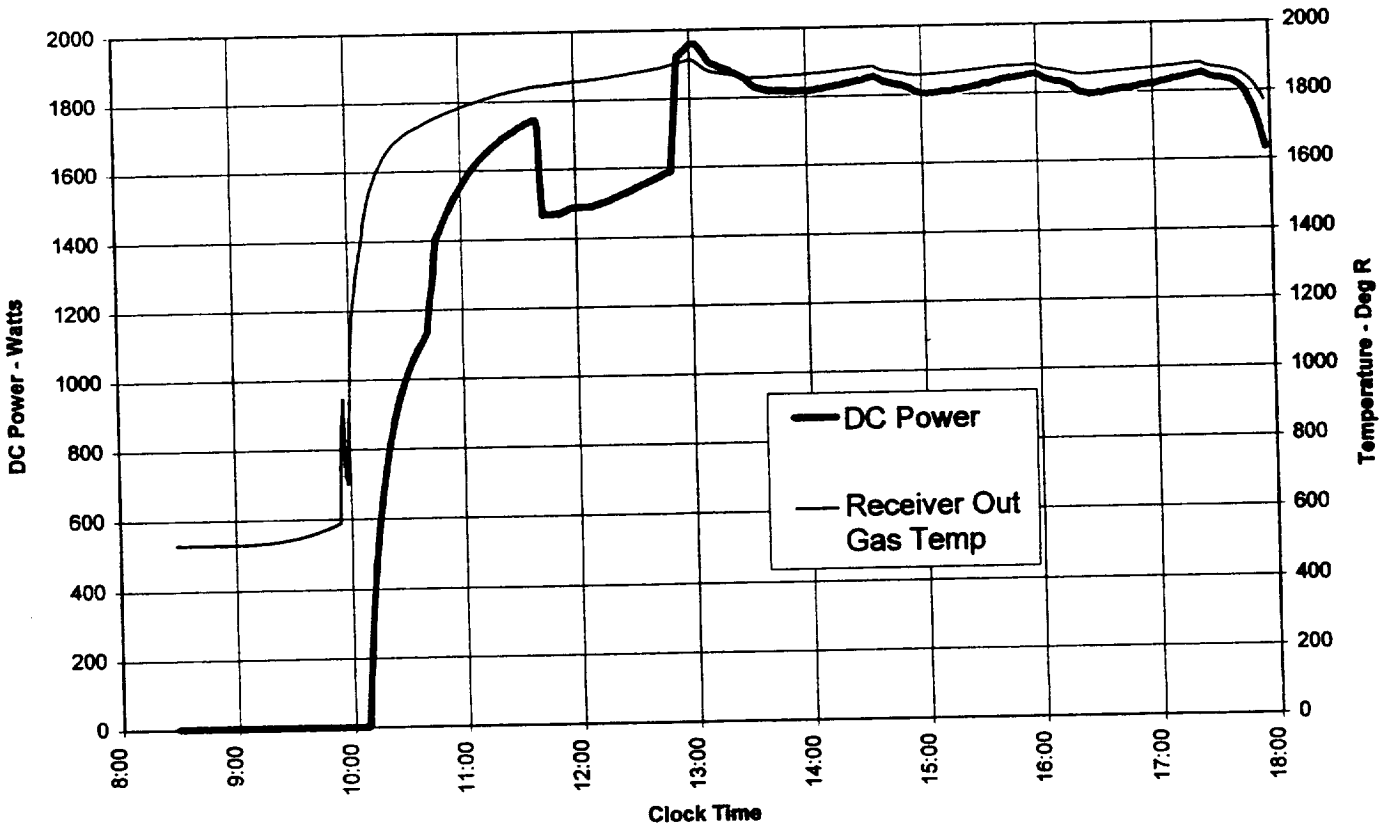

Figure 2-4. 17 Feb 95 Power and Temp. vs. Time (Orbital Cycles Only)

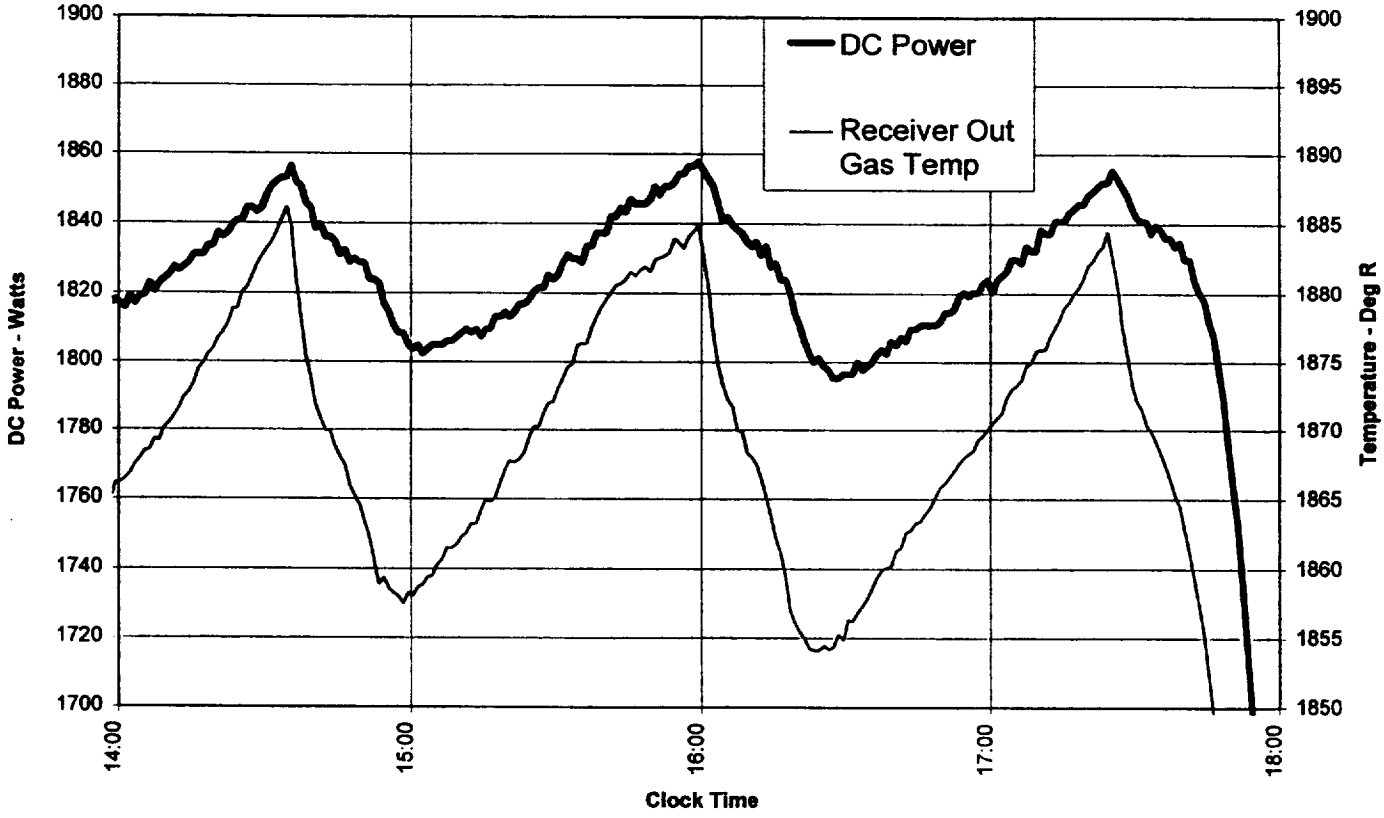

Many claims are made concerning efficiency of power generating equipment which tend to ignore certain parasitic losses for the sake of inflating the actual efficiency of the system. We believe that the real efficiency of the system should be the ratio of the usable electrical power delivered to the vehicle divided by the solar energy intercepted by the system. This efficiency should be based not on instantaneous power generated at one point during the orbit but on integrated energy (W-hr) over the entire orbit. The calculated efficiency delivered during the 2-17-95 tests is calculated as follows:

2.4.3.2 Delivered Electrical Energy

During the last orbital period of the 2-17-95 test an average of 1823 W (at 120 Vdc) was delivered by the power conditioning and control unit. This power is downstream of the control and downstream of the rectifier. During this test the liquid loop pump and the 2 shutdown valves were powered by external power supplies. The power consumption of these devices has been measured as 25 and 14 (7 each) W respectively. This leaves a residual 1784 W available to the user for the 85 minute orbital period: 1784 * 85/60 = 2528 W-hr of energy to the user.

2.4.3.3 Input Optical Energy

Dc electrical power is very easy to instrument and measure. Optical power is much more difficult. Two methods were used to calculate the optical power delivered during the test.

2.4.3.4 Method 1 - Receiver Calorimetry

The receiver can be used as a calorimeter. Instrumentation in the gas loop allows calculation of the power delivered by the receiver to the gas loop in terms of mass flow, Cp, and temperature rise across the receiver. Thermal losses of the receiver were modeled and include reradiation losses out the aperture and skin losses off the surface of the MLI. A receiver high temperature cool down, with the engine not operating, was conducted and the decay of the receiver temperature agreed precisely with the thermal losses model. During orbital operation if the beginning and end of each orbit are at identical temperatures then there is no net thermal storage (or discharge) of energy into (or from) the thermal storage medium. Therefore, the energy coming through the aperture over the orbit must be the sum of the energy delivered by the receiver to the gas and the energy losses out the aperture and off the surface. During the 2-17-95 orbital case the average aperture power was calculated at 10.5 kW. This was delivered for 66 minutes and results in 10.5 * 66/60 = 11.55 kW-hr of energy. Further calculations based on analytical and measured results are required to account for the losses associated with the concentrator. These losses are as follows:

Loss	Efficiency	Basis	Energy at Location
Aperture Losses	95.5%	Analysis	12.09 kW-hr
Concentrator Reflectivity	86%	Test Data	14.06 kW-hr
Facet Blockage by Structure	96.7%	Analysis	14.54 kW-hr

This method calculates that 14.54 kW-hr of energy was delivered to the concentrator optical surfaces. The efficiency which results is

$$System\ Efficiency = \frac{User\ Electrical\ Energy}{Concentrator\ Optical\ Energy} = \frac{2.528\ kW-hr}{14.54\ kW-hr} = 17.4\%$$

2.4.3.5 Method 2 - Optical Radiometer

The solar simulator consists of nine lamps which each fully illuminate the concentrator surface. The intensity of the light which falls upon the concentrator is not uniform. NASA conducted a test to map this intensity and the results appear as Figure 4-4 in Section 4 of this report. This map of the intensity of the light beam was made with a radiometer placed on a rotating and translating arm. This same radiometer was placed on a known location of the concentrator and its measurement of the light recorded during the tests. In addition to the nonuniformity of the beam, the concentrator optics are not at uniform distance from the beam, so the local intensity varies with the square of the distance from the optical window. Assuming that the nonuniformity of the light beam stays constant with optical power and time, an analysis was conducted to determine the light energy delivered based on the reading of the radiometer, the light intensity uniformity map and the physical geometry locations of the individual facets. For the 2-17-95 test the average light intensity based on this method was 16.44 kW. The delivered light energy for the 66 minute eclipse period would then be 16.44 * 66/60 = 18.09 kW-hr.

$$System\ Efficiency = \frac{User\ Electrical\ Energy}{Concentrator\ Optical\ Energy} = \frac{2.528\,kW-hr}{18.09\,kW-hr} = 13.98\%$$

Neither method is accurate for determining the level of delivered solar energy. Both methods require assumptions and analysis to arrive at the delivered solar energy. An aperture calorimeter which is maintained at low temperature to minimize reradiation losses is being constructed by NASA LeRC. This device will be placed directly in front of the receiver aperture plane and will measure energy delivered to the aperture as well as spillage on the area adjacent to the aperture. This measurement will provide better resolution of this difference.

An additional check on light energy was done. The receiver thermal design code SOLREC-TSD predicts individual receiver canister temperature and outlet gas temperature as a time-varying function of aperture input light power and inlet gas temperature and flowrate. As discussed in Section 6 or this report, the predicted temperatures are consistently lower than the test data if the aperture light intensity is 10.5 kW. A much better match with the test data is achieved if the aperture light power is assumed to be 11.0 kW.

Based on these approaches the demonstrated system efficiency is in the range of 14 to 17.4 percent. It should be remembered that the SDGTD is not an optimized design. It consists of engine hardware designed and fabricated in the mid-1970s and concentrator, receiver, and radiator designs which were extracted from other projects. Considering this, the demonstrated end-to-end efficiency is very good

compared to comparable large photovoltaic systems. End-to-end orbital efficiency of photovoltaic systems is currently estimated to be about 4 percent for *ISSX*.

2.4.3.6 Thermal Control Methodology

Work done on solar dynamic power for Space Station *Freedom* (Work Package 4) analytically investigated various means of thermodynamic control required to accommodate the differences in annual orbital insolation and varying orbital eclipse and insolation periods. There is no satisfactory method of directly measuring the energy stored in the salt of the receiver, because measuring the latent heat content of salt requires a measurement of the percentage of salt which is melted. This is not something which is easy to accomplish. The approach taken on SDGTD was to suggest that a direct measurement of energy storage was not required. Instead, it was postulated in AlliedSignal Report 41-12065 that a properly charged receiver (with most salt melted at sunset) would show less thermal and power variations from sunset to sunrise compared with a receiver which was undercharged. This characteristic is evident by comparing Figures 2-2 and 2-4. The 2-2-95 test was conducted in a manner to operate the engine too fast for the amount of thermal input energy. Relatively high operating speed for a given thermal input extracts too much energy from the receiver during the sunlight portion of the orbit and consequently stores too little energy in the salt for the eclipse portion. Large temperature and power swings result from sunrise to sunset. The swing in electrical power generation is 100 W out of an average of 1380 W, or 7.5 percent variation. The test conducted on 2-17-95 was operated at a speed more consistent with the orbit and thermal input, and a variation of only 60 W out of an average 1825 (3.3 percent) was observed. If large variations in output power are observed then the engine is operating too fast and extracting too much power during the sunlight portion of the orbit. All that is required is to sense the maximum-to-minimum power ratios and, if large, slow the engine speed. To do this the only parameters which need to be measured are output voltage and current. These parameters are already measured by the electrical control system and do not require additional instrumentation transducers.

2.5 Bibliography

Specifications

System	N10115
Solar Concentrator	N10116
Solar Receiver	N10117
Radiator	N10118
Parasitic Load Radiator	N10119
Power Conditioning & Control	N10120
Data Acquisition & Control	N10121
Liquid Utilities Pallet	N10132

Interface Control Drawings (ICDs)

Power Conversion Subsystem	213000016
Solar Concentrator	213010116

Receiver	213010117
Radiator	213010118
Parasitic Load Radiator	213010119
Power Conditioning & Control	213010120
Liquid Utilities Pallet	213010132

System Drawings

System Layout	213000001
Piping and Instrumentation	213000002
Intercabling Diagram	213000014
Instrumentation List	213000017
Wire List	213000019
Connector List	213000020
Grounding Network	213000021

Technical Reports, Plans & Procedures

System Test Planning Instructions	213TI000001
Receiver/PCS Pallet Installation Procedure	213TI000003
System Installation Flow	213TI000005
Preliminary Hazards Report	213SRR000001
Final Hazards Analysis	213SRR000001 Rev. A
Test Plan Summary	213TPS000002
System Test Plan	213TP000002
System Test Procedure	213DTP000001

3. SOLAR CONCENTRATOR

This section discusses the activities and results for the concentrator subsystem, including the facets. The essential time period is during the hardware phase, from CDR through concentrator subsystem testing at NASA LeRC.

3.1 Summary and Conclusions

The concentrator was fabricated, delivered and tested ahead of the prescribed project schedule and fully met or bettered the technical specifications. The critical steps of assembling the support structure and concentrator hex panel structure were first performed at the Harris facility; they were then reassembled in NASA LeRC Tank 6. The completed solar concentrator, installed in Tank 6, is shown in Figure 3-1. The facets produced by Solar Kinetics, Inc. (SKI) met their technical specifications and were shipped directly to NASA LeRC, right on the program schedule. Figure 3-2 provides a close up photograph of a completed facet assembly prior to installation on the concentrator. The facets were final prepared and installed and aligned into the hex panels, and aligned using the Harris laser based facet alignment system to within 0.5 milliradians of ideal - the internal requirement was 1.0 mr. The resulting flux distribution was measured using the Harris Flux Distribution Special Test Equipment, in the solar thermal vacuum environment of Tank 6. The measured peak flux and the total side wall power were within 10 percent of the predicted analytical value. The following table compares test results to requirements:

Parameter	Requirement	Test Result
Total power into receiver with 1.700 kW/m^2 at Optical Control Surface (OCS)	> 11.568 kW	results scale to 13.35
Power at OCS required to produce 11.5 kW/m^2 in aperture (derived req.)	<1.700 kW/m^2	1.46 kW/m^2
Maximum flux peak	< 42.9 kW/m^2	29.8 kW/m^2
Tube to tube variation	Best effort (worst case predict = 0.75/1.53)	0.90/1.25

It has been shown that a thermoelastically stable structure can be fabricated and optically precise/thermal vacuum compatible facets can be assembled with excellent reflective characteristics. It was also shown that the analytical tools used to predict concentrator performance and perform structure and facet alignment compared well with actual hardware performance.

Figure 3-1. Solar Concentrator Installed in Tank 6

NASA
C-94-05857

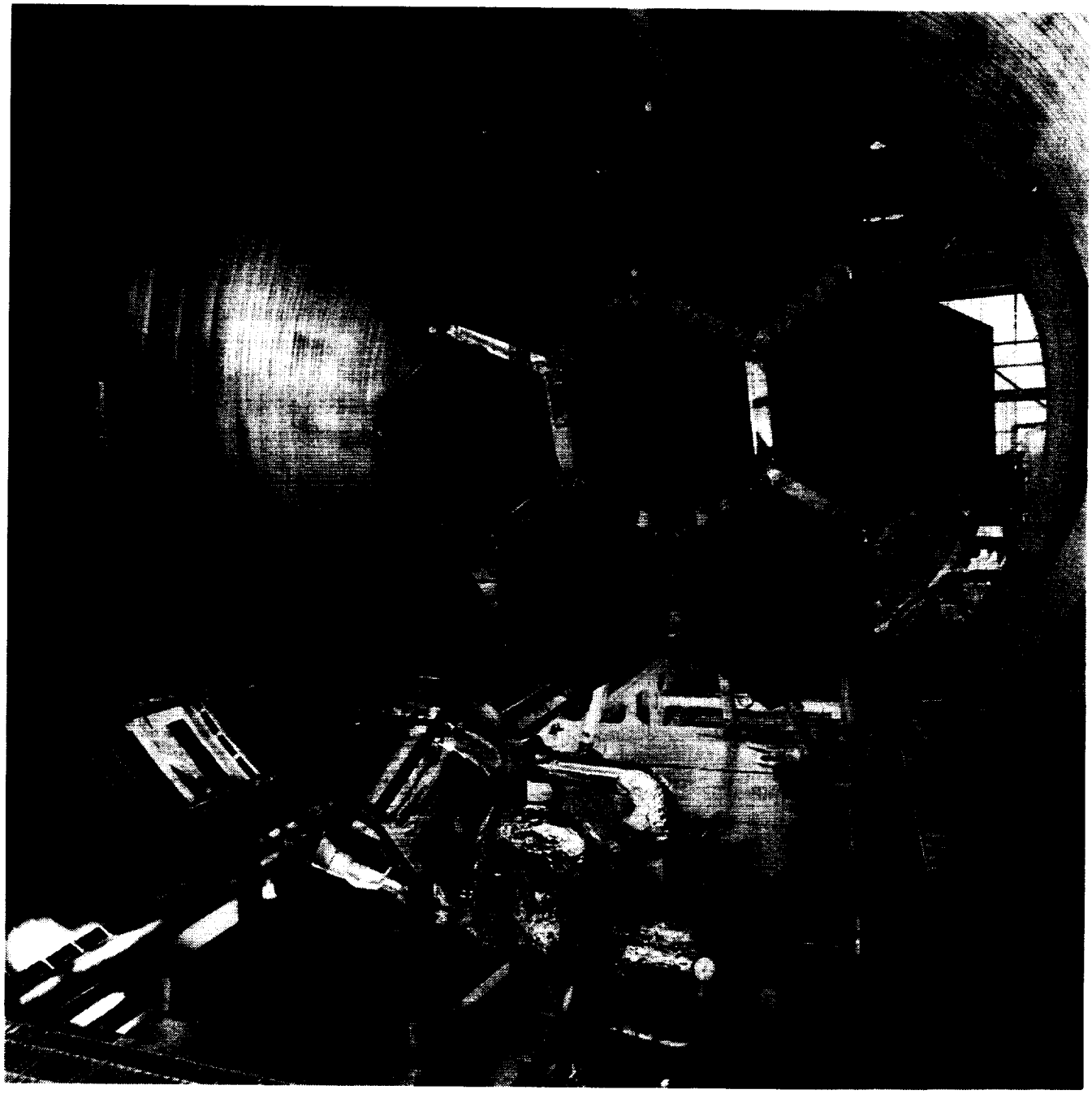

k:\ger\14056-3.doc

Figure 3-2. Facet Assembly Prior to Installation on the Concentrator

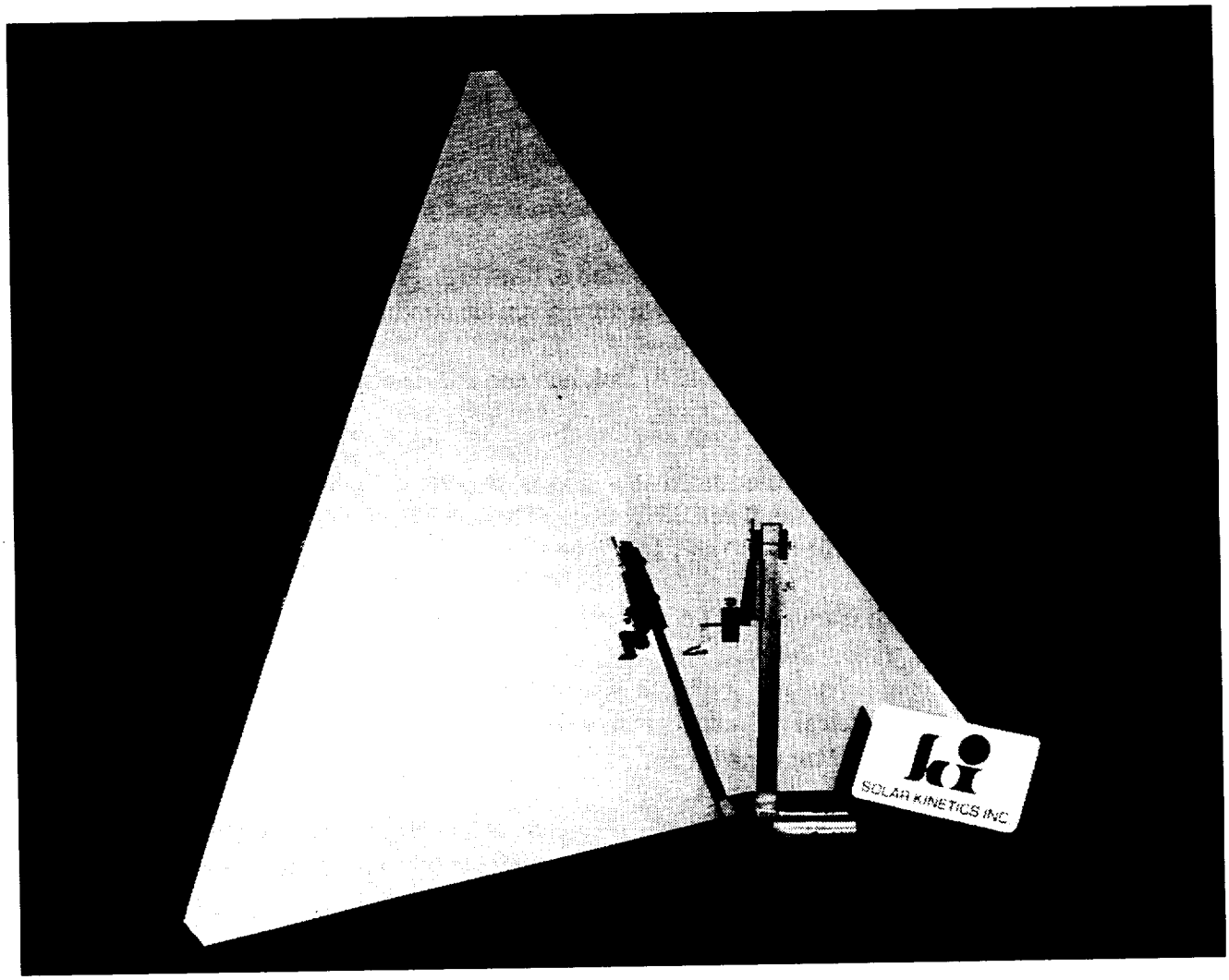

3.2 Design Changes after PDR

The following changes were made after CDR in the design of the concentrator, facets and concentrator support structure. All changes have been noted as engineering change orders in the drawing package.

1. Support structure leg to Buildup Assembly Platform (BAP) if modified per NASA request. Change made in interface bolt hole pattern and pattern location.

2. Added 4-layer MLI blankets around all latch/striker pairs to help reduce temperature excursions during illuminated to eclipsed conditions.

3. Facet-to-hex panel standoff lengths (and item numbers) changed with final flux tailoring.

4. Thermal control tape (Sheldahl tape G408050) added to drawings. This was the coating on the back side of the facets to keep their temperature down during sun-on conditions.

5. Switched from EA9394 epoxy to Loctite 242 to lock hub and corner fittings. This was easier for the manufacturing process.

6. Facet radii count and placement updated from 16 at 205 in. and 26 at 255 in. to 22 at 205 in. and 20 at 255 in.). This better optimized the flux distribution. (These are the predictions of their in-the-sun radii; the facets were built to radii of 200 and 247 inches.)

7. Power requirements dropped from 15 to 11.5 kW/m2 due to improvements in the predicted Brayton Cycle engine efficiency.

8. Facet solar averaged hemispherical reflectivity rose (0.85 to 0.88). This was a byproduct of trying to achieve the specular goal for a 7 mr cone angle.

9. Flux transducer changed from pyroheliometer to solar cell. This was more adaptable to the geometry of the flux region of interest, a rectangle representing a receiver canister, was just as accurate and less expensive.

10. Facet alignment gimbals with crossed mirrors. At CDR the design concept was to use an azimuth/elevation positioner to move a laser. Final design that was implemented used a pair of galvanometer-driven mirrors to direct only the laser beam instead of the entire laser assembly.

3.3 Fabrication Summary

Fabrication of the solar concentrator occurred in multiple phases and locations. The facet assemblies were built and inspected by SKI and direct shipped to NASA LeRC. The hex panel assemblies (less the facets) were built up at Harris, where they were tested and inspected, and finally shipped to NASA LeRC. The support structure was also fabricated at Harris and then shipped to NASA. Top-level

assembly of the concentrator, including alignment, occurred at NASA LeRC. The following paragraphs discuss each phase of the fabrication process in detail.

3.3.1 Support Structure Fabrication

The support structure (Drawing 3007157) consists of several components that were fabricated in local machine shops. It was assembled in Harris GASD Building 19 high bay onto a triangular shaped tooling plate (Drawing 3007162) that represents the anticipated interface pattern of the NASA Build Up Assembly Platform (BAP). Shimming was required to get the legs and table to align properly, and all shim thicknesses and locations were recorded. It was then proof loaded to 3 times the vertical load, and a combination of 2 times vertical/1.5 times horizontal time the expected loading due to the facet populated concentrator. It successfully passed the proof load with no degradation, cracks or yielding.

After disassembly (into hex panel assemblies) and shipment to NASA LeRC, it was first reassembled onto the BAP in May 1994. It was proof loaded at NASA LeRC in September 1994 to verify proper assembly readiness for final use.

3.3.2 Concentrator Hex Panel Assembly

The concentrator hex panel assembly consists of many components. The major components are the graphite epoxy box beams, the corner fitting assemblies, the hub fitting assemblies, the standoff brackets, the latches and the strikers.

The box beams were re-used from the previous Solar Concentrator Advanced Development (SCAD) project, although they were cut to new lengths in a Harris shop. The latches and striker assemblies were also re-used from the SCAD project. The use of existing latches and strikers from the larger SCAD concentrator resulted in larger gaps between hexes than would have existed with new designs. The standoff brackets were used from SCAD.

The corner and hub fitting assemblies were new designs, and were built up at Harris from aluminum and steel components that were made in local machine shops.

The hex panel was assembled on an assembly fixture that was the SCAD assembly fixture cut down to the proper size and angles. This fixture was also used to proof load the hex panel for workmanship verification.

The first hex panel assembly was successfully loaded to loads higher than those anticipated in handling and operation. But, it was discovered that it was slightly misaligned - it was several mils out of being coplanar. It was fixed, and loaded again. During the second loading there was some slight slipping of joints at the corner fitting to box beam interface. The slipping was due to the liquid shim material, epoxy, actually forming a bond instead of a sliding joint. The surfaces under the epoxy had been coated with a mold release agent, and this design has been used successfully elsewhere at Harris. The hex assembly was also thermal cycled, and it was found that it wasn't stable under the proofread of 2x the working load. Hence, a design change was made to increased the clamping force of two of the four

fasteners holding each box beam to a corner fitting. The hex assembly was proof loaded again to the 2x working load and the assembly remained structurally stable, no joints slipped, and the structural test was deemed complete.

3.3.3 Facet Assembly

The facets were designed and assembled at Solar Kinetics, Inc. (SKI) of Dallas, Texas. The basic flow for assembly was

1. Rough bending of the aluminum face sheets - the aluminum sheets were press formed over a coarse mandrel to approximate the radii of curvature
2. Cutting of face sheets and honeycomb core to rough dimensions - cut to dimensions that best work for the steps that follow, and have planned excess material that is scrapped around the edges
3. Degrease and de-oxidize face sheets - removes oils, all oxidation and other possible coatings on the aluminum, prepares the surfaces for bonding and leveling
4. Spin coating of polyimide applied to front of facet to make smooth surface. This critical step gives the facet its smooth surface that later is measured as slope error
5. Etch of levelized sheet
6. Aluminum core has been trimmed and degreased
7. Assembly and bonding of front sheet, core and rear sheet, with core dipped in adhesive, and pulled down over a precise mold with vacuum and vacuum bag over entire assembly. Assembly allowed to cure.
8. Installation of cup inserts
9. Facet trimmed to size. The excess material is cut from the sides, facet is in its final dimensions.
10. Facet sent to EMF (Evaporated Metal Films, Inc.) for application of the vacuum deposited aluminum layer and final thin coating of SiOx. Returned to SKI for curvature and optical measurements.

Two different radius of curvature facets were produced, and were designated F for the 205 inch radius and G for the 247 inch radius. The production line ran very smoothly with the slight exception of a series of facets in the middle of the run that had polyimide cracks in the reflective surface. It did not effect the reflectance of the facets, but did cause concern visually. The small cracks were noted on facets G20, F18, F24, F34, G33, G37, F36, G39, G38 and G41, refer to the As-Built package from SKI for details. The cracking effect was corrected with a slight modification to the spin coating process and the cure oven temperature ramp rates. Many of the facets have what appears to be scratch marks when viewed at some angles. This source was never tracked down (possibly scratches from the metallizer's cleaning process), but, they did not effect the functionality or performance of the facet. Table 3-1 provides a comparison of achieved (demonstrated) performance to program goals. The specific locations of installed facets is shown in Figure 3-3.

Table 3-1. Summary of the Specifications and Actual Values for Various Parameters Characterizing the Facets Used in SDGTD

	Spec	Actual
Weight, lb/ft^2	0.5	0.57
Reflectivity, total, AMO	>0.85	0.88
Reflectivity, at 15 mrad at 660 nm	>0.85	0.88
Radius of curvature, inch	±10	0.2
Slope error (mrad)	<2	0.3
Irregular surface area	$<1\ in^2$	
Irregular sites/facet	≤2	
Max temp, °F	207	170
Min temp, °F	-50	-5*
Outgassing, %	1	2
(As condensible), %		0.2
Thickness, in	0.28	0.28
Thermal control backing	TBD	Yes

*Tested to these levels

Figure 3-3. Final Facet Locations

Facet Radii
F_{series} = 205 in
G_{series} = 255 in

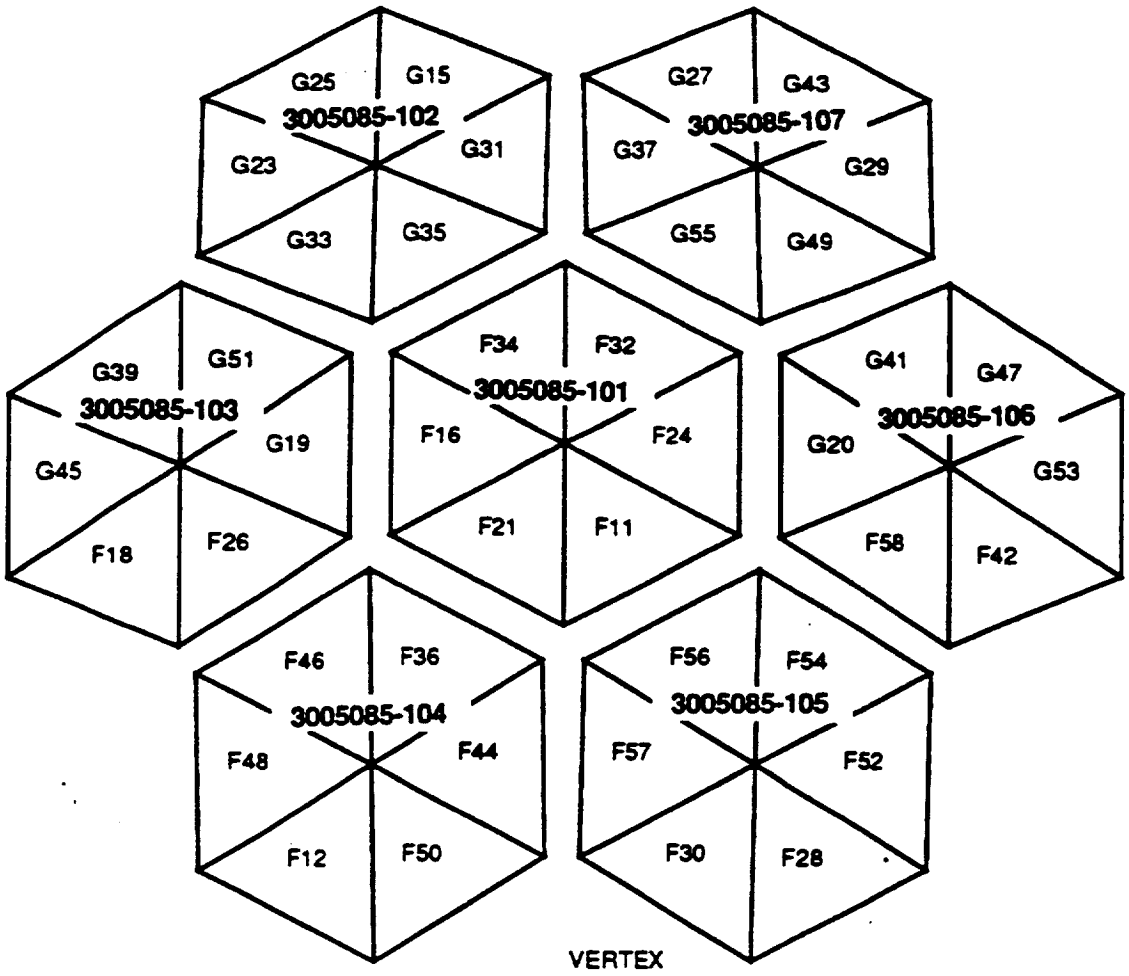

3.3.4 Final Hex Panel Assembly and Installation of Facets

Upon receipt of the facets at NASA, the facets were visually inspected and their rear side covered with silvered Teflon thermal control tape. This operation took place in September 1994. The facets were then installed into the hex panel assemblies, using the prescribed standoff lengths, initial standoff adjustments and the as-designed locations of the two types of facets (by radius of curvature). The hex assemblies were ready for final installation into the concentrator assembly. This operation is discussed as part of the next section, and is covered under the concentrator structure alignment and facet alignment paragraphs.

3.4 Component Testing Summary

Tests were performed at the subassembly level and the assembly level of the concentrator.

3.4.1 Facet Testing

Facet coupons were subjected to a humidity cycling test, 100 thermal cycles and a thermal vacuum test to verify stability of the reflective surface and structural integrity of the honeycomb. The tests were conducted at SKI, Harris and NASA-Lewis, respectively. The tests were successful.

One full size facet was subjected to a thermal vacuum/3 cycle test at NASA-Lewis. It successfully passed this test and the design was deemed ready for production.

3.4.2 Harris activities at NASA LeRC

Harris activities at NASA LeRC included the bulk of the system alignment and identification, installation and integration to the solar concentrator, and finally, functional testing of the concentrator.

3.4.2.1 Tank Surveying and System Alignment

Harris established a global coordinate system in the tank from which all components, including the solar simulator, could be referenced. This involved the Harris owned theodolite system and the Harris proprietary software used to reduce the theodolite measurements into a set of coordinates in the established coordinate system. The setup includes three theodolites, two located inside the tank and one on the walkway adjacent to the pit that the tank door slid. Their specific location is not important, as long as they are stable over the prescribed period of time.

Harris drew sketches of a tapered steel rod that had a small hollow point. This rod was attached to the side of the tank wall in three locations at an elevation off the floor of about 8 feet. The rod was firmly affixed to tank penetration plates. The points of the rod served as the three reference points for the tank coordinate system for the duration of the setup.

Harris then helped NASA by measuring the optical axis of the solar simulator relative to the fixed points of the three rods, which was then placed in the now established tank coordinate system.

Neither Harris nor NASA measured the actual location of the Build Up Assembly platform (BAP) relative to the coordinate system. This was a risk that the SDGTD team chose to accept.

The concentrator support structure had been previously (early summer 1994) installed on the BAP outside of the tank. The support structure went together in approximately the same fashion as first assembled back at Harris, with no major problems interfacing (for the first time) with the BAP.

The step of installing the hex panel assemblies (complete with installed, initially aligned facets) also went well. The hex panels fit together just as they had back at Harris, and in earlier assembly sequences at NASA when they were assembled for various tours and two tank thermal tests. This final assembly was the only time the hexes contained facets.

The targets (little balls of the end of small spires) on the concentrator box beams were then measured in reference to the coordinate system. It was determined that the concentrator was mispositioned laterally with respect to the simulator optical axis by 1.3 inches. It was fortunate that the interfaces and the tolerances were good enough to not require this adjustment.

3.4.2.2 Facet Alignment

The entire facet alignment test report was delivered as a stand alone document, but is summarized here for completeness.

The facet alignment system consisted of a low power laser, a pair of galvanometer controllable laser turning mirrors, a translucent screen with reference points and a video camera; plus the necessary control cards and a 486 personal computer. The laser, turning mirrors and laser screen were precisely located using the previously described theodolite system. The PC was located outside of the tank, the laser and turning mirrors were very near the solar simulator source, and the screen very near the receiver aperture location.

After initial calibration, the system operated automatically to give the precise pointing vector of each of the 42 facets on the concentrator. The facet adjustments necessary were also reported by the alignment software, which were implemented by a person adjusting the standoff lengths between the facets and the hex panel assembly attachment point. A cherry picker was used to reach the upper facets.

The facets were aligned within an acceptable pointing error (0.5 milliradians) after only one iteration. However, it was determined a day later that the target the facets were pointed at was probably just beyond the location of the receiver aperture, so the procedure was repeated in two days to point to a location well within the aperture adjustment capability. This only took one iteration.

The whole alignment routine, which was somewhat challenged at CDR as overly complex, proved to be very valuable and made quick and accurate alignments. The development of the hardware and software was not costly.

As mentioned above, a cherry picker was used to reach the facets in the top most hex panels for adjustment. This was awkward, but safe and workable. Because of the accuracy of the adjustment software, the cherry picker was only needed once when the final alignment was made.

3.4.2.3 TE Distortion Testing

The first thermal distortion test on the project was conducted by NASA. The test article was the concentrator (structure only) on the support structure installed on the BAP. One facet was installed. The concentrator structure, support structure and BAP were sparsely populated with thermocouples. A bright light bulb near the solar source location illuminated the facet, and reflected onto a screen near the future location of the receiver aperture. The tank was pumped down to a vacuum, and the walls were filled with liquid nitrogen. The temperatures were recorded and the movement of the light spot on the screen was noted/photographed and compared to the starting point. The results did not match the expectations. It was noted that it seemed that the BAP thermal gradient was not close to what NASA had predicted (3 degrees measured versus 17 degrees F predicted). It was further noted that the supporting structure hadn't reached steady state conditions.

NASA decided to repeat the test with more thermocouples the second time. Steady state conditions were achieved, and the BAP gradient was closer to expectations. The net system distortion was noted for later consideration for biasing the pointing of the concentrator. It was deemed close enough to predictions to move on.

3.4.2.4 Flux Distribution Testing

The Flux Distribution Test was described fully in the delivered test report. The following is a summary of the test.

The test objective was to measure the reflected solar flux in a simulated receiver behind a simulated aperture plate in environmental conditions like the conditions that would exist for the full GTD test. A special test fixture was designed, built and calibrated to accomplish this. The fixture consisted of a calibrated rake of solar cells that rotated and simulated the cylinder of the receiver. The STE was aligned by Harris personnel using the theodolites and the established tank coordinate system. Partial power and full power cases with eclipse periods were conducted in the evacuated chamber with walls full of liquid nitrogen.

Of note is that interpretation of results is highly dependent upon the intensity and distribution of the flux field on the concentrator. NASA had performed a flux survey before the test, reported the results, and then made adjustments to the solar simulator with an estimate of how it would change the flux field. A second flux survey was conducted several months later, revealing the estimate was not accurate. Integrated flux measurements at the flux fixture indicate a 6% lower optical energy than solar simulator

output estimates. This is similar to the differences noted during engine testing and discussed in paragraph 2.4.3.3 of this report.

The results of the Flux Distribution Test are contained in the test report 7002233. Highlights include the following:

Receiver Flux Mapping - the maximum flux peak was 24.9 kW/m^2 when total sidewall power was 8.23 kW (which scales to 28.8 at power of 9.5 kW/m^2). This compares to a worst case prediction of 42.9 kW/m^2. This shows that the peak fluxes are well within the worst case design expectations. The worst case tube to tube flux variation, as measured in normalized values, was 0.90/1.25, as compared to a worst case prediction of 0.75/1.53. Both the peak flux values and the tube to tube variation are quite acceptable to the limitations of the receiver, and achieve the concentrator requirements. A comparison in measured flux distribution and predicted values is provided in Figure 3-4 and Figure 3-5.

Temperatures and Thermal Analysis Comparison - bulk temperature predictions for the cold soak condition were all within 10 °F of measured results, and gradients for this case were good for most components except the BAP (NASA prediction) and the facet (Harris prediction). The facet problem was determined to be a poor installation of a thermocouple, because the measured 12 °F gradient is entirely impossible. The orbital steady state temperatures did not correlate well with measurements, the measured temperatures were all much cooler than the predictions. This is attributed to conservative analyses (properties, etc.) which assumed a higher intensity optical source (1.44 kW/m^2 assumed versus 1.2 kW/m^2 test) and a warmer tank end wall temperature (wall 20 ° cooler than assumed). Since correlation was not required, and the results were more benign - thus hardware safety not of concern, no better correlation was attempted. The temperatures were all well within their qualification limits during this test and subsequent system testing.

Optical Performance and Analysis Comparison - the real meaningful data in the optical sense is that which was summarized in the section above on receiver flux mapping, with the conclusion that the tube to tube, peak flux and total power into the aperture hole are within requirements and satisfy the needs of the receiver. In addition to that, the thermoelastic effects of all of the structure in the concentrator was reviewed. It was decided that the biasing of intentionally aligning an offset of 0.3 inches into the concentrator/receiver aperture setup was not needed. It was intended to provide the optimal alignment for a combination of hot, cold and orbital steady state conditions in which the concentrator points in a slightly different direction for each due to the thermoelastic distortion (due to different temperatures). This was the setup then for the real aperture on the real receiver. The only bias that was added to the test setup was the bias discussed in paragraph 2.3 (Item 4) to account for the thermal growth differences between the receiver (hot) and the flux test fixture (cold).

Figure 3-4. Predicted Flux Distribution for Conditions of Scan 1858

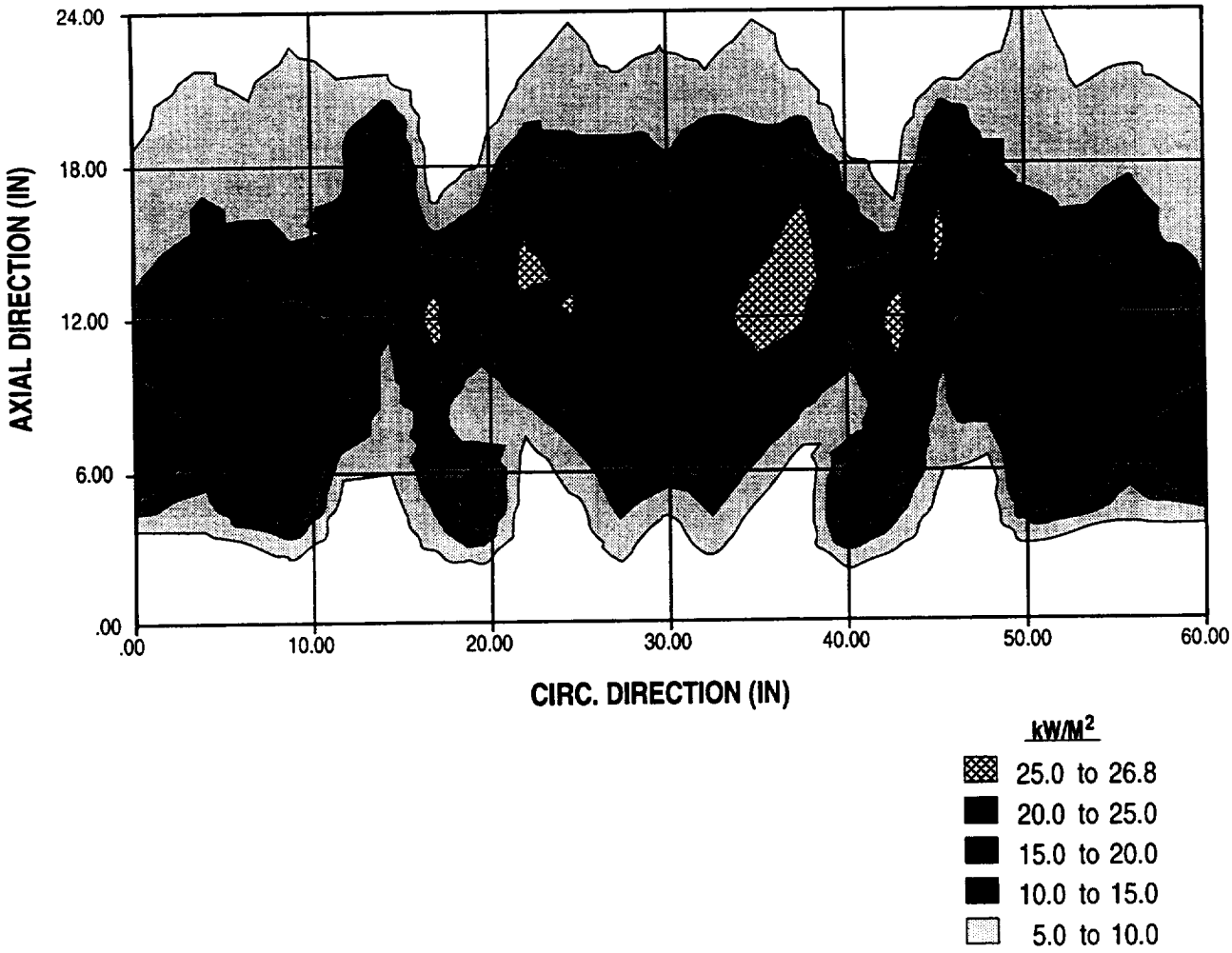

Figure 3-5. Measured Flux Distribution for Conditions of Scan 1858

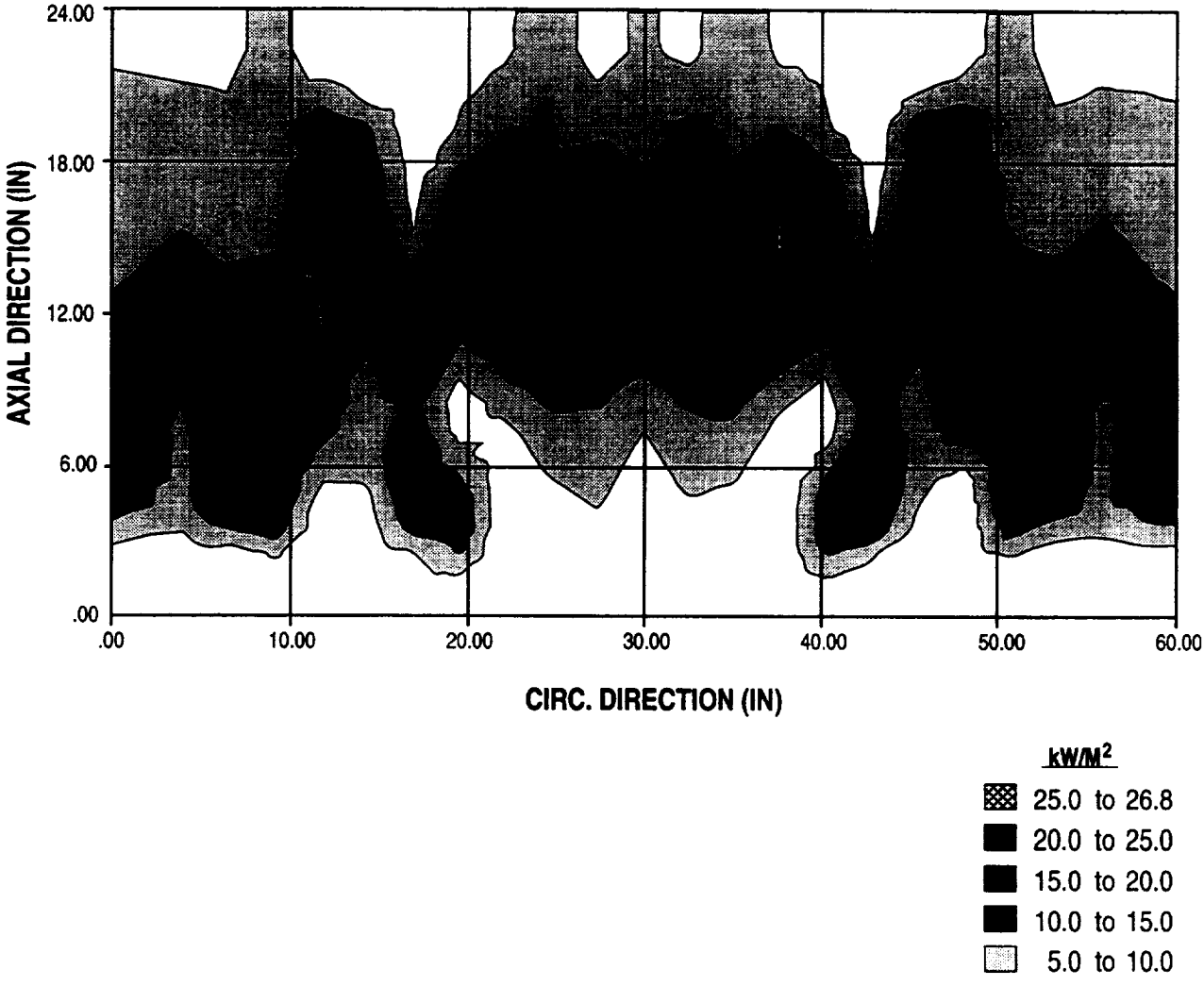

3.5 Bibliography

3.5.1 Specifications and Statements of work

Solar Dynamic Ground Test Demonstration Design requirements specification for concentrator.

Solar Dynamic Ground Test Demonstration SOW for concentrator.

Reflective Facet Assembly Procurement Specification 2001423, Rev. B

Reflective Facet Assembly SOW 7000493, Rev. B

3.5.2 Review Packages

Solar Concentrator SRR package
Solar Concentrator PDR package
Solar Concentrator CDR package, 13 April 1993

Reflective Facet PDR package, 29 July 1993
Reflective Facet CDR/MRR package, 21 December 1993

3.5.3 General

Calibration Report for the Flux Distribution STE Solar Cells. Harris Corp., 7002231, Feb. 1994.

Concentrator Acceptance Test Plan. Harris Corp., 7000495, Rev. A, March 15, 1993.

Concentrator Acceptance Test Procedure. Harris Corp., 7000495, Rev. A, June 6, 1994.

Concentrator Acceptance Test Report. Harris Corp., 7002232, Jan 19, 1995

Facet Alignment Test Plan. Harris Corp., 7000498, Rev. A, March 10, 1993.

Facet Alignment System Checkout Test Report. Harris Corp., 7002230

Facet Development & Acceptance Test Plan. Harris Corp., 7000494, Rev. A, March 15, 1993.

Flux Distribution STE Checkout Plan. Harris Corp., 7000504, April 30, 1993

Flux Distribution STE Checkout Report. Harris Corp., April 22, 1994

Flux Distribution Test Plan. Harris Corp., 7000496, Rev. A, March 10, 1993.

Flux Distribution Test Procedure. Harris Corp., 7000496, April 25, 1994.

Flux Distribution Test Report. Harris Corp., 7002233, Jan 19, 1995

Hazard Analysis, Harris Corp., DRD MA-05, Rev. A, 3 May 1993.

Hex Assembly and Support Structure Proofread Test Report. Harris Corp. 10 November 1993.

Hex Beam Pin Bearing Development Test. Harris Co. Dave Brangwin, Internal Memo, June 3, 1993.

Hex Proofread Verification Test Plan. Harris Corp., 7000499, Rev. A, Jan 25, 1993

Test Report for Environmental Exposure of Small Scale Coupons. Paul Schertz, Solar Kinetics, Inc., 16 March 1994.

Test Report for Environmental Exposure of a Full Size Facet. Paul Schertz, Solar Kinetics, Inc., 17 March 1994.

Manufacturing Plan. Harris Co., 7000503, Jan 31, 1993

Spares List. Harris Co. 7000502, Oct 16, 1992

Thermal Cycle Test Results for 100 Cycle Facet Coupon Testing. Jeff Dupper, Harris Co. Internal Memo, Nov 18, 1993

Vacuum Thermal Cycling of Solar Concentrator Coupons for the Solar Dynamic Ground Test Demonstration Program. Eric J. Bruckner, Cleveland State Univ. and Joyce A. Dever, NASA LeRC, Dec 16, 1993

Vacuum Thermal Cycling of Solar Concentrator Coupons for the Solar Dynamic Ground Test Demonstration Program, Phase II. Eric J. Bruckner, Cleveland State Univ. and Joyce A. Dever, NASA LeRC, Feb. 1, 1994

Vacuum Thermal Cycling of Full-Sized Facet for the Solar Dynamic Ground Test Demonstration Program, Phase II. Don Jaworski, Kim DeGroh and Carol Tolbert, NASA LeRC, Dec 12, 1993

Design of a Solar Concentrator for the Solar Dynamic Ground Test Demonstration Program. Bahnman, D.W. and Jensen, P.A. ASME paper, 30 March 1994.

Design, Analysis and Test of a Solar Concentrator for Space Applications. Campbell, J.S. and Jensen, P.A. ASME paper, 30 March 1994.

4. SOLAR SIMULATOR

The NASA solar simulator (SS) shown in Figure 4-1 nominally provides 1.37 kW/m^2 (1.8 kW/m^2 maximum) of light at a subtense angle of <1 degree over a 4.5 m diameter test area, illuminating the SD concentrator. The optic and power systems are located at the western end of Tank 6 as shown in Figure 4-2. Cooling subsystems are located in the Tank 6 pump room, on its roof, and directly outside on the ground floor. Control and monitoring of the simulator is accomplished with two 486 PCs running Paragon software in the Tank 6 control room.

The heart of the system is a cluster of nine 30 kW xenon arc lamps supported by the following subsystems: optics, power supplies, data acquisition and control, cooling, radiometer, and structure. As shown in Figure 4-3, light from each lamp is gathered with its own collector which directs the light through a lens and onto a turning mirror. A water cooled shutter is commanded to intercept the light beams just above the mirrors to simulate the sun-shade cycle encountered in space. The turning mirror, consisting of nine segments, reflects and focuses the light into the vacuum tank through a quartz window. Each lamp is powered by its own power supply and igniter, and can be controlled manually at the power supply, or remotely via the SS DACS (Solar Simulator Data Acquisition and Control Subsystem). Water cooling of the lamp electrodes is provided by a dedicated deionized water system, while the quartz lamp envelope is cooled by the air cooling system. The collector and turning mirrors are cooled principally by the domestic water system with some additional cooling from the air cooling system. The lens is air cooled, as is the window which utilizes pressure blowers to provide a large cooling capacity. Except for the lenses, the temperatures of all components of the optic train are monitored by the SS DACS either directly, as in the case of the turning mirrors and window, or indirectly by their cooling water outlet temperatures. A protection system provides lamp shutdown in the event of a loss of air or water coolant flow or violation of component temperature limits, in addition to other automatic or operator-initiated shutdowns.

Prior to system testing, a survey of the solar simulator beam was made to characterize the general uniformity and overall intensity of the light. The survey was conducted using photodiodes and a radiometer mounted on a mechanical arm which was swept through the beam in an arc. The radiometer is water cooled and held at a constant temperature (20 ± 2 °C) and provides a direct measurement of the light intensity. Sensor readings were recorded in a fine grid for each of the nine lamps and compiled into a final representation as shown in Figure 4-4. Both uniformity and intensity were found to match reasonably well with design requirements (± 10 percent uniformity, up to 1.8 kW/m intensity). The data was also used to develop a model that predicts concentrator input power based on lamp power settings and the radiometer signal for any combination of lamps.

Once operational, the simulator proved to be a relatively simple system to run. Start-up is done locally on the power supply platform, with monitoring of system parameters occurring both at the control room and the power supply platform. After a nominal start, control is transferred to the control room. Operation activities consist principally of monitoring system parameters and setting power levels and opening and closing the shutter at the test engineers request. Radiometer and power supply from a typical run (4-3-95) is shown in Figure 4-5. As of May 1995 the simulator has nearly two hundred hours of run time.

Figure 4-1. NASA Solar Simulator for Tank 6

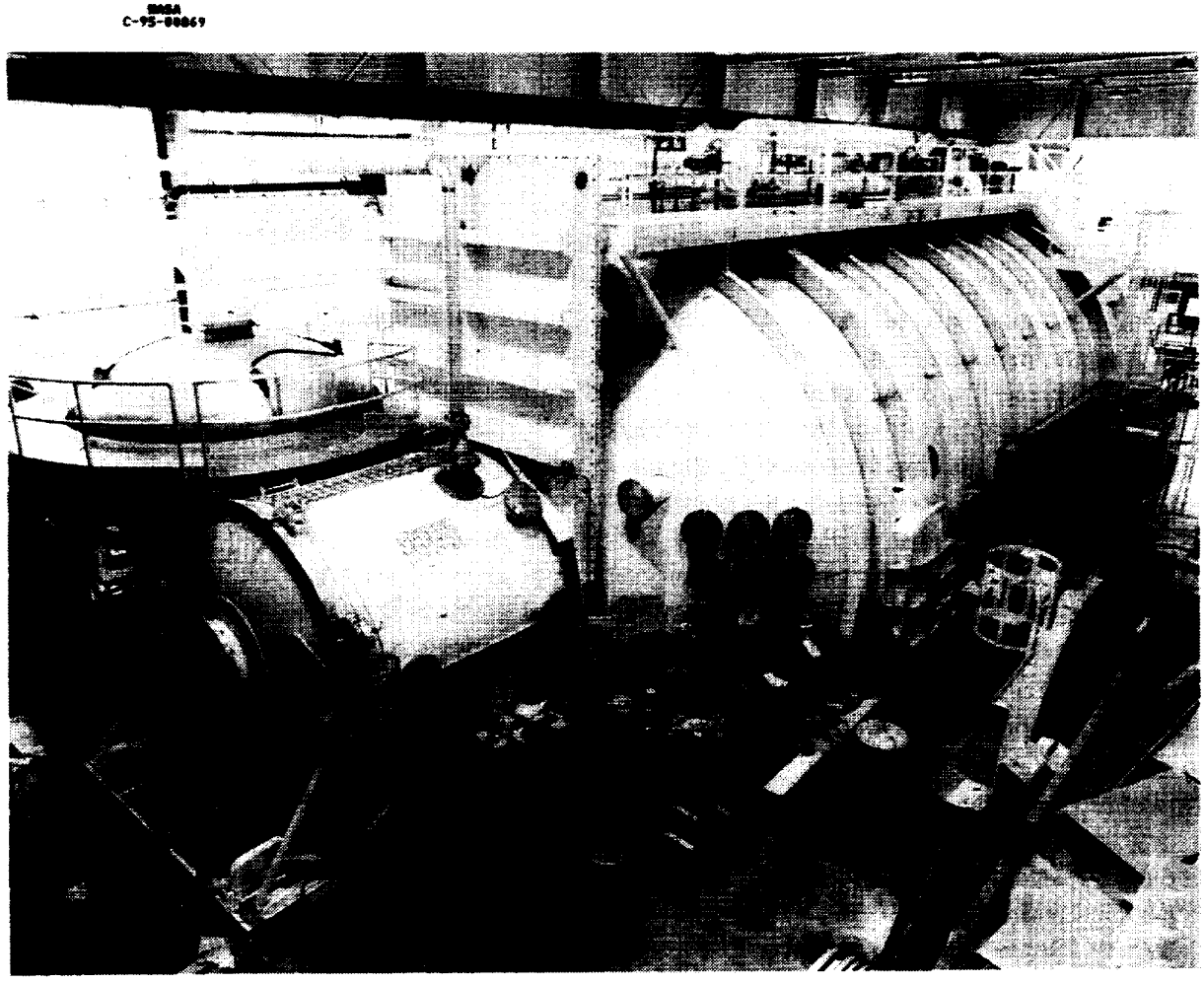

Figure 4-2. Solar Simulator and Supporting Equipment

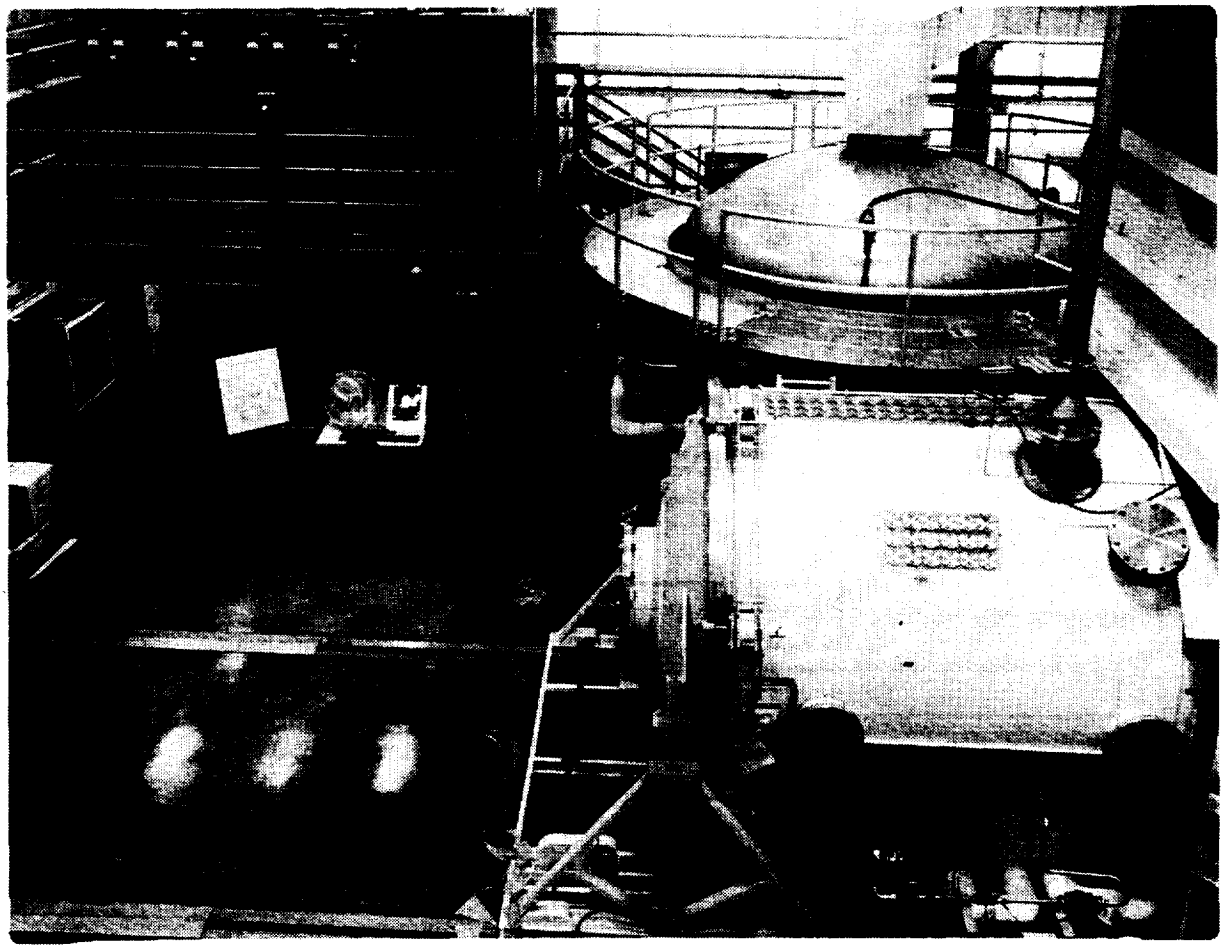

Figure 4-3. Solar Simulator Configuration

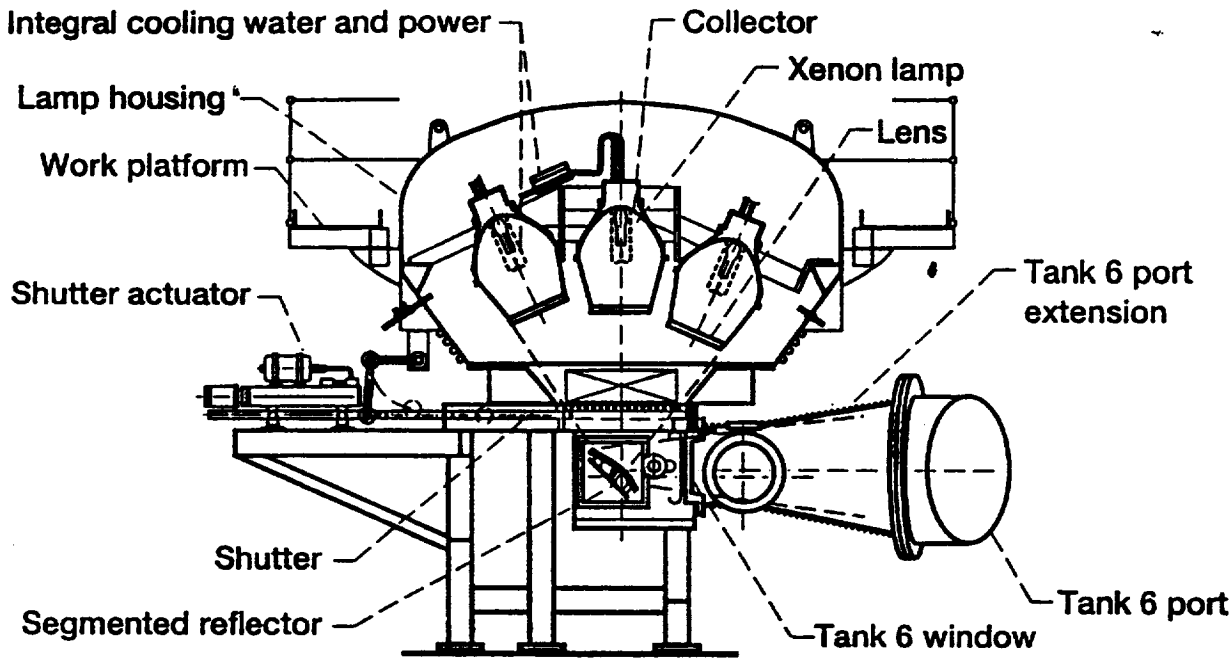

Solar simulator characteristics	
Beam size	188.5-in. diam at 56-1/2 ft from apparent sun
Collimation	None - point source
Irradiance	1.8 kW/m^2 (1.27 sun) max
Uniformity	±10%
Subtense angle	About 1 deg

CD-94-68893

Figure 4-4. Solar Simulator Intensity Data

Figure 4-5. Solar Simulator Functional Test Data

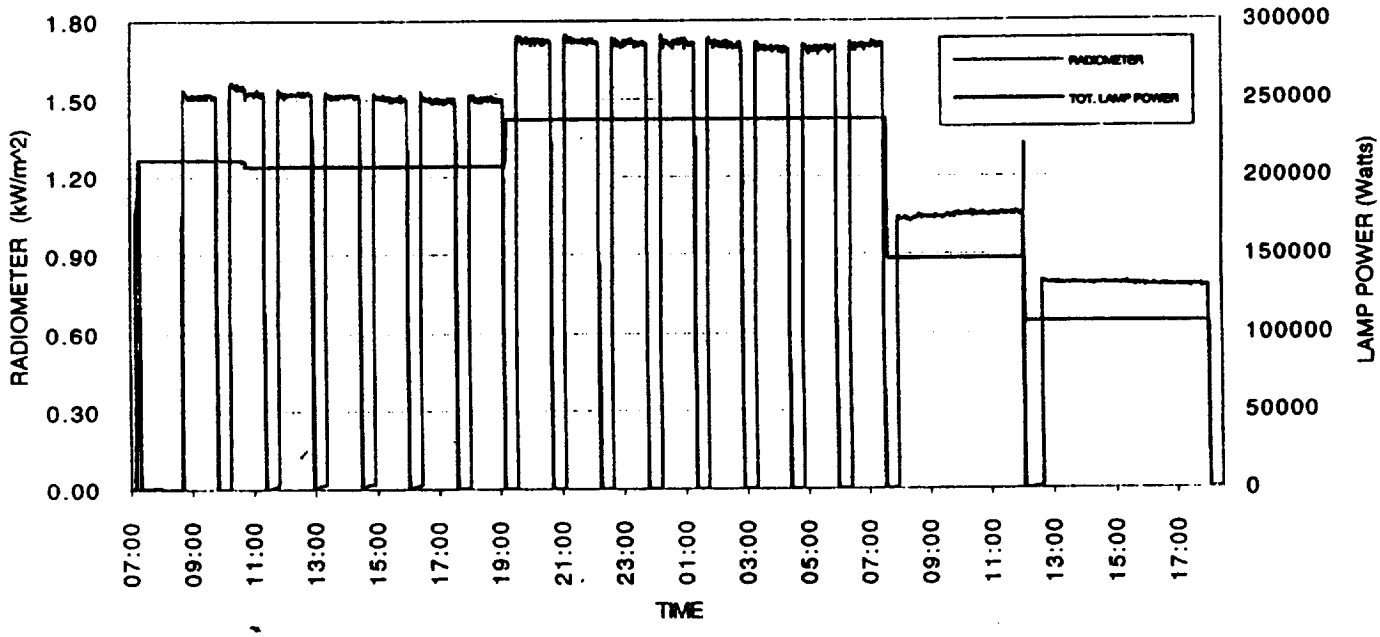

5. TANK 6 AND FACILITY TEST SUPPORT HARDWARE

5.1 Tank 6 Vacuum Facility

Vacuum Facility 6 (Tank 6), shown in Figure 4-1, consists of a 4.6 m diameter by 22 m long main chamber, with a 3 m diameter by 3 m long test port which may be isolated from the main chamber by a 3 m diameter gate valve. The main chamber is pumped by twenty 0.8 m diameter oil diffusion pumps charged with DC-705 silicon oil. These pumps are backed by four Roots Blowers and three Kinney roughing pumps. The diffusion pumps utilize Freon cooled (-45 °C) chevron baffles to minimize oil backstreaming. The chamber base pressure is approximately 3x10E-06 torr (8x10E-07 torr with cold walls on).

Space thermal simulation is provided by a three-section liquid nitrogen cooled coldwall capable of 0.24 MW thermal loading (80 kW per section). The liquid nitrogen usage is approximately 1400 l/hr for no test article thermal load. Liquid nitrogen storage is provided by a 20800 l dewar.

A rehabilitation project started in March 1990 and completed in 1994 decontaminated Tank 6 of mercury, and replaced the liquid nitrogen cold walls and pumping train. A new 40 ton Freon refrigeration system and cooling water tower system were also installed.

The thermal vacuum facility is computer controlled for start up and shutdown as well as health monitoring during operation. Corrective actions take place automatically if an off condition occurs. The liquid nitrogen system must be manually started at which point it is switched to automatic operation.

5.2 Buildup Assembly Platform (BAP)

The NASA-LeRC BAP was designed and built to provide a stable platform for buildup, handling and positioning of the SDGTD concentrator, solar receiver, and power conversion system. The prime technical requirements were to position the test article in an accurate and repeatable manner within the solar simulator light beam inside of Tank 6, and to maintain the concentrator and solar receiver optical alignment under test conditions. The BAP also minimizes Tank 6 down time by providing a platform on which pretest activities, such as build up, rough alignment, and electrical checks, can be performed outside of and independent of other Tank 6 activities.

The BAP, shown in Figure 5-1, is a 20 ft x 10 ft stainless steel frame constructed of six inch square by 1/4 inch wall stainless tubing, weighing approximately 3260 pounds without system components. Mounting surfaces are provided for the concentrator and the independently adjustable subpallet which supports the solar receiver and PCS. Four lift points are provided for transport by the Tank 6 overhead crane onto the Modular Rail System (MRS). The BAP's wheels (two flat and two V groove) mate to the MRS rails and permit the BAP to be rolled along the MRS and into position inside Tank 6. Final horizontal positioning is accomplished with two precision pins which anchor the BAP to support mounting pads at the east end of the tank. Vertical positioning is accomplished with three BAP jackscrews which raise the BAP wheels clear of the MRS. Jack screw contact is made at two points near

Figure 5-1. Tank 6 and Buildup Assembly Platform

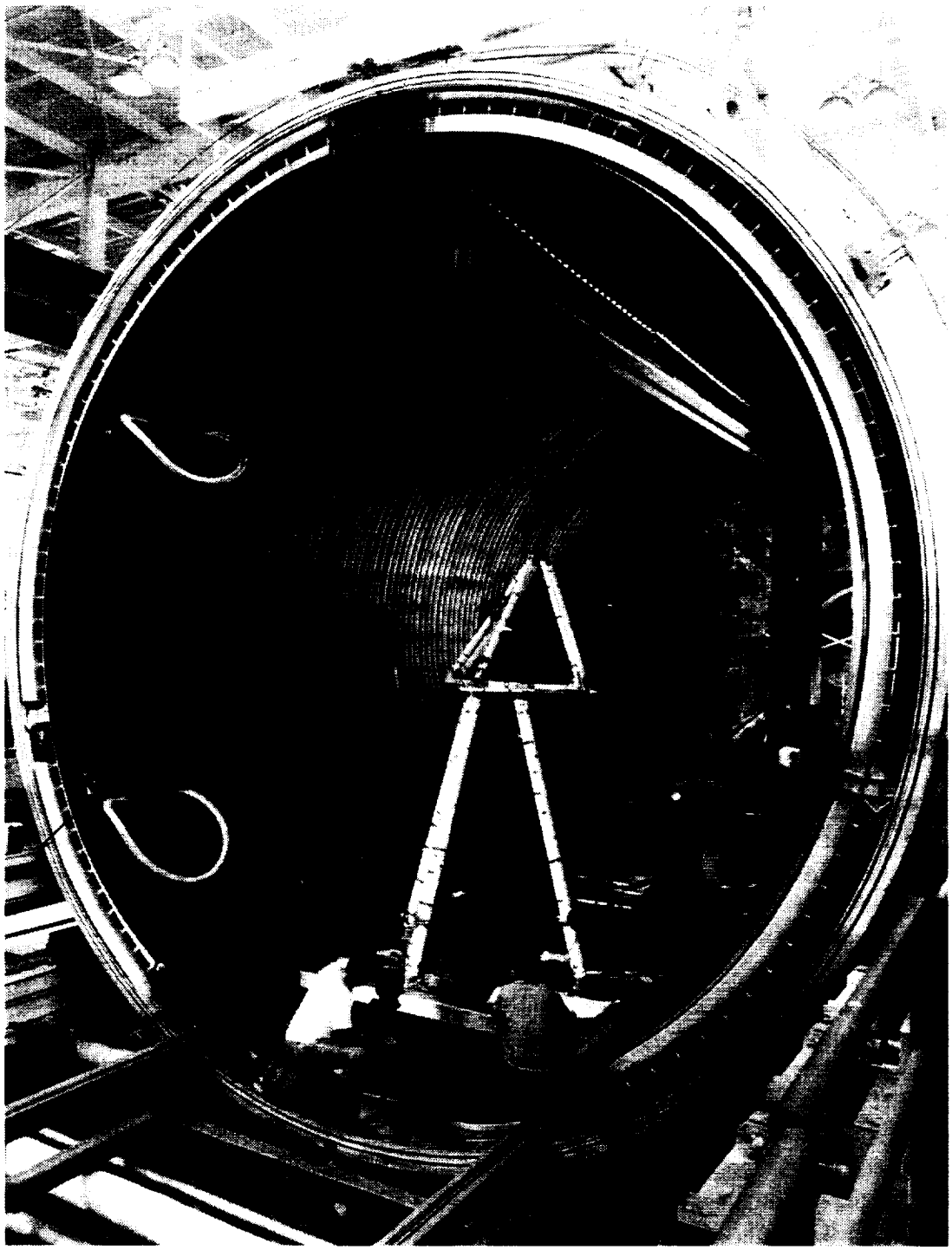

the concentrator (east) end of the BAP and one central point at the receiver (west) end. The east contact points coincide with Tank 6 hard mount points, while the west support point contacts a column which passes through a bellows-sealed Tank port and is anchored to the facility floor. The west support provides vertical support only and minimizes any effects tank movement and BAP thermal movement might have on SDGTD positioning.

BAP positioning repeatability was determined by rolling the BAP out of the tank on the MRS rails and then back into position several times, measuring final positions each time with theodolites. Final positioning accuracy was repeatable to less than 0.017 inches. The BAP was also subjected to a thermal vacuum test prior to SDGTD system testing to determine distortion levels as it cooled in the coldwall environment. Light was projected onto a concentrator facet and its image at the receiver aperture was monitored for movement. Facet image movement was approximately 0.5 inches downward (approximately half the predicted movement) as the BAP cooled from room temperature to its cold soak conditions.

5.3 Thermal Modeling

A thermal model (SINDA and TSS) was created by NASA LeRC for the SDGTD project to provide temperature data for design and performance predictions of the test hardware. A representation of the model is shown in Figure 5-2. Prior empirical data was not available due to the refurbishment and reconfiguration of Tank 6 (new cold walls, internal floor, etc.).

Thermal boundary conditions were calculated for various LeRC and Contractor components. Particular attention was paid to the radiator, concentrator and BAP. Sink temperatures of -155 °F and -91 °F for the radiator east and west panels were predicted. The west panel prediction was found to be low by approximately 60 °F when compared to an instrumented sink temperature gauge average reading of -30 °F. BAP temperature gradients were also less than predicted. Localized heating of the tank end cap was observed on the order of 100 °F (typical was 70 °F) in those areas where the simulator beam missed the concentrator. Most differences between measured and predicted temperatures can be attributed to heating affects of the diffusion pump heaters on the tank floor and higher-than anticipated convection due to shop ambient air currents on the end caps.

Sufficient data now exists to adjust the thermal model to compensate for inaccuracies uncovered during testing. This is a recommended activity as significant effort went into creation of the model and its use in future Tank 6 tests is probable and desirable.

Figure 5-2. Tank 6/SDGTD Thermal Model

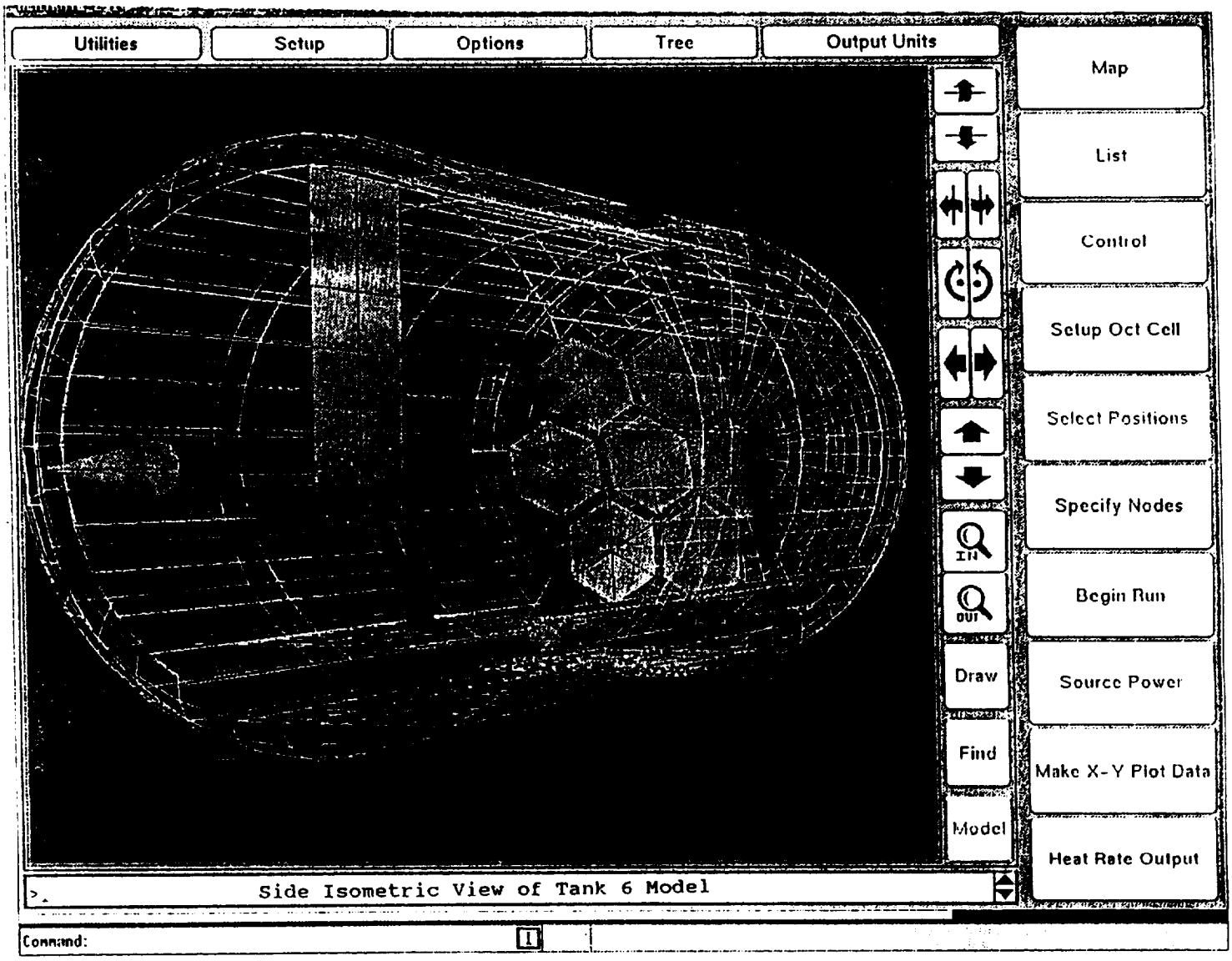

5.4 Uninterruptible Power Supply (UPS)

A UPS, backed by a natural gas fired, electric generator was installed on the ground floor outside Building 301 to provide the SDGTD with backup electrical power in the event of a facility power failure. Of prime importance was maintaining power to the SDGTD liquid loop radiator heater and pumps to prevent freezing of the n-heptane fluid. Secondary to this was powering the ELS, solar simulator, and DACS (data systems) to maintain monitoring and control capabilities during a facility power loss. The UPS also provided power conditioning, although this was not a prime consideration. Switch-over to the UPS following a power outage is automatic and immediate.

The 18 KVA UPS is a set of batteries providing at least 10 minutes for the test engineer to manually start the generator switch over to generator power. Once started, the Kohler generator provides 50 kW to the SD experiment. Power is provided via a distribution system composed of 208 and 110 Vac receptacles located alongside Tank 6, in the control room, and on the solar simulator power supply platform.

Monitoring of the UPS status is done on a 286 PC located in the Tank 6 control room.

5.5 PCS Helium-Xenon Charge System

The primary purpose of the helium-xenon gas charging system is to fill the power conversion system (PCS) gas loop with the proper inventory of working fluid. The working fluid is a high purity mixture of helium and xenon gases (63 percent xenon and 37 percent helium) with a molecular weight of 83.8. The system is nominally charged to a loop pressure of between 38 and 49 psia at ambient temperature.

The gas charging system is shown in Figure 5-3. Most of the equipment comprising the gas charging system is mounted outside of Tank 6. Vacuum feedthroughs connect the exterior piping system with the PCS, inside Tank 6. The gas charging system is operated manually.

In addition to supplying the required quantity of the helium-xenon gas mixture to the PCS, the charging system also provides:

1. a means for supplying additional He-Xe gas to, or removing excess helium-xenon gas from the PCS following the initial fill,

2. a means for evacuating the Power Conversion System prior to filling the PCS with the helium-xenon working fluid,

3. a means for filling the PCS with alternative gases such as He to allow leak checking of the PCS,

4. a method for acquiring representative He-Xe gas samples from the PCS during system operation, by means of a flow through gas sampling loop.

Figure 5-3. Cycle Gas Charging System

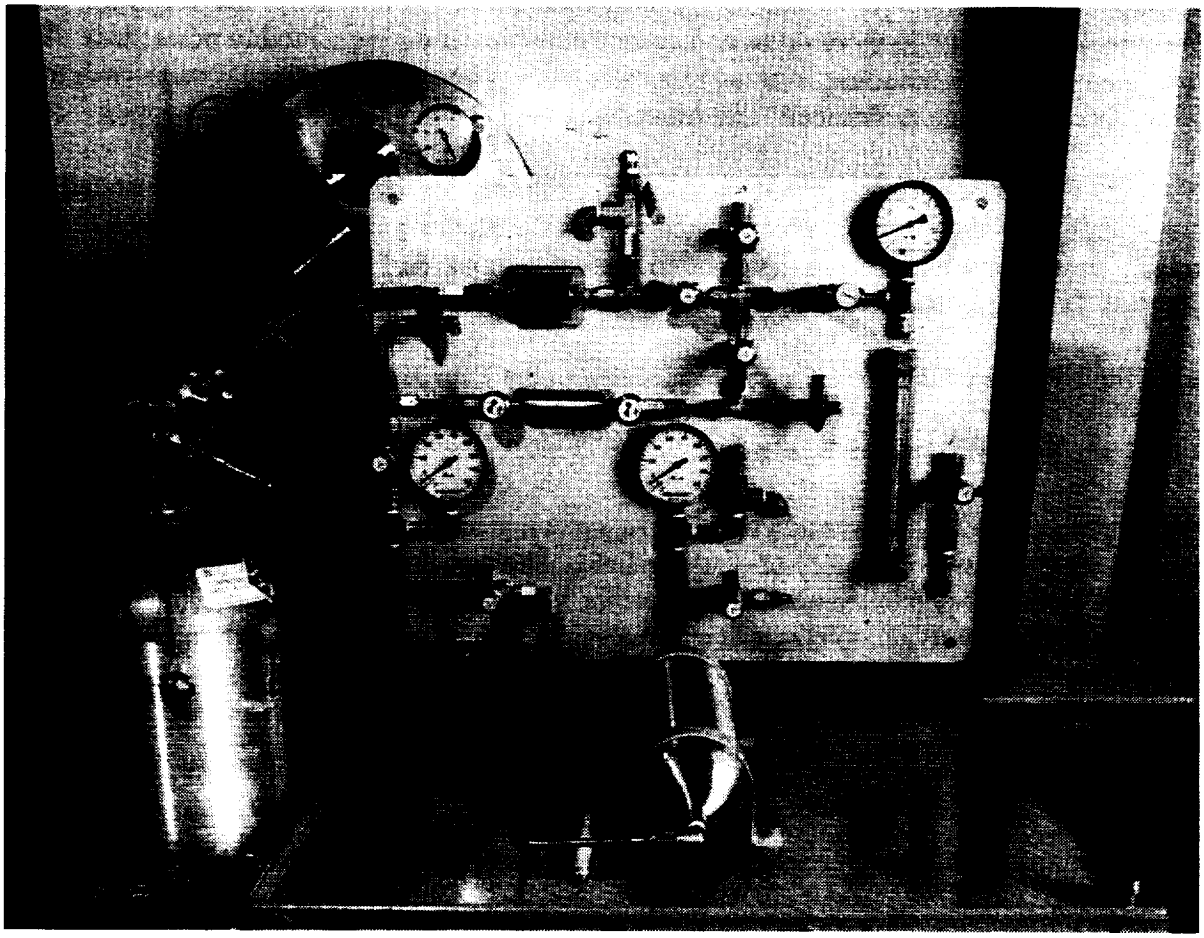

5.6 Radiometer Thermal Control System

The closed-loop radiometer thermal control system is designed to provide a continuous flow of constant temperature cooling water to the Kendall MK-IV Radiometer. The Kendall radiometer is mounted inside Tank 6 for the measurement of solar simulator flux levels at the concentrator. The radiometer main body is maintained at a relatively constant room temperature. The cooling water system is mounted external to Tank 6 on a cart and plumbed to the existing radiometer body via 1/4 inch lines routed through a vacuum feedthrough in the Tank 6 wall. Power to the pump is supplied by the SDGTD uninterruptible power supply.

The closed-loop thermal control system is shown in Figure 5-4. The primary components of the system are the refrigerated bath/circulator and the diaphragm metering water pump. The remainder of the system consists of various flow control components, tubing, and the necessary instrumentation for monitoring system performance. The system delivers conditioned water to the radiometer at a flow rate of approximately 10 GPH, and a pressure between 30-60 psig. The water is pumped from a five liter refrigerated water bath, which maintains the water at a constant temperature, within + 0.1 °F (maximum permissible variation + 4 °C). A 2.5 micron filter has been installed in the system, downstream of the water pump. Thermocouples are located in the radiometer supply and return water lines at the radiometer. Additional instrumentation in the system includes a flow gauge for monitoring the water flow rate, and pressure gauges for measurement of water pressure and filter pressure drop.

5.7 Fill/Drain System

The NASA LeRC n-heptane fill and drain system for the SDGTD is used for the safe transfer of approximately two gallons of n-heptane from a dedicated pressure vessel into the SDGTD coolant liquid loop system. The fill and drain system is also used to drain the n-heptane from the coolant system to another dedicated pressure vessel. The fill drain system is shown in Figure 5-5.

The n-heptane fill and drain system consists of three fluid subsystems:

1. a portable n-heptane supply system
2. piping hardware within the vacuum chamber to provide the fluid to the various component fill ports and to provide verification of fluid fill
3. a fixed n-heptane drain system located below the vacuum chamber.

The fill portion of the system consists of a cylindrical pressure vessel for n-heptane storage, a liquid tight piping system for n-heptane transfer, and a low pressure gaseous helium system for purging the vapor space of the fill pressure vessel and pressurizing the n-heptane during filling. The fill verification hardware consists of shutoff valves and sight flow indicators mounted at the uppermost points of the coolant piping system. These components are used by personnel to determine when the coolant system has been completely filled with n-heptane. The n-heptane drain subsystem consists of another dedicated pressure vessel and piping system that provides the capability of draining the n-heptane from the coolant system, as part of an end-of-experiment shutdown or at any other desired time (at the operator's discretion).

Figure 5-4. Radiometer Thermal Control System

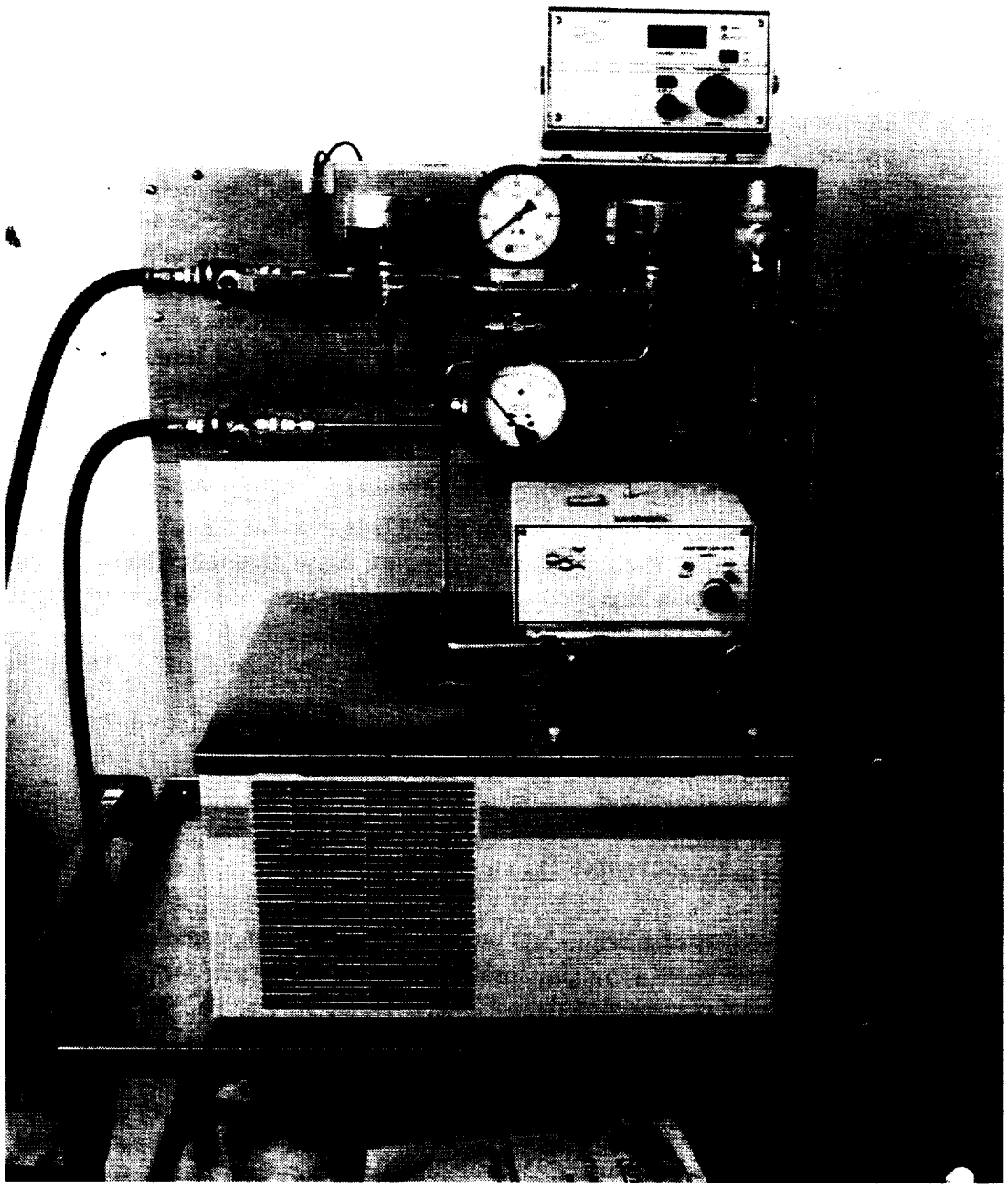

Figure 5-5. N-heptane Fill and Drain System Schematic

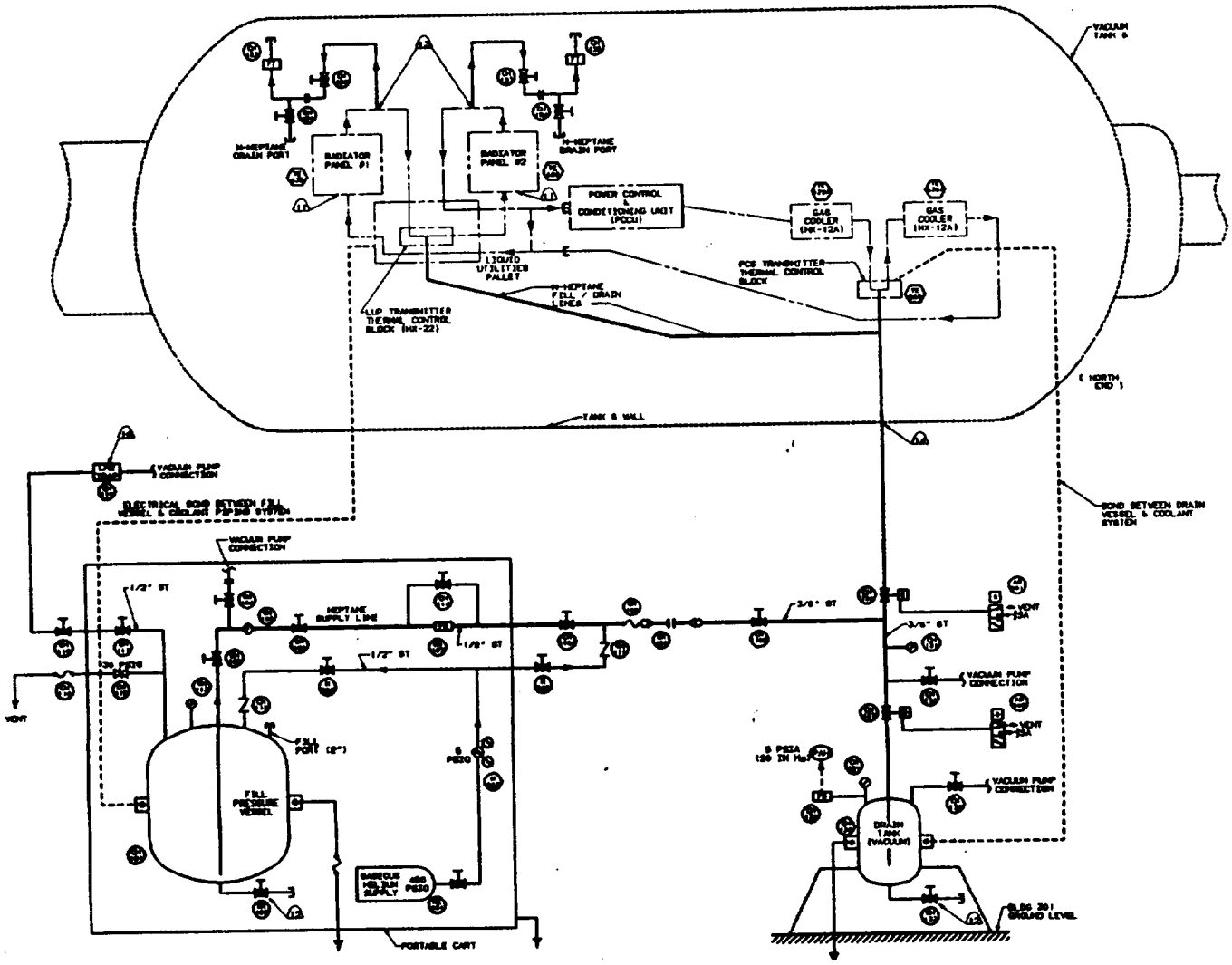

5.8 Electric Load Simulator

The ELS (Electric Load Simulator) was developed by NASA LeRC for the SDGTD project to provide representative user load variations that may be encountered during actual space missions. The system provides a means for evaluating the SD electrical system response to sudden and/or random load variations.

The ELS main components are two water cooled programmable load modules controlled by a 486 PC running LABVIEW software. As configured, the system is capable of absorbing approximately 2 kW dc per module, although the actual number is limited via a DACS-supplied maximum value. (ELS to DACS communications are over an IEEE bus.) Electric loads may be simulated in three modes: constant current, constant resistance, and constant power. Within each mode, a sinusoidal, step, or ramp function may be selected to vary the absorbed power over time. Selection of the modes and control of the ELS is accomplished through a touch screen interface in the Tank 6 control room. The ELS Operator's Screen is shown in Figure 5-6.

Figure 5-6. ELS Operator Screen

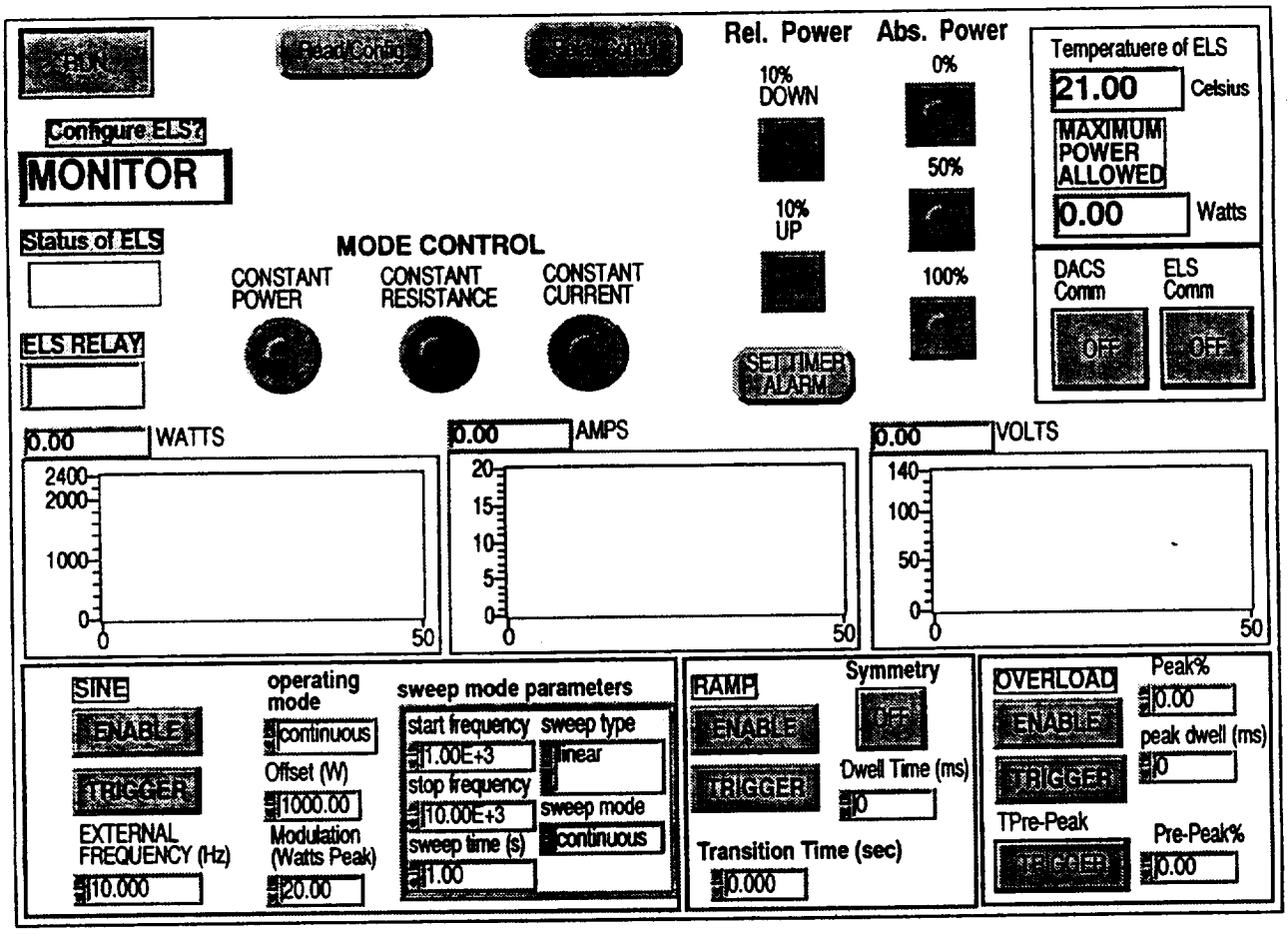

6. RECEIVER

6.1 Summary and Conclusions

The heat receiver component for the solar dynamic ground test demonstrator space power system was designed, developed, fabricated, and tested. The design of the heat receiver is based on the solar receiver developed for the solar dynamic power option as part of Work Package 4 of Space Station *Freedom*. The *Freedom* receiver was a much larger unit, corresponding to an engine power output of over 30 kW(e) compared to 2 kW(e) for the present unit.

The receiver design (shown in Figure 6-1) comprises a cylindrical receiver cavity, the walls of which are lined with a series of tubes running the length of the cavity. The receiver incorporates integral thermal storage, using a eutectic mixture of lithium fluoride and calcium difluoride as the thermal storage solid-to-liquid phase change material (PCM). This thermal storage is required in order to enable power production during an eclipse period in low-earth orbit. The eutectic has a melting point of 1413 °F.

The cycle working fluid flows through a finned annular region in the tubes (shown in Figure 6-2). The center of the tube is blocked to increase the flow velocity. A significant enhancement in heat transfer rate is afforded by this configuration.

As shown in Figure 6-1, both the inlet and outlet ends of each tube are bent. The bending accommodates differential tube-to-tube thermal expansion and reduces thermal stresses. The differential thermal expansion is due to the circumferentially asymmetric incident flux arising from the offset parabolic concentrator. There are no fins in the bent tube ends.

The PCM is contained in a series of hermetically sealed metal containment canisters (see Figure 6-3). The canisters are stacked and brazed to the working fluid tube, as shown in Figure 6-6.

The use of individual containment canisters for the PCM is a key attribute of the receiver design. This configuration affords a readily fabricated and highly reliable design. Failure of a canister would affect only that individual canister, and have minimal impact on receiver operation. The compartmentalization also reduces the chance of failure by localizing void formation upon freezing (due to the lower density of the liquid as compared to the solid), minimizing the likelihood of high stress buildup.

The receiver cavity walls consist of a metallic shell with an inner ceramic cloth liner. The shell is externally insulated.

The receiver gas circuit, outer shell assembly, and aperture assembly are each independently mounted to a support frame, using tie rods, as shown in Figure 6-5. The approach minimizes weight-induced and thermally-induced stresses by off-loading weight from the gas circuit and allowing thermal growth.

The receiver design is summarized in Table 6-1.

Figure 6-1. SDGTD Receiver

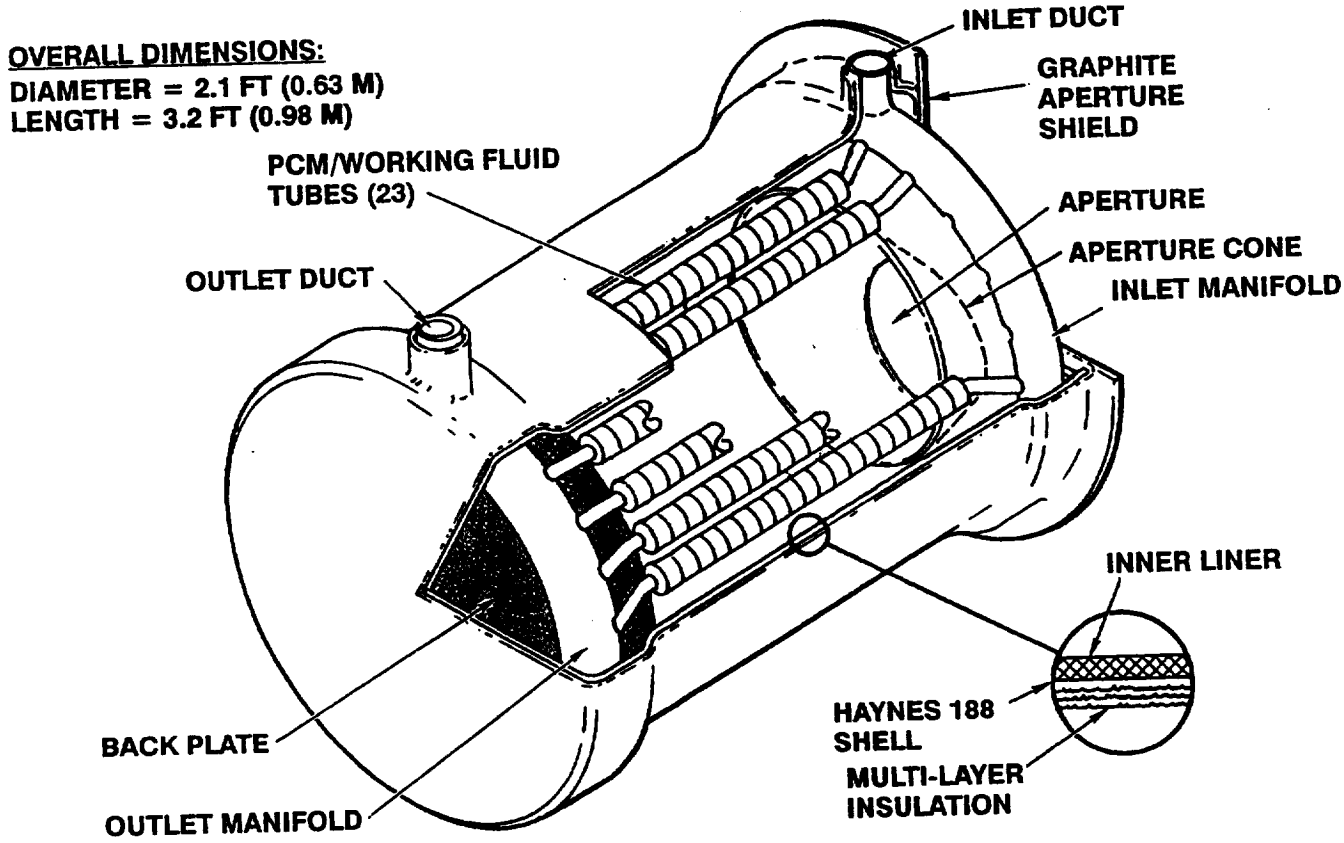

Figure 6-2. Finned Tube Cross Section

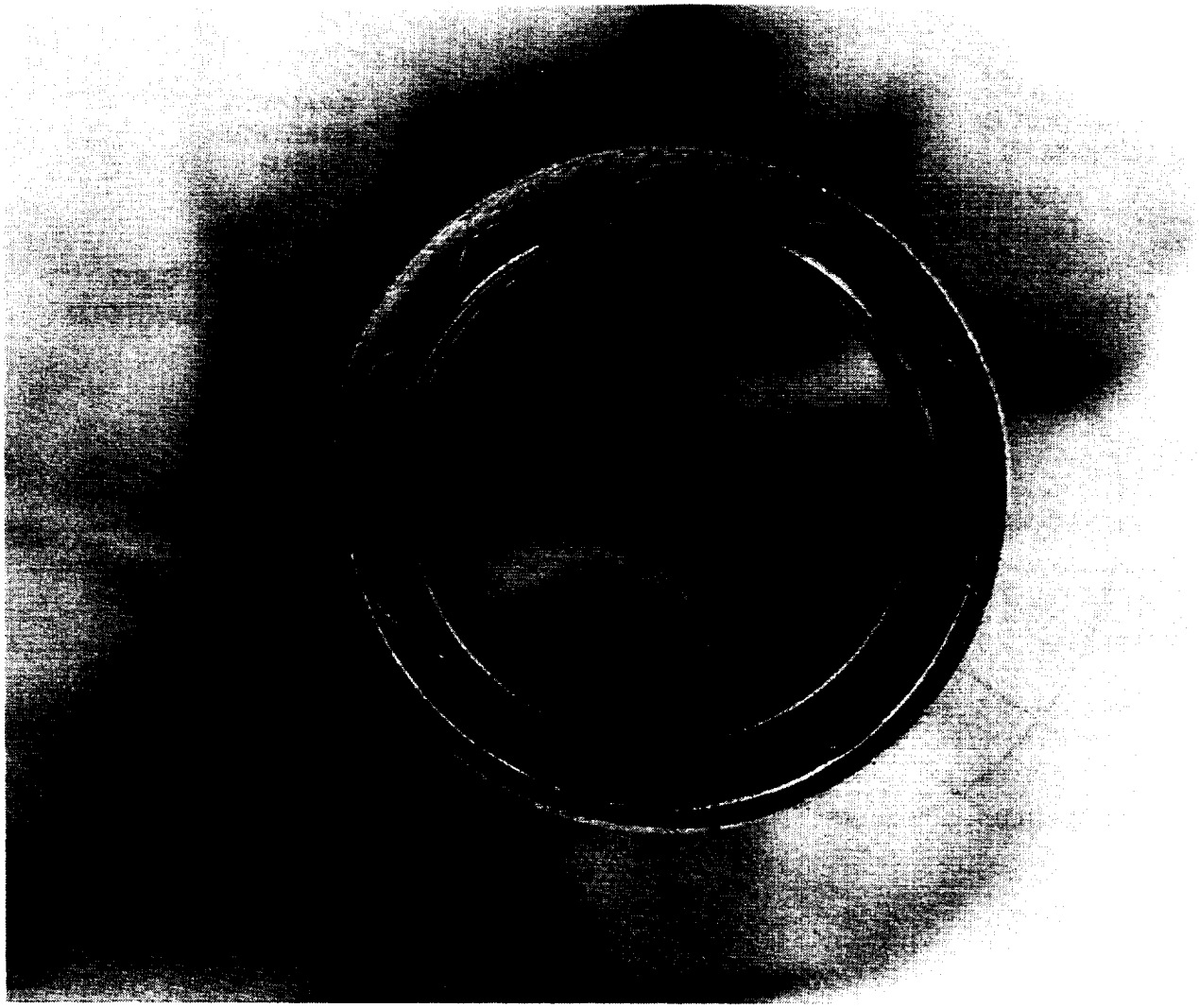

101756-2

Figure 6-3. Containment Canister

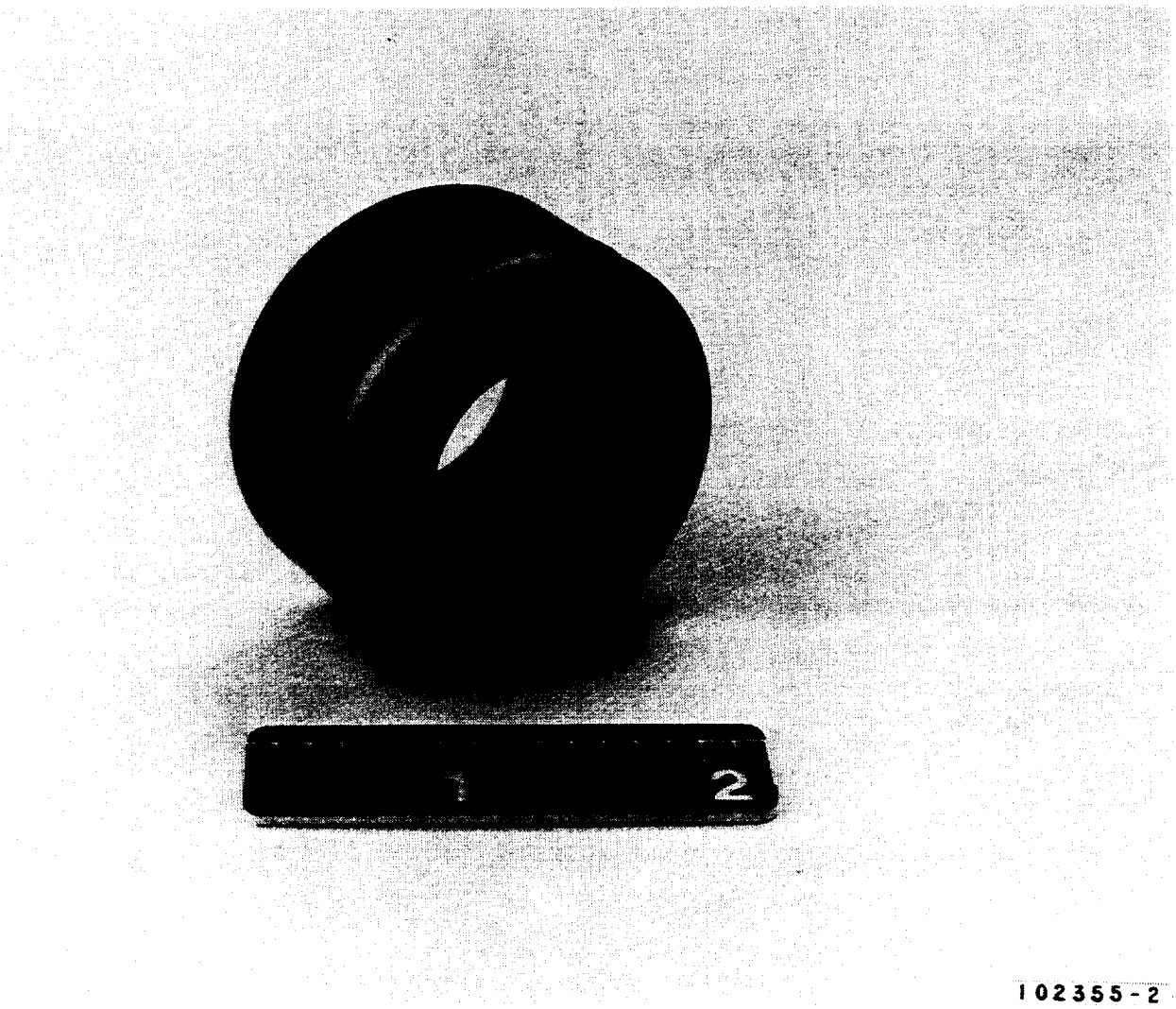

Figure 6-4. Canisters Brazed to Working Fluid Tube

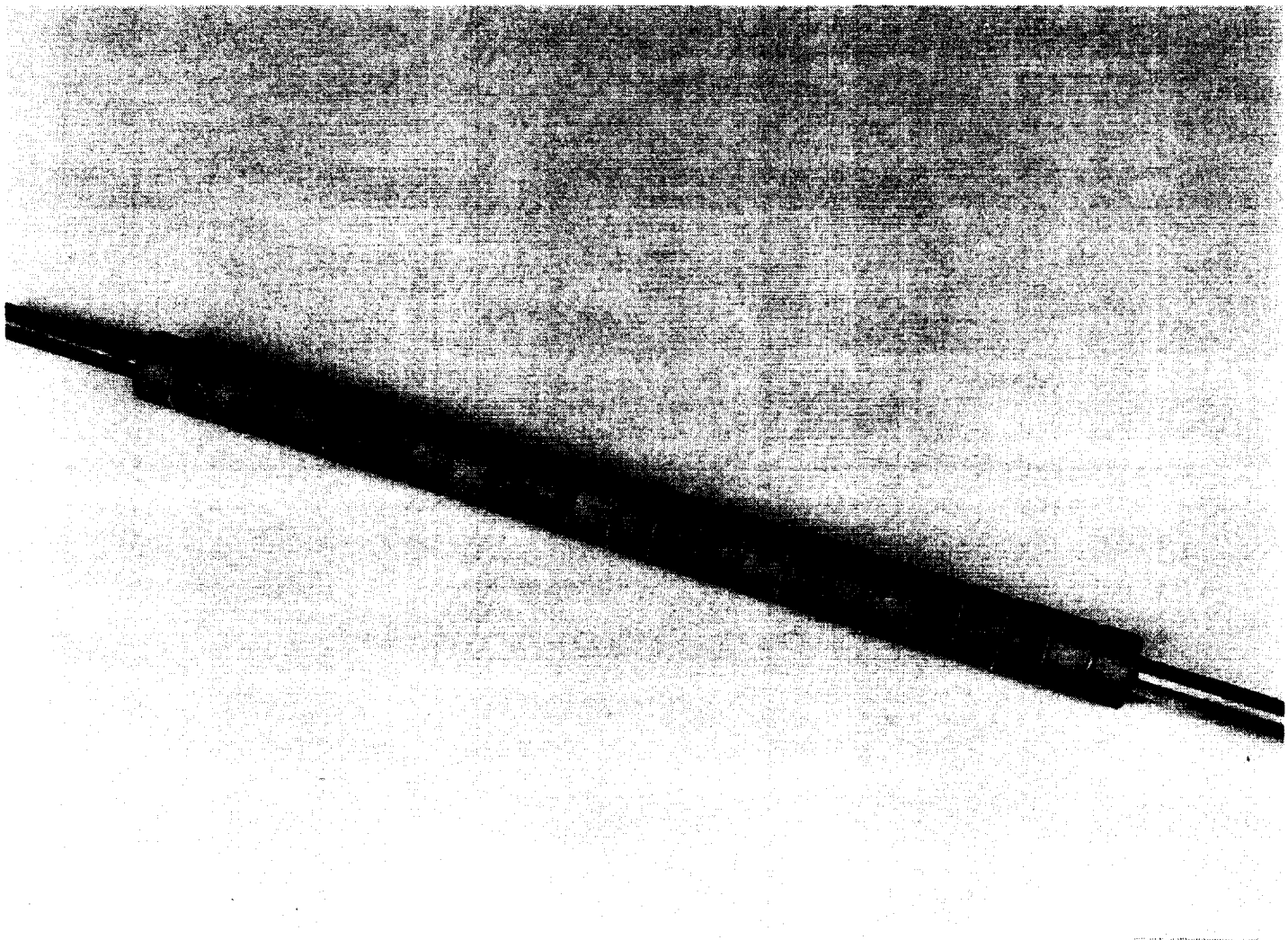

102312-3

Figure 6-5. Receiver Assembly Overview

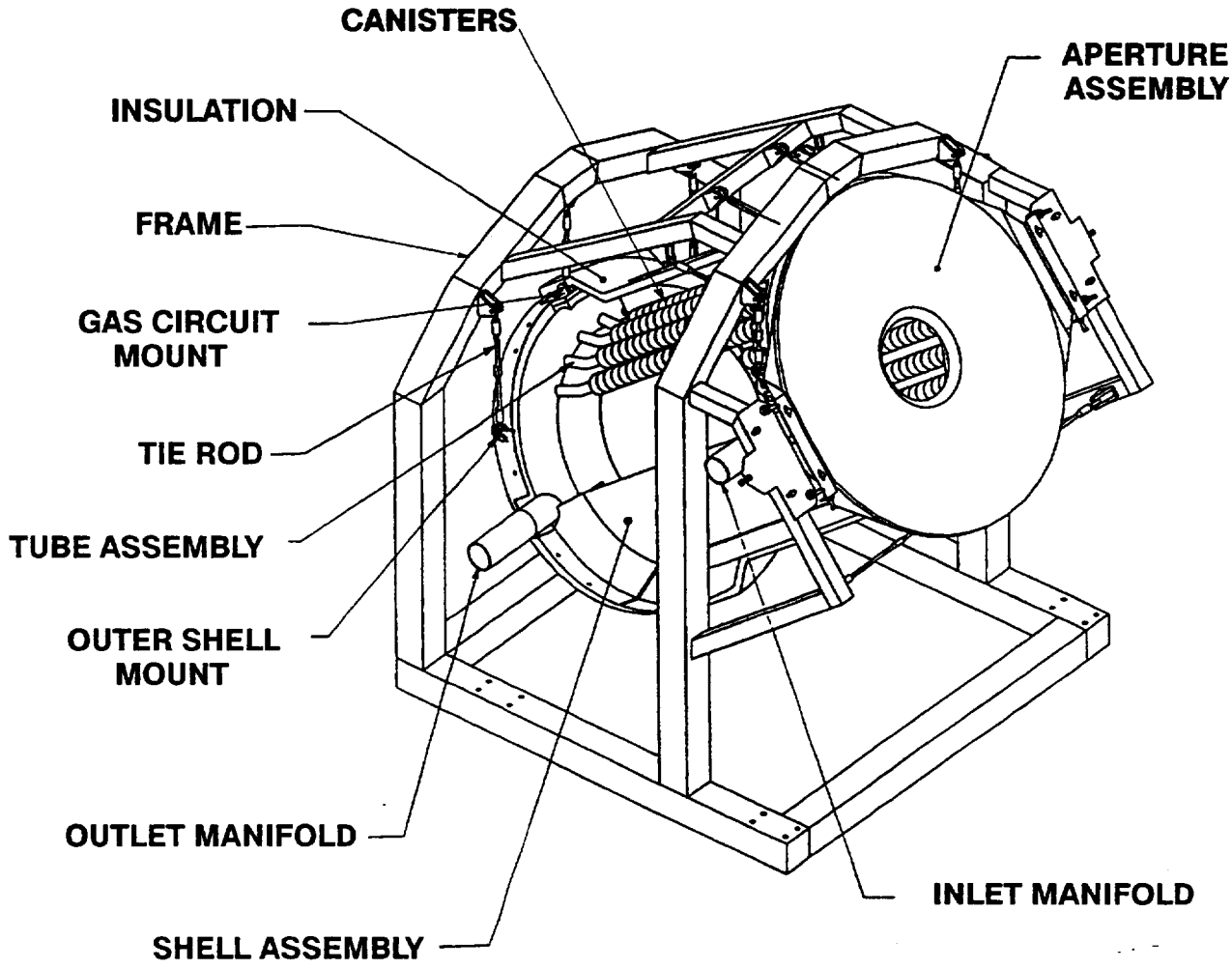

Table 6-1. Receiver Design Summary

Tube and containment material	Haynes 188
Pcm material	Lif-CaF_2 Eutectic (M.P. = 1413 °F)
Active tube length, Ft	2.0
Number of tubes	23
Number of containment canisters	24 Per Tube
Fluid tube OD, in.	0.875
Tube wall thickness, in.	0.035
Containment canister inner wall thickness, in.	0.032
Containment canister outer wall thickness, in.	0.060
Containment canister sidewall thickness, in.	0.060
Containment canister OD, in.	1.780
Containment canister length, in.	1.00
Tube spacing, center-to-center, in.	2.60
Receiver outside diameter, ft	2.06
Receiver outside length, ft	3.22
Aperture diameter, in.	7.0
Aperture offset from centerline, in.	1.5
Receiver weight, lb	440
Frame weight, lb	230

The system testing at NASA-Lewis revealed two items that needed correction. The first was contaminant canister outgassing from Nextel thread used as canister spacers. Nextel thread with a rayon filament was provided by the supplier instead of pure Nextel as requested. The second item was a measured pressure drop considerably higher than predicted. This was due to idealized modeling of the flow passages and has been corrected.

Measured cycle fluid and containment canister temperatures were compared to predictions from the receiver performance computer code SOLREC-TSD. The comparison seems to be quite good.

6.2 DESIGN CHANGES AFTER CDR

Several adjustments to the design were made as fabrication and assembly of the receiver progressed. In every instance the drawings were updated and the changes became part of the as-built drawing package delivered to NASA at the completion of the project. The first change was necessitated by the need to apply an emissivity coating to the canister surfaces. The detonation process used to apply the coating damaged the ceramic felt spacers between the canisters. The wafers were replaced with a Nextel ceramic thread wrapped between the canisters and tied off after twelve wraps. The second revision to the gas loop occurred at the tube-to-manifold joint. The complex ported joint configuration at the inlet manifold was found to be unnecessary and was replaced with a simpler butt joint.

The aperture shield support plate was noted to be less rigid than desired. It was replaced with a heavier 0.25 inch thick plate. The added weight of the plate required strengthening of the support brackets which were stiffened by adding doublers. The aperture shield was further revised by reproportioning the graphite sections on the face. Reproportioning resulted in sections which were closer to being the same size. Attachment of the sections was changed from two bolts per section to one bolt per section. Bolts were changed from carbon-carbon material to corrosion resistant stainless (CRES).

As a final revision the instrumentation panel was changed to a subassembly which could be wired and fabricated without the need to have it attached to the frame. The change allowed parallel assembly of the two components and moved the wiring operation from the shop floor to the laboratory bench where it could be more easily controlled.

6.3 Fabrication Summary

The receiver is made up of four subassemblies identified in Figure 6-6. The gas loop subassembly consists of toroidial manifolds, gas transport tubes, and salt containment canisters. Exterior to the gas loop is the outer shell subassembly, consisting of a thin metal shell covered on the outside with multilayer insulation and on the inside with a refractory shielding. At the aperture opening to the receiver is the heat shield subassembly, consisting of a graphite heat shield with its support and adjustment hardware. These three subassemblies are independently fastened to the support frame subassembly.

6.3.1 Gas Loop Subassembly

Canisters--Canisters are required to be of uniform wall thickness with a precision machined inside diameter for fit-up to the gas transport tubes of the receiver. Canisters are made of Haynes 188 alloy, and formed by a multiple-step deep drawing process.

The starting material was a flat circular disk. The center of the disk was formed upward to create the inside wall of the canister, and the outer edge was formed upward to create the outer wall. Thinning was a problem at the inner wall, since not enough metal was available at the center of the disk to raise the wall. The solution called for moving metal from the outer portions of the disk toward the center. Annealing and subsequent forming operations resulted in wall thinning of no more than 20 percent. This was sufficient for machining to the required wall thickness.

After forming, the canisters were selectively trimmed to size to produce the two canister sections (see Figure 6-7). The sections differed because it was necessary to position the weld joints for access and inspection.

The canister sections were joined by electron beam welding on an automated turntable. Weld joints were radiographically inspected using computer-enhanced real-time X-ray techniques. The resultant X-rays, on video tape, have excellent resolution and display defects as small as 0.005 in. in the canister walls.

Figure 6-6. Receiver Subassemblies

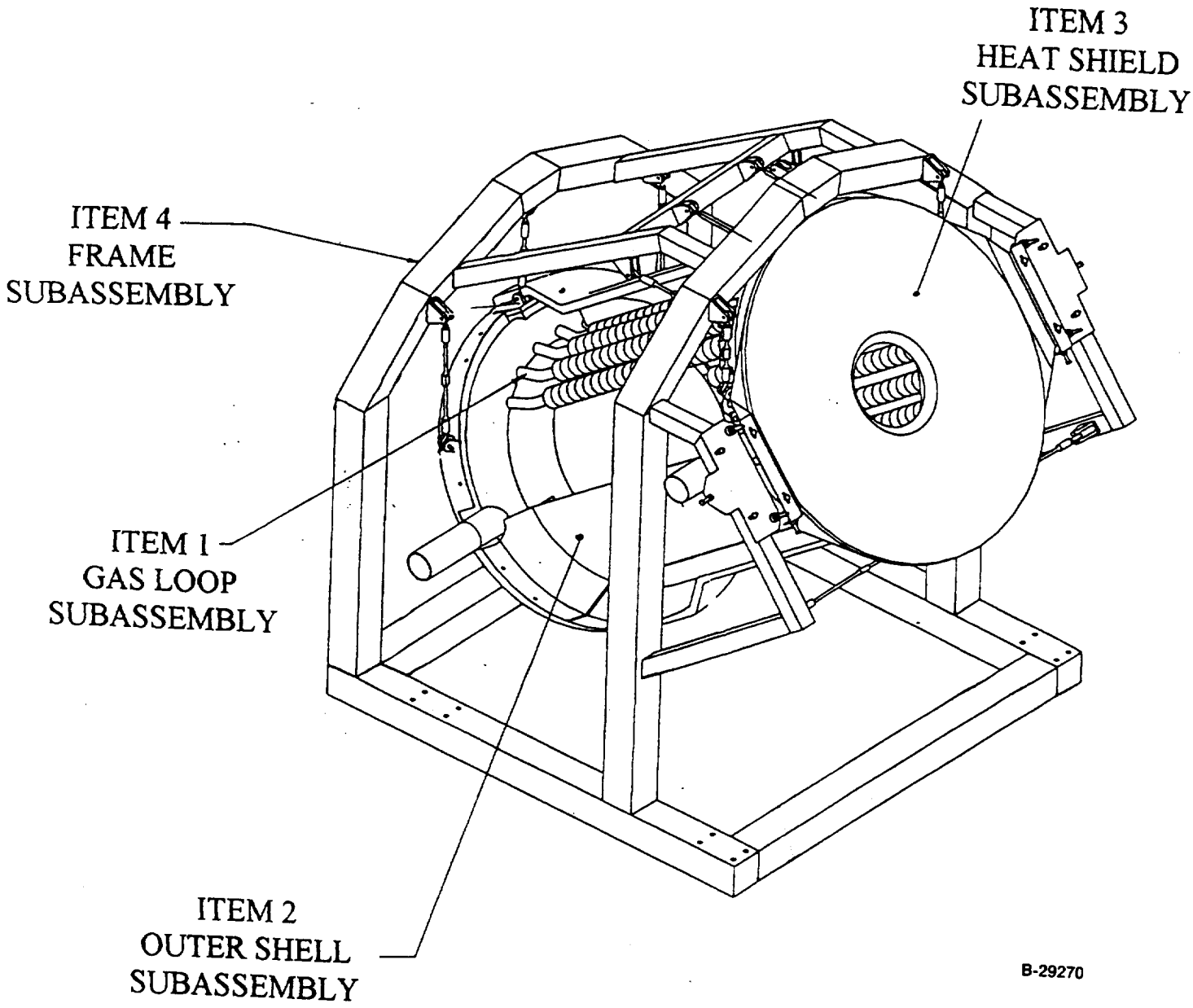

Figure 6-7. Canister Forming Sequence

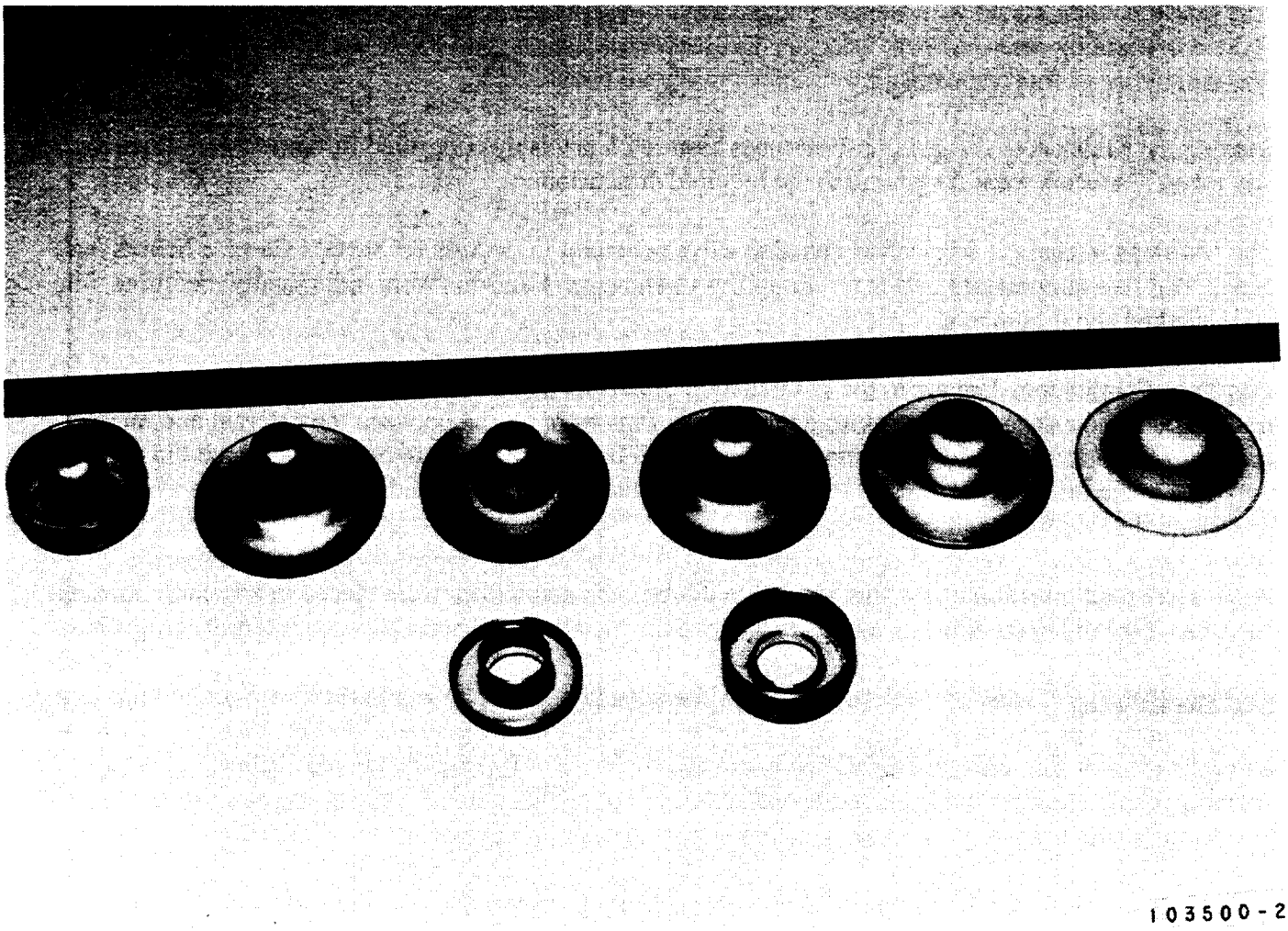

103500-2

A small-diameter access hole was provided in the side wall of the canister for salt fill. Salt in a coarse powder form was funneled into the canister to a specified weight. The powder was too bulky to allow the full charge to be placed in one operation, thus requiring a final fill after the first had been compacted by melting. The second fill to full charge weight and a subsequent second melt yielded the full canister. An inert cover gas was introduced into the furnace after the melt operation to prevent moisture contamination of the purified salt.

The canisters were sealed with a small plug of Haynes 188 material closing off the hole. The plug was welded in place by electron beam welding. Subsequent to welding, all joints were examined by X-ray for soundness. A finished canister was shown in Figure 6-3.

Brazing the canisters to the gas transport tubes required a precisely controlled fit-up between canisters and tubes. Canisters were ID ground to the required dimension.

The last steps in canister fabrication included a dye penetrant inspection for surface flaws, a helium leak check, and five temperature cycles for durability verification. Canisters were individually identified with laser marked serial numbers.

Gas Tube Fabrication--Unique to the gas transport tube is its internal structure, which includes heat transfer fins and a second (concentric) internal tube. Fins were placed between the external and internal tubes as shown in Figure 6-2. Insertion was simplified by the use of a thin braze foil, which did triple duty as a braze foil, lubricating surface, and insertion aid. The foil provided a sliding surface which prevented the fins from galling.

After successful insertion of the fins and internal tubes, the assemblies were placed in a vacuum brazing furnace where the braze foil was melted to achieve the metallurgical bond between internal components.

Canister Brazing--Canisters were positioned on the outside of the completed tubes. A circular wire ring of braze alloy was placed adjacent to each canister. Canisters were separated by thin spacers of amorphous silica refractory material. The entire assembly was subjected to a braze cycle to metallurgically bond the canisters to the outside of the tube. This braze cycle was run at a lower temperature than the previous braze cycle to prevent a remelt of the internal fin braze alloy.

Emissivity Coating--A coating was applied to provide a high thermal emissivity surface on the canisters. The refractory spacers between canisters are torn away by this process. The replacements consisted of strands of refractory fiber wound into the spaces between canisters and knotted for retention.

Tube-to-Manifold Attachment--The manifolds, formed in a hydraulic press and laser trimmed to receive the gas transport tubes, were mounted in a horizontal carousel tool. The carousel had 23 indexed positions, one for each tube in the assembly. Tubes were manually welded to the manifolds using Haynes 188 filler rod. Welds were sequenced to minimize heat distortion. Two tubes spaced at 180 degrees to each other were welded first. The second pair of tubes was spaced at 90 degrees to the first, and so forth. Each weld was allowed to cool before the next was executed. Extensive X-ray evaluation

was performed on all gas loop joints. A verification test was conducted on the entire assembly to ensure that flow pressure drop was within specification. This was followed by a helium leak check to confirm that the gas loop was free of detrimental leakage. Figure 6-8 shows some tubes welded to the manifolds.

6.3.2 Outer Shell Subassembly

Details of the shell subassembly are shown in Figure 6-9. The curved panels were formed from Haynes 188 sheet material. Eight panels make up the cylindrical portion of the shell assembly. An internal liner made of woven refractory material (not shown in Figure 6-9) is attached to the concave surface of each panel. Attachment is with Nichrome wire threaded through predrilled holes in the panels. The panels are subsequently bolted to the circular end caps shown. The end caps are of Haynes 188 flat sheet material welded to formed flanges. A cone section is welded to one end cap to make the entry aperture of the receiver. After the bolted components have been assembled to construct the full shell, insulation is layered over the outside to complete the subassembly. Each layer of the multilayered stack-up is form fit to the contours of the previous layer and contours of the shell.

6.3.3 Heat Shield Subassembly

Figure 6-10 shows components of the heat shield subassembly. The purpose of the subassembly is to support a graphite heat shield at the aperture of the receiver. The primary structural member is the heavy cross section plate made of A286 alloy. To reduce weight, a substantial amount of the plate was removed by laser cutting, leaving the structural webbing shown in Figure 6-10. The graphite shield is machined in eight pieces. All eight are indexed to adjacent pieces, and all have stair-step edges for overlap at the join lines. A single bolt centrally located on each graphite segment fastens the segment to the backplate. All other components serve to attach the backplate and shield to the support frame. The brackets shown are made from flat sheet metal bent to the desired shapes. The brackets are reinforced with doublers in critical areas.

6.3.4 Frame Subassembly

The support frame subassembly shown in Figure 6-6 is a welded structure made of stainless steel. The structure is built to the same standards as a precision tool, since it is the interface datum for all positioning and alignment measurements during assembly and installation. The frame is supplied with multiple mounting clevises, half of which suspend the gas loop. The remainder support the shell subassembly. Suspension rods that support the gas loop are machined from Haynes 188 and are cut with left- and right-hand threads for adjustment in turnbuckle fashion.

6.3.5 Final Assembly

Final assembly of the receiver starts with installation of the gas loop subassembly, which is suspended from the frame. Optical and mechanical measuring equipment is used to align the gas loop with the frame data. The turnbuckle suspension arrangement allows for fine adjustment of position. The outer shell is assembled around the gas loop, starting with the end caps, which are suspended from adjustable

Figure 6-8. Welding in Process - Tubes to Manifolds

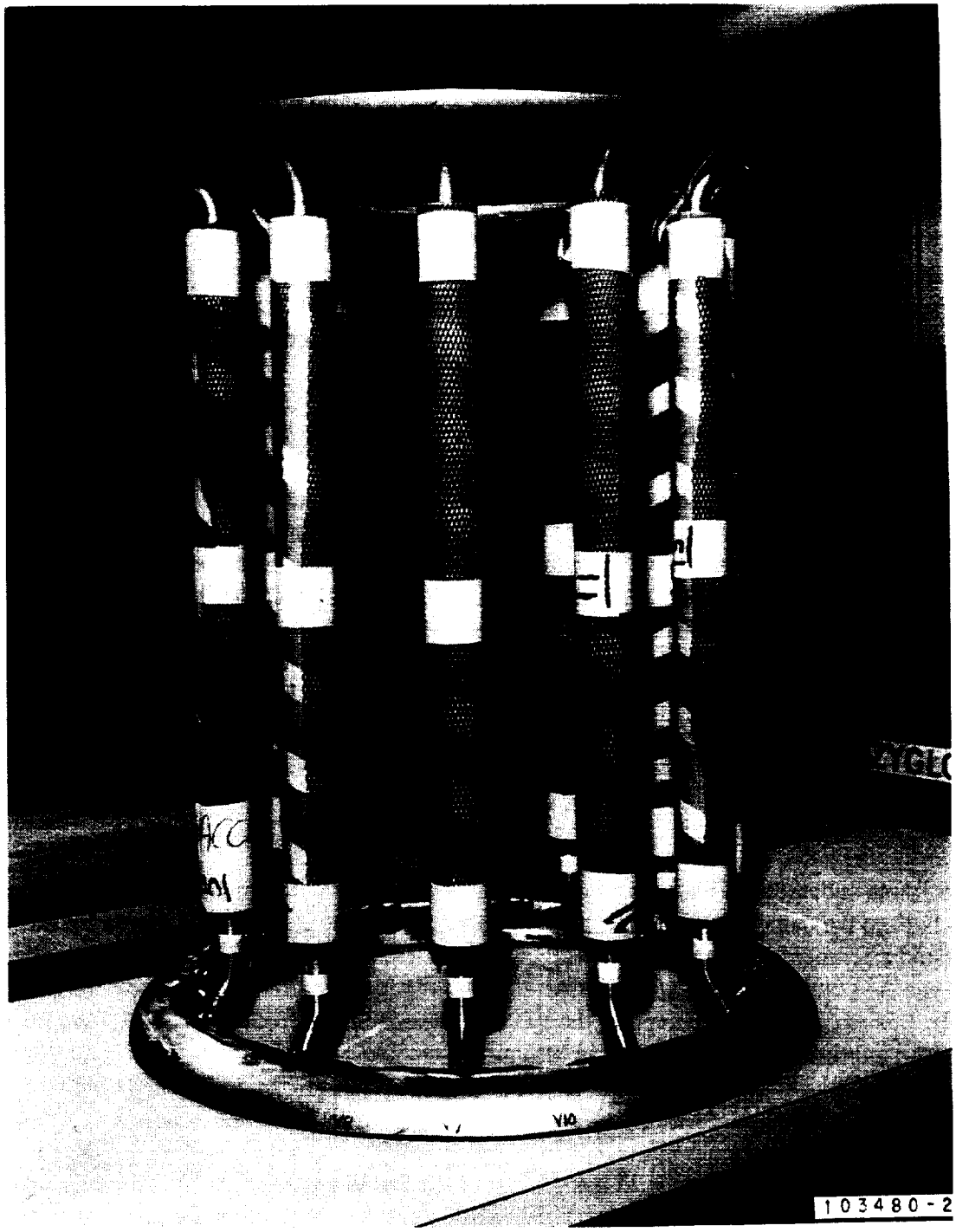

Figure 6-9. Receiver Shell Details

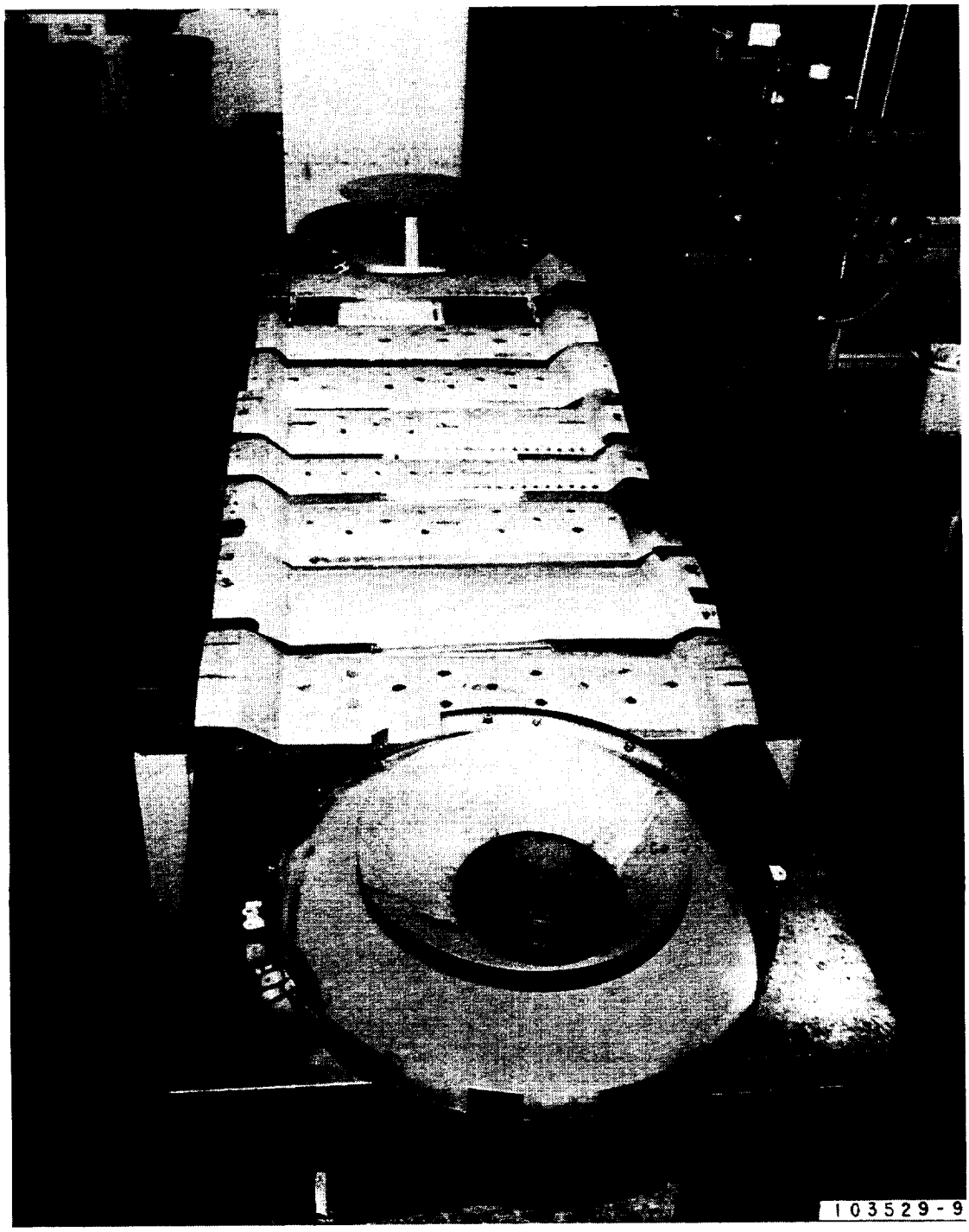

Figure 6-10. Heat Shield Details

rods. Side panels are attached, and the shell subassembly is aligned with the datums to provide a 1.0-in. clearance between the shell and tubes of the gas loop. The multilayer insulation is then installed. Each of the insulation layers is made of several individual panels butted at seam joints. Metal foil layers are, likewise, multipaneled and overlapped. Foil panels are welded at the overlaps for retention.

The most critical positioning involves the heat shield, which is bolted to the frame at the aperture of the receiver. A laser-marked target disk with crosshairs is inserted into the shield opening to enable optical targeting. Shield position is controlled with various adjustment features in the mount hardware which vary elevation and translation.

6.4 Component Testing

6.4.1 Single Tube

To verify the integrity of the receiver tube and attached canisters, a full-size tube was fabricated and tested. Thermal performance verification was conducted on a different tube on the Space Station *Freedom* program.

To test the tube, a solar simulator test rig was assembled. The rig comprises a vacuum vessel for the test section; a heated air supply; solar simulator heaters; temperature, pressure, and flow measurement; and control and recording capability. The test rig provides hot air to the test section inlet. The solar simulator heater panel is cycled on and off to simulate the sunlight/eclipse pattern. Air is used as the working fluid to minimize test cost.

The fully instrumented tube is shown in Figure 6-11. The tube is enclosed in an Inconel 625 shell, which also houses the electrical heaters. The shell is covered with multilayer insulation. The insulated shell is enclosed and supported within a stainless steel vacuum tank. The tank has removable elliptical ends through which the test specimen and instrumentation can be accessed. The test rig is mounted on a test pallet with an adjustable pivot (see Figure 6-12). The 37-deg angle corresponds to the installation angle of the receiver in the GTD vacuum tank.

The tube was successfully run for around 1500 hr (approximately 1000 cycles). Each cycle caused the canisters to go through a freeze and thaw condition. The test was run with the heater both above and below the tube. This corresponds to the extreme melt orientations in the operating receiver.

Typical thermocouple traces for a single simulated orbit are shown in Figure 6-13. The heater is on for the first 66 min of the 95-min cycle. These cycles were reproducible throughout the test. The PCM melting temperature is 1413 °F.

After the test period, the tube was visually examined. The external appearance was very similar to the pretest appearance.

Figure 6-11. Single Tube Test Unit

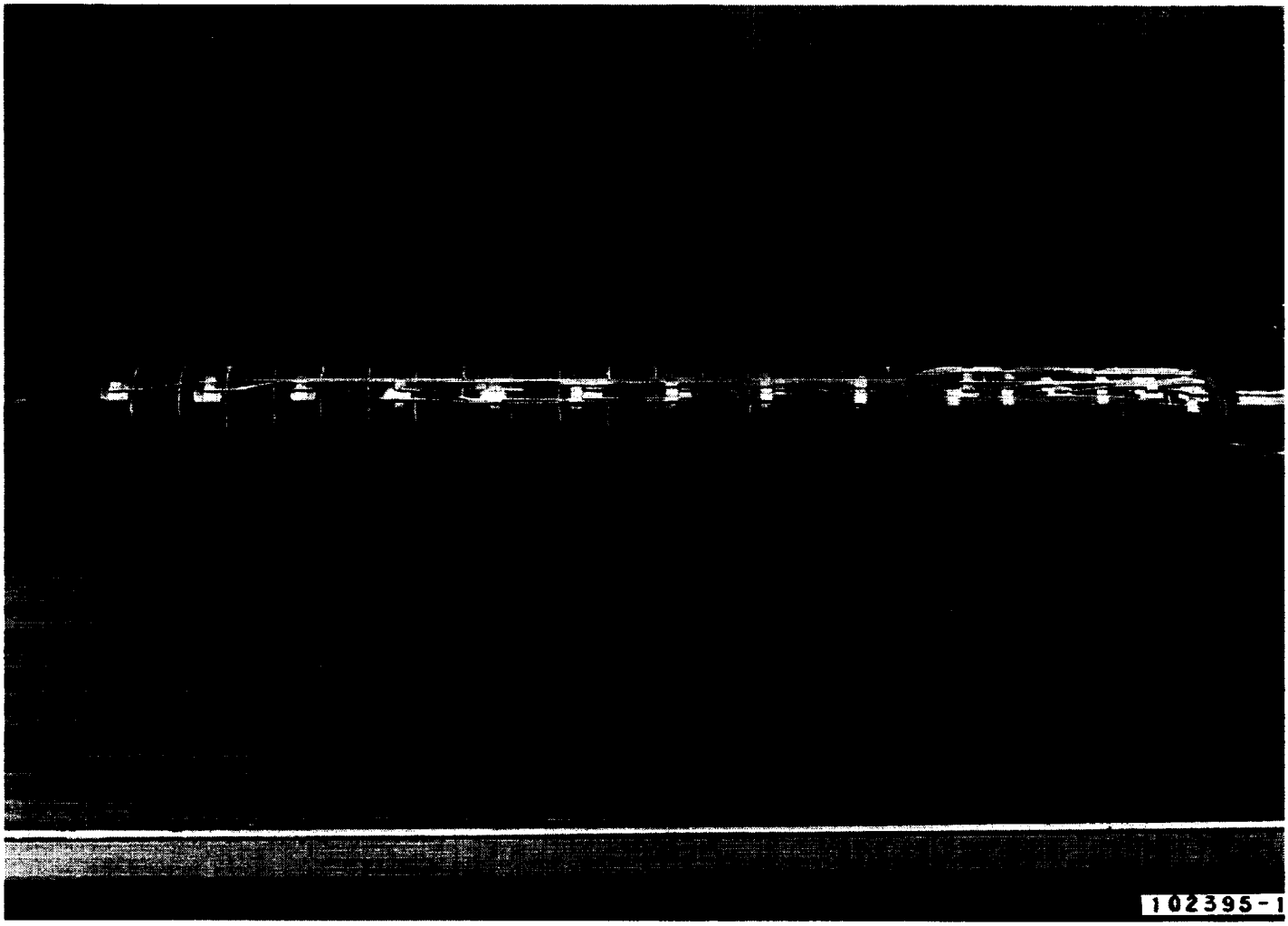

Figure 6-12. Single Tube Test Configuration

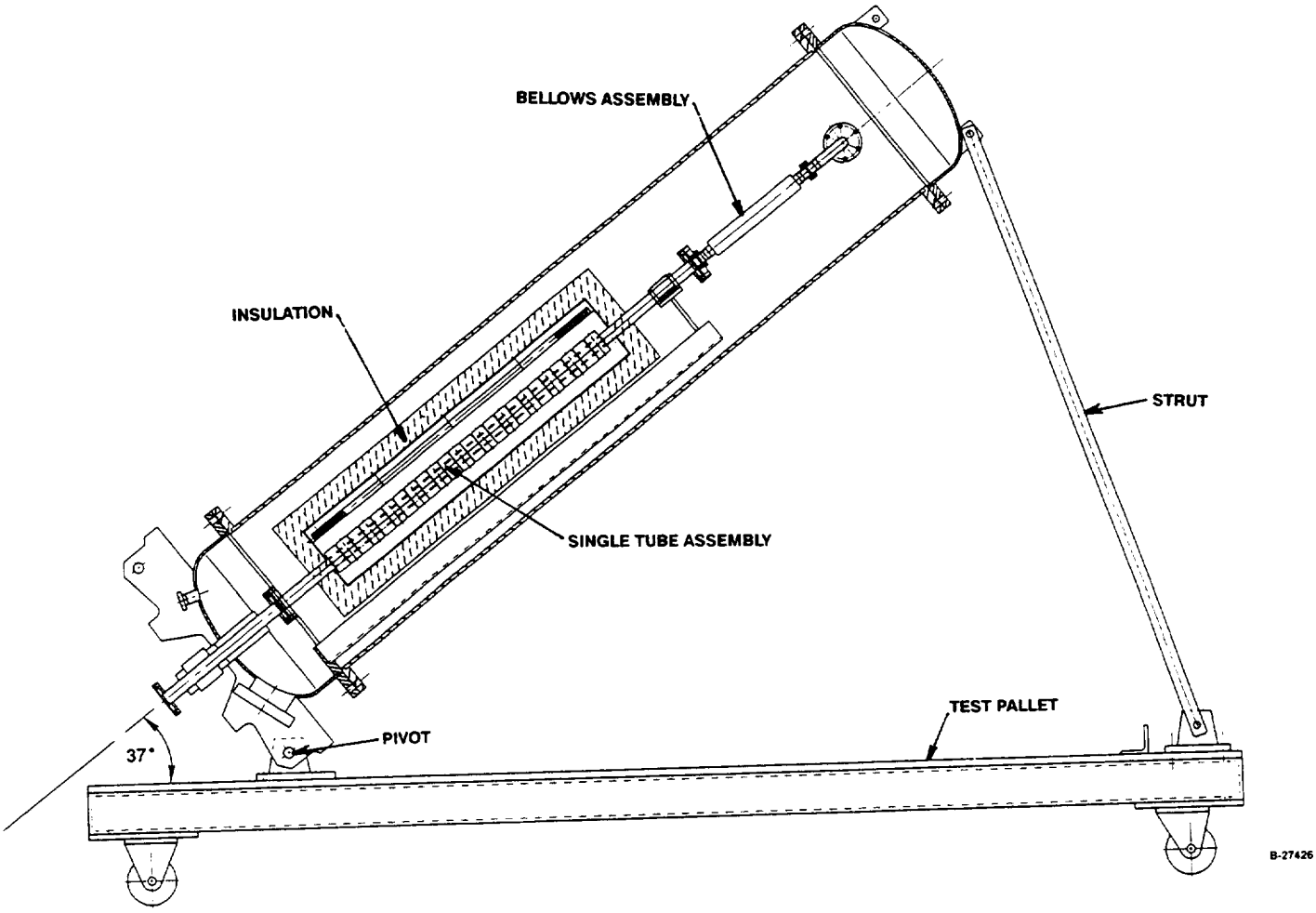

Figure 6-13. Single Tube Test Results

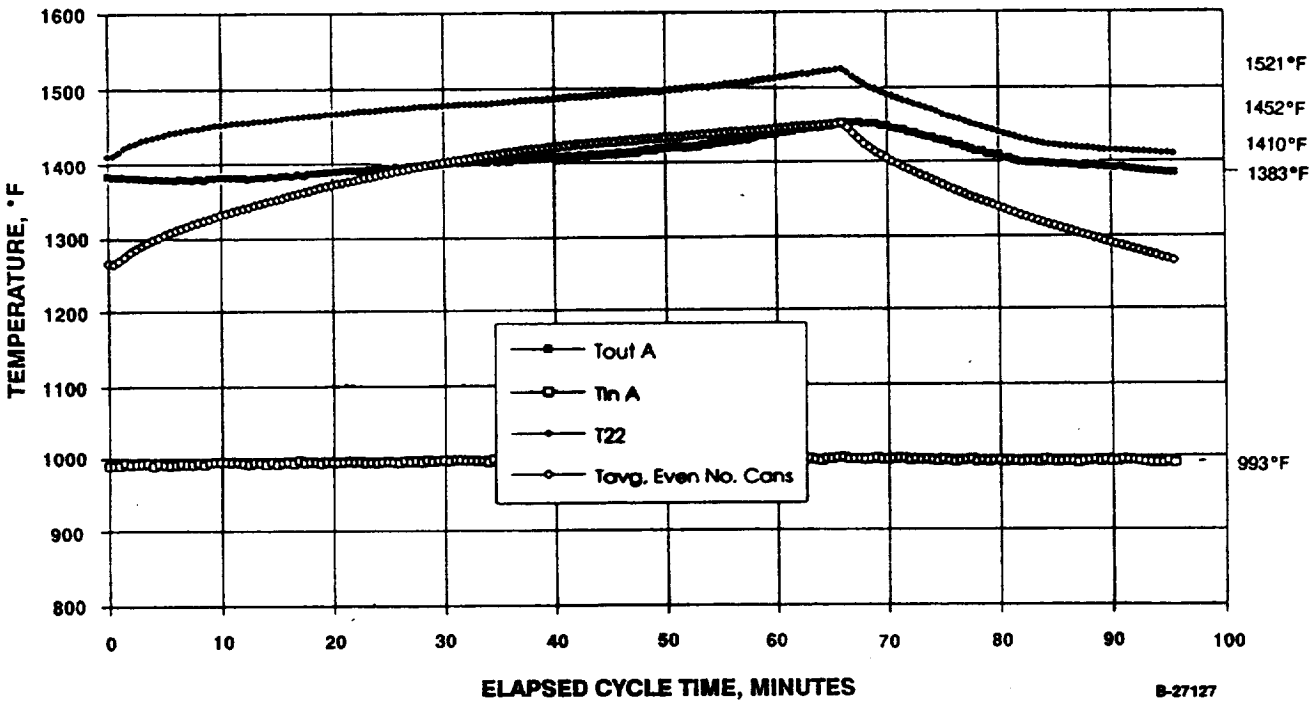

6.4.2 Acceptance Test (Pressure Drop)

The acceptance test of the solar receiver was conducted without incident. The Data from the test revealed that the pressure drop of the gas circuit was higher than predicted. The implication of this are discussed in paragraph 6.5.1. At the specified flow of 4.8-5.0 lb/min, the actual static-to-static pressure drop measured and corrected for inlet and outlet flange losses was 1.03-1.30 psid versus the predicted 0.51 psid as defined by the Acceptance Test Procedure 94-66786.

6.4.3 Systems Test (Tank 6)

Data taken for receiver fluid and canister temperatures were compared to predictions from the receiver performance prediction computer code, SOLREC-TSD. The incident flux distribution was generated by Harris Corporation based on flux rake data for the receiver cavity cylindrical walls and calculations for the receiver back wall. For the cylindrical walls, Harris flux file 2132.CL was used. The unadjusted file showed 8.12 kW deposited on the cylindrical surface. The back wall data were from Harris file DDR05.BWD. The data in this file were multiplied by 0.969 and divided by 1.194. After this correction, the back wall deposited power was 1.66 kW. This resulted in a total incident power into the receiver aperture of 8.12 + 1.66 = 9.78 kW.

The data used for comparison were extracted from the simulated orbital run on 2/17/95 from AES-Tempe file 02-17-95.XLS. The third (and last) orbit was selected. Figure 6-14 shows the measured receiver outlet temperature for the last three orbits of the run. It can be seen that orbital steady state has not yet been attained, as the outlet temperature at the end of eclipse has not entirely stabilized.

The inputs to SOLREC-TSD were the time varying receiver inlet temperatures and pressures. The flow rate was assumed to be essentially constant at 0.349 lb/sec. This value was derived from the calculated flow rates given on page 18 of AES-Tempe Report 41-13692, April 21, 1995. The incident flux data were scaled to yield a total input power of 10.5 kW, as determined in Report 41-13692, page 17.

The predicted receiver gas outlet temperatures from SOLREC-TSD are compared to the measured temperatures in Figure 6-15. Comparison of SDGTD 2-17-95 Test with Predicted Receiver Gas Outlet Temperatures for 10.5 kW Input Power. The comparison is quite good, with some divergence prior to and just after sunrise. The divergence may be due to a number of reasons. First, as shown in Figure 6-14, steady state was not attained in the text with temperatures continuing to drop. Thus, the measured data in Figure 6-15 and higher than the steady state temperatures would be. Second, the assumed input power of 10.5 kW may be low. NASA-Lewis has estimated a considerably higher input power. See paragraphs 2.3.4 and 2.4.3.5 of this report. A SOLREC-TSD run was made with the incident flux data scaled to 11.0 kW. These results show less divergence with the measured data, as indicated in Figure 6-16.

Figure 6-14. SDGTD 2-17-95 Test Receiver Gas Outlet Temperature (3 Orbits)

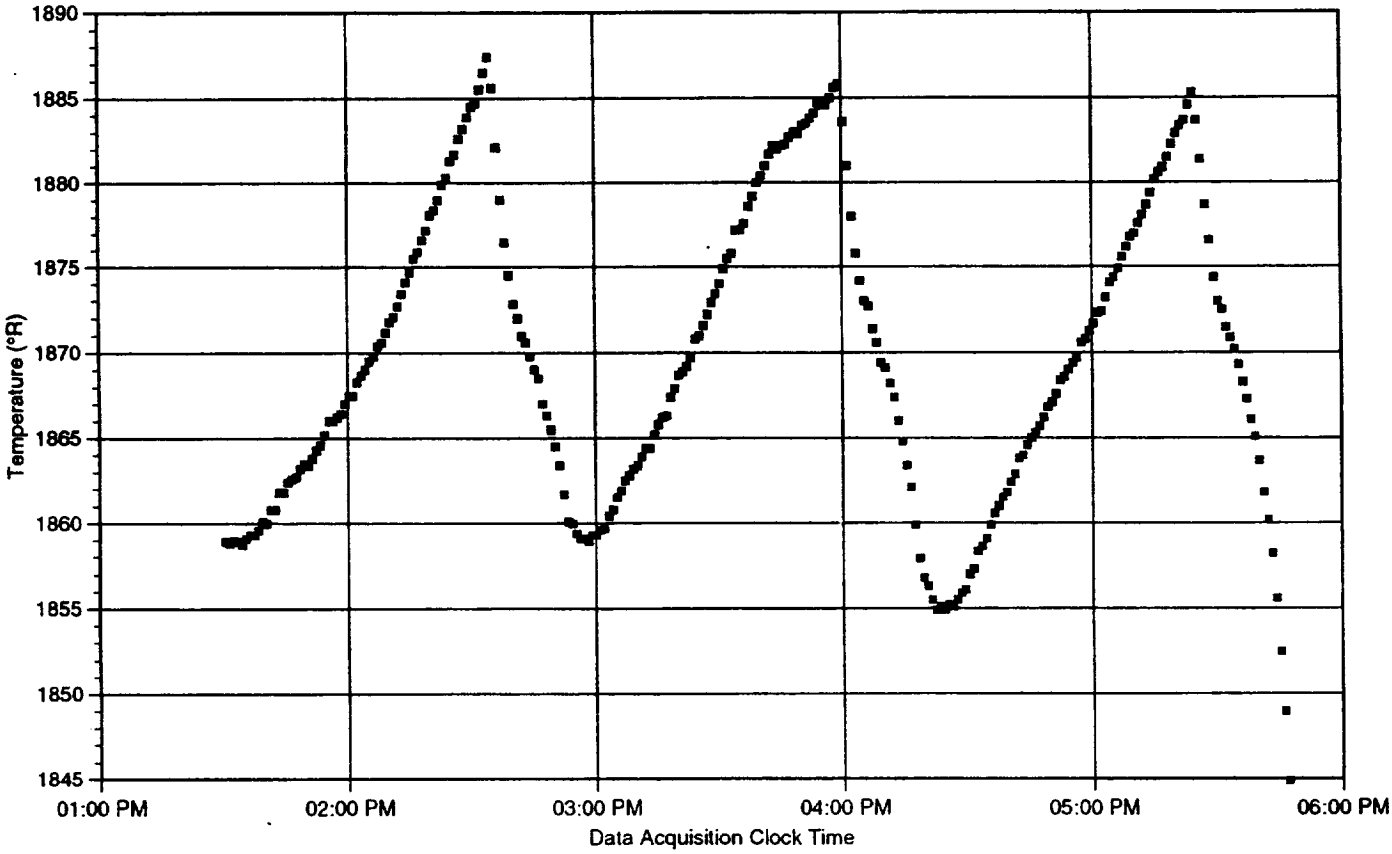

Figure 6-15. Comparison of SDGTD 2-17-95 Test with Predicted Receiver Gas Outlet Temperatures for 10.5 kW Input Power

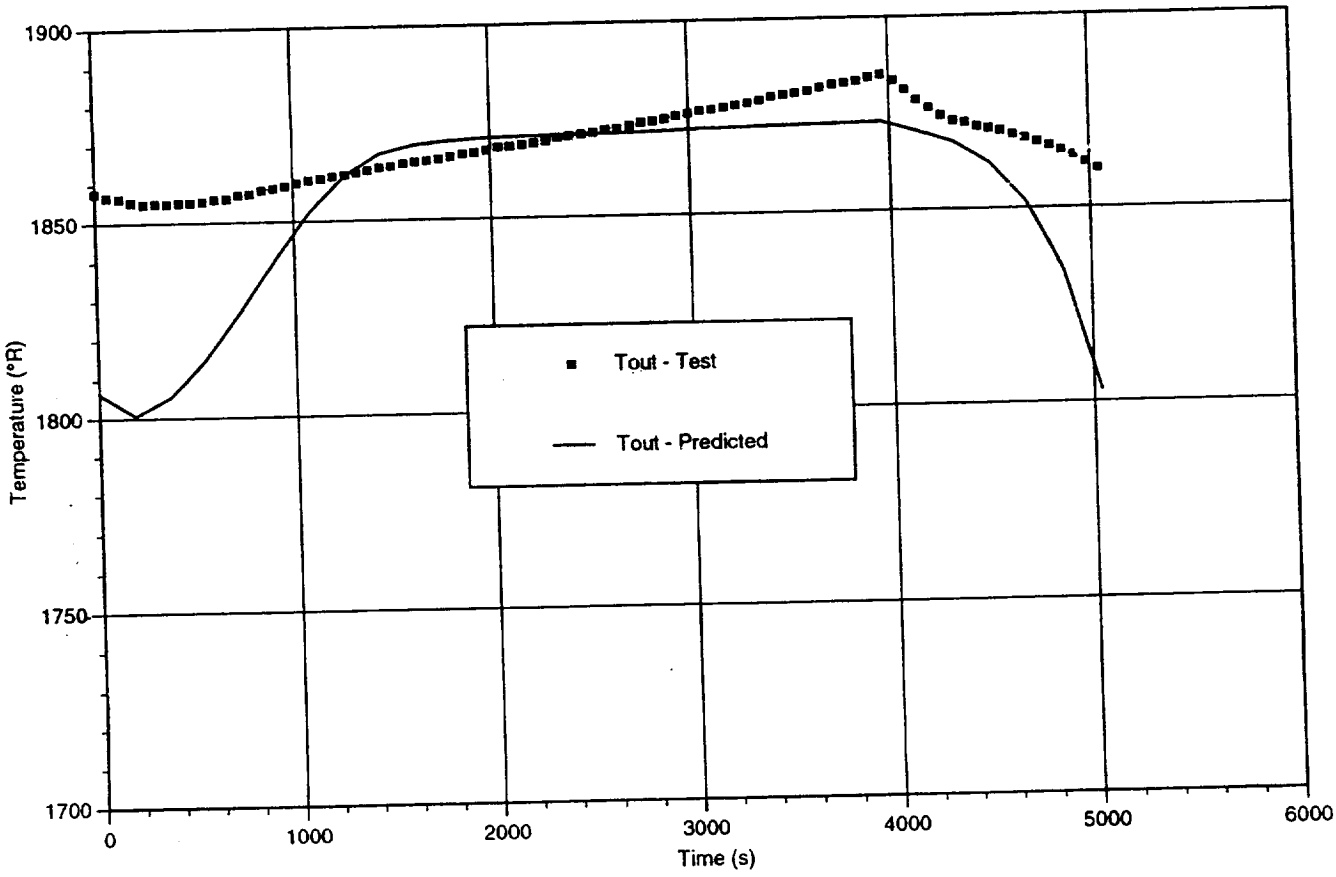

Figure 6-16. Comparison of SDGTD 2-17-95 Test with Predicted Receiver Gas Outlet Temperatures for 11.0 kW Input Power

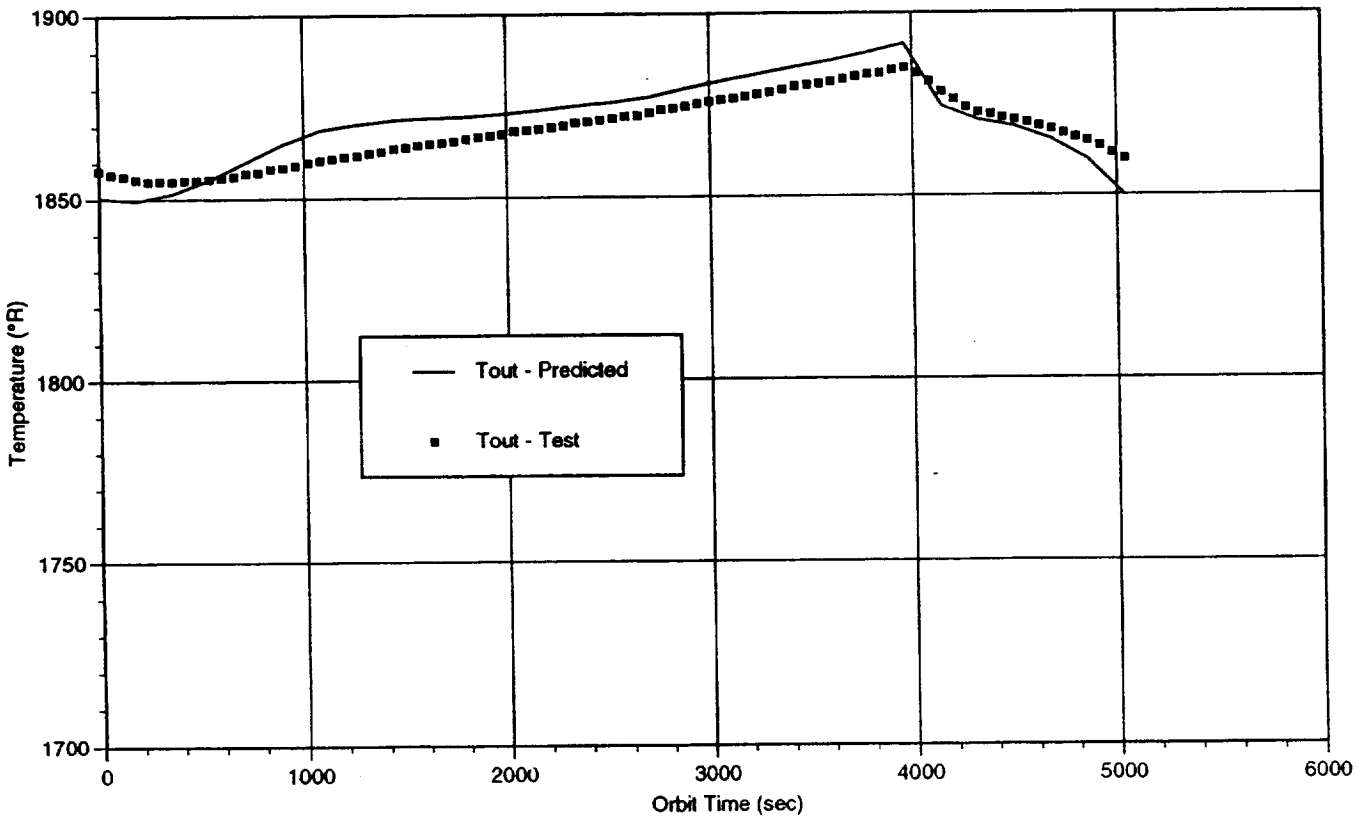

A third potential reason is the contribution of the outlet manifold. The predicted temperatures from SOLREC-TSD represent the mixed-mean temperature at the outlet of the receiver tubes. The measured temperatures are taken downstream of the outlet manifold. The thermal capacitance of the outlet manifold offers additional heat transfer to the gas. To try to quantify this effect, the outlet temperatures from SOLREC-TSD (10.5 kW power) were input to an outlet manifold thermal model (see Figure 6-17). The model was run for a number of orbits until orbital steady state was attained. The results, presented in Figure 6-18, indicate a reduction in the divergence. The total energy into the gas does not change with inclusion of the manifold in the model. Also shown is the average predicted manifold solid temperature. As can be seen, depending on the time, the gas can be either heated or cooled by the manifold.

The manifold model does not include radiation heat transfer to the manifold from the receiver back wall. Inclusion of the radiation might further reduce the divergence, but would not change the total energy into the gas.

Receiver actual pressure drop is compared to revised predictions (see paragraph 6.5.1) in Figure 6-19. The comparison is very good.

Comparisons were made between predicted and measured receiver canister temperature. All predictions were for the 10.5 kW input power case. Twenty canisters were instrumented. Each canister had two thermocouples--one facing the centerline of the cavity and the other 180 degrees away facing the canister wall. Data from the inward facing thermocouples proved to be unreliable, recording significant radiation effects due to insufficient shielding of the thermocouple beads. This is indicated in Figure 6-20, which shows the inward and outward facing temperature readings for a typical canister. As soon as the solar simulator is turned off, removing the radiative heat source, the apparent inward facing temperature readings drop rapidly and approach the outward facing temperature readings. As such, comparisons with predicted temperature are based on the outward facing thermocouple only.

The comparisons are shown in Appendix 2. SOLREC-TSD produces one temperature per canister. The canister nomenclature shows tube number and canister number. The canister numbering starts from the inlet end. Also shown is the thermocouple instrumentation number. The comparisons can be seen to be quite good, with similar trends and temperature levels between predicted and measured data in all canisters.

The predicted canister temperatures are independent of whether the outlet manifold is included in the model. The general trend of the predicted temperatures being lower than the measured temperatures could be due to not reaching steady state in the test or using too low an input power for the predictions. The input power used in the prediction was that power which was calculated by the Brayton Cycle performance model. As discussed in paragraphs 2.4.3.4 and 2.4.3.5, a variation in predicted optical energy exists based on several different methods used to estimate it.

Figure 6-17. Outlet Manifold Thermal Model

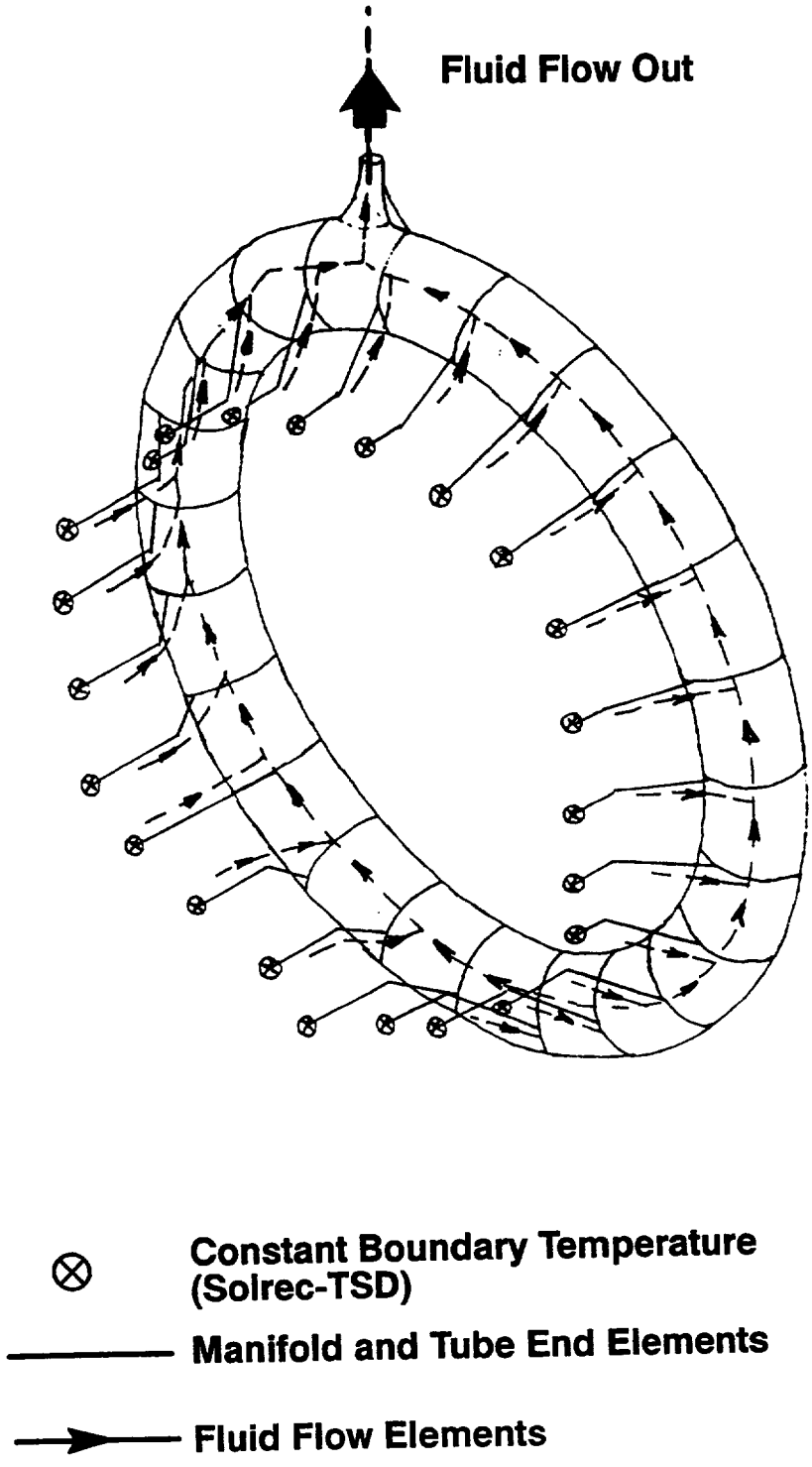

Figure 6-18. Effects of Outlet Manifold on Receiver Gas Outlet Temperatures

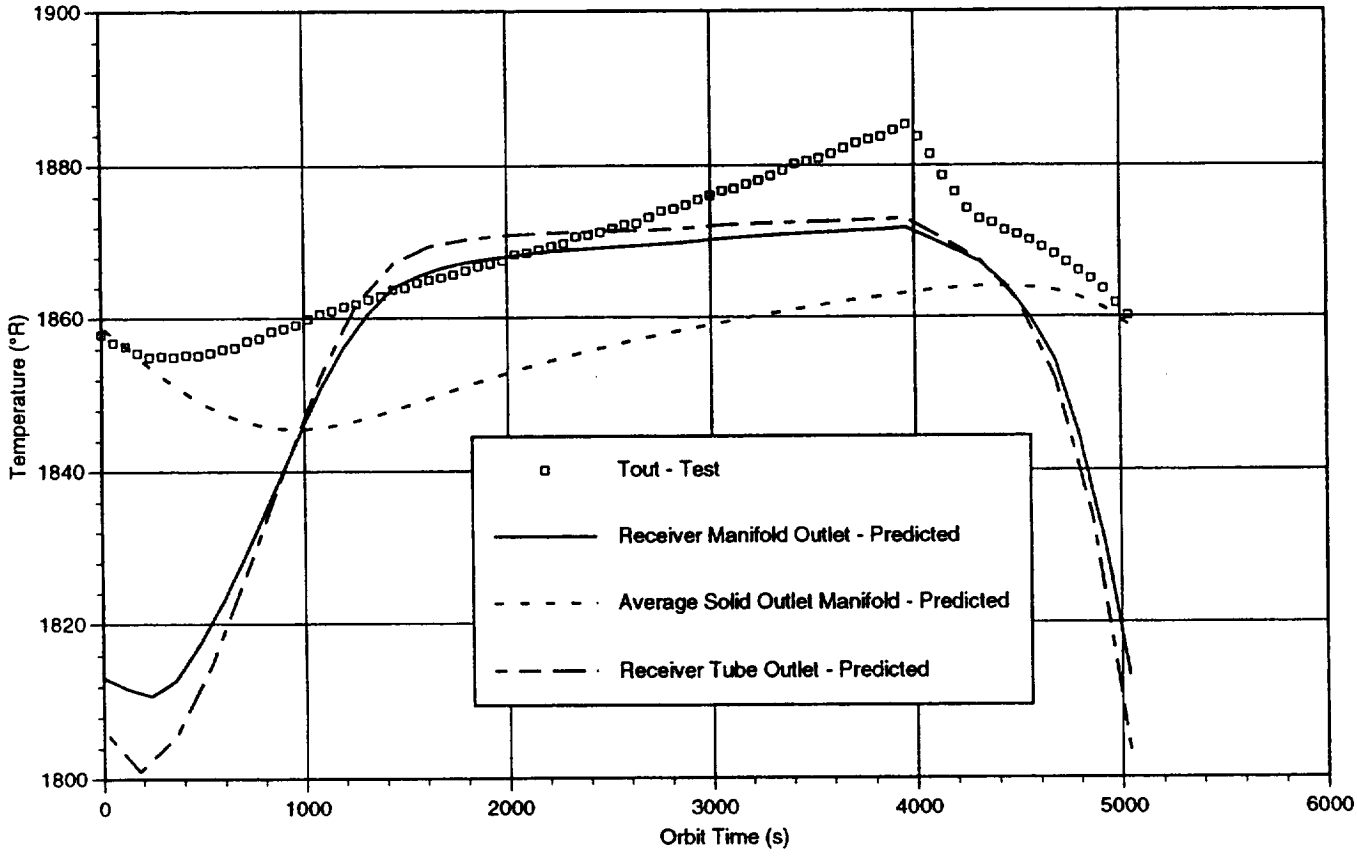

Figure 6-19. Comparison of SDGTD 2-17-95 Test with Predicted Receiver Gas Pressure Drop

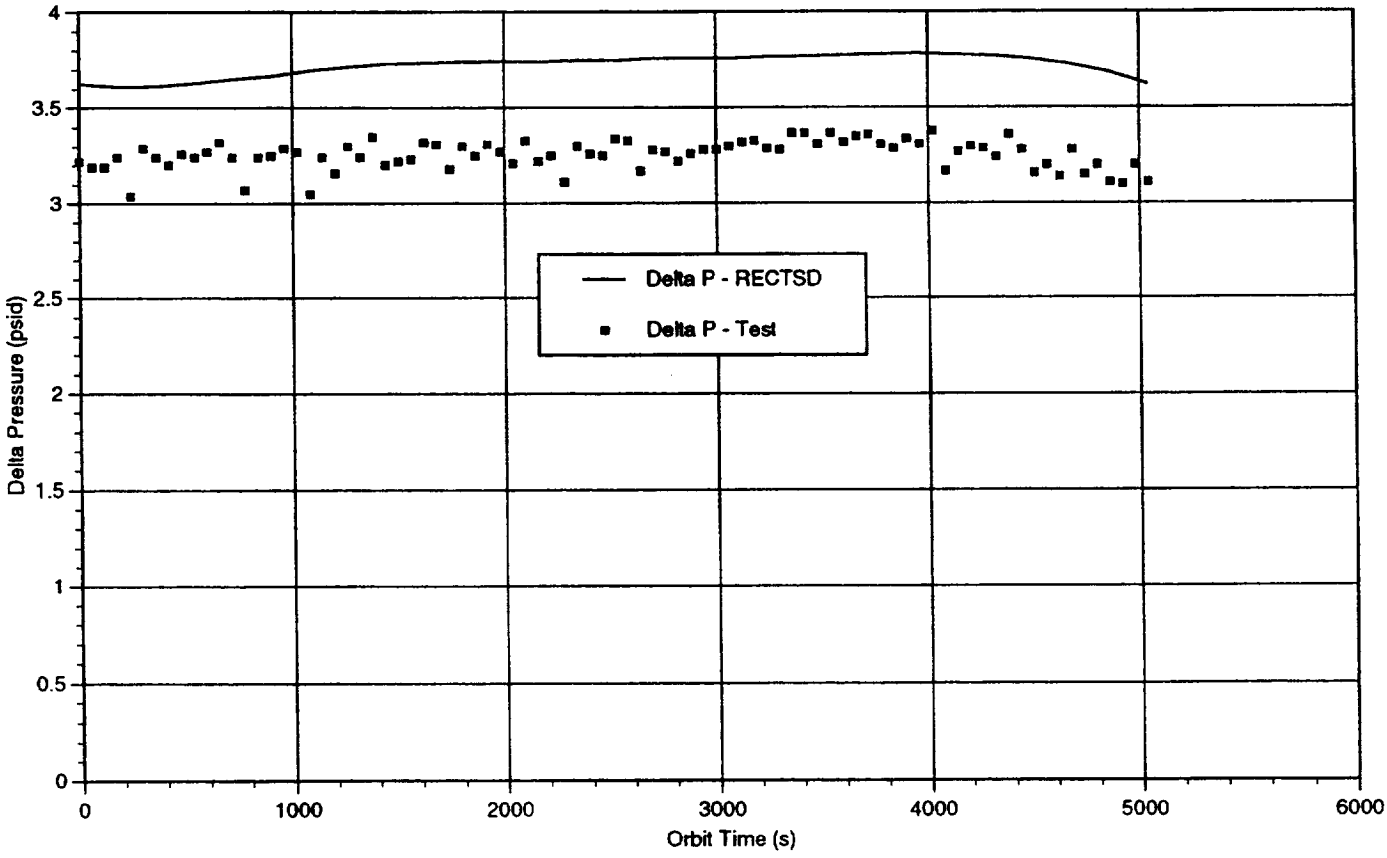

Figure 6-20. Receiver Measured Canister Temperatures - SDGTD 2-17-95 Test (Canister 4 on Tube 7, 3rd Test Orbit)

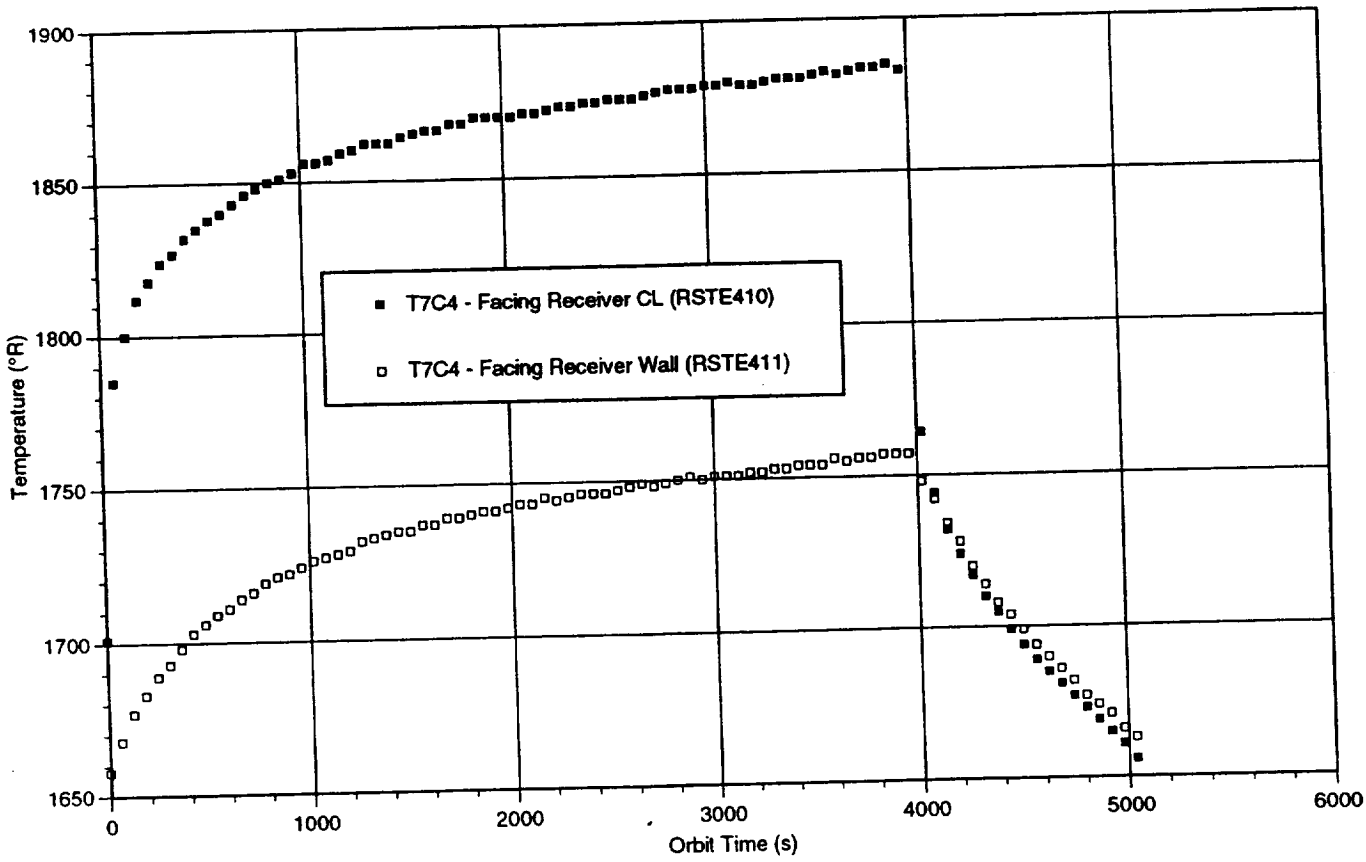

6.5 Lessons Learned

6.5.1 Receiver Pressure Drop

The system test in Tank 6 resulted in a receiver pressure drop considerably greater than initially predicted (approximately a factor of two). A review of the Engineering records confirmed that the receiver pressure drop test had exceeded the ATP limits, as discussed in Section 6.4.2. The pressure drop measured in the single tube test (Section 6.4.1) was also higher than expected. As explanation, it can be said that the receiver was designed, fabricated, and tested as a Research category unit. This category allows Engineering the flexibility to pass judgment with respect to problems encountered during the development, and thus affords cost and schedule savings.

The effect of the increased pressure drop on system performance was not well appreciated. It had been assumed that a lower receiver performance, either high pressure drop or increased thermal losses, could be made up by allowing the gas temperature to rise. In addition, the delivery schedule requirement and the inability to correct the problem once identified, let Engineering to allow the receiver to ship to NASA LeRC.

The pressure drop discrepancy was found to be due to the idealized model of the flow passages in SOLREC-TSD. The code modeled an annular flow passage with continuous rectangular fins. The fabricated tubes have triangular-type fins (see Figure 6-2). In addition, the fins are discontinuous, with eight sections in the flow direction.

These differences result in two additive effects of similar magnitude. First, the triangular passages result in a considerably smaller hydraulic radius which lowers the Reynolds number and increases the friction factor. Second, the discontinuous fins prevent development of laminar flow, also increasing the apparent friction factor.

SOLREC-TSD has been upgraded to better reflect the as-fabricated geometry. The new code predictions were used in the present report.

For the flight demonstration receiver, the tube annulus geometry has been revised to increase the flow area and reduce the pressure drop, so as to limit the impact on engine performance.

6.5.2 Nextel Thread

Nextel thread, as previously discussed, was used as a filler between the canisters on the gas loop after the tissue quartz spacers had been damaged during application of the emissivity coating. The thread is the source of the outgassing which resulted in the need to interrupt the test to remove residue from the concentrator and the test facility.

The Nextel thread was initially purchased in small experimental quantity for trial purposes. The thread proved to be successful and was adopted for used on the receiver. A follow-on purchase order was issued for six spools to supply the necessary quantity to wrap the entire receiver. The thread was

purchased in the same manner as the previous experimental spool. At the time of purchase it was not known that two virtually identical Nextel fiber products existed which were, ultimately, differentiated only by their MSDS numbers. Nextel fibers designated with MSDS 10-4844-6 contain 1 to 3 percent volatiles. The Nextel fibers designated with MSDS 10-4848-7 contain 6 to 22 percent volatiles. The latter contains approximately 16 percent lubricant and strengtheners to allow processing with a sewing machine. The lubricant is believed to be the source of the outgassing which contaminated the test facility.

Future purchases of Nextel fibers will be accompanied by MSDS numbers and all fibers will be verified on a per-spool basis to preclude mix-up of product.

6.5.3 Canister Leak

During fabrication of the receiver, one containment canister developed a salt leak during a rebraze cycle of a tube assembly. The rebraze was required for other reasons (undercut braze fillets). Subsequent to the second braze, white contaminants were found around a canister. Chemical analysis determined that the contaminates were salt from the phase change material (lithium fluoride and calcium difluoride).

The salt leakage of this canister was caused by a combination of factors. An initial flow (surface fissure) was apparently introduced by the deep-draw forming process. The stresses from the electron beam girth welding propagated the fissure, but not through the wall thickness. The thermal stresses from the two braze cycles further propagated the fissure until it became a through-crack.

The suspect canister was removed from the tube assembly and subjected to extensive non-destructive testing followed by destructive testing both at AES Torrance and at NASA LeRC. As part of the non-destructive analysis, the suspect area was subjected to real-time radiography. Dissection allowed visual inspection of the fissure. High magnification confirmed the existence of a Z shaped flaw. Higher magnification revealed the presence of checking adjacent to the flaw. Penetrant inspection from the inside highlighted the extent of the flaw. A review of the real-time X-ray video shows that the flaw existed prior to the salt filling or brazing operation.

Real-time X-ray video tape recordings of all canisters utilized in the GTD receiver were reviewed to verify that other canisters did not contain flaws or fissures similar to that found on the defective canister.

For the flight demonstration receiver, all canister halves will be visually and penetrant inspected prior to girth welding. In addition, real-time X-ray will be conducted over the entire canister cylindrical surface.

6.6 Bibliography

Monthly Technical Schedule Status Reports: 92-65615-1 (i)

PDR Briefing Charts: 92-65656 (November 1992)

CDR Briefing Charts: 93-66201, Rev. 1 (May 1993)

Program Management Reviews: 92-65694 (i)

Receiver Single Tube Assembly Test Report: 93-66722 (December 1993)

Strumpf, H. J., Krystkowiak, K., and Killackey, J., "Design of the Heat Receiver for the Solar Dynamic Ground Test Demonstrator Space Power System," Paper 93028, 28th IECEC, 1993.

Strumpf, H. J., Avanessian, V., Ghafourian, R., and Huang, F., "Thermal and Structural Analysis of the Heat Receiver for the Solar Dynamic Ground Test Demonstrator," Proceedings of the 1994 International Solar Energy Conference, San Francisco, CA, pp. 222 to 234, 1994.

DeGroh, K. K., Roig, D. M., Burke, C. A., and Shah, D. R., "Performance and Durability of High-Emittance Heat Receiver Surfaces for Solar Dynamic Power Systems," prepared for the 1994 ASME International Solar Energy Conference, San Francisco, CA, March 27-30, 1994.

Strumpf, H. J., et al., "Fabrication and Testing of the Solar Dynamic Ground Test Demonstration Heat Receiver," 29th IECEC, 1994.

7. RADIATOR

7.1 Summary and Conclusions

The SD Waste Heat Radiator (WHR) rejects waste heat from the SDGTD Closed Brayton Cycle (CBC) system. Waste heat from the CBC is transported to the SDWHR via a liquid n-heptane coolant that is pumped and controlled by the AlliedSignal provided Liquid Utilities Pallet (LUP). The waste heat is rejected by thermal radiation from the SDWHR to the NASA-Lewis Tank 6 facility liquid nitrogen cold wall system. Radiator panels radiation is enhanced by Chemglaze A276, a white thermal control coating with a low solar absorbtivity and a high infrared emissivity.

The SDWHR subsystem, illustrated in Figure 7-1, has two radiator panels connected in series through the LUP. A structural attachment system of support rods and straps, support the radiator panels from the tank ceiling monorail as shown in Figure 7-2. Fluid connections between the panels and the LUP are made through standard fittings. The radiator panels are prevented from swinging by anti-swing brackets mounted at the bottom.

The radiator requirements were derived from studies accomplished under the Space Station *Freedom* Solar Dynamic Project contract. SDGTD project continued this effort. Hardware detail design and fabrication picked up where the SSF program had stopped. Fabrication was accomplished in the LV manufacturing facility established for the International Space Station radiators. People, tools, processes and procedures from the Space Station Program were utilized thus maximizing efficiency.

The Ground Test Demonstration Project was streamlined to maximum extent possible. The decision to use Space Station *Freedom* requirements and design substantially reduced the analysis and design effort.

Dedication of AlliedSignal and NASA-Lewis management to stabilize technical requirements and program requirements, such as funding, throughout the entire period of contract performance prevented the inefficiency of starts, stops and replans. The radiators were designed, fabricated, and tested on an accelerated schedule which reduced level of effort costs.

This approach resulted in radiators that performed as predicted; redesigns were not required and the overall SDGTD performance and schedule was fully supported.

7.2 Design Changes after CDR

There were no changes in performance, design requirements or design after CDR. Several minor interface problems were identified during the fabrication cycle, such as the anti-swing brackets location (these were used to connect the panel lower edge to the AlliedSignal LUP) and the bracket holes size and location on the bottom edge of the panels. These minor items resulted from evolving interface documentation and were rapidly resolved by AlliedSignal drawing changes to accommodate the panel as fabricated.

Figure 7-1. WHR Subsystem

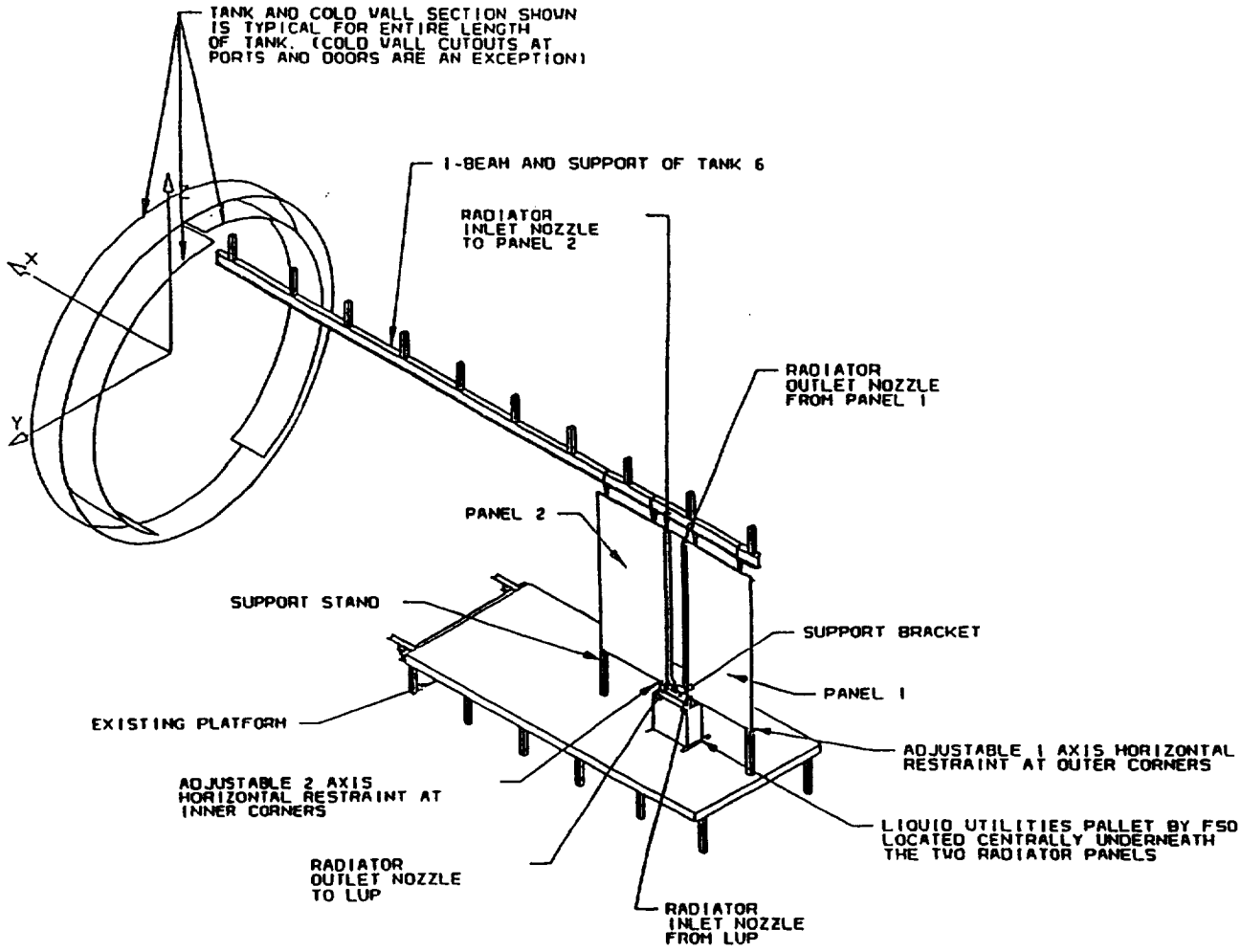

Figure 7-2. Radiator Panels Installed in Tank 6

NASA
C-94-02593

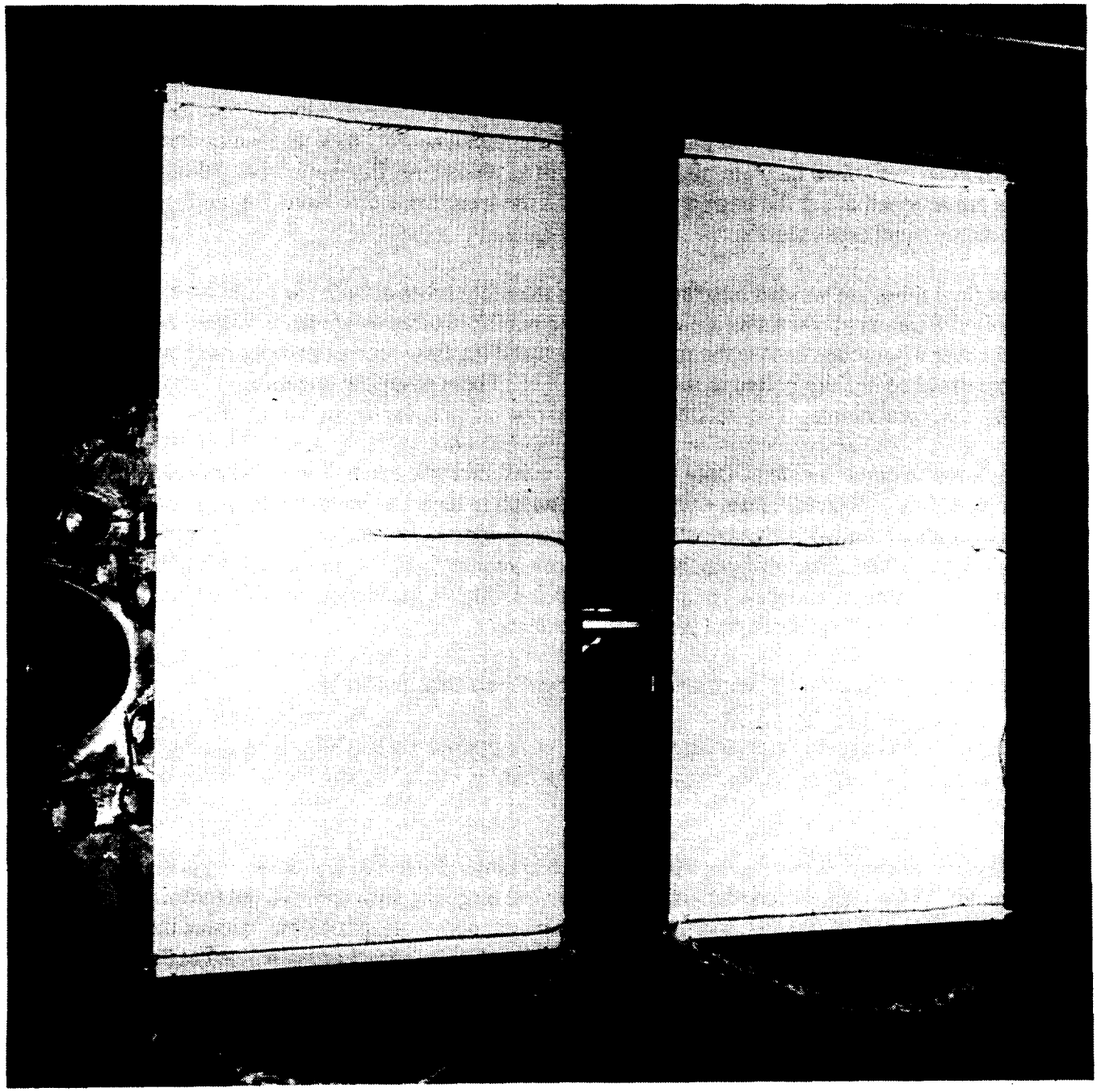

k:\ger\14056-3.doc

7.3 Fabrication Summary

The Solar Dynamic Waste Heat Radiator (WHR) panels are similar in construction to those on the current Heat Rejection System (HRS) and Photo Voltaic Radiator (PVR) Space Station programs. The radiators are bonded aluminum honeycomb panels containing 22 aluminum flow tubes, eleven active and eleven non-active tubes. The flow tubes are one piece aluminum extrusions with a 0.07 inch internal diameter flow tube in the center. The flow tube has extensions which provide impact protection from the low earth orbit micrometeroid/debris environment. The flow tube extrusion cross section is shown in Figure 7-3. The active and non-active flow tubes are equally spaced and alternate across the panel width as shown in Figure 7-4. Honeycomb core bonded to the extrusions with a foam adhesive is placed between the tubes to provide panel structural rigidity. The flow tube and honeycomb core is bonded between two 0.010 inch aluminum skins with an aluminum-filled adhesive. Aluminum sheet closeouts are attached along the edge of the panels in the lengthwise direction. Figure 7-5 shows a partial radiator panel cross section.

Extrusion flow tubes are welded into the aluminum manifold tubes at both the panel inlet and outlet ends. Only the eleven active tubes are welded to the manifold tubes as shown in Figure 7-4. Aluminum manifold cover assemblies encase the manifold tubes and the flow tube extensions as shown in Figure 7-6. The manifold covers are bolted to the radiator panel. These manifold covers are supported by bulkheads at several points. The bulkheads also provide support for the manifold tubes.

Fabrication was without incident. Only one issue of substance occurred. The small extrusion flow tube was welded to a 1/4 inch aluminum extension tube which in turn was welded into the manifold tube. The initial welds of the 1/4 inch extension tube to manifold tube exhibited signs of excessive porosity and possible cracking. After analysis, weld schedules were revised and all 42 tube/manifold welds were accomplished with no rejections. The welds passed full Quality inspection procedures including X-ray, dye penetrate, helium leak check and proof pressure tests.

7.4 Component Testing Summary (including Tank Integration)

Successful ambient environment Acceptance Tests were performed at LV in the presence of AlliedSignal representatives. These tests are documented in items 7 and 10 of the bibliography (Section 7.5 below).

Further component tests were conducted in the NASA-Lewis Tank 6 in a simulated space vacuum environment. These tests included thermal performance mapping with and without thermal insulation blankets covering part of Panel 2, thermal performance mapping using the final thermal insulation blanket coverage configuration, cold start transient simulation, nominal mission simulation, and steady state off-design mission simulation. Due to the longer than expected time required for achieving steady state conditions for thermal performance mapping and the physical limitations of the accumulator volume, the number of steady state thermal performance test points were reduced. However, sufficient test points were conducted to define the Radiator System thermal performance map.

Figure 7-3. Flow Tube Assembly Detail

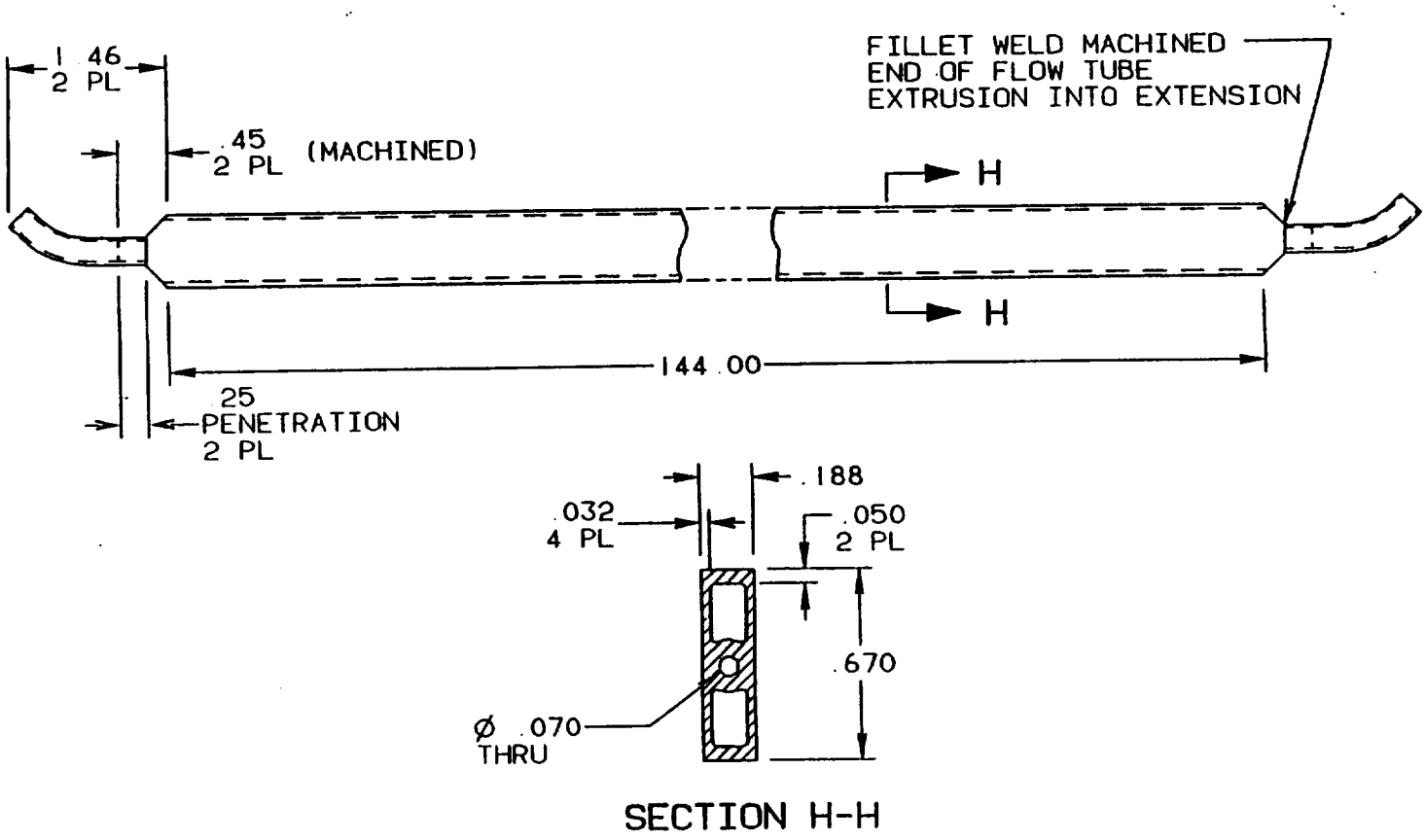

Figure 7-4. Radiator Panel Bond Assembly

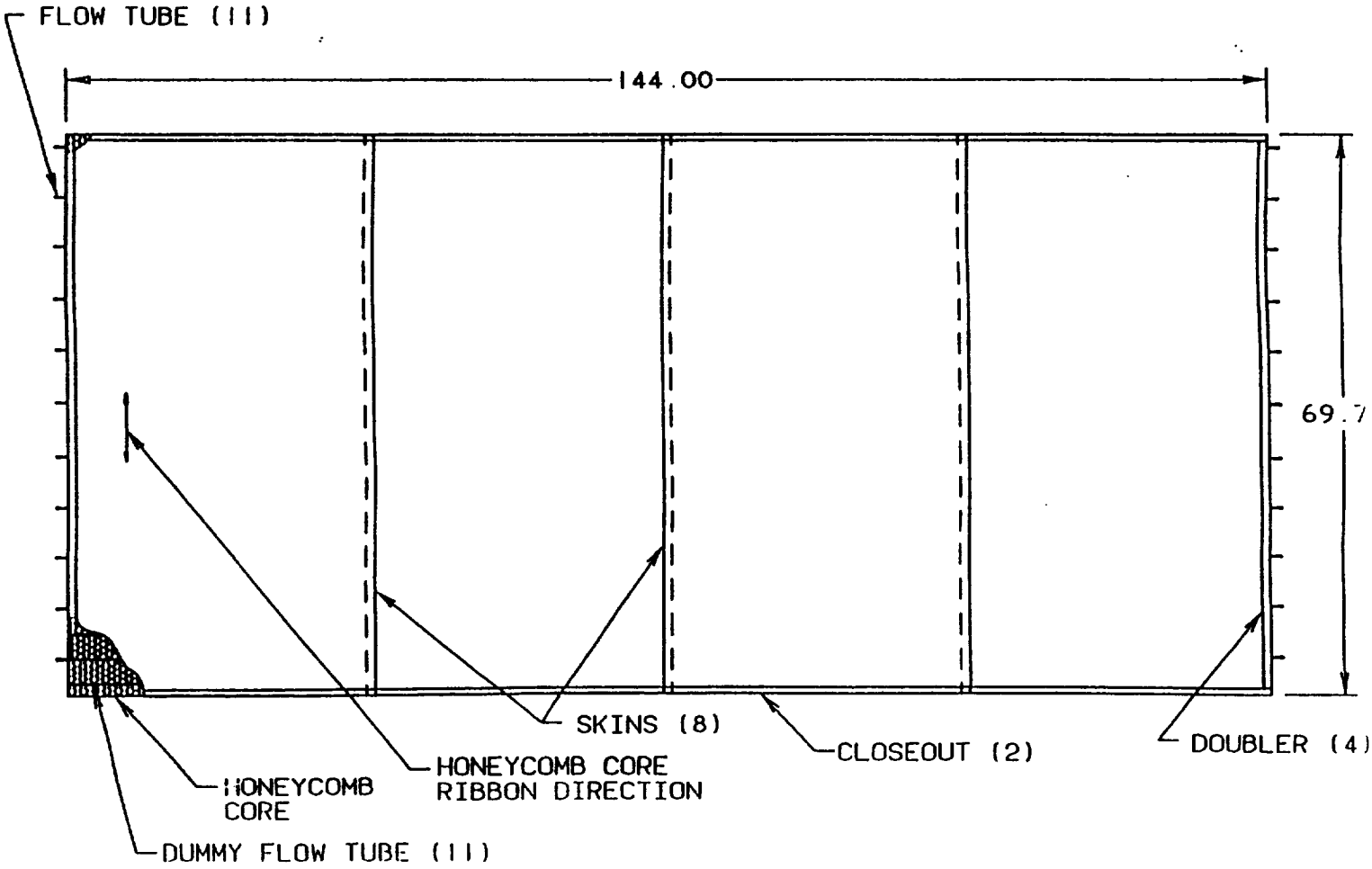

k:\ger\14056-3.doc

Figure 7-5. Panel Cross Section Configuration

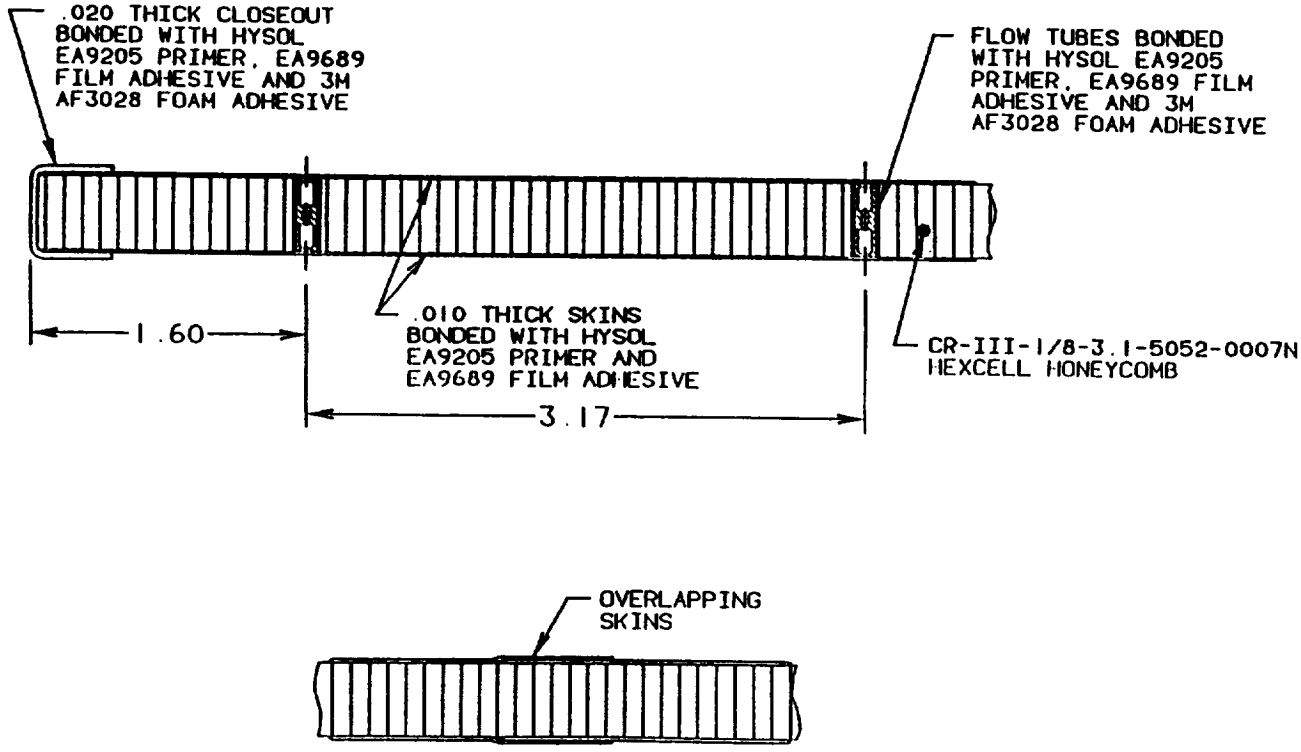

Figure 7-6. Manifold Cover Configuration

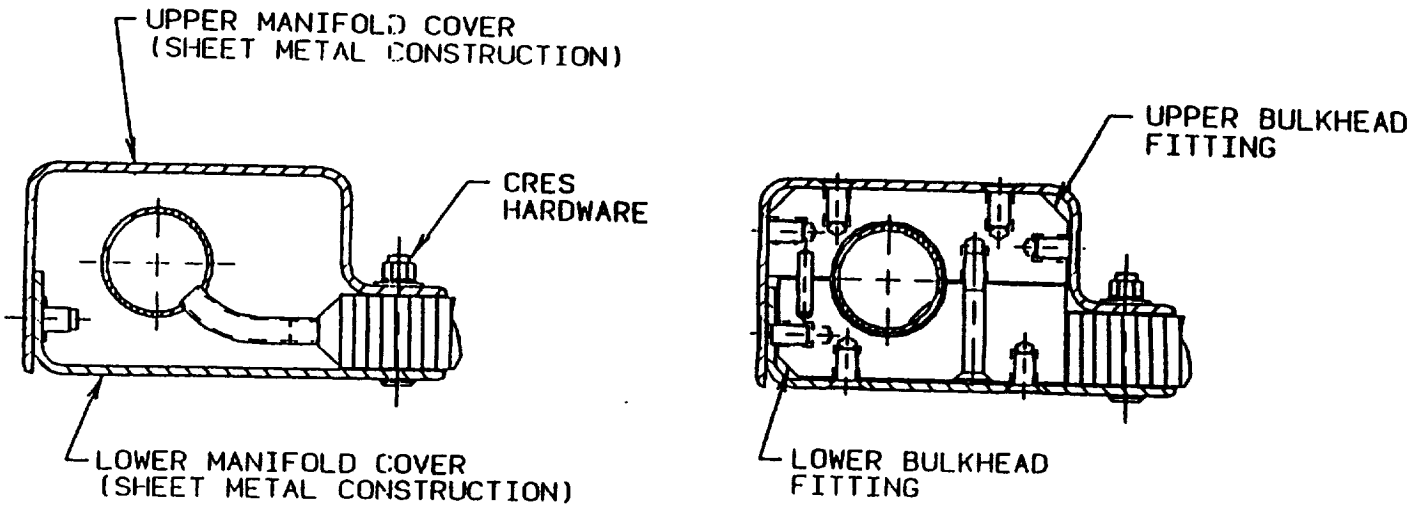

A helium leak check was conducted on the components and plumbing. A Veeco vacuum pump was connected to the n-heptane fill and drain line located below the tank. A vacuum was pulled on the HRS system and a helium source was applied to all fittings and connections. Several leaks were found around fittings and these fittings were tightened and sealed. Leaks were still detected and the source was believed to be the interconnection flex hoses. These flex hose lines were replaced with stainless steel hard lines and the system was able to hold vacuum with no further leaks detected.

A proof pressure test was accomplished on the HRS system. The system was pressurized to 65 psia and held for 15 minutes with no damage noted.

In the subsequent thermal vacuum testing, steady state thermal mapping tests were conducted first with no insulation blanket on the second panel. After the first series of tests, the insulation blanket was raised to cover a predetermined length of Panel 2 at the panel bottom, and the thermal mapping test series was repeated. After completing the second series of tests, the insulation blankets were adjusted to achieve the desired fluid outlet temperature at nominal operating conditions and the thermal mapping tests were repeated. A cold start transient test was then conducted followed by nominal and off-design performance.

Forty-four steady state test points and 11 transient test points were conducted during the radiator component testing. Table 7-1 and Table 7-2 list the test points and the conditions established for each. The two 12 feet long radiator panels plumbed in series give an effective 24 foot radiator length with no insulation blanket coverage. When the insulation blanket was used to cover part of the second radiator panel the effective radiator length was shortened. The radiator length is listed in Table 7-1 below. The insulation blanket on the second panel covered the inlet manifold end. The first 13 test points (test points 1-13) were conducted with no insulation blanket the next 10 test points (test points 14-23) were conducted with the insulation blanket covering 5 feet of the second panel. The remainder of the test points (test points 24-43, 49) were conducted with the insulation blanket readjusted to cover 4 feet of the second panel.

The radiator component test objectives were met and the radiator panels performed as expected. No hardware damage was observed from shipment to NASA-Lewis from LV. During proof and leak testing, no leaks were found to originate from the weld joints. After filling the HRS system with n-heptane liquid, the radiator panels functioned properly with the LUP. A thermocouple test checkout was performed and the panel thermocouple instrumentation were found to be operational. At nominal design conditions the HRS system maximum pressure drop was 10.5 psid. To achieve the desired fluid outlet temperature at SDGTD nominal operating conditions, Panel 2 was covered about 4 feet from the inlet end (bottom) by the insulation blankets. Various flow rate and inlet temperature combinations were conducted to map the thermal performance with and without thermal blanket coverage. The n-heptane fill procedure was finalized. No gas or vapor bubbles were introduced into the system. The only test objective not fully met was the correlation of the analytical models to the test data for both steady state and transient cases. The variations in sink temperatures across the panels during various times of the day made this correlation impractical. It was judged the correlation data was not worth the effort required to accomplish the task.

Table 7-1. Steady State Radiator Test Points

Test Point Number	Date Conducted	Total Panel Length, FT	Flow Rate pph	Fluid Inlet Temperature, °F	Heater Power %
1	7/27/94	24	173.3	140.6	77.0
2	7/27/94	24	175.5	150.1	77.0
3	7/27/94	24	175.3	178.8	94.0
4	7/27/94	24	174.8	190.7	100.0
5	7/28/94	24	196.8	175.6	100.0
6	7/28/94	24	196.7	123.3	70.0
7	7/28/94	24	200.8	97.6	60.0
8	7/28/94	24	175.2	96.5	58.5
9	7/28/94	24	179.1	121.6	72.0
10	7/28/94	24	179.2	178.2	100.0
11	7/28/94	24	150.5	195.1	90.0
12	7/28/94	24	148.0	152.5	72.0
13	7/28/94	24	142.6	101.0	52.5
14	8/01/94	19	177.5	138.9	69.0
15	8/01/94	19	177.4	177.1	87.0
16	8/01/94	19	174.6	200.9	97.5
17	8/01/94	19	199.2	192.0	100.0
18	8/01/94	19	201.4	149.1	79.0
19	8/01/94	19	201.9	98.8	57.5
20	8/01/94	19	153.2	96.5	48.5
21	8/01/94	19	150.8	142.5	69.0
22	8/01/94	19	151.5	197.8	90.0
23	8/01/94	19	177.3	99.2	53.0
24	8/04/94	20	175.4	138.6	69.5
25	8/04/94	20	177.7	150.5	77.0
26	8/04/94	20	201.3	151.8	84.0
27	8/04/94	20	151.2	155.0	67.7
28	8/04/94	20	124.3	149.4	58.0
29	8/04/94	20	102.3	148.1	53.0
30	8/04/94	20	100.7	171.5	60.0
31	8/04/94	20	127.3	174.5	72.5
32	8/04/94	20	151.9	177.3	81.0
33	8/04/94	20	175.4	174.9	89.0
34	8/04/94	20	201.4	175.7	96.0
35	8/04/94	20	201.8	186.0	100.0
36	8/04/94	20	178.8	189.3	96.0
37	8/04/94	20	151.7	200.3	87.0
38	8/04/94	20	125.6	197.3	75.4
39	8/04/94	20	101.6	196.4	67.0
40	8/04/94	20	96.8	128.9	44.6
41	8/05/94	20	121.1	125.6	53.0
42	8/04/94	20	175.8	140.8	75.0
43	8/05/94	20	173.0	139.2	68.3
49	8/05/94	20	175.7	138.8	68.5

k:\ger\14056-

Table 7-2. Transient Test Points

Transient Case	Time	Flow rate	Heater Power	Action	Comment
	H:M	pph	%		
1	11:57	105	75	Increase flow to 145 pph	Hold for 30 minutes
2	12:27	145	75	Increase flow to 150 pph	Hold for 30 minutes
3	12:57	150	75	Increase flow to 175 pph	Hold for 30 minutes
4	13:27	175	75	Increase flow to 200 pph	Hold for 30 minutes
5	14:00	200	75	Increase htr pwr to 100%	Hold until temperatures stabilized
6	15:10	200	100	Shut off heater power	Hold until accumulator reaches lower limit
7	15:24	200	0	Increase htr pwr to 100 %	Hold until temperatures stabilized
8	16:34	200	100	Shut off heater power	Hold until accumulator reaches lower limit
9	16:48	200	0	Increase htr pwr to 100%	Hold until temperatures stabilized
10	17:36	200	100	Reduce flow rate to 130 pph	Hold for 1 minute
11	17:37	130	100	Increase flow rate to 200 pph	Hold for 5 minutes

7.5 Bibliography

1. "Final Test Report for HRS Radiator Component Tests," Flores, 3-47300/4R-005 10 April 1995.

2. "Solar Dynamic Ground Test Demonstration Radiator Design and Test," Fleming, Flores, Sharpe, 29th IECEC.

3. "Solar Dynamic Radiator Design Development," Fleming and Flores 1994, ASME International Solar Energy Conference.

4. "SDGTD Radiator Panel Sizing," Flores 3-47300/2DIR-542 22, October 1992.

5. "Stress Analysis of Solar Dynamic Ground Test Panel," Miniatas 3-47300/3DIR-006, February 9, 1993.

6. "Test Plans and Test Procedures for HRS Radiator Component Test and System Integration Test (HRS Only)," 3-47300/4DIR-005, Rev. A, June 27, 1994.

7. "Solar Dynamic Ground Test Demonstration Acceptance Test Report," 3-47300/3R-007 June 13, 1994.

8. "SDGTD Radiator Panel Instrumentation Vacuum Bake Out," August 23, 1993.

9. "SDGTD Radiator Panel Instrumentation Fabrication and Acceptance Testing" Rev. A, June 14, 1993.

10. "SDGTD Radiator Panel Instrumentation Fabrication and Acceptance Testing," February 21, 1994.

11. "Acceptance Test Requirements and Procedures and Radiator Panel Installation Procedures for NASA-Lewis Tank 6 Facility and Radiator Component Test Plan and Procedures and SDGTD System Test Radiator Test Plan," 3-47300/3R-021, January 7, 1994.

8. INTRODUCTION

This final report describes the effort by Aerospace Design & Development (ADD) on the Solar Dynamic Ground Test Demonstration (SDGTD) Radiation Shields Project. The objective of this project was to design and fabricate radiation shields consisting of multifoil insulation blankets to insulate various portions of the SDGTD system. The radiation shields allowed heat losses from the system to be reduced to the level required for acceptable performance of the SDGTD system. ADD performed analysis, design and fabrication of insulation blankets for the following items: 1.) Receiver, 2.) Recuperator, 3.) TAC, 4.) Receiver Inlet Duct, 5.) Turbine Inlet Duct and 6.) Turbine Exhaust Duct. In addition, coupon level thermal performance testing was performed to verify the thermal performance of the candidate blanket layups.

8.1 Summary and Conclusions

The multifoil insulation blankets used on the SDGTD system consist of layers of 0.001 inch thick foils alternating with layers of a pure quartz fabric spacer material. Figure 8-1 shows a typical layup used on a straight section of duct. To assemble each layer, the foil and spacer is wrapped around the duct with a one inch overlap of the foil. The foil layer is then spot welded together at the overlap. Thus, each layer essentially is one contiguous shell with the spacer material entirely contained within the foil. Thirty layers of insulation were used on lower temperature components (Recuperator, Receiver Inlet Duct and Turbine Exhaust Duct) and 50 layers were used on the high temperature components (Receiver, TAC and Turbine Inlet Duct). Due to the temperature gradient along the length of the Recuperator, a staggered layup was used with 30 layers on the hot end gradually reducing down to only one layer on the cold end.

Figure 8-1. Typical Multifoil Insulation Layup

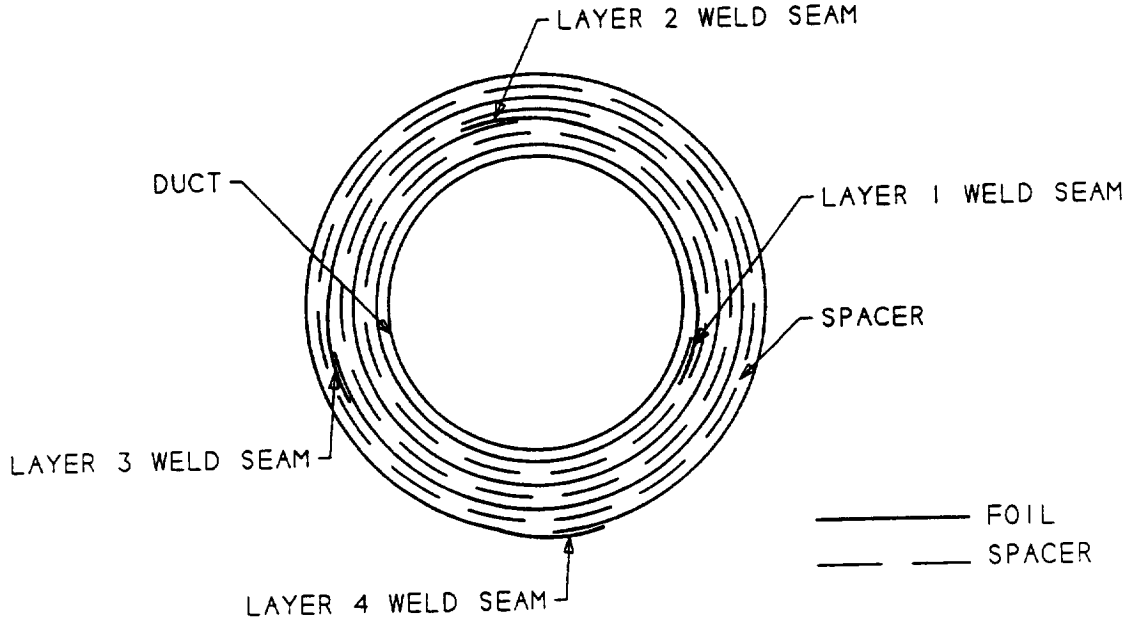

Nickel 201 foil was used in the inner layers of the blanket with ten outer layers of Aluminum 1100. The aluminum allowed a reduction in the total number of layers used because the emissivity of aluminum is much less than that of nickel, and thus provides a higher level of insulation. Aluminum could not be used for the entire blanket since the insulated components operated at temperatures near and exceeding the melting point of aluminum. The quartz spacer material used was Tissuquartz, manufactured by Pallflex Corporation.

Preliminary thermal analysis was performed early in the project and baselined a layup of 20 layers nickel with ten outer layers of aluminum for the lower temperature (1100 °F) components and 30 layers of nickel with ten outer layers of aluminum for the high temperature (1400 °F) components. Detailed thermal models were then produced for each component to be insulated. The detailed models included effects of penetrations, corrections based on completion of final component layouts, and correlations to the coupon test data.

The results of the final updated thermal analyses is presented in Table 8-1. This table lists system heat loss by component and summarizes the boundary conditions used for analysis as well as the final blanket layup configuration. The total system heat loss through the insulation blankets was predicted to be 685 W. The main impact of the final analysis was a decision to use a 50 layer blanket on the receiver and the turbine inlet duct. The additional ten layers added approximately 0.2 inches to the layup thickness on both items, for a total of 0.9 inches. The additional layers were needed for two reasons: 1.) This would ensure that if 1500 °F hot spots occur on the receiver wall the innermost aluminum layer would not be closer than 200 °F to its melting point. 2.) This gave sufficient margin on total system heat leak to ensure that the 750 W total heat loss requirement would be met. The total heat loss of 685 W was based on the coupon test data correlations. Thus, the models reflected actual thermal performance of a blanket that has several penetrations for instrumentation wires as well as three support tubes. This fact, coupled with the fact that the models were designed to be conservative ensured that the system heat loss goals would be met.

8.2 Post CDR Design Changes

There were two significant changes to the design following the Critical Design Review. The first was that the total number of layers on the Receiver and Turbine Inlet Duct was increased from 40 to 50. The reasons for the change were discussed above. The second change was that removable insulation shells were not used on the welded flanges that mate the Receiver and PCS. The reason for not using them was that during layup of the insulation at NASA it was noted that there was insufficient clearance between the receiver inlet duct and receiver frame to allow mounting the insulation shell. Also, interference between the shell and duct instrumentation leads precluded moving the shell outside of the interference zone. As a result, the flanges were insulated with a standard layup after the flanges were welded.

Table 8-1. Insulation Heat Leak Summary

	Area, In^2	T_{hot}, °F	T_{sink}, °F	No. Layers	Heat Loss, W
Receiver Inlet Duct	461	1080	-70	30	36.8
Turbine Exhaust Duct	329	1110	-70	30	28.1
Turbine Inlet Duct	668	1365	-70	50	89.2
Solar Receiver	4200	1400	-70	50	393.6
Bellows Restraint	400	1365	-70	40	51.8
Recuperator	1166	1100	-70	30	46.6
Rcvr Inlet Duct Flange	92	1080	-70	30	14.4
Turb Inlet Duct Flange	67	1365	-70	40	24.8
Total System Heat Loss					685.3

8.3 Fabrication Summary

Installation of the Receiver and PCS insulation was performed at NASA LeRC. This eliminated the potential problem of a leak developing in the Receiver and/or PCS during shipment to LeRC. If such a leak were to develop after the insulation was installed, pinpointing the location of the leak would be extremely difficult, if not impossible, and portions of the insulation would need to be removed and replaced in order to repair the leak.

Precutting of most insulation gore sections was done at ADD in the months of July - September 1994. Installation of the Receiver and PCS insulation was performed at NASA in September and October. At the same time, personnel at ADD completed the TAC external insulation assemblies. These were shipped to LeRC for installation by ADD personnel once the blanket installation was completed.

There were several lessons learned during the layup of the insulation. The first was that the layup thickness grew faster than estimated. As a result, the overlap of foils required for spot welding was often inadequate on outer layers, and extra material had to be patched in. The second lesson learned had to do with the method used to insulate the duct elbows. Foil and Tissuquartz tape 1.5 and 3.0 inches wide was wrapped around the elbow, much like a bandage, as shown in Figure 8-2. This caused a large overlap, up to 90 percent, on the inside radius of the elbow resulting in a much larger buildup of insulation thickness than anticipated. This was most evident on the Turbine Inlet Duct (TID), which had the most insulation layers of any of the ducts. The layup on the TID ended up being nearly three inches thick, rather than the baselined one inch thick. Also, it would have been better to install the TAC external insulation shells prior to insulating the Turbine Inlet Duct. The TAC external shell insulation terminated with a 45 degree interface where the 1.5 inch turbine inlet ducts entered the shell. Installing the shells first would have allowed the TID insulation to be installed completely up to the shell.

Figure 8-2. Duct Elbow Insulation Layup

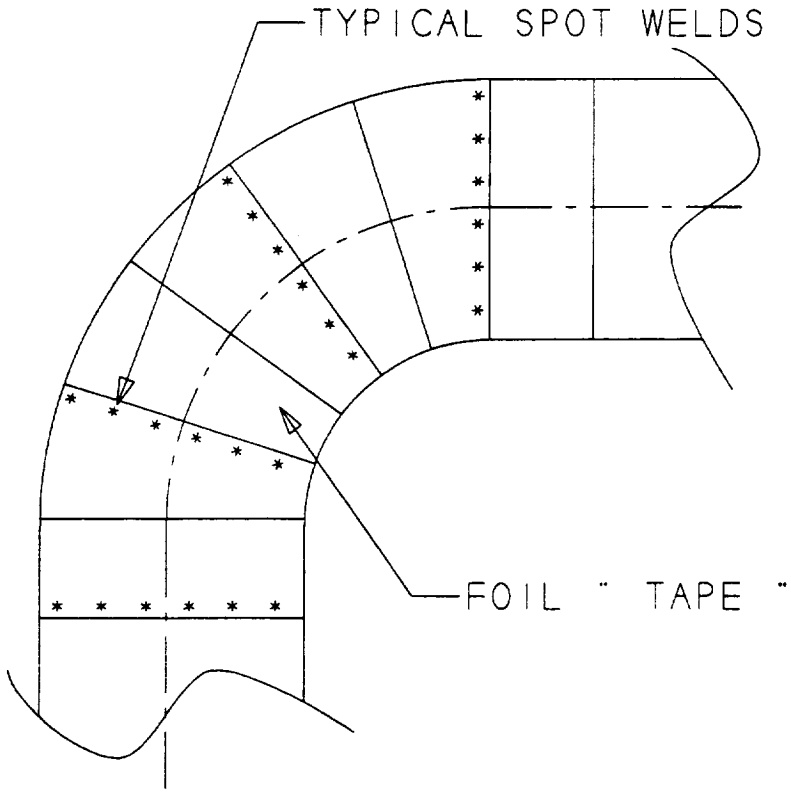

Instead, the insulation was terminated several inches away from the shell envelope, and a four inch section of TID insulation had to be patched in following installation of the shell. One final note is the need for large clearances around items being insulated, with the Recuperator being a prime example. On paper, there appeared to be sufficient clearances for the insulation itself (e.g., one inch) around the Recuperator supports. However, in reality 4-6 inch clearances are actually needed in order to have enough space to freely move the foil and spacer when installing. Smaller clearances do not give enough room for your hands to get behind supports and often resulted in tearing of the foil and spacer against the supports.

8.4 Test Summary

As a portion of the SDGTD radiation shields development project, ADD performed coupon level thermal performance testing of candidate insulation blanket configurations. This testing was required to verify the insulation blanket thermal analysis and ensured the thermal performance goals of this contract were achieved. Another reason for coupon testing was to verify the integrity of the blankets if exposed to the atmosphere while at high temperature should that condition be necessary.

The overall arrangement of the test hardware and data acquisition system is presented in Figure 8-3. It consists of ADD's thermal test calorimeter, instrumentation, vacuum pump, and data acquisition system. The test calorimeter consisted of a four inch diameter, 24 inch long copper rod that provides a high conductivity isothermal surface. The rod was insulated with the test blanket and placed in a vacuum jacket that contains feedthroughs for the heater and for thermocouples internal to the copper rod and on every tenth insulation layer. Six thermocouples were also placed on the vacuum jacket to measure the outside sink temperature. The heater is a 200 W cartridge heater placed in a well that passes into the center of the copper bar. The vacuum jacket also has a pump-out port for a vacuum pump and ports for thermocouple and ion vacuum gauges. The heater is connected to a Variac to control the heater power, and a watt meter was used to measure heater power.

Figure 8-3. Coupon Test Schematic

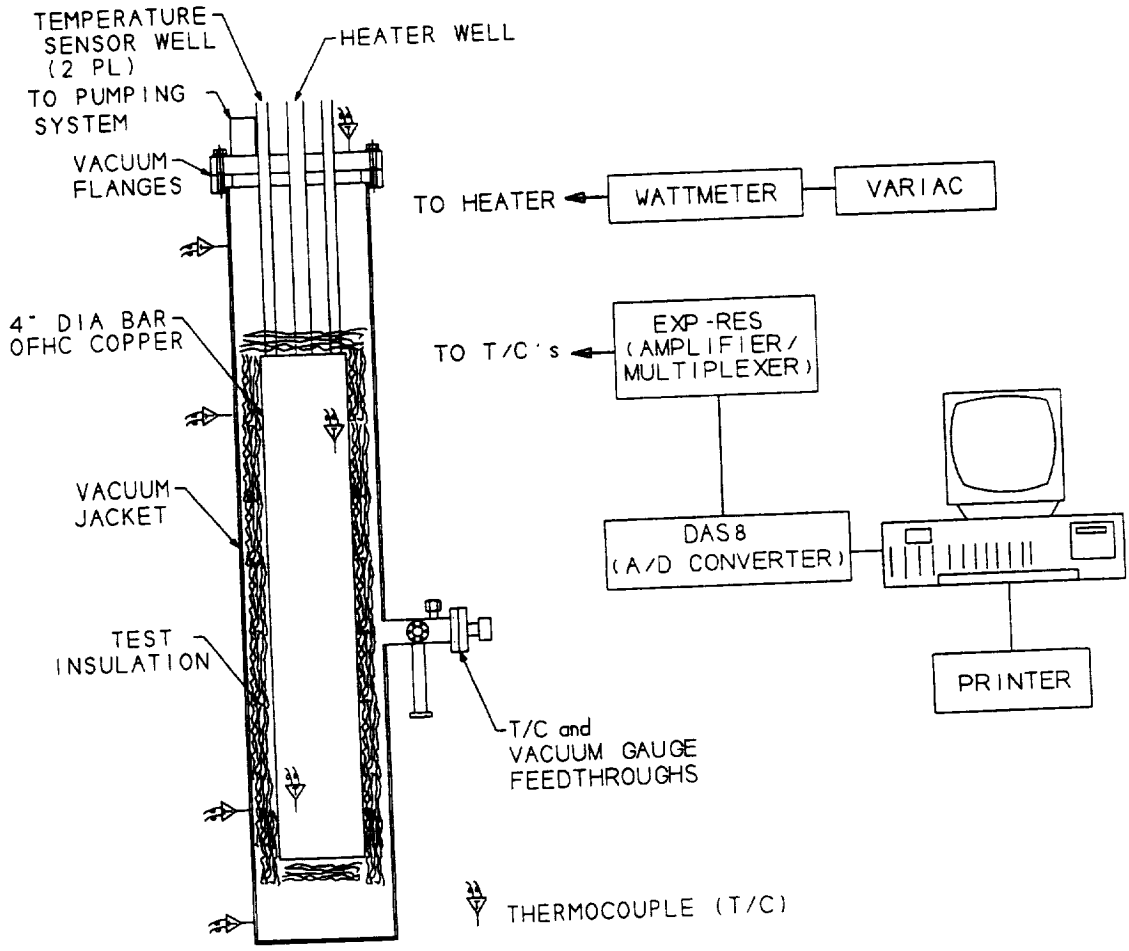

Five tests were performed, each with a different layup configuration. Table 8-2 summarizes each of the tests. For each test, several steady state temperature points were obtained between ambient and the maximum expected operating temperature for the blanket configuration. Once steady state at the maximum temperature was reached, the apparatus was cooled down with steady state temperature data points again measured during cooldown. To reach a steady state point, the heater power was set to a constant level and the apparatus was allowed to remain at constant temperature for a period of at least 12 hours. At that point, the heater power was measured with a multimeter and the apparatus was either cooled down or ramped up to the next desired steady state point. The ramp-up/cooldown cycle was performed at least two times for each test.

Table 8-2. Coupon Test Summary

Test Date	Foil Configuration	Spacer Material
11/10/92 - 12/14/92	20 Nickel, 10 Aluminum	FiberFrax
05/26/93 - 08/06/93	20 Nickel, 10 Aluminum	Tissuquartz 2500QA
10/08/93 - 12/22/93	40 Nickel, 10 Aluminum	Tissuquartz 400QA
01/18/94 - 03/15/94	40 Nickel	Tissuquartz 400QA
04/07/94 - 07/05/94	30 Nickel, 10 Aluminum	Tissuquartz 400QA

The heater power and blanket temperature profiles obtained at the steady state points were then used to correlate a thermal model of the test apparatus for each configuration. Once the model was correlated, the insulation blanket portion of the model was used in the detailed thermal analysis effort. Correlation between the test data and the thermal model was excellent. Figure 8-4 shows a plot of heater power vs. temperature for the 30 layer Tissuquartz spacer test. Both test data and analytic data from the thermal model are shown, depicting the close correlation

Figure 8-4. MLI Thermal Model Test Correlation Results

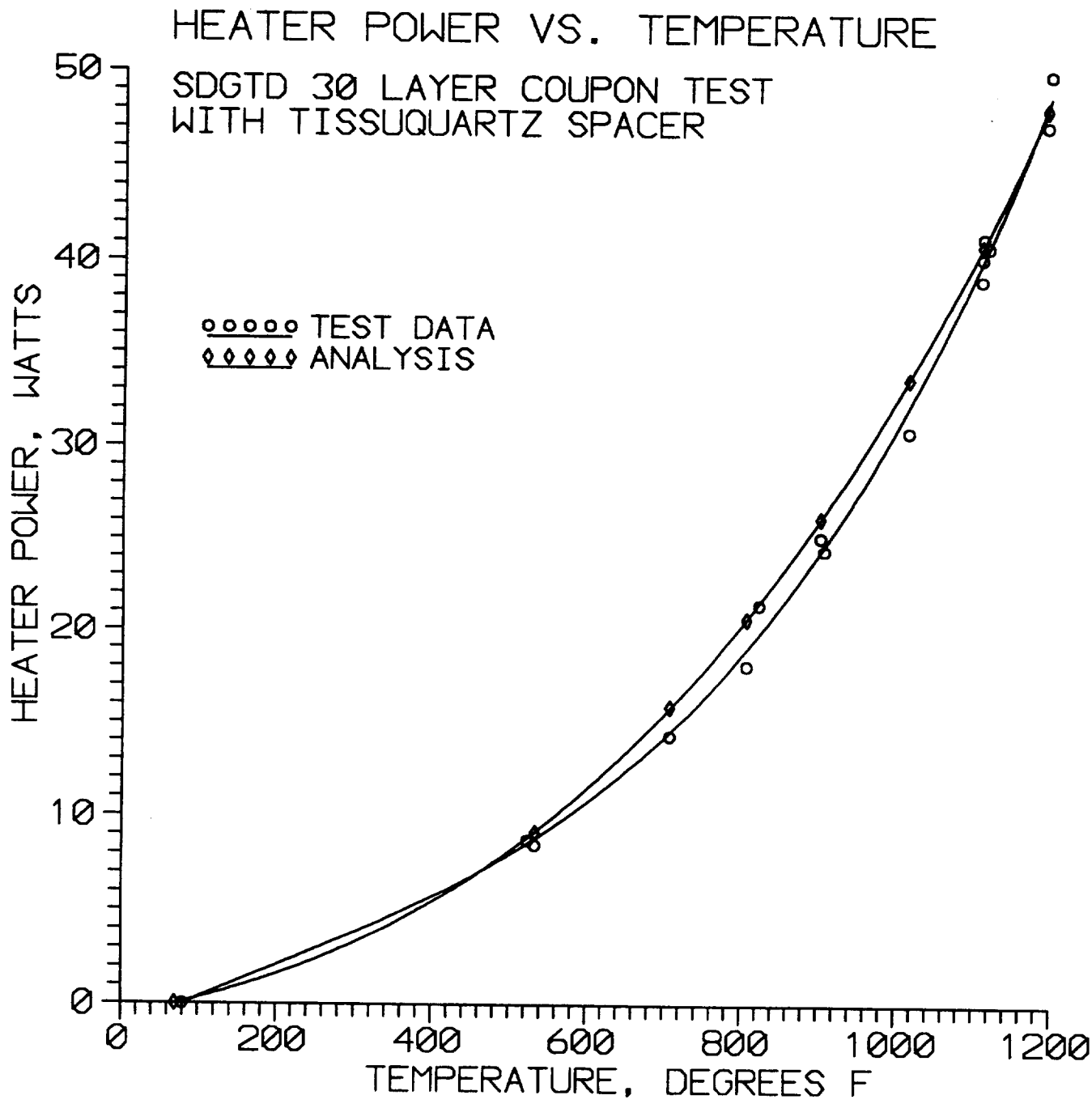

k:\ger\14056-3.doc

9. POWER CONVERSION SUBSYSTEM (PCS)

The Power Conversion Subsystem (PCS) of the Solar Dynamic Ground Test Demonstrator consist of the following functional components:

- Turboalternator Compressor (TAC)
- Recuperator
- Cooler (cycle gas to waste heat loop heat exchanger)
- Ducting
- Supporting Structure

Except for the Cooler (2) this hardware was originally designed, fabricated and tested as part of the Brayton Isotope Power System (BIPS) Project conducted by AlliedSignal (then Garrett) for DOE/NASA in the mid 1970s. After the completion of that project this hardware was sent to Plumbrook, Ohio for long term storage. In storage, this hardware was subjected to significant rodent infestation and resultant ammonia contamination. On the SDGTD project this hardware was retrieved, cleaned, refurbished, modified, instrumented, assembled and tested prior to integration into the complete system test setup of Tank 6. The Cooler (P/N 2340374-1) consisted of two identical heat exchangers operated in series. These heat exchangers were originally designed, fabricated and tested for Phillips Lab for use as a cryocooler for space application. The integrated PCS is shown in its test and shipping stand prior to the installation of multilayer insulation in Figure 9-1. A photographic collage of the components is shown in Figure 9-2.

9.1 Summary and Conclusions

Substantial performance testing had previously been accomplished on the components of this subsystem as part of the BIPS project and during the qualification testing of the cooler. No significant discrepancies with prior performance characteristics were noted during the subsystem or system testing. The following conclusions were drawn concerning the PCS components as a result of the activities of this project:

1. The TAC had previously been designed to operate at 2.0 kWe and had previously been tested on the BIPS project to 1.3 kWe. The SDGTD successfully operated the TAC up to 2.08 kWe. However, capacitance probes installed to monitor the radial and axial motion of the rotor indicated that the foil thrust bearing was operating near its steady state load capacity at 52,000 rpm. Increasing speed above 52,000 rpm increases pressure ratio hence thrust load and is not recommended at design SDGTD gas inventory and pressure levels.
2. TAC rotor dynamic operation was satisfactory. The concern of increased negative spring rate resulting from increased attraction of the rotor by the alternator stator at higher electrical loads did not materialize. The concern had been that the radial foil bearings low spring rate would be further reduced by attraction of the rotor to the stator at higher electrical loads which would effectively reduce the bearing spring rate and increase the potential for rotor dynamic instability.

Figure 9-1. Power Conversion Subsystem Prior to MLI Installation

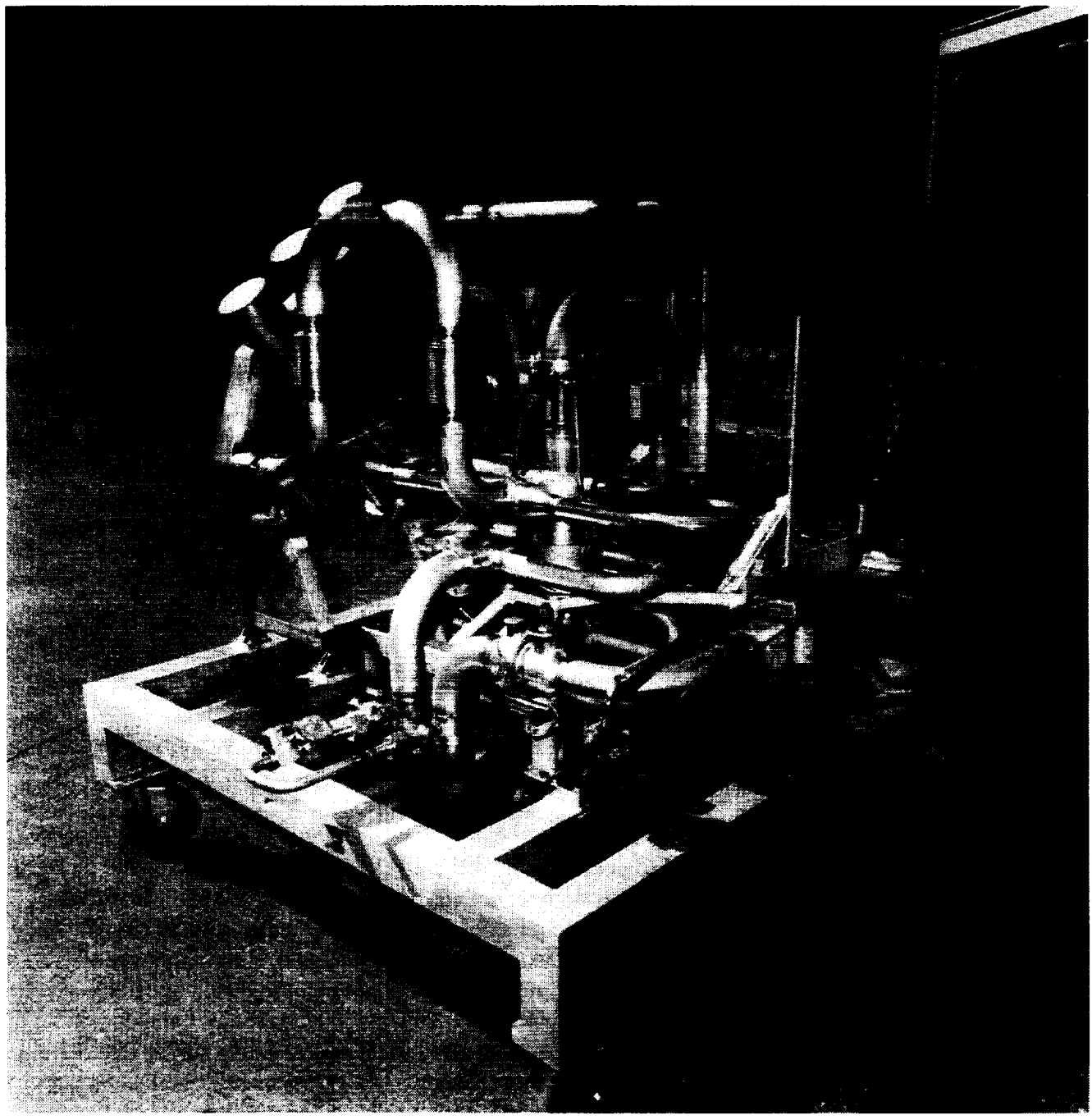

Figure 9-2. Power Conversion Subsystem Components

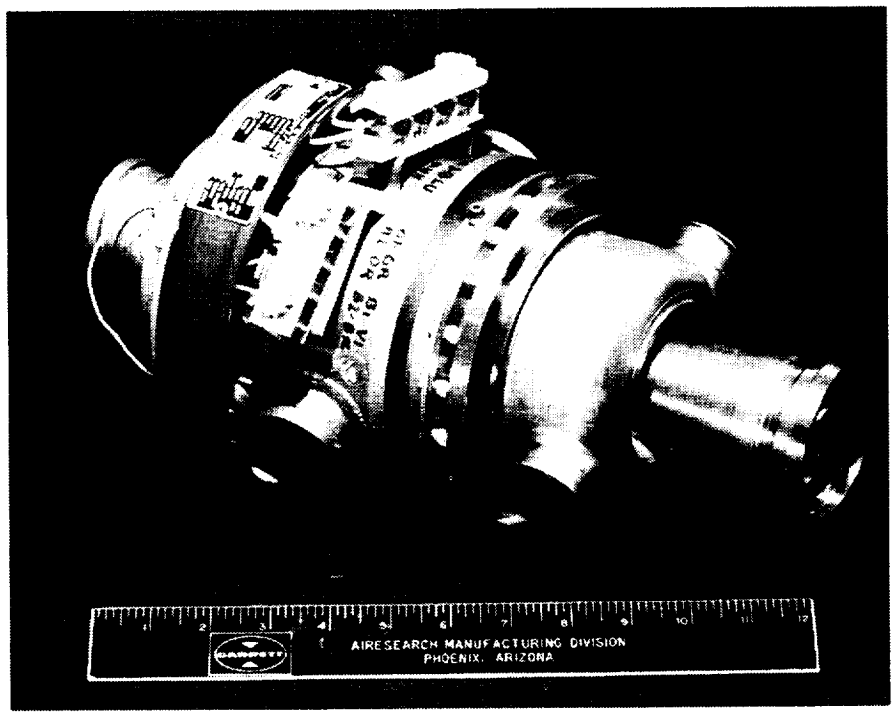

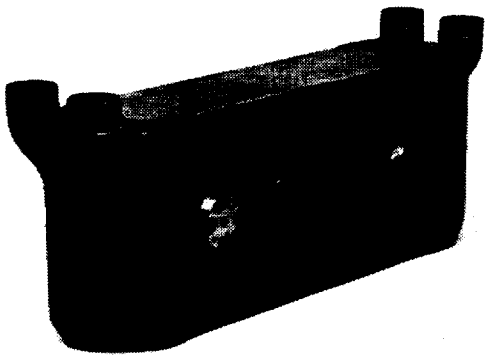

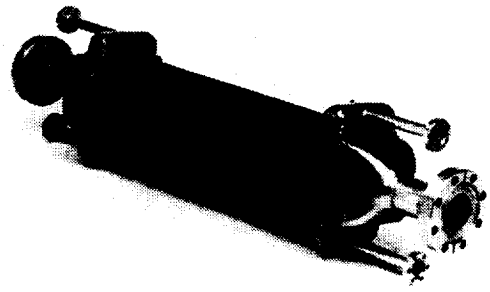

3. It was discovered that preheating the turbine prior to starting was required to keep the compressor from going into surge during the start.
4. Shutdown from normal operating temperatures, without extracting the heat from the receiver, did not result in any appreciable thermal soakback into the TAC turbine bearing cavity. Bearing temperatures increase only 20-30 degrees R after shutdown.

9.2 Design Changes After CDR

9.2.1 Turboalternator Compressor

Changes to the BIPS TAC identified at CDR were the following:

- Upgrading radial foil bearings to new configuration offering improved damping, load capacity and coating. These bearings were derivatives of the V-22 environmental control unit.
- Incorporation of 2 axial and 2 radial capacitance probes to monitor thrust rotor axial excursion and shaft radial runout.
- Modifications to secondary flow system to accommodate higher internal losses associated with operation at higher gas pressure levels.
- Replacement of the Waspalloy turbine plenum with a Hastalloy X plenum which was fabricated as part of the BIPS project but was new.

The following changes were incorporated into the TAC after CDR.

- During initial motoring tests the compressor impeller rubbed the compressor shroud. The primary cause was traced to an assembly error which shimmed the compressor impeller 0.005 in. closer to the shroud then was desired. In addition to revising the procedure bumpers were added to the radial bearing housings. These bumpers had been used on the BIPS unit but were not incorporated into the SDGTD initial TAC design
- Hot Loop testing showed poor subsystem performance which was traced to leak paths in passages installed to route instrumentation and alternator electrical wiring across the compressor flow path. These leak paths were eliminated.

The final assembly part number for the Turboalternator Compressor is AlliedSignal Fluid Systems drawing 3793271.

9.2.2 Cooler

No changes in the cooler configuration was made after CDR

9.2.3 Recuperator

No changes in the recuperator configuration was made after CDR. However, recuperator thermocouple instrumentation (tag numbers PCSTE530-536) were not incorporated as called for by the test plan and instrumentation list available at CDR. The final release of the instrumentation list (Rocketdyne document 213000014) reassign these parameters.

9.2.4 Ducting/Piping

The bolted flange in the compressor inlet duct was eliminated and replaced with a welded joint to eliminate as many elastomeric gas boundary seals from the unit. After this flange was eliminated, the only elastomeric joint was in the gas check valve joining flange. No other changes were made to the gas ducting configuration. The final released drawings reflected the compressor flange change.

The liquid loop piping between the two gas coolers was rerouted to incorporated a cold plate for the pressure transducers which were connected to the PCS.

Further, turbine discharge instrumentation (PCSTE521-523 and PCSPT520) was shown at CDR to be in the turbine discharge duct just downstream of the outlet bellows support structure. These instrumentation elements were relocated further downstream in that same duct to a point 2 in. upstream of the recuperator inlet interface. This was done to make it easier to apply multi-layer insulation to the turbine plenum.

9.2.5 Supporting Structure

A set of brackets were added to support the pressure transducer cold plate which was added to the liquid loop piping as discussed above. The cold plate was added directly above the 2nd cooler.

9.3 Fabrication Summary

9.3.1 Turboalternator Compressor

The Turboalternator Compressor had previously been developed as part of the 1970s BIPS project. Except for new radial bearings and incorporation of capacitance probes, hardware had previously been fabricated. Procedures for assembling the unit were also available. The build procedure were republished to reflect the new parts incorporated during the SDGTD project. Two lessons were learned in the assembly aspect:

- The procedure for shimming the compressor axial clearance to the shroud produced a result which was 0.005 in. too tight. This procedure was revised: 41-12251A should be used for any future TAC assembly activity.
- Instrumentation and alternator electrical pathways across the compressor flow path did not incorporate sealing features. These leak paths were eliminated by filling with RTV. The RTV was pulled into each void using vacuum.

9.3.2 Recuperator

The recuperator(s) were previously fabricated. Activity on the SDGTD involved only cleaning. No lessons learned were accumulated in this activity.

9.3.3 Cooler

Like the recuperators, these heat exchangers were previously fabricated and no lessons learned were accumulated here.

9.3.4 Ducting/Piping

Ducting was assembled primarily from bellows and ducting lengths which were salvaged from the BIPS design. No fabrication lessons learned were identified for this hardware.

9.3.5 Support Structure

No lessons learned were identified for the PCS support structure.

9.4 Test Results

9.4.1 Component Testing Results

9.4.1.1 Turboalternator Compressor

Initial motoring testing conducted on the TAC resulted in a compressor impeller rub which was traced to an error in the assembly instructions. Further, when attempting to motor the TAC with a cold turbine the compressor was forced into surge. This characteristic required changes in the subsystem and system starting procedures. No performance information on the TAC was developed during TAC acceptance as this was purely a mechanical integrity check.

9.4.1.2 Recuperator

Two recuperators were previously made. One, serial number D-1, had accumulated approximately 1000 hours of testing as part of the BIPS project. The other, serial number R-1, had been used in an accelerated aging thermal shock fatigue test. Serial number D-1 was subjected to proof pressure and leakage test. Leakage was measured from high pressure side to low pressure side as well as internal to external. The leakage results were as follows:

- High side to low side - $1.67 * 10^{-3}$ scc/sec of helium at 15 psid
- Internal to external leakage - $4.4 * 10^{-9}$ scc/sec of helium at 15 psid

The internal leakage appears to be high, but when compared with the through flow, which is 0.33 lb/sec, this leakage is insignificant and would remain insignificant at 1000 times that leak rate. The system performance model was run with an internal leakage and it took a leakage rate of 1 percent of through flow before the differences were greater than the instrumentation error.

9.4.1.3 Cooler(s)

The coolers were cleaned, proof pressure tested and leak checked. Again, leak check included an internal and external leakage. Internal leakage for all coolers was less than 2×10^{-9} scc/sec helium at 15 psid. External leakage was less than 3×10^{-7} scc/sec of helium at 15 psid.

9.4.1.4 Ducting/Piping

All ducting elements were individually penetrant inspected and helium leak checked to better than 1 * 10-6 scc/sec helium at 15 psid prior to incorporation into the integrated PCS. In this manner final system leak check required testing only the final weld closures and instrumentation. With the complex ducting geometry of the Brayton cycle components trying to do a system leak check without checking the duct welds first would have been a very difficult task.

9.4.2 Power Conversion Subsystem Testing

9.4.2.1 Testing at Fluid Systems Prior to Delivery to NASA LeRC

Testing of the Power Conversion Subsystem was conducted at Fluid Systems prior to delivery to NASA LeRC. This testing was referred to as the Hot Loop tests and incorporated the following hardware:

- The Power Conversion Subsystem
- An electric heater to replace the Solar Receiver (Section 6)
- The Data Acquisition Subsystem (Section 12)
- The breadboard PCCU (Section 10)
- FiberFrax insulation of hot components
- A liquid nitrogen cooled tank of ethylene glycol/water to act as a heat sink
- Pumps and flow meter from the Liquid Utilities Pallet (Section 13)

This was a test of the Brayton engine which maximized the use of other deliverable components to minimize test setup cost and to maximize the amount of components which were tested prior to delivery to Tank 6 and NASA Lewis. During the test sequence the Electric Load Simulator (Section 11) was delivered by NASA to Fluid Systems and was included in the Hot Loop test to resolve interface issues between the ELS, PCCU and DACS.

The first of two test sequences (Hot Loop A) was conducted from 25 March 94 to 26 May 94 and accumulated approximately 14 hours of hot TAC operation. A maximum of 1300 W was generated during this test sequence. Two significant findings were uncovered during this testing:

1. With the TAC installed in the closed loop of the PCS it was discovered that the compressor would go into surge if the turbine was at room temperature and the TAC was motored by the alternator. The turbine is 2.8 inches in diameter while the compressor is only 2.0 inches. When motoring, both units want to act like compressors and the turbine, being larger, wins and forces the compressor into surge. Figure 9-3 provides a plot of the predicted temperature ratio turbine to compressor necessary to keep the compressor out of surge and establish normal flow through the turbine. A small pump was added to the gas loop. After the electric heater had been heated to approximately design temperatures, the small pump was turned on which forced a small amount of gas to move through the loop. In this manner some preheated gas was moved from the heater to the turbine. No temperature sensors were located within the turbine inlet plenum and we do not know how hot we preheated the turbine, but it wasn't very much. Subsequently, and by accident, we discovered that if the shutdown valves were left open and the TAC was motored the compressor did not go into surge and positive flow was established through the turbine. Opening the shutdown valves which connect the compressor exit to the inlet were anticipated to eliminate the compressor surge problem as these work exactly like bleed valves used on open cycle gas turbines for precisely the same purpose. Why a positive flow was established through the turbine was and remains unclear.... but it does. This allowed for the elimination of the small pump and associated lines and valves. Instead, the heater was brought up to operating temperature, the shutdown (bypass) valves were opened, and the TAC was motored for approximately 2 minutes. During this time a definite change in heater temperature profile was observed and a very small rise in turbine discharge temperature could be observed.
2. The performance of the system was initially very low and analysis of the data indicated that a large internal secondary flow leak(s) was present inside the TAC. The compressor shroud was removed and a leak was found were the capacitance probe electrical leads were brought across the compressor exit flow path. This leak path was eliminated. The compressor shroud was reinstalled and subsequent testing showed that the performance was improved but was still low and analysis of the data indicated internal leakage was reduced be still present.

The TAC was removed from the PCS and fully disassemble. Fixtures were built to leak test the internal TAC cavity and leakage was found to exist where alternator electrical leads and instrumentation wires crossed the compressor flow path radial outboard of the alternator heat exchanger. These leak paths were plugged with RTV and the TAC was reassembled. The TACS was reinstalled in the PCS and the second test sequence was initiated on 26 August 95 and was completed on 31 August 95. During this test sequence 1825 W of electrical power was produced and 5 hours and 25 minutes of hot test time was accumulated. Performance analysis of the test data showed good correlation to the test model. Operation at design conditions was not possible due to the large heat loss from the FiberFrax insulation. During this test sequence the DACS and the PCCU operation were also satisfactorily demonstrated.

Table 9-1 summarizes the significant test points accumulated during Hot Loop testing.

Figure 9-3. Turbine Compressor Temperature Ratio Required to Achieve Closed-Loop System Flow

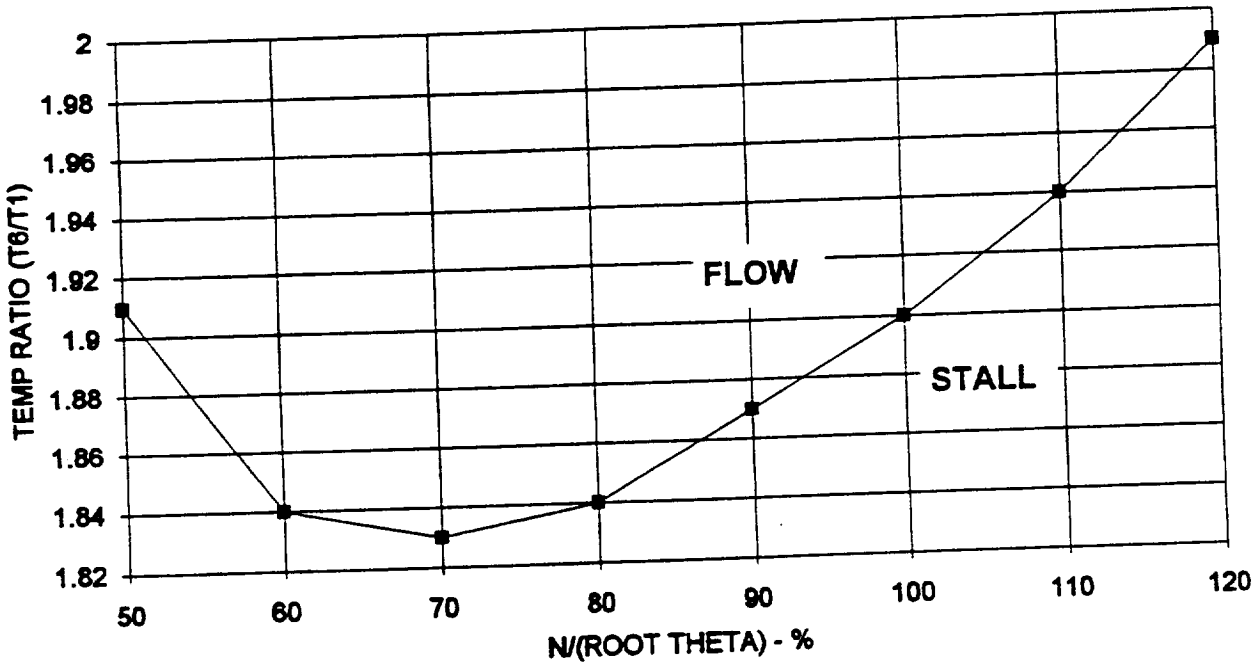

Table 9-1. Runs 83, 84, and 87 (Hot Loop A) and 106 and 108 (Hot Loop B)

TAG No.	PARAMETER	UNITS	RUN 83	RUN 84	RUN 87	RUN 106	RUN 108
HRSCE663	ACCUMULATOR VOLUME	%	4.18	1.83	50.25		
HRSFT628	LIQUID LOOP FLOW	GPH	39.88	39.88	33.24	33.39	37.52
HRSPT627	LIQ LOOP PUMP INLET	PSIA	36.68	35.20	35.70		
HRSPT628	LIQ LOOP PUMP EXIT	PSIA	42.20	41.96	38.34		
HRSTE629	LIQ LOOP COOLER IN	R	454.00	452.02	436.08	433.15	436.788
HRSTE630	LIQ LOOP COOLER EXI	R	570.85	570.16	601.85	581.20	566.002
	MONOPOLE SPD-PCCU	RPM					52004.4
PCSPT500	COMPRESSOR DISCHARG	PSIA	85.87		89.73	86.88	89.876
PCSPT504	COMPRESSOR INLET	PSIA	55.29	59.75	56.63	53.83	55.136
PCSPT508	TURBINE INLET	PSIA	84.46	91.40	88.23	85.25	88.284
PCSPT512	COOLER INLET(GAS)	PSIA	55.70	60.26	57.05	54.17	55.61
PCSPT516	RECEIVER INLET	PSIA	85.78	92.86	89.69	86.68	89.668
PCSPT520	TURBINE DISCHARGE	PSIA	56.23	60.78	57.56	54.68	56.174
PCSPT554	COMP BRG CAVITY	PSIA	73.26	79.20	73.63	70.57	72.59
PCSPT555	COMP BRG CAVITY	PSIA	82.79	89.49	77.41	70.99	72.978
PCSPT556	TURBINE BRG CAVITY	PSIA	81.90	88.51	76.61	70.04	72.01
PCSPT557	TURBINE BRG CAVITY	PSIA	72.06	77.89	72.13	68.10	70.138
PCSSE572	SPEED	RPM	52272.10	52205.42	52621.50	52631.11	52627.7
PCSSE573	SPEED	RPM	52305.01	52270.38	52444.97	52455.77	52456.018
PCSTE501	COMPRESSOR EXIT	R	601.69	599.22	599.84	596.96	600.132
PCSTE502	"	R	602.76	599.83	600.35	597.58	600.806
PCSTE503	"	R	598.77	599.49	599.60	596.32	599.918
PCSTE505	COMPRESSOR INLET	R	458.00	456.32	448.65	446.46	444.342
PCSTE506	"	R	464.52	457.27	453.59	451.19	446.238
PCSTE509	RECEIVER OUTLET	R	1705.82	1782.15	1778.77	1771.35	1860.942
PCSTE510	"	R	1710.87	1790.05	1792.99	1782.24	1874.37
PCSTE513	COOLER INLET(GAS)	R	675.59	683.28	661.29	636.01	627.364
PCSTE514	"	R	675.71	682.73	660.38	634.68	626.752
PCSTE515	"	R	677.21	683.96	661.73	636.42	627.432
PCSTE517	RECEIVER INLET	R	1346.18	1403.32	1417.92	1358.26	1461.71
PCSTE518	"	R	1343.59	1394.19	1409.23	1383.15	1453.542
PCSTE519	"	R	1348.33	1400.82	1415.69		1460.734
PCSTE521	TURBINE DISCHARGE	R	1387.08	1443.78	1470.99	1467.96	1527.516
PCSTE522	"	R	1382.37	1442.68	1470.60	1467.63	1528.048
PCSTE523	"	R	1383.79	1437.92	1466.15	1460.42	1520.644
	TIT-DUCT EXT.	R			1703.79	1676.65	1769.624
	"	R			1692.69		
PCSTE556	COMP BRG TEMP	R	642.97	640.02	666.04	592.27	579.74
PCSTE559	TURB BRG TEMP	R	663.50	660.02	698.18	716.80	720.412
PCSTE560	COMP BRG CAVITY-CS	R	579.59	575.88	558.13		
PCSTE561	COMP BRG CAVITY-TS	R	616.99	613.63	651.02	705.98	698.192
PCSTE562	TURB BRG CAVITY-CS	R	634.55	631.90	648.60	666.17	667.848
PCSTE563	TURB BRG CAVITY-TS	R	669.09	666.28	705.79	738.39	744.832
PCSTE564	THRUST BRG-CS	R	550.32	546.82	564.24	673.50	658.254
PCSTE565	THRUST BRG-TS	R	593.86	591.71	575.35	683.84	670.52
PCSTE566	COMP DISCHARGE	R	600.12	596.41	589.64		
PCSTE567	ALT END TURN	R	637.00	635.89	666.37	684.08	683.34
PCSTE568	ALT FIELD ID	R	636.52	635.40	666.26	684.08	683.29

Runs 83, 84, and 87 (Hot Loop A) and 106 and 108 (Hot Loop B)

PCSTE569	ALT FIELD OD	R	625.92	623.49	639.66	650.00	649.048
PCSTE570	ALT SLOT	R	638.43	637.25	674.37	697.04	697.37
PMCEE108	DC OUTPUT VOLTAGE	VOLTS	120.82	120.30	119.77	117.07	115.112
PMCEE111	PHASE A - RMS VOLTS	VOLTS	55.65	56.89	57.77	58.70	59.266
PMCEE112	PHASE B - RMS VOLTS	VOLTS	55.66	56.50	58.00	58.45	59.18
PMCEE113	PHASE C - RMS VOLTS	VOLTS	55.37	56.43	57.92	58.82	59.314
PMCIE105	ACCY AMPS	AMPS	0.08	0.15	0.15	0.15	0.38
PMCIE106	PROP FIELD AMPS - DC	AMPS	0.19	0.28	0.46	0.57	0.66
PMCIE107	PWM FIELD AMPS - DC	AMPS	0.55	0.51	0.55	0.55	0.56
PMCIE108	OUTPUT AMPS - DC	AMPS	4.17	6.54	10.66	12.52	14.452
PMCIE109	PLR AMPS - DC	AMPS	4.29	6.65	10.81	13.18	15.212
PMCIE110	USER LOAD - DC	AMPS	-0.01	-0.03	0.01	0.01	0.012
PMCIE111	PHASE A - RMS AMPS	AMPS	2.78	4.50	7.78	9.68	11.154
PMCIE112	PHASE B - RMS AMPS	AMPS	3.22	5.04	8.39	10.29	11.852
PMCIE113	PHASE C - RMS AMPS	AMPS	2.94	4.62	7.67	9.81	11.298
	LIQ LOOP HEATER OUT	R	575.40	570.55	603.13		
	ETHYLENE GLYCOL	R	423.86	424.40	416.04	414.55	421.736
PMCTE140	HEATER INLET	R	1655.22	1685.71	1692.46	1686.68	1732.636
PMCTE141	"	R	1737.00	1759.94	1762.84	1756.79	1799.786
PMCTE142	HEATER MID	R	1782.24	1847.92	1846.06	1845.18	
PMCTE143	"	R	1830.07	1898.73	1897.16	1902.83	1900.306
PMCTE144	HEATER EXIT	R	1915.08	2018.72	2009.56	2021.77	2082.518
PMCTE145	"	R	1989.51	2108.05	2103.68	2122.60	2063.978
PMCTE146	HEATER MOUNT- EXIT	R	1115.96	1171.56	1186.06	1007.02	1035.47
RSPDT424	RECUP HP DELTA P	PSID		0.24	0.25	0.24	0.254
	SPEED-PCCU	RPM					52000.678
	Speed Set Point	RPM					51999.08
	ALTERNATOR POWER	WATTS	496.72	800.57	1380.32	1746.77	2032.58
	DC OUTPUT POWER	WATTS	518.32	800.00	1294.71	1542.57	1751.08
							1825.44

9.4.2.2 Testing at NASA Lewis Tank 6

At the completion of the Hot Loop Testing the Power Conversion Subsystem was delivered to NASA Lewis as shown in Figure 9-1. The test cart was used as the shipping fixture and the electric heater was left in place to support the ducting. When the unit was received at NASA Lewis

- the ducts to the electric heater were disconnected by grinding down the attachment welds
- the electric heater was removed and placed in government storage by NASA
- the PCS was lifted off the test cart and placed on the PCS Pallet, which is part of the NASA buildup Assembly Platform (see Section 5)
- the Receiver was mounted to the Pallet
- the PCS ducts were welded to the Receiver
- the PCS/Receiver Pallet was placed into the tank and functionally checked using procedure 41-13166
- the PCS and Receiver were covered with multilayer insulation (see Section 8).

During the installation process only two minor difficulties were encountered and these had to do with the ducting attachment to the receiver. When the ducts were disconnected from the electric heater the receiver outlet duct flange was ground down to far to permit welding to the receiver. A special adapter flange was fabricated in NASA's shop from a spare duct flange. This adapter was welded into the duct and then to the receiver. Secondly, when the PCS was placed on the pallet either the duct interface between the PCS and Receiver was correct of the mounting flange interface between the PCS and the Pallet was correct but not both simultaneously. Rather than spend time investigating this anomaly, the duct interface was established and the PCS mounting flanges were tack welded to the PCS mounting surface in the position that the duct interface dictated. The final installation of the PCS in the tank is shown in Figure 3-1.

System testing was conducted from 12 Dec 94 to 17 Feb 95 as discussed in Section 2. During that testing approximately 36 hours of hot TAC operation was accomplished and a maximum of 2080 electrical watts (ac) were produced at the alternator output terminals. The efficiency of the PCS can be defined by the following equation:

PCS Eff = Alternator Electrical Power Output/Receiver Gas Power Input

Receiver gas power = mass flow * Cp * Receiver delta T. During the maximum power point of the 17 Feb 95 test a PCS efficiency of 29 percent was demonstrated. 2080 W of electrical power was measured and 7137 Btu/hr or gas power was calculated to be delivered from the receiver to the gas.

Operationally the PCS performed according to analytical predictions. Thrust bearing axial capacitance probe measurements indicate that, at design inventory and speed (52,000) the TAC rotor is moving toward the turbine with a force which has the thrust bearing at steady state maximum limits. No margin exits for operating at higher speeds or at higher inventories without jeopardizing the turbine side thrust bearing.

Table 9-2 presents the significant PCS test data taken during the systems testing in Tank 6.

Table 9-2. PCS Data Summary

TAG No.	PARAMETER	UNITS	RUN 108	02/02/95	2/17/95
HRSFT628	LIQUID LOOP FLOW	GPH	37.52	30.02	34.37
HRSTE629	LIQ LOOP COOLER IN	R	437	441	433
HRSTE630	LIQ LOOP COOLER EXI	R	566	596	577
PCSPT500	COMPRESSOR EXIT	PSIA	89.88	90.7	93.46
PCSPT504	COMPRESSOR INLET	PSIA	55.14	55.52	56.39
PCSPT508	TURBINE INLET	PSIA	88.28	87.04	89.67
PCSPT512	COOLER INLET (GAS)	PSIA	55.61	55.89	56.65
PCSPT516	RECEIVER INLET	PSIA	89.67	90.45	93.1
PCSPT520	TURBINE DISCHARGE	PSIA	56.17	56.33	57.2
PCSPT554	COMP BRG CAVITY	PSIA	72.59	72.92	74.48
PCSPT555	COMP BRG CAVITY	PSIA	72.98	73.08	74.68
PCSPT556	TURBINE BRG CAVITY	PSIA	72.01	72.14	73.57
PCSPT557	TURBINE BRG CAVITY	PSIA	70.14	69.79	71.22
PCSSE572	SPEED	RPM	52000	52000	52000
AVG'D VALUE	COMPRESSOR EXIT	R	600	597	584
AVG'D VALUE	COMP. INLET (TYPE T)	R	445	445	433
AVG'D VALUE	RECEIVER OUTLET	R	1868	1880	1915
AVG'D VALUE	COOLER INLET (GAS)	R	627	642	631
AVG'D VALUE	RECEIVER INLET	R	1459	1559	1581
AVG'D VALUE	TURBINE DISCHARGE	R	1526	1588	1610
AVG'D VALUE	COMP. INLET (TYPE K)	R		449	437
PCSTE556	COMP BRG TEMP	R	580	575	564
PCSTE559	TURB BRG TEMP	R	720	701	689
PCSTE561	COMP BRG CAVITY-TS	R	698	689	679
PCSTE562	TURB BRG CAVITY-CS	R	668	651	638
PCSTE563	TURB BRG CAVITY-TS	R	745	729	716
PCSTE564	THRUST BRG - CS	R	658	649	638
PCSTE565	THRUST BRG - TS	R	671	667	654
PCSTE567	ALT END TURN	R	683	673	666
PCSTE568	ALT FIELD ID	R	683	673	666
PCSTE569	ALT FIELD OD	R	649	638	628
PCSTE570	ALT SLOT	R	697	693	682
RSPDT424	RECEIVER DELTA P	PSID		3.28	3.46
PMCEE108	AC POWER (PF=1.00)	WATTS	2032	1833	2129

9.5 Bibliography

DOCUMENT NUMBER	DOCUMENT TITLE	DOCUMENT SUBTITLE
41 11529	TAC DISASSY INSTRUCT	
41 12010	TAC REFURB REPORT	INITIAL SUBMIT
41 12095	TEST PLAN TAC	CDR UPDATE
41 12098	TEST PLAN HOT LOOP A	CDR UPDATE
41 12099	TEST PLAN HOT LOOP B	CDR UPDATE
41 12103	TAC DESIGN PACKAGE	CDR INPUT
41 12104	PCS DESIGN PKG	CDR INPUT
41 12112	TEST PLAN S/D VALVE	CDR SUBMIT
41 12162	PCS VIEWGRAPH	CDR INPUT
41 12181	TAC VIEWGRAPHS	CDR INPUT
41 12251	TAC ASSY INSTRUCT	
41 12412	TEST PROCEDURE	TAC
41 12923	TEST PROCEDURE	HOT LOOP B
41 12967	TEST PROCEDURE	HOT LOOP A
41 12969	TEST REPORT PCS	HOT LOOP A
41 13085	TEST REPORT PCS	HOT LOOP B
41-13166	TANK 6 INSTALLATION	PROCEDURE
41-13692	TANK 6 TEST REPORT	PCS
ATP3605427XO	TEST PROCEDURE	SHUTDOWN VALVE
3793301	PCS ASSEMBLY DWG	
3793271	TAC ASSEMBLY DWG	
41-12010	TAC REFURB REPORT	INITIAL SUBMIT
41-12095	TEST PLAN-TAC	CDR UPDATE
41-12098	TEST PLAN-HOT LOOP A	CDR UPDATE
41-12099	TEST PLAN-HOT LOOP B	CDR UPDATE
41-12103	TAC DESIGN PACKAGE	CDR INPUT
41-12104	PCS DESIGN PKG	CDR INPUT
41-12112	TEST PLAN-S/D VALVE	CDR SUBMIT
41-12162	PCS VIEWGRAPH	CDR INPUT
41-12181	TAC VIEWGRAPHS	CDR INPUT
41-12251	TAC ASSY INSTRUCT	
41-12412	TEST PROCEDURE	TAC
41-12923	TEST PROCEDURE	HOT LOOP B
41-12967	TEST PROCEDURE	HOT LOOP A
41-12969	TEST REPORT-PCS	HOT LOOPA
41-13085	TEST REPORT-PCS	HOT LOOP B
41-13166	TANK 6 INSTALLATION	PROCEDURE
41-13692	TANK 6 TEST REPORT	PCS
ATP3605427X0	TEST PROCEDURE	SHUTDOWN VALVE

10. POWER CONDITIONING AND CONTROL UNIT

This section discusses the final design, fabrication, and testing of the Power Conditioning and Control Unit from the CDR through final integration at Tank 6, NASA Lewis.

10.1 Summary and Conclusions

The Power Conditioning and Control Unit was fabricated essentially in accordance with the hardware design shown at the CDR. Some minor design changes were incorporated during fabrication to improve accessibility and modularity of the various subassemblies in the Heat Sink Assembly. Figure 10-1 shows PCCU outside Tank 6.

Two sets of printed circuit wiring assemblies, referred to as the B boards and the C boards, were fabricated and delivered to NASA. The B boards were prototype boards used to prove out the hardware design of the printed circuits. These boards were fully socketed to allow easy trouble shooting and parts replacement. The C boards were designed for use in the vacuum environment of Tank 6, and contained soldered in components, with the exception of programmable parts such as PALs and PROMs. The C boards also incorporated an aluminum heat sink under all the electronic parts to conduct heat away to the n-heptane-cooled heat sink, as described at the CDR.

During development of the PCCU, certain minor modifications were required from the design presented at the CDR, but the final product performed essentially as was stated at the CDR. These modifications are explained in Section 10.2.

The PCCU in its final configuration is performing in accordance with its design goals, except for its ability to operate in the cold vacuum of Tank 6. Speed control, voltage regulation, start performance, and user load/PLR load sharing function in accordance with all design goals. As discussed below in Section 10.2, the PCCU failed to function while operating in the cold vacuum of Tank 6. In lieu of troubleshooting the PCCU to determine the reasons for this, it was decided that the SDGTD Project goals could be met by simply operating the unit with the PCCU outside the vacuum tank. This is the way it is operating today.

10.2 Design Changes After CDR

The PCCU was fabricated essentially in accordance with the schematic design presented at the CDR and subjected to development tests in the Tempe test facility. As a result of those tests, and additional tests after installation at NASA Lewis, some changes were incorporated into both the schematic design and the mechanical design of the unit. The following sections define those changes.
Voltage Regulator PWM Driver

Figure 10-1. Power Conditioning and Control Unit (PCCU)

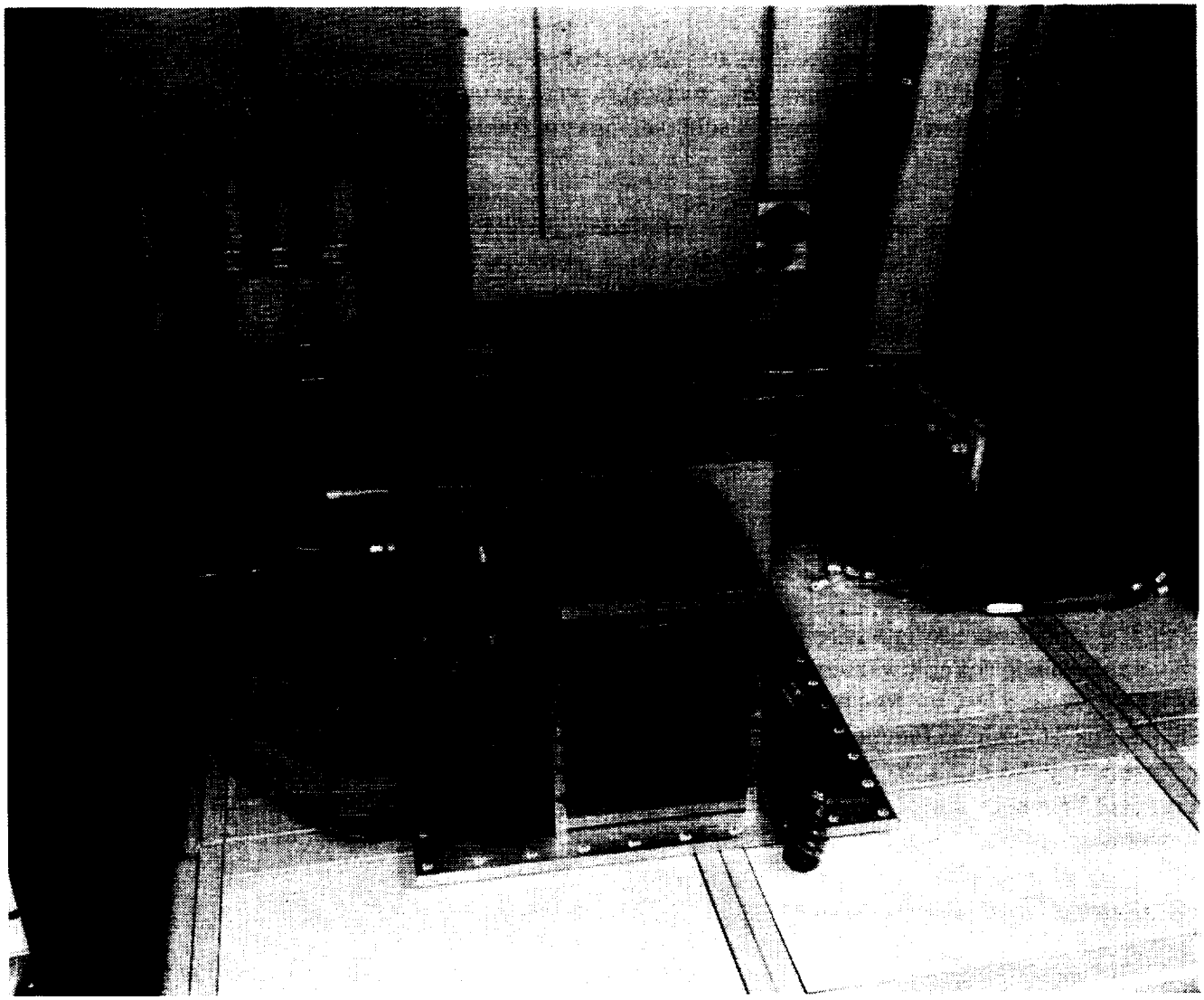

The configuration of the Voltage Regulator Pulse Width Modulated (PWM) Driver circuit was changed to improve output power quality.

As originally configured at the CDR, the TAC had two sources of field current: current transformers wrapped around the alternator output power leads, and the output dc voltage of the PCCU in series with a PWM transistor.

Current from the first source is essentially proportional to the load on the system and contributes nothing to the ripple and noise at the output terminals of the system.

The current from the second source is drawn from the output of the system after the output voltage has been filtered by the LC filter at the output of the main rectifier. This PWM current tended to have an adverse effect on power quality due to the approximately one half amp of field current being drawn in pulses from the output.

To correct this, a separate rectifier/filter was installed to provide power to the PWM transistor. This rectifier filter was located upstream of the main rectifier/filter and its effect on output power quality proved to be negligible.

10.2.1 PCCU Single Point Ground

As configured at the CDR, the PCCU was intended to set up an isolated local single point ground at the output of its rectifier, which was to be connected to earth ground via wiring to the earth ground in the ICPC. Testing at Tank 6 showed that this configuration was not acceptable, as the PCCU experienced noise problems that were eliminated when the PCCU's earth ground was moved to the vicinity of the PCCU. The local single point ground in the PCCU is currently connected to the PCCU chassis which is tied to the facility ground near (within 6 feet of) the PCCU.

10.2.2 Thermally Conductive Grease

As configured at the CDR, all power transistors in the PCCU were to be dry mounted to their heat sinks. This approach was selected under the mistaken belief that the use of thermally conductive grease in a vacuum would not be permitted due to outgassing considerations. The first test of the PCCU in a warm vacuum (i.e., no cold walls) showed that that was not a good decision, as one of the PLR drive transistors failed due to overheating. The PCCU was removed from the tank, and all PLR drive transistors were treated with thermally conductive grease.

10.2.3 Fabrication Summary

Two major assemblies make up the PCCU: a card file assembly and the heat sink assembly. Each assembly is bolted to a common n-heptane cooled base plate for temperature control in a vacuum.

Fabrication of the PCCU was straight forward with no problems worth noting. Two sets of printed wiring boards were fabricated. The prototype set, or B boards, included sockets for the electronic parts and were fabricated to prove out functionality of the circuit board design.

The vacuum compatible C boards were fabricated with all components except the programmable components soldered in place, with an aluminum heat sink installed between the parts and the board to conduct away heat. Sockets were used for all programmable parts.

The B boards and C boards are completely interchangeable in lab ambient conditions.

10.2.4 Component Testing Summary

Prior to delivery to NASA Lewis, the PCCU was completely tested at the test facility in Tempe using first the SIPS to simulate the TAC, then the ATR, and finally the Hot Loop Test setup.

Power quality tests were conducted using the ATR as the power source. All power quality test objectives were met. The user load simulator was shipped to Tempe for testing with the PCCU and ATR prior to shipment to NASA Lewis.

Integration tests at NASA Lewis using the SIPS, ATR, and TAC were successful.

Test of the PCCU in the vacuum tank revealed the need for thermally conductive grease under power devices. This became apparent when one of the PLR driver transistors failed after initial testing in the vacuum.

Cold testing of the PCCU revealed a problem when the PCCU n-heptane-cooled cold plate was cooled below 0 °F. For reasons that were never determined, the PCCU lost communication with the DACS at that point, only to regain communications when the cold plate was returned to ambient.

Because the test objectives of the SDGTD project could be met with the PCCU controlling the system while located outside the vacuum tank in the lab ambient conditions, the decision was made to not take the time to test the PCCU under cold conditions again, but to continue the project with the PCCU outside the tank.

10.2.5 Bibliography

The following AlliedSignal reports contain material related to the PCCU development and test project:

41-11725	TEST PLAN
41-11764-5	PDR REVIEW CHARTS
41-12044	PCCU SOFTWARE DEVELOPMENT PLAN
41-12083	PCCU SOFTWARE REQMTS DOC
41-12084	PCCU SOFTWARE DESIGN DOC
41-12094	TEST PLAN PCCU S/W
41-12097	TEST PLAN PCCU
41-12105	PCCU DESIGN PACKAGE
41-12158	PCCU VIEWGRAPH
41-13227	TEST REPORT PCCU

11. DATA ACQUISITION AND CONTROL SUBSYSTEM

11.1 Summary And Conclusions

11.1.1 Summary

11.1.1.1 Equipment

Instrumentation Console (IC) and the Control Room Console (CRC).

The IC assembly consists of the following major components:

- Equipment Rack, 2 each
- Instrumentation Console Personal Computer (ICPC), 1 each
- Monitor, 1 each
- Data Acquisition Chassis, 3 each
- Heater Controller (P16M-04-018), 1 each
- Signal Conditioning Buffer (P16M-13-115), 1 each
- Liquid Coolant Pump Controller (P16M-04-017), 1 each
- Capacitance Probe Signal Conditioner, 4 each
- IEEE-488 Extender, 1 each
- Sorensen Power Supply, 2 each
- Lambda Power Supply, 2 each
- BNC Lexan Bulkhead Adapter Panel (P16F-07-117), 1 each
- Patch Panel, 2 each

The CRC assembly consists of the following major components:

- Equipment Rack, 5 each
- Data Display Personal Computer (DDPC), 4 each
- Monitor, 4 each
- Printer, 1 each
- Analog Instrumentation Panel (P16M-13-114), 1 each
- Speaker Panel (P16M-01-186), 3 each
- Speaker Panel w/Volume Control (P16M-01-187), 1 each
- Mass Storage Backup Unit (Tape), 1 each
- Parch Panel, 2 each

Note: See drawing STE7406967 for the location of the components within the assemblies

11.1.1.2 Functions

The DACS provides the following functions:

a. Control:
   1. Control the operation of the shutdown (compressor bypass) valves
   2. Liquid control loop pump power and speed control
   3. Liquid control loop auxiliary heater power and temperature control
   4. TAC speed control via command set point to PCCU
   5. SDGTD output voltage control via command set point to PCCU
   6. User connect/disconnect from the SDGTD
   7. Sun light shutter open/close
   8. Control the operation of the gas charge (PCS) valve
   9. Start inverter control interface
b. Provide alternate power for the PCCU when the SDGTD is not operating.
c. Collect, process, display and store the data acquired from the testing.
   1. Low rate of 1 scan/5 seconds (low speed)
   2. High rate of 50 scans/1 second (high speed)
d. Provides CRT monitoring and man-machine interface for the test monitoring and control.
e. Provide discrete panel meters to monitor the following:
   1. PCCU output voltage
   2. Total output current
   3. TAC speed
   4. Turbine inlet temperature
   5. Compressor inlet temperature
   6. Liquid coolant loop flow
f. Provide buffered outputs for the following analog signals:
   1. TAC speed
   2. Radial and axial shaft runout
   3. Alternator phase A, B & C line-neutral voltage
   4. Alternator field 1 & 2 voltage
   5. Alternator field 1 & 2 current
   6. PCCU output voltage
   7. Accessory load current
   8. Total output current
   9. Parasitic load total current
   10. User load current
   11. Alternator phase A, B & C current

The DACS software provides the following tasks:

a. Data acquisition and storage
b. On line data analysis and presentation
c. Orbital operation at constant speed
d. Orbital operation at constant power
e. Start-up and shut-down sequencing
f. Data communication
g. Calibration
h. Alarm processing
i. System control
j. Hard copy output
k. Security

11.1.2 Conclusions

The following is a lessons learned for more efficient processing of acquired data:

The original design of the DACS required the initial storage of the acquired data in engineering units. This required the conversion of each parameter using a 5th order polynomial equation for temperatures and an mx + b equation for all other parameters. These real time calculations performed by the ICPC take large amounts of processor time.

A more efficient method would have been to take the raw data and store this data with a conversion file that would have included the calibration data, engineering units, data type and thermocouple type. To perform the alarm functions, each alarm function would be back calculated to the raw voltage level for the limit specified at the start up of the ICPC. Each individual DDPC would then acquire that conversion file and perform the polynomials and slope formulas for each of the parameters and then display the data appropriately. Any post analysis would also require the same conversion file.

If this method had been used, the overall load on the ICPC processor would have been 30 percent less.

In conclusion, with the exception of the DACS high scan rate the DACS fulfills all requirements set forth in the Data and Control Subsystem, Solar Dynamic Ground Test Demonstrator Specification (N10121).

11.2 Design Changes After Critical Design Review (CDR)

Note: Figure 11-1 is the block diagram presented at CDR. Figure 11-2 is the block diagram for the final configuration.

Control function changes after CDR:

- At CDR, it was stated that the DACS would control the BAP and LUP pressure transmitter box temperatures through a heater element located in each of these units. After CDR another means of controlling the pressure transmitter temperature has been implemented. The LUP coolant is kept at a constant temperature prior to, and during, the running of the PCS. It was decided to flow the LUP coolant through a block to which the pressure transmitters are attached. This keeps the transmitters at a constant temperature which is within their stated operating parameters and eliminates the need for the temperature control loops described at CDR.
- A switch was added to the CRC, Analog Instrumentation Panel to enable or disable the contactor switch located in the SIPS.
- At CDR, it was proposed that the SIPS be controlled by a discrete IEEE-488 card located in the ICPC and the ELSS and SSS be controlled by another IEEE-488 card located in the ICPC. The final configuration has the SIPS, ELSS and SSS all controlled by a single IEEE-488 card located in the ICPC and the other IEEE-488 card has been removed from the ICPC.
- The IEEE-488 Extender Card originally located in the CRC has been relocated in the ELSS rack. The IEEE-488 cable runs directly to the ELSS rack and bypasses the CRC.
- The network communication between the computers of the DACS, CRC and IC proposed at CDR was the IEEE-488. The present configuration uses an Ethernet network for communication.
- A single power supply in the IC was proposed to drive the PCS Shut Down Valves and the PCS Gas Charge Valve. The final configuration uses one power supply to drive both Shut Down Valves and another to power the Gas Charge Valve. Both power supplies are located in the IC.

Measurement parameters changed after CDR:

a. Measurement sampling rates from CDR to the final configuration are as follows:
   1. CDR:
      (a) Low sample rate of 1 scan/10 seconds (minimum)
      (b) High sample rate of 100 scans/1 second (minimum)
   2. Final released form:
      (a) Low sample rate of 1 scan/5 seconds (minimum)
      (b) High sample rate of 50 scans/1 second (minimum)
b. Compressor inlet temperature was added to the CRC, Analog Instrumentation Panel.
c. Strain measurements located on the Concentrator Subsystem were removed. Consequently, the number of SCXI chassis in the IC decreased from four to three and both an AT-MIO-16X data acquisition card and PC-DIO-24 card in the ICPC were removed.
d. The DACS software does not compute the available energy reserves.
e. The LUP Accumulator Volume parameter was added.

Figure 11-1. DACS - Block Diagram CDR Configuration

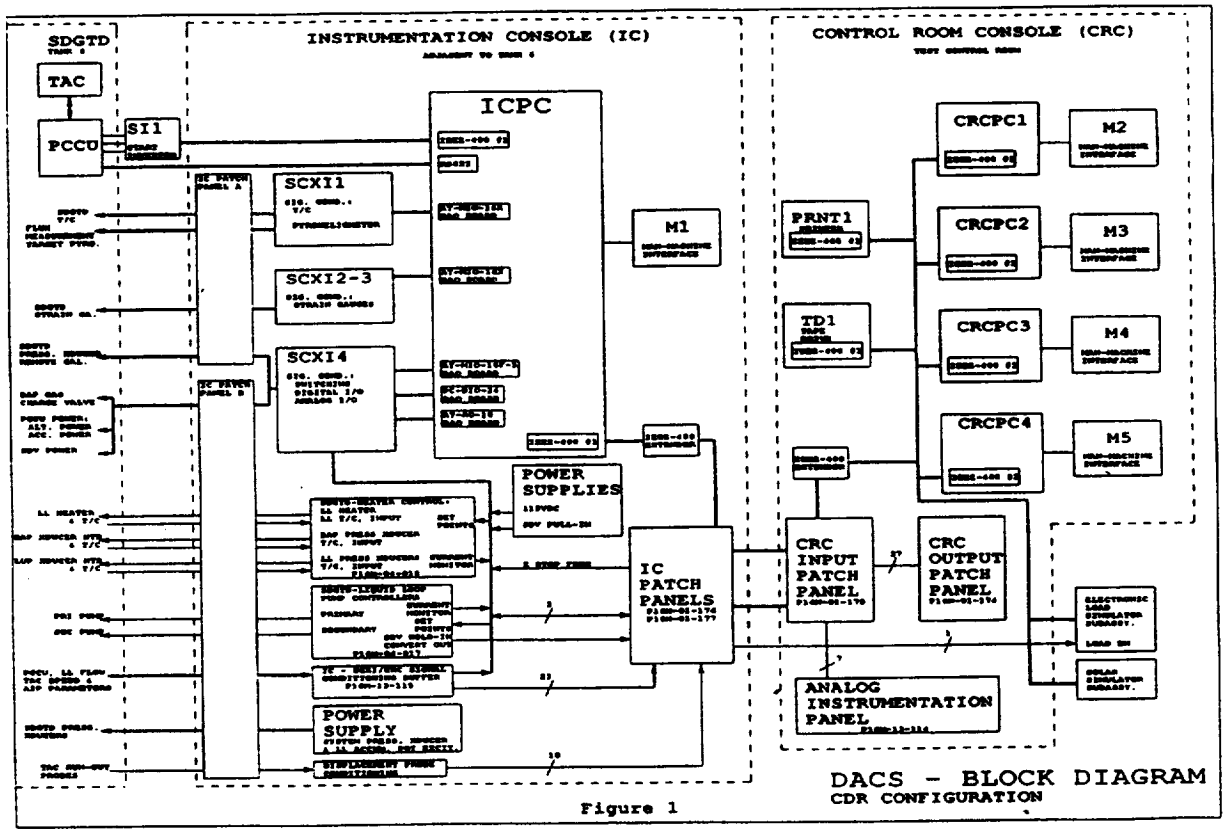

Figure 11-2. DACS - Block Diagram Final Configuration

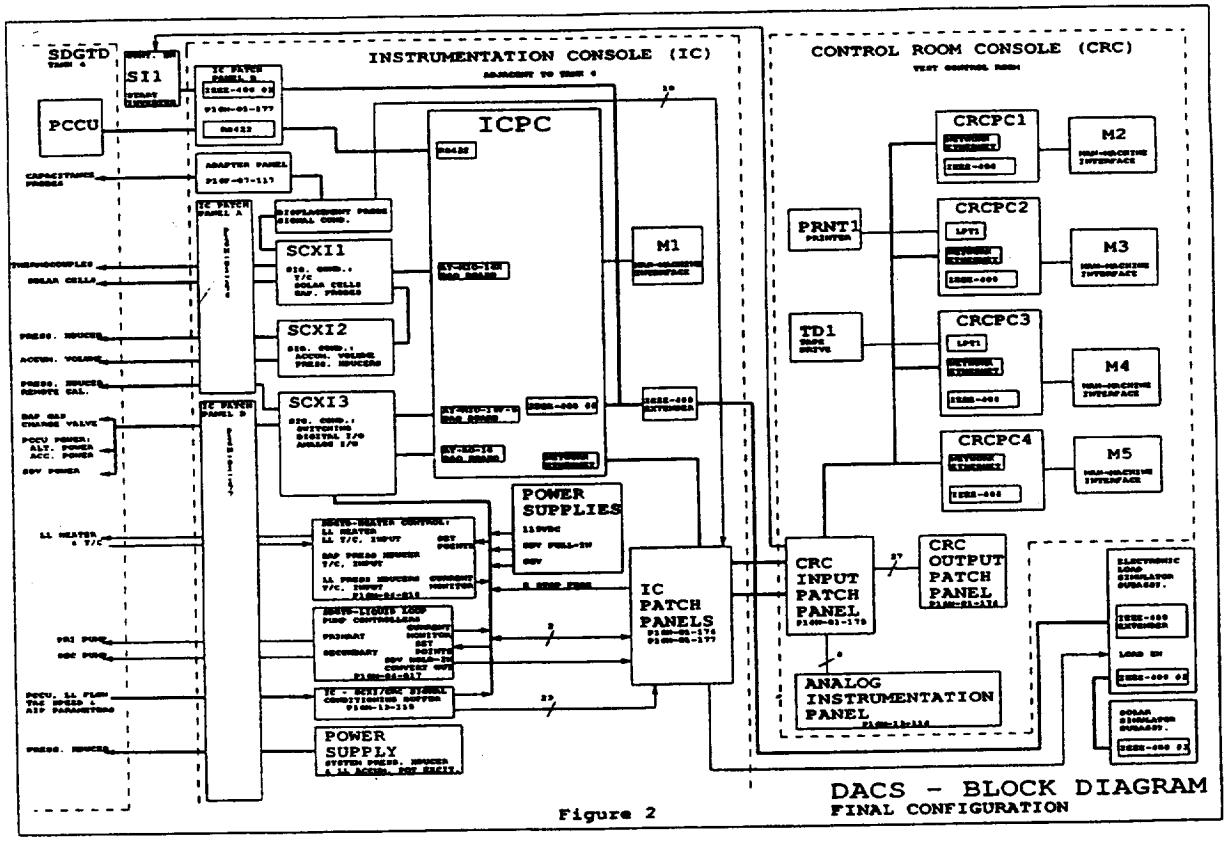

f. The instruments for measurement of light intensity on the Concentrator Subsystem were changed from pyroheliometers to solar cells.
g. It was proposed at CDR that all thermocouples monitored by the DACS be the ungrounded type. The final configuration of thermocouples monitored by the DACS contains both grounded and ungrounded types. The Concentrator Subsystem is the only subsystem in the final configuration to contain ungrounded types exclusively.
h. The conditioned signals of the capacitance probes monitoring the TAC shaft run-out were to go to the CRC Output Patch Panel exclusively in the CDR configuration. In the Final Configuration these signals are also being monitored by the ICPC at the low sample rate for display on the CRC Custom Screens.

11.3 Fabrication Summary

There were no major unexpected or unanticipated problems which occurred in the fabrication of the DACS hardware or software which are noteworthy.

11.4 Component Testing

The DACS software and hardware were tested per the Software Test Plan (41-12093) and the Certification Test Plan (41-13165) for the Data Acquisition and Control Subsystem Software.

11.5 Software Discussion

DACS Software

National Instruments, LabView for Windows, provided a unique environment to generate the DACS software at an impressive rate. LabView allowed for rapid software changes, necessary with the dynamics of the project. The programming concepts of LabView were found to be different from other languages and took some time to get use to. In addition, National Instruments released four upgrades of LabView during the life of this project. Each new release carried its share of bugs that had to be overcome from file access techniques, memory management, display driver conflicts and printing. Microsoft Windows for Workgroups provided a perfect environment for the software. The workstation network environment, allowed for transparent use of the network and the data could easily be imported to MS Office packages. The structure of the ICPC software is shown in Figure 11-3. Figure 11-4 shows the software structure of the TCPC. The man-machine interface is shown in Figure 11-5. The control of the system and presentation of data was accomplished through the use of touch screen monitors. The primary control screen is shown in Figure 11-6 while the overall system data screen is presented in Figure 11-7. Numerous screens, defined in Figure 11-5, were available for component data presentation, graphical data plots, file management, and alarm and password control.

Figure 11-3. ICPC Software Structure

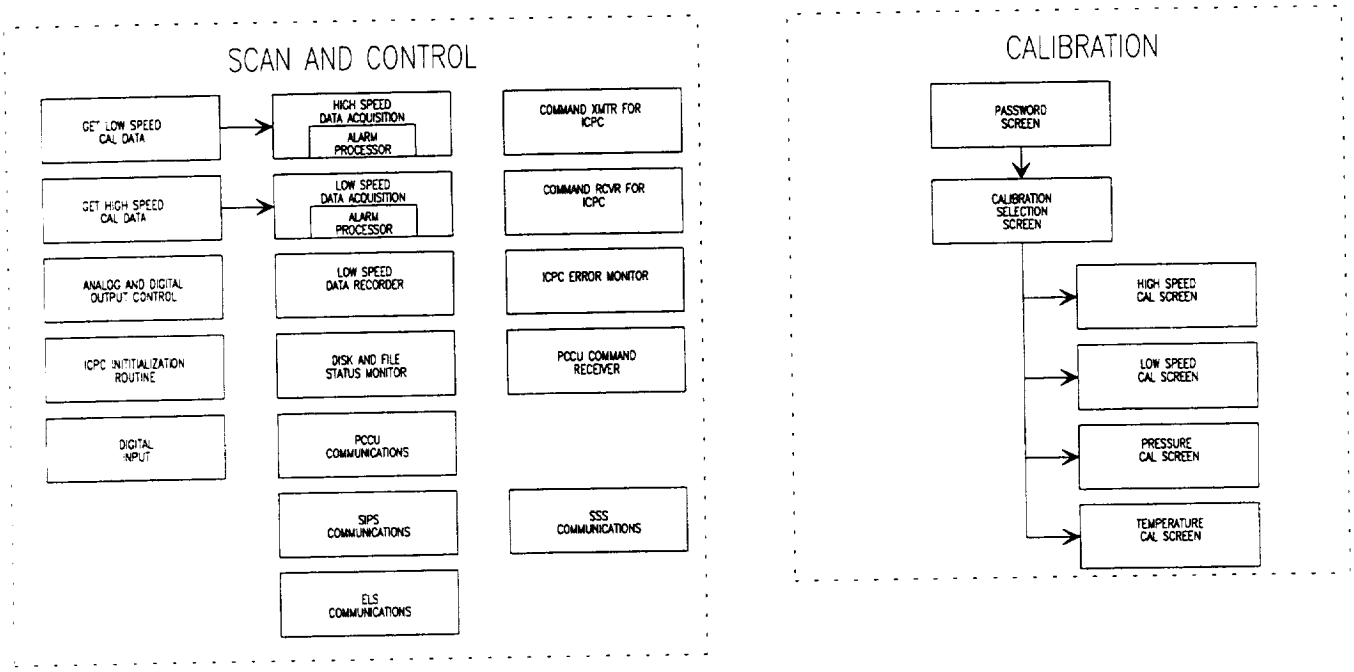

Figure 11-4. TCPC and DDPC Software Structure

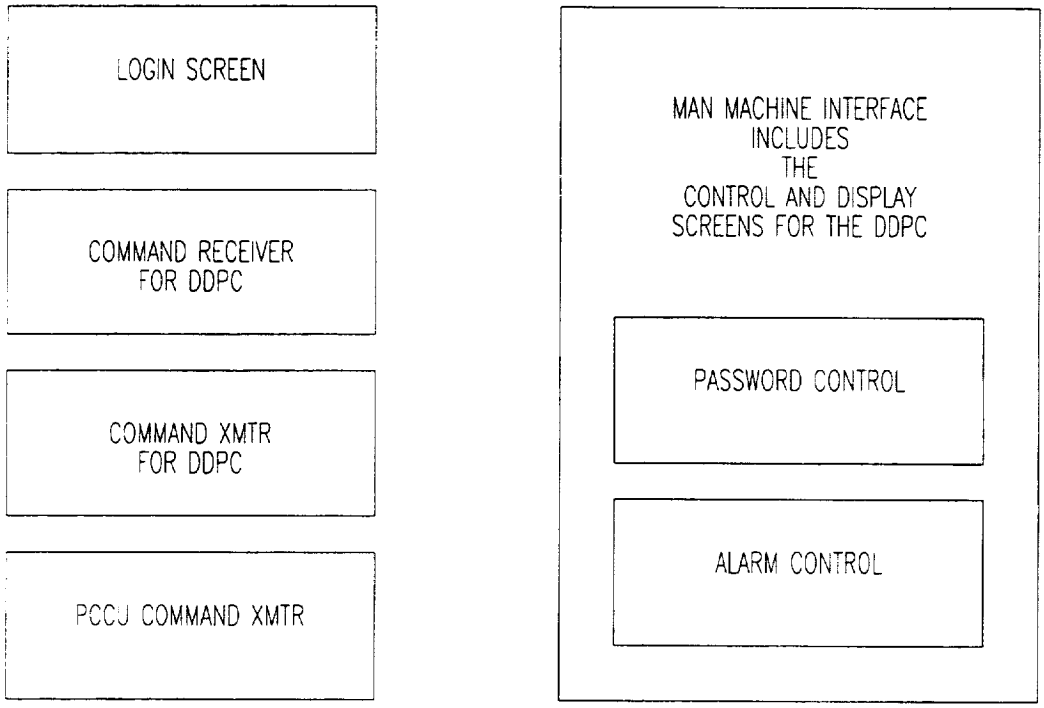

Figure 11-5. TCPC and DDPC Man Machine Interface Menu Flow

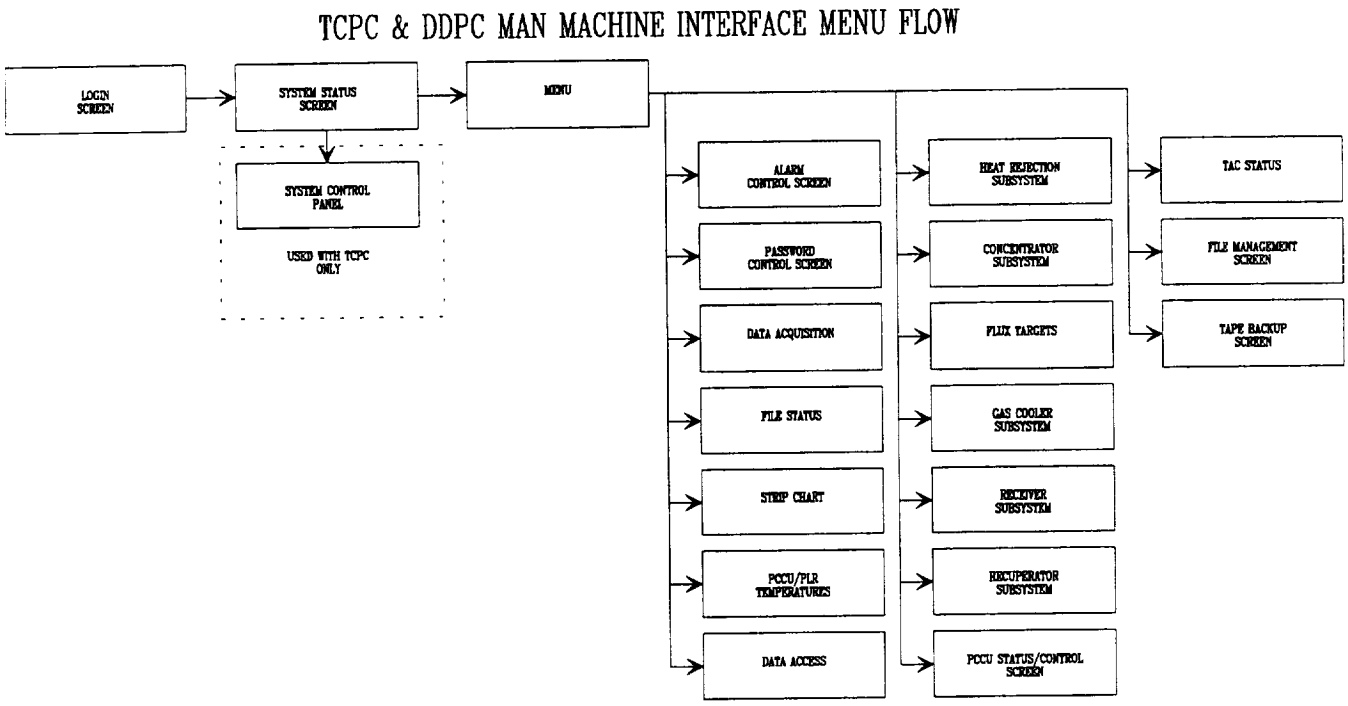

Figure 11-6. System Control Screen

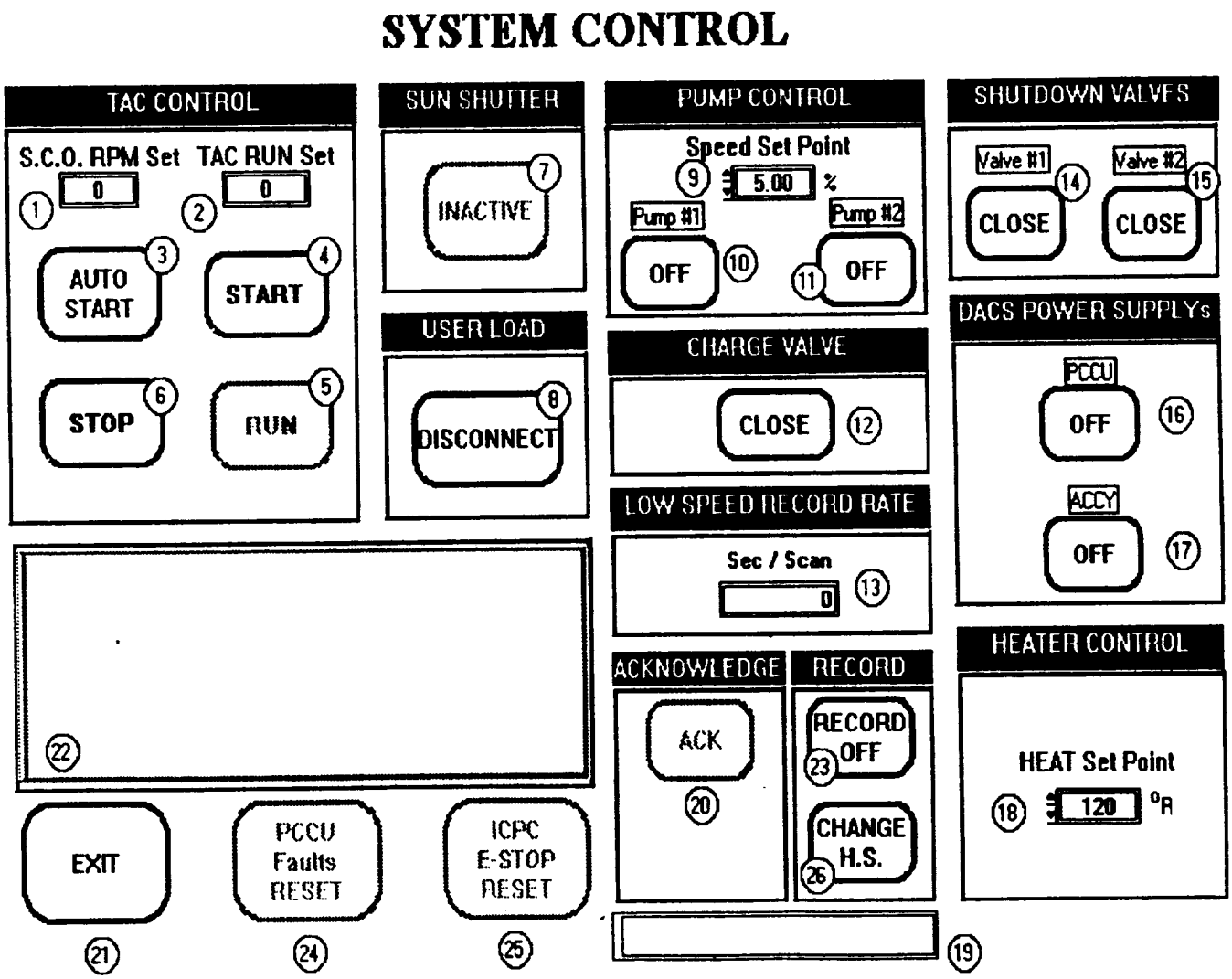

Figure 11-7. System Status Screen

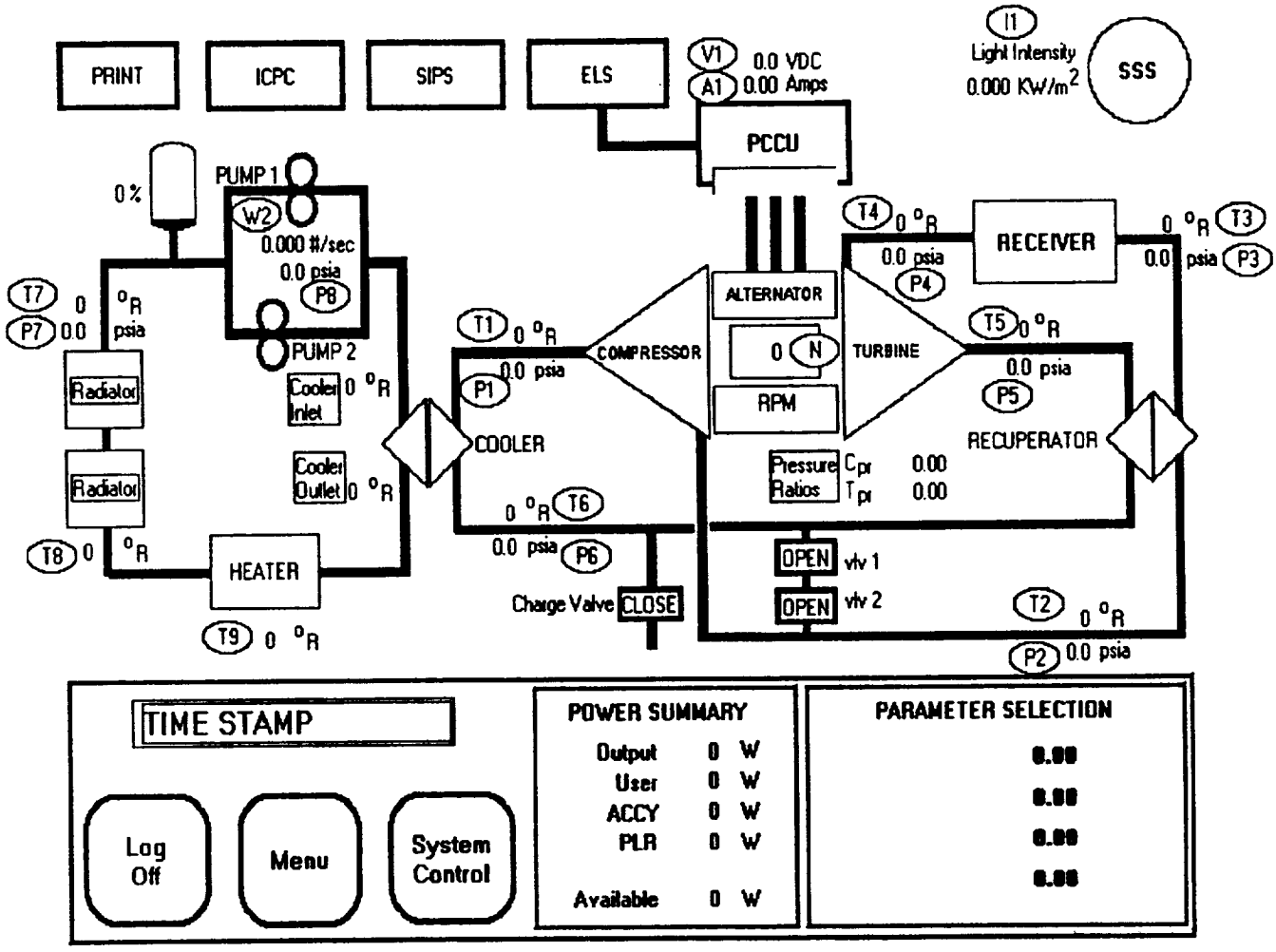

The DACS software initial design started with the primary communication between computers as GPIB, which is a well known bus used in test equipment.

However, it was learned that the National Instruments GPIB boards would cause the computer to stop all operation while waiting for a response from the GPIB board. The use of a network looked to better suit the needs. Other areas of change included the removal of the orbital performance screen and adding a time vs. amplitude strip chart screen. The structure of the software was changed so only one general menu was used on the TCPC computers. For convenience the alarm control, file status, communication status and data acquisition screens were moved from the ICPC to the TCPCs.

The primary difficulty associated with software design was ICPC processor time or the lack of same. On reflection, the software design could have been simplified to allow the ICPC to have more time available. The ICPC was designed to acquire the raw data and immediately perform the calculations to convert the data to engineering values. The TCPCs could have performed data conversions, allowing more processor time available for other processes.

11.6 Bibliography

11.6.1 DACS Software Documentation Compendium

41-12071 Software Requirements Specification for the Data Acquisition and Control Subsystem Software, Solar Dynamic Ground test Demonstrator. AlliedSignal AES, Tempe, Arizona

41-12092 Software Design Document for the Data Acquisition and Control Subsystem Software, Solar Dynamic Ground test Demonstrator. AlliedSignal AES, Tempe, Arizona

41-12093 Software Test Plan for the Solar Dynamic Ground test Demonstrator Data Acquisition and Control Subsystem Software. AlliedSignal AES, Tempe, Arizona

41-13165 Certification Test Plan for the Data Acquisition and Control Subsystem Software, Solar Dynamic Ground test Demonstrator. AlliedSignal AES, Tempe, Arizona

41-13428 Version Description Document for the Data Acquisition and Control Subsystem Software, Solar Dynamic Ground test Demonstrator. AlliedSignal AES, Tempe, Arizona

11.6.2 DACS Hardware Documentation Compendium

AlliedSignal Generated Documents:

41-12604 System Calibration Procedure for the Solar Dynamic Ground Test Demonstrator Data Acquisition and Control Subsystem AlliedSignal AES, Tempe, Arizona

41-12088 Uncertainty Analysis for the Data Acquisition and Control Subsystem of the

	Solar Dynamic Ground Test Demonstrator AlliedSignal AES, Tempe, Arizona
42-1238	IC-SCXI/CRC Signal Conditioning Buffer (P16M-13-115) Checkout and Alignment Procedure, AlliedSignal AES, Tempe, Arizona
N10121	Data Acquisition and Control Subsystem (DACS), Solar Dynamic Ground Test Demonstrator. Rockwell International Corporation, Rocketdyne Division, Canoga Park, California
P16F-07-117	BNC Lexan Bulkhead Adapter Panel
P16M-01-007	SDGTD - DACS Drawing Tree
P16M-04-017	SDGTD - Liquid Coolant Pump Controls
P16M-04-018	SDGTD - Heater Control LCL and BAP & LUP Pressure Transducers
P16M-06-036	SDGTD - DACS: Instrumentation Console (IC) Layout
P16M-13-114	Analog Instrumentation Panel (AIP)
P16M-13-115	IC - SCXI/CRC Signal Conditioning Buffer
P16M-15-033	SDGTD - DACS System Block Diagram
P16M-20-038	SDGTD - DACS: Wiring
P16N-01-174	Control Room Console (CRC) Output Patch Panel
P16N-01-175	Control Room Console (CRC) Input Patch Panel
P16N-01-176	SDGTD - DACS IC Patch Panel A
P16N-01-177	SDGTD - DACS IC Patch Panel B
P16N-01-186	SDGTD Speaker Panel
P16N-01-187	SDGTD Speaker Panel W/Volume
STE7406967	SDGTD - (DACS)

OEM Generated Documents:

320266-01 DATE2-93	National Instruments: SCXI, AT-MIO-16F-5 User's Manual
320488-01 DATE1-93	National Instruments: SCXI, AT-MIO-16X User's Manual
320379-01 DATE12-92	National Instruments: SCXI, AT-AO-6/10 User's Manual
320426-01 DATE3-93	National Instruments: SCXI-1121 User's Manual
320513-01 DATE12-92	National Instruments: SCXI-1160 User's Manual
320408-01 DATE11-92	National Instruments: SCXI-1100 User's Manual
320423-01 DATE10-92	National Instruments: SCXI-1000/1001 User's Manual
320576-01 DATE1-93	National Instruments: SCXI-1163 User's Manual
320572-01 DATE1-93	National Instruments: SCXI-1162 User's Manual
320424-01 DATE11-91	National Instruments: SCXI-1180/1181 User's Manual
IM-LLS-6000 REV. B	Lambda LLS-6040 Power Supply User's Manual
1063986	SORENSEN DCS 150-7 Power Supply User's Manual
10997ML-02 REV. A	NEWPORT METERS User's Manual

12. LIQUID UTILITIES PALLET (LUP)

12.1 Summary and Conclusions

The Liquid Utilities Pallet is a subsystem which conditions the components necessary to condition the fluid (n-heptane) in the waste heat removal loop. The LUP, installed below the radiator panels, is shown in Figure 7-1. No attempt was made to make any of this equipment space prototypic. The project objective was to provide the needed functions as inexpensively as possible. Overall, the LUP did provide the functions required, was low cost, and did not develop any appreciable problems. The components contained within the LUP included:

- Redundant pumps with commercial brushless dc motors
- Accumulator
- Flowmeter
- 6 kWe heater
- Cold plate for heat sinking pressure transducers
- Thermocouples and pressure transducers (4)

The pump was a magnetically driven Tuthill gear pump (P/N B9045 MC-B6729). The brush type dc motor supplied by Tuthill was removed and replaced with a Inland brushless dc motor (P/N RBEH - 01200). These brushless dc motors were driven by an Inland controller (P/N BLS-1500-170/8/12-CL-15) which was mounted outside the vacuum tank and contained within the DACS. To reduce cost these motors were operated open loop and no speed feedback control was implemented.

The Accumulator was a custom designed unit provided by Metal Bellows Inc. The accumulator was placed within the loop to accommodate the expansion and contraction of the fluid due to thermal expansion changes of the liquid loop components and of the fluid. The sizing analysis which was done at CDR showed that hot side expansion approximately equaled cold side contraction. We did not find this to be true during test and consistently the contraction of the cold side components was much greater than the expansion of the hot side resulting in complete depletion of the accumulator. An accumulator with larger capacity then the SDGTD accumulator (30 in^3) would be desirable. The SDGTD accumulator design provided adequate proof pressure capability of the exterior housing to assure that the accumulator did not leak. However, once assembled, the bellows internal to the accumulator could not tolerate high overpressures. One accumulator was damaged (failed bellows) when attempting to proof pressure (at 150 psig) the complete liquid loop during the radiator acceptance test at Loral Vought. The remaining accumulator should not be operated at a maximum pressure of 50 psia and should not be exposed to system proof pressures above 75 psia.

The electric heater was added to the liquid loop to prevent freezing of the radiator when exposed to the liquid nitrogen cold walls of Tank 6 and the test unit was not operating. It was sized so that it could also be used to provide a thermal input larger than anticipated from the Brayton cycle cooler. The heater was then used as the heat source need to conduct radiator acceptance testing at Loral Vought and radiator/Tank 6 integration tests at NASA LeRC. This unit was designed by AlliedSignal so that n-heptane did not come in contact with electric heating elements. Heating elements were commercial

Watlow heating elements operated at 110 Vac to prevent formation of corona. Heating elements appear to have a life of approximately 100 hours when operated near maximum power. Resistance checking elements is periodically accomplished to determine when replacement is required. This unit worked as anticipated.

12.2 Design Changes After CDR

Two changes were incorporated into the LUP after CDR:

1. Redundant pump assemblies connected in parallel are used within the LUP to provide test continuity in case one pump fails. To prevent leakage through the non-operating pump check valves were installed downstream of each pump. One of these check valves failed during tank operation. Each pump has a volumetric capacity much larger than the design flowrate and the minor leakage through the non-operating gear pump was consider acceptable. The check valves were then eliminated as unnecessary.
2. At the time of CDR it was thought that the pressure transducers within the LUP would require heating to maintain them at temperatures consistent with good linearization. However, it was subsequently learned that the transducers selected consumed approximately 2 W of electrical power and would get hot in a vacuum in not actively cooled. For this reason the electric heated box for the transducers was eliminated and a cold plate was added to the liquid loop between the radiator panels. The Chromolox controllers for the pressure transducer electric heater remains in the DACS and is unused.

12.3 Fabrication Summary

Comprised mostly of commercial items no lessons learned of any consequence were developed during the fabrication of the LUP.

12.4 Testing Summary

The LUP components were incorporated into the Hot Loop testing, the radiator acceptance testing, and the radiator/Tank 6 integration testing to provide opportunity for checkout prior to incorporation into the system test. The following events of note occurred:

1. During the radiator acceptance testing an accumulator was failed during test setup proof pressure test. It was found that the bellow, internal to the accumulator, would not tolerate the high proof pressure used on the liquid loop plumbing. There was a misinterpretation of the accumulator proof pressure requirement. The accumulator supplier applied the proof pressure requirement to the external boundary shell but did not make the internal bellows design capable of tolerating the proof pressure requirement. When the accumulator was installed in the radiator test setup it was proof tested to 150 psig and did not function after the pressure test. It was then determined that the maximum capability of the bellows was no greater than 75 PSIA (60 psig).
2. During radiator/tank integration test the liquid loop pump controllers were removed from the data acquisition system and connected with temporary wiring and power supplies. At several times the

controllers were fried by connecting them incorrectly. When repaired and placed back within the DACS no further difficulties were encountered.

3. It was determined that the heating elements contained within the liquid loop heater have a life expectancy of approximately 100 hours at high electrical power. Normal operation of the system does not operate the heater at levels above 50 percent and the elements should last significantly longer.

12.5 Bibliography

DOCUMENT NUMBER	DOCUMENT TITLE	DOCUMENT SUBTITLE
41 12127	LUP DESIGN PACKAGE	CDR INPUT
41 12162	LUP VIEWGRAPH	CDR INPUT
3793316	LUP ASSEMBLY DRAWING	

Appendix 1. Bibliography of Technical Papers

[1] Amundsen, P. C., et al., BIPS Turboalternator-Compressor Characteristics and Application to the NASA Solar Dynamic Ground Demonstration Program, Proc. 29th IECEC; 1994.

[2] Bahnman, D. W. and Jensen, P. A., Design of a Solar Concentrator for the Solar Dynamic Ground Test Demonstration Program, ASME; 1994, pp. 193-203.

[3] Brown, M., et al., Solar Dynamic Power System Deployment Structures and Pointing Controls System Study, Naval Research Lab, Naval Center for Space Technology, Washington D. C.; 1992.

[4] Calogeras, J. E., et al., Solar Dynamic Power for Earth Orbital and Lunar Applications, Proc. 26th IECEC; 1991.

[5] Calogeras, J. E., et al., The Ground Testing of a 2 kW Solar Dynamic Space Power System, Proc. 27th IECEC; 1992, Vol 1, pp. 455-460.

[6] Campbell, J. S. and Jensen, P. A., Design, Analysis and Test of a Solar Concentrator for Space Applications, ASME; 1994, pp. 205-216.

[7] de Groh, K. K., et al., Performance and Durability of High Emittance Heat Receiver Surfaces for Solar Dynamic Power Systems, ASME; 1994.

[8] Fleming, M. L., et al., Solar Dynamic Ground Test Demonstration Radiator Design and Test, Proc. 29th IECEC; 1994

[9] Fleming, M. L. and Flores, R. R., Solar Dynamic Radiator Design Development, ASME; 1994.

[10] Huckins, E. and Ahlf, P., Space Station Power Requirements and Issues, Proc. 29th IECEC; 1994, pp. 608-612.

[11] Jaworske, D.A.; Jefferies, K. S.; and Mason, L.S., Alignment and Initial Operation of an Advanced Solar Simulator, AIAA 96-0102, 34th Aerospace Sciences Meeting, Reno, NV, 1966.

[12] Jefferies, K. S., Ed., Solar Dynamic Power System Development for Space Station *Freedom*, RP1310, May 1993.

[13] Jefferies, K. S., Solar Simulator for Solar Dynamic Space Power System Testing, NASA TM 106393, ASME; 1994, pp. 217-222.

[14] Mason, L. S., et al., Solar Dynamic Ground Test Demonstration System Test Plans, ASME; 1994.

[15] Mock, E. A., Solar Dynamic Ground Test Demonstrator System Orbital and Startup Control Methods, ASME; 1994.

[16] Schertz, P., et al., Development of an Improved Facet for Space Applications, NASA CR-189109, 1991.

[17] Shaltens, R. K. and Boyle, R. V., Overview of the Solar Dynamic Ground Test Demonstration Program, NASA TM 106296, Proc. 28th IECEC; 1993, Vol 2, pp. 831-836.

[18] Shaltens, R. K. and Boyle, R. V., Update of the 2 kW Solar Dynamic Ground Test Demonstration Program, NASA TM 106730, Proc. 29th IECEC; 1994, pp. 359-365.

[19] Shaltens, R. K. and Boyle, R. V., Initial Results From the Solar Dynamic (SD) Ground Test Demonstration Project at NASA Lewis, TM 107004, Proc. 30th IECEC; 1995, pp. 363-368.

[20] Shaltens, R. K., Overview of the Solar Dynamic Ground Test Program At NASA Lewis Research Center, NASA TM 106876, 1995.

[21] Strumpf, H. J., et al., Design of the Heat Receiver for the Solar Dynamic Ground Test Demonstrator Space Power System, Proc. 28th IECEC; 1993, Vol 1, pp. 469-475.

[22] Strumpf, H. J., et al., Fabrication and Testing of the Solar Dynamic Ground Test Demonstration Heat Receiver, Proc. 29th IECEC; 1994, pp. 372-377.

[23] Strumpf, H. J., et al., Thermal and Structural Analysis of the Heat Receiver for the Solar Dynamic Ground Test Demonstrator, ASME; 1994, pp. 223-234.

Appendix 2. Bibliography of Project Documentation

DOCUMENT NUMBER	DOCUMENT TITLE	DOCUMENT SUBTITLE
** REPORTS OF AEROSPACE DESIGN & DEVELOPMENT		
41 11757A	PRELIM HAZARD ANAL	MLI
** REPORTS OF ALLIEDSIGNAL AEROSPACE EQUIPMENT SYSTEMS (TORR.)		
92 65635	TEST PLAN	HEAT EXCHANGERS
92 65652	PRELIM HAZARD ANAL	ALAD HEAT EXCH.
92 65708	RECUP REFURB PLAN	
93 65811	TEST PLAN	SINGLE TUBE
93 66093	TEST PROC, RECUP	
93 66138	RECUP REFURB RPT	FINAL SUBMIT
93 66141	TEST PLAN, RECEIVER	CDR UPDATE
93 66142	TEST PLAN, COOLER	CDR UPDATE
93 66172	REVIEW DOC.	CDR PACKAGE
93 66189	HAZARD ANALYSIS	CDR UPDATE
93 66189 REV. 1	HAZARD ANALYSIS	CDR HEAT EXCH
93 66201	REVIEW DOC.	CDR CHARTS
93 66201 REV. 1	REVIEW DOC	CDR CHARTS REV
93 66232	SNGLE TUBE TEST PROC	
93 66722	TEST REPORT	SINGLE TUBE TST
94 66786	TEST PROC, RECEIVER	
** REPORTS OF ALLIEDSIGNAL FLUID SYSTEMS		
41 11367 1(N)	TECH/SCD STATUS RPT	MONTHLY (N=38
41 11460(1)	THERMODYNAMIC REQMTS	SRR
41 11460(2)	THERMODYNAMIC REQMTS	PDR
41 11460(3)	THERMODYNAMIC REQMTS	CDR
41 11468 BK 1	REVIEW DOC.	SRR MINUTES
41 11468 BK 2	REVIEW DOC.	SRR PACKAGE
41 11468 BK 3	REVIEW DOC.	SRR CHARTS
41 11529	TAC DISASSY INSTRUCT	
41 11611	DP/P CYCLE STUDY	HI UA RECEIVER
41 11685	THERMO ANALYSIS	PDR RESULTS
41 11725	TEST PLAN	PDR UPDATE
41 11743	REVIEW DOC.	PDR PACKAGE
41 11744	SPARES LIST	INITIAL SUBMIT
41 11744A	SPARES LIST	INTERM
41 11757A	PRELIM HAZARD ANAL	GFSD EQUIP
41 11764 (5 BKS	REVIEW DOC.	PDR CHARTS

DOCUMENT NUMBER	DOCUMENT TITLE	DOCUMENT SUBTITLE
41 11929	REVIEW DOC.	PDR MINUTES
41 11946	PROD ASSURANCE PLAN	FINAL SUBMITAL
41 11982	ALT TEST RIG EAI	
41 12000	THERMO ANALYSIS	STARTING SCENAR
41 12010	TAC REFURB REPORT	INITIAL SUBMIT
41 12044	PCCU S/W DEVEL PLAN	CDR SUBMIT
41 12060A	CONFIG MGMT PLAN	CDR UPDATE
41 12065	SYSTEM CNTRL METHODS	
41 12071	DACS S/W REQMTS DOC	CDR
41 12072	1ST SYSTEM START	ANALYSIS
41 12083	PCCU S/W REQMTS DOC	CDR RELEASE
41 12084	PCCU S/W DESIGN DOC	CDR
41 12088	UNCERTAINTY ANALYSIS	CDR
41 12091	TEST REPORTDACS	LABVIEW PROTO.
41 12092	DACS S/W DESIGN DOC	CDR
41 12093	TEST PLAN DACS	CDR UPDATE
41 12093	TEST PLAN DACS S/W	CDR UPDATE
41 12094	TEST PLAN PCCU S/W	CDR UPDATE
41 12095	TEST PLAN TAC	CDR UPDATE
41 12096	TEST PLAN PLR	CDR UPDATE
41 12097	TEST PLAN PCCU	CDR UPDATE
41 12098	TEST PLAN HOT LOOP A	CDR UPDATE
41 12099	TEST PLAN HOT LOOP B	CDR UPDATE
41 12102	DACS REVIEW PKG	CDR INPUT
41 12103	TAC DESIGN PACKAGE	CDR INPUT
41 12104	PCS DESIGN PKG	CDR INPUT
41 12105	PCCU DESIGN PACKAGE	CDR INPUT
41 12106	PLR DESIGN PKG	CDR INPUT
41 12112	TEST PLAN S/D VALVE	CDR SUBMIT
41 12119	REVIEW DOC.	CDR PACKAGE
41 12127	LUP DESIGN PACKAGE	CDR INPUT
41 12139	DACS VIEWGRAPHS	CDR INPUT
41 12158(+CHGS)	PCCU VIEWGRAPH	CDR INPUT
41 12162	PCS VIEWGRAPH	CDR INPUT
41 12162	LUP VIEWGRAPH	CDR INPUT
41 12167	PLR VIEWGRAPH	CDR INPUT
41 12181	TAC VIEWGRAPHS	CDR INPUT
41 12250	CDR SUMMARY REPORT	
41 12251	TAC ASSY INSTRUCT.	
41 1238	DACS IC SCXI/CRC	CHECKOUT PROC.
41 12412	TEST PROCEDURE	TAC
41 12600	STARTUP PROCEDURE	DACS IC

DOCUMENT NUMBER	DOCUMENT TITLE	DOCUMENT SUBTITLE
41 12600A	STARTUP PROCEDURE	DACS IC
41 12601	STARTUP PROCEDURE	DACS CRC
41 12603	CALIB. PROCEDURE	DACS
41 12604A	CALIB. PROCEDURE	DACS
41 12923	TEST PROCEDURE	HOT LOOP B
41 12967	TEST PROCEDURE	HOT LOOP A
41 12969	TEST REPORTPCS	HOT LOOP A
41 13085	TEST REPORTPCS	HOT LOOP B
41 13157	PROCEDURE STARTING	SIPS
41 13165	DACS & DACS S/W	S/W CERT.
41 13166	PROCEDURE INSTALL.	PCS/PCCU/DACS
41 13227	TEST REPORT PCCU	POWER QUALITY
41 13428	VER. DESCRIPTION	DACS S/W
41 13428A	VER. DESCRIPTION	DACS S/W
41 13507	PROCEDURE CHECKOUT	PCCU OUT OF TNK
41 13511	PROCEDURE CHECKOUT	PCCU IN TANK
ATP3605427XO	TEST PROCEDURE	SHUTDOWN VALVE
** REPORTS OF HARRIS CORP.		
7000494A	FACET TEST PLAN	CDR
7000495	TEST PROCEDURE	CONCENTRATOR
7000495A	CONCENTRATOR ATP	CDR
7000496	TEST PROCEDURE	FLUX DISTRIB.
7000496A	FLUX DIST. TEST PLAN	CDR
7000498	FACET ALIGN TECH	CDR
7000499	HEX PROOF TEST PLAN	CDR
7000500	SUPP STRUCT TEST PLN	CDR
7000502	CONC SPARES LIST	PDR SUBMITTAL
7000502 REV. A	CONC SPARES LIST	CDR UPDATE
7002232	TEST REPORT	CONC ALIGNMENT
7002233	TEST REPORT	FLUX DISTRIBUT.
	PRELIM HAZARD ANALY	CONCENTRATOR
UNNUMBERED	REVIEW DOC.	PDR PACKAGE
UNNUMBERED	REVIEW DOC.	CDR PACKAGE
UNNUMBERED	REVIEW DOC.	PDR CHARTS
UNNUMBERED	REVIEW DOC.	CDR CHARTS
UNNUMBERED	HAZARD ANALYSIS	CDR CONCENTRATO
** REPORTS OF LORAL VOUGHT		
3 47300/2DIR542	RAD THERMAL ANALYSIS	
3 47300/2R 518	PRELIM HAZARD ANAL	RADIATOR

DOCUMENT NUMBER	DOCUMENT TITLE	DOCUMENT SUBTITLE
3 47300/3DIR005	RADIATOR WEIGHT ANAL	CDR RELEASE
3 47300/3DIR006	RADIATOR STRESS ANAL	CDR RELEASE
3 47300/3R 002	HAZARD ANALYSIS	RADIATOR
3 47300/3R 005	SAFETY PLAN	
3 47300/3R 007	TEST REPORT	RADIATOR ATP
3 47300/3R 021	TEST PROCEDURE	RADIATOR
3 47300/4R 005	TEST PROCEDURE	RADIATOR
3 47300/4R 005	TEST REPORT RADIATOR	TANK INTEG TEST
3 47300/4R 005A	TEST PROCEDURE	RADIATOR
UNNUMBERED	REVIEW DOC.	PDR PACKAGE
UNNUMBERED	REVIEW DOC.	PDR CHARTS
UNNUMBERED	REVIEW DOC.	CDR CHARTS
VARIOUS	REVIEW DOC.	CDR PACKAGE

** REPORTS OF ROCKETDYNE

213000001	SYSTEM LAYOUT	PROPOSAL SUBMIT
213000001 ISS 1	SYSTEM LAYOUT	SRR UPDATE
213000001 ISS 2	SYSTEM LAYOUT	PDR UPDATE
213000001 ISS 3	SYSTEM LAYOUT	CDR UPDATE
213000001 N/C	LAYOUT, SYSTEM	APPROVD RELEASE
213000002 ISS 1	P & ID	SRR SUBMIT
213000002 ISS 3	P & ID	PDR UPDATE
213000002 ISS 4	P & ID	CDR UPDATE
213000002 N/C	P & ID, SYSTEM	APPROVD RELEASE
213000014 ISS 1	EI&C CABLING DIAGRAM	PDR SUBMIT
213000014 ISS 2	EI&C CABLING DIAGRAM	CDR UPDATE
213000014 N/C	CABLING DIAGRAM	APPROVD RELEASE
213000015 ISS 1	WIRE LIST	PDR SUBMIT
213000016 ISS 1	ICD, PCS	PDR SUBMIT
213000016 ISS 2	ICD, PCS	CDR UPDATE
213000016 N/C	ICD, PCS	APPROVD RELEASE
213000017 ISS 1	INSTRUMENT LIST	PRE CDR RELEASE
213000017 ISS 4	INSTRUMENT LIST	CDR RELEASE
213000017 N/C	INSTRUMENTATION LIST	APPROVD RELEASE
213000018 N/C	INSTALLATION DWG	APPROVD RELEASE
213000019 ISS 1	WIRE LIST	CDR UPDATE
213000019 N/C	WIRE LIST	APPROVD RELEASE
213000020 ISS 1	CONNECTOR LIST	CDR SUBMIT
213000020 N/C	CONNECTOR LIST	APPROVD RELEASE
213010116 ISS 1	ICD, CONCENTRATOR	PDR SUBMIT
213010116 ISS 2	ICD, CONCENTRATOR	CDR UPDATE

DOCUMENT NUMBER	DOCUMENT TITLE	DOCUMENT SUBTITLE
213010116 N/C	ICD, CONCENTRATOR	APPROVD RELEASE
213010117 ISS 1	ICD, RECEIVER	PDR SUBMIT
213010117 ISS2	ICD, RECEIVER	CDR UPDATE
213010117 N/C	ICD, RECEIVER	APPROVD RELEASE
213010118 ISS 1	ICD, RADIATOR	PDR SUBMIT
213010118 ISS 2	ICD, RADIATOR	CDR UPDATE
213010118 N/C	ICD, RADIATOR	APPROVD RELEASE
213010119 ISS 1	ICD, PLR	PDR SUBMIT
213010119 ISS 2	ICD, PLR	CDR UPDATE
213010119 N/C	ICD, PLR	APPROVD RELEASE
213010120 ISS 1	ICD, PCCU	PDR SUBMIT
213010120 ISS 2	ICD, PCCU	CDR UPDATE
213010120 N/C	ICD, PCCU	APPROVD RELEASE
213010121 ISS 1	ICD, TEST CONTRL	PDR SUBMIT
213010122 ISS 1	ICD, ACCUMULATOR	PDR SUBMIT
213010123 ISS 1	ICD, COOLER	PDR SUBMIT
213010132 ISS 1	ICD, LUP	CDR UPDATE
213010132 N/C	ICD, LUP	APPROVD RELEASE
213SRR000001	PREL HAZARD ANAL	SYSTEM
213SRR00002	HAZARD ANALYSIS	CDR
213TI000001	INSOLATION PARAMETER	SELECTION OF
213TI000003	PRACA(3)	SYSTEM TEST
213TI000004	PROCEDURE SYSTEM	PALLET INSTALL.
213TI000005	DIAGRAM SYSTEM	INSTALL. LOGIC
213TI000006	DRAWING INSTRUMENTA.	RADIATOR T/Cs
213TP000002 IS2	TEST PLAN, SYSTEM	CDR UPDATE
213TP000002ISS1	TEST PLAN, SYSTEM	PDR SUBMIT
213TPS000001/3	TEST PLANSUMMARY	CDR UPDATE
213TPS000001IS1	TEST PLANSUMMARY	SRR UPDATE
213TPS000001IS2	TEST PLANSUMMARY	PDR UPDATE
N10115	SYSTEM SPEC	INITIAL SUBMIT
N10115 ISS 3	SYSTEM SPEC	SRR UPDATE
N10115 ISS 4	SYSTEM SPEC	PDR UPDATE
N10115 ISS 5	SYSTEM SPEC	CDR UPDATE
N10115 N/C	SPEC, SYSTEM	APPROVD RELEASE
N10116 ISS 1	SPEC, CONCENTRATOR	PDR SUBMIT
N10116 ISS 2	SPEC, CONCENTRATOR	CDR UPDATE
N10116 N/C	SPEC, CONCENTRATOR	APPROVD RELEASE
N10117 ISS 1	SPEC, RECEIVER	PDR SUBMIT
N10117 ISS 2	SPEC, RECEIVER	CDR UPDATE
N10117 N/C	SPEC, RECEIVER	APPROVD RELEASE
N10118 ISS 1	SPEC, RADIATOR	PDR SUBMIT

DOCUMENT NUMBER	DOCUMENT TITLE	DOCUMENT SUBTITLE
N10118 ISS 2	SPEC, RADIATOR	CDR UPDATE
N10118 N/C	SPEC, RADIATOR	APPROVD RELEASE
N10119 ISS 1	SPEC, PLR	PDR SUBMIT
N10119 ISS 2	SPEC, PLR	CDR UPDATE
N10119 N/C	SPEC, PLR	APPROVD RELEASE
N10120 ISS 1	SPEC, PCCU	PDR SUBMIT
N10120 ISS 2	SPEC, PCCU	CDR UPDATE
N10120 N/C	SPEC, PCCU	APPROVD RELEASE
N10121 ISS 1	SPEC, TEST CONTROL	PDR SUBMIT
N10121 ISS 2	SPEC, DACS	CDR UPDATE
N10121 N/C	SPEC, DACS	APPROVD RELEASE
N10122 ISS 1	SPEC, ACCUMULATOR	PDR SUBMIT
N10123 ISS 1	SPEC, COOLER	PDR SUBMIT
N10132 ISS 1	SPEC, LUP	CDR UPDATE
N10132 N/C	SPEC, LUP	APPROVD RELEASE
UNNUMBERED	REVIEW DOC.	PDR PACKAGE
UNNUMBERED	REVIEW DOC.	PDR CHARTS
UNNUMBERED	REVIEW DOC.	CDR CHARTS
UNNUMBERED	REVIEW DOC.	CDR PACKAGE

Appendix 3. Comparison Between Predicted and Measured Receiver Canister Temperatures

Each of these plots provides a comparison between test data and predictions for a specific receiver canister. The receiver consists of 23 tubes. Each tube contains 24 canisters. Canister No. 1 is closest to the aperature and the receiver gas inlet. The annotation of T1C4 on the first plot indicates that this is the fourth canister on Tube No. 1.

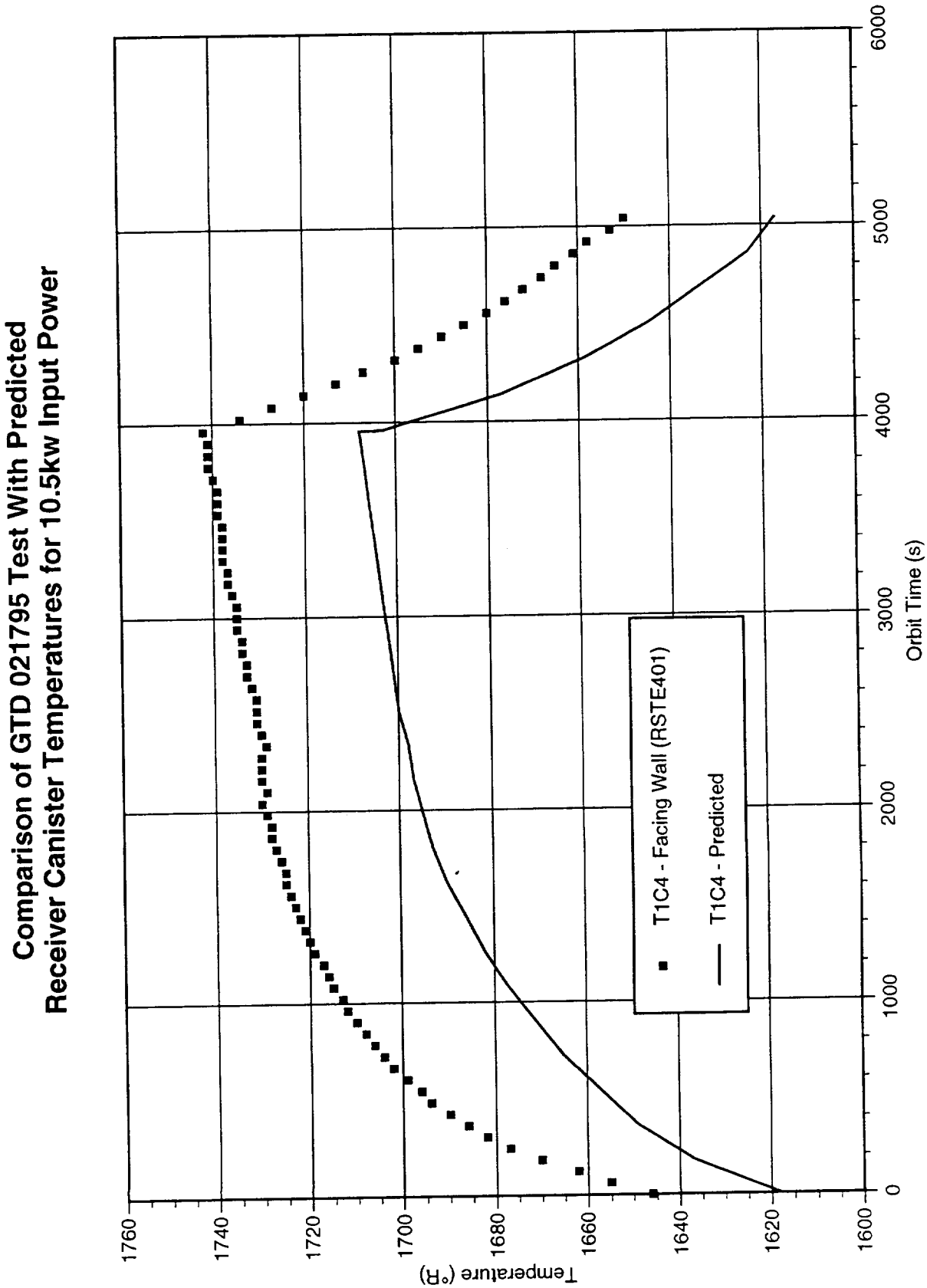
Comparison of GTD 021795 Test With Predicted
Receiver Canister Temperatures for 10.5kw Input Power
Temperature (°R)
1760
1740
1720
1700
1680
1660
1640
1620
1600
0
1000
2000
3000
4000
5000
6000
Orbit Time (s)
T1C4 - Facing Wall (RSTE401)
T1C4 - Predicted

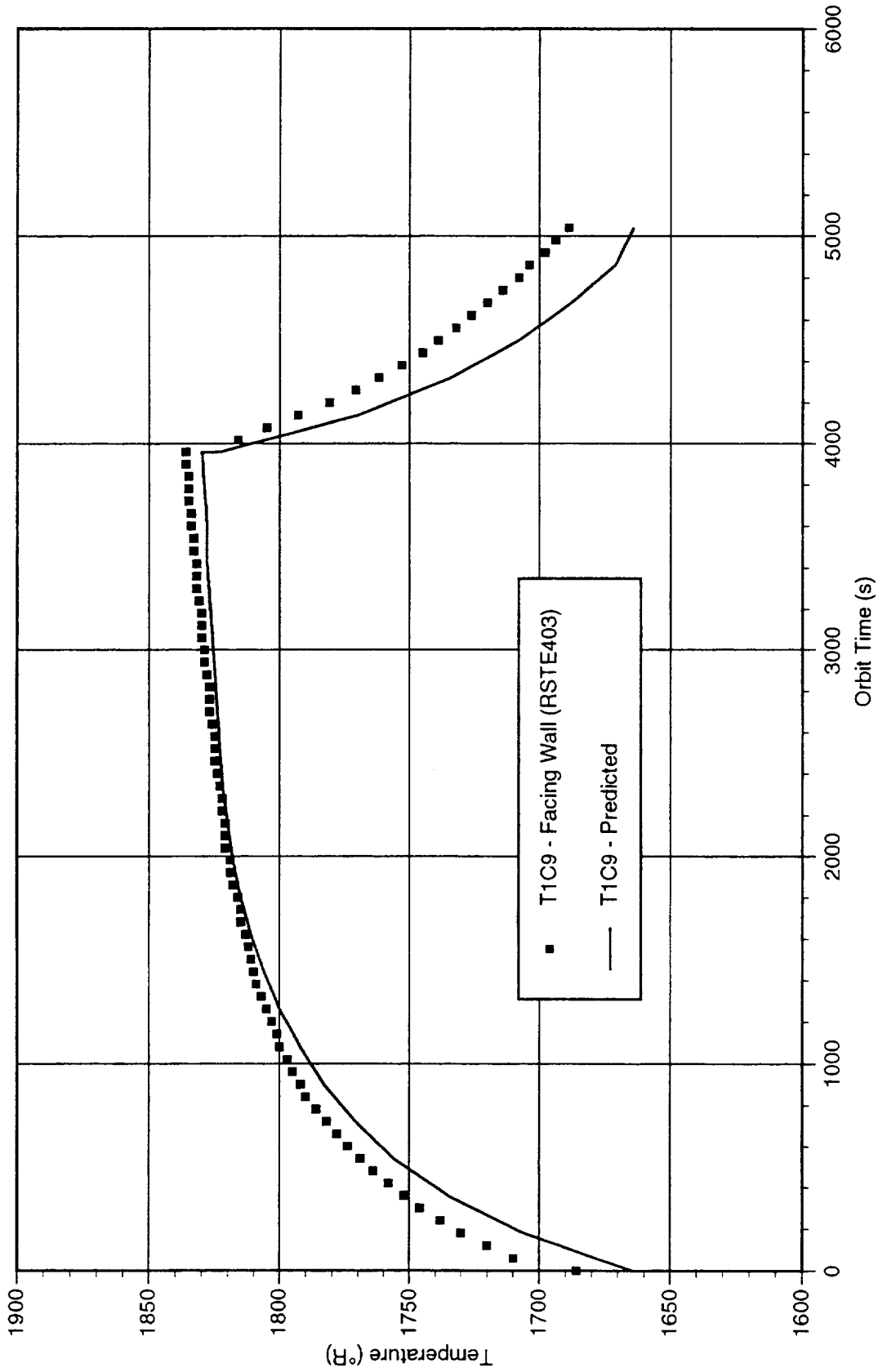
Comparison of GTD 021795 Test With Predicted
Receiver Canister Temperatures for 10.5kw Input Power
Temperature (°R)
1900
1850
1800
1750
1700
1650
1600
0
1000
2000
3000
4000
5000
6000
Orbit Time (s)
T1C9 - Facing Wall (RSTE403)
T1C9 - Predicted

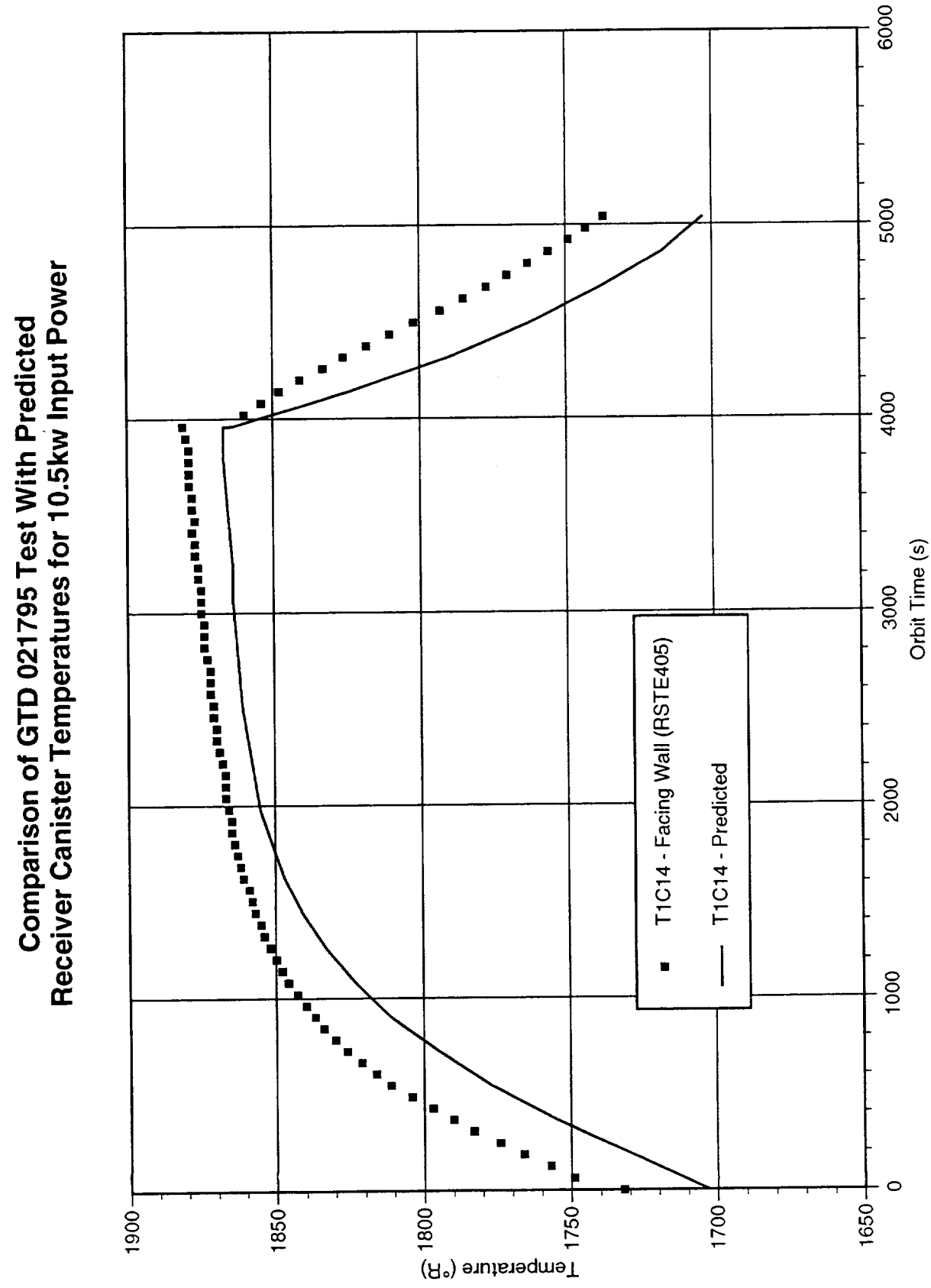
Comparison of GTD 021795 Test With Predicted
Receiver Canister Temperatures for 10.5kw Input Power
Temperature (°R)
1900
1850
1800
1750
1700
1650
0
1000
2000
3000
4000
5000
6000
Orbit Time (s)
T1C14 - Facing Wall (RSTE405)
T1C14 - Predicted

Comparison of GTD 021795 Test With Predicted Receiver Canister Temperatures for 10.5kw Input Power

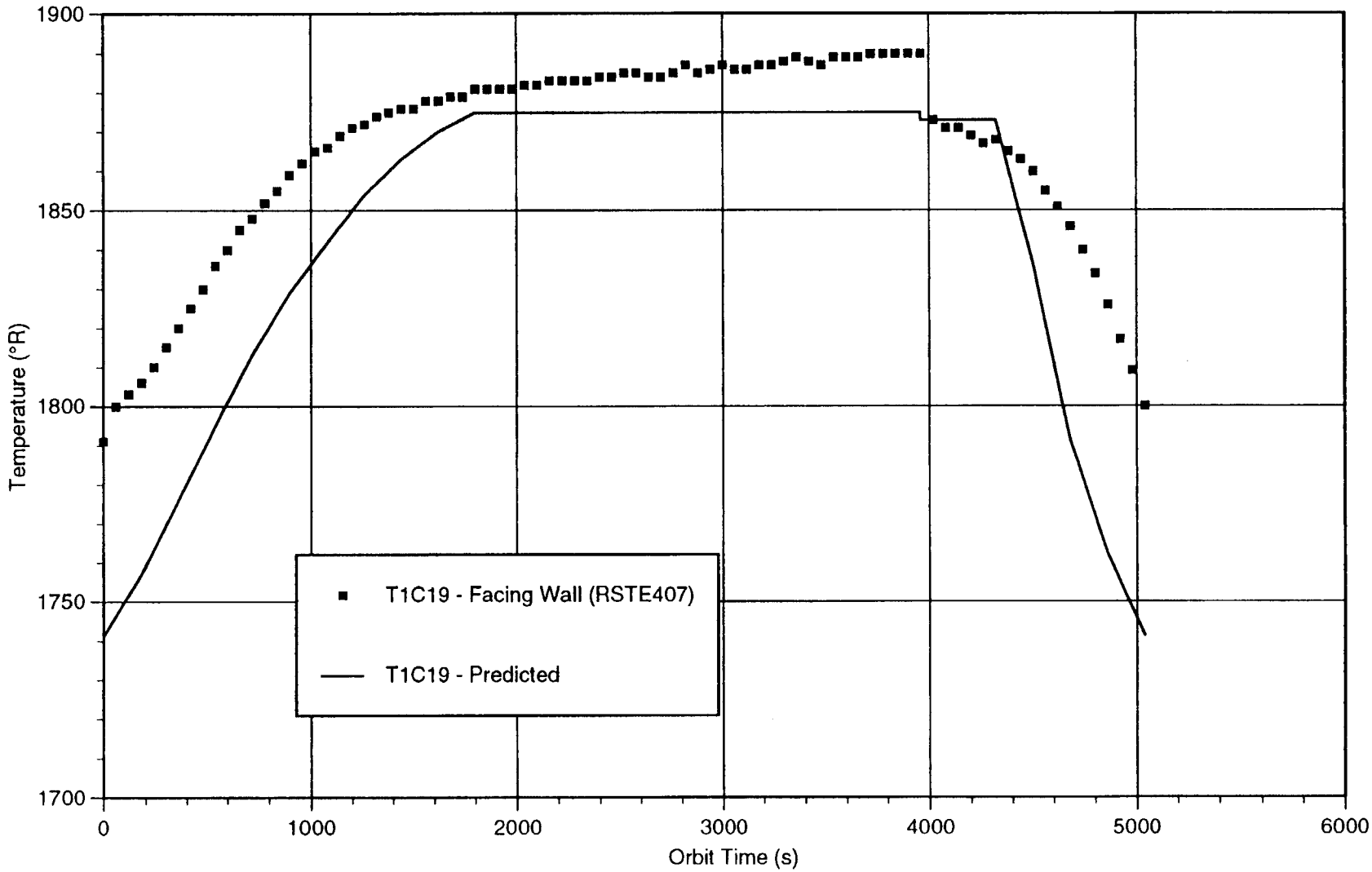

Comparison of GTD 021795 Test With Predicted Receiver Canister Temperatures for 10.5kw Input Power

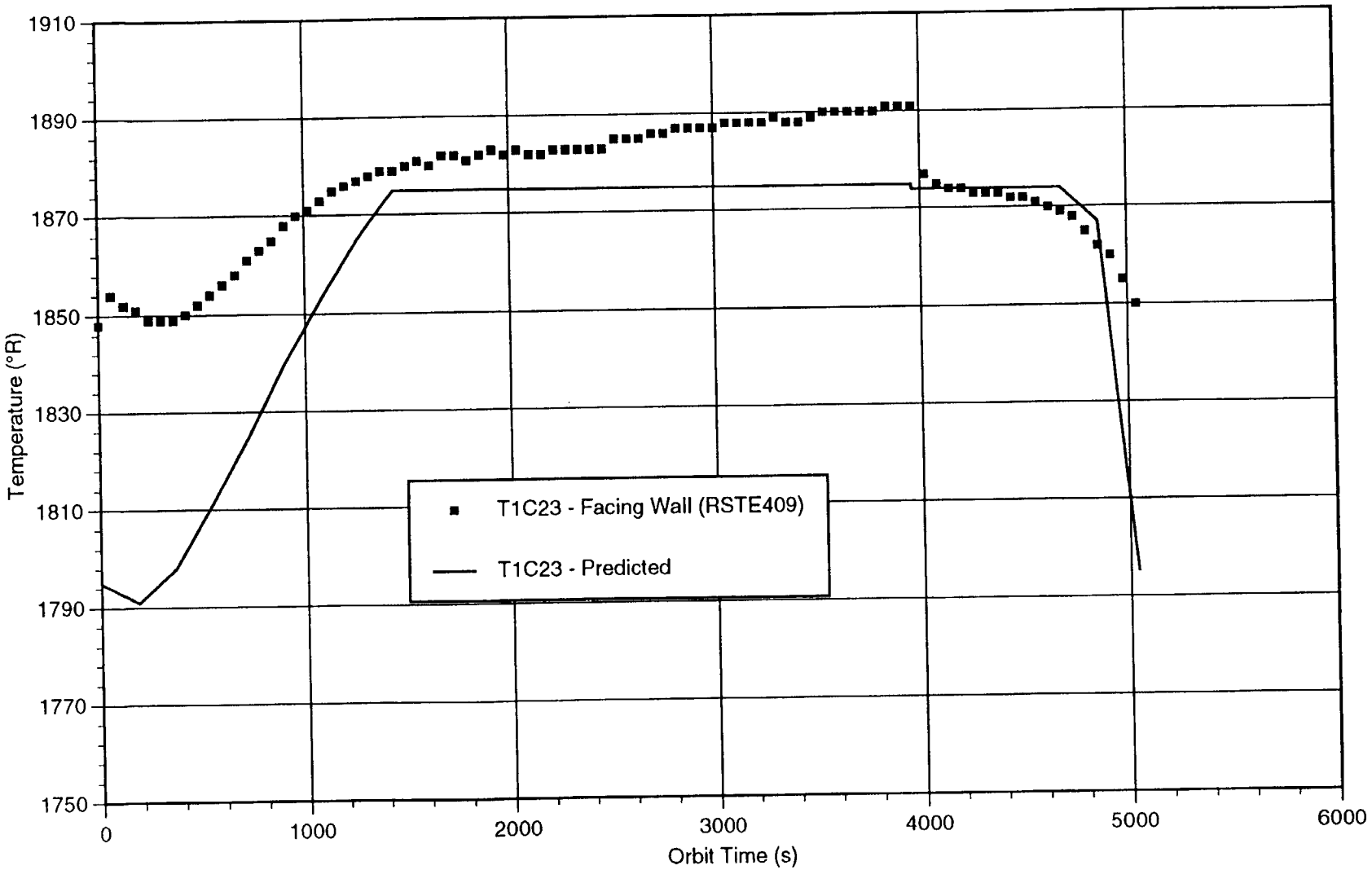

Comparison of GTD 021795 Test With Predicted Receiver Canister Temperatures for 10.5kw Input Power

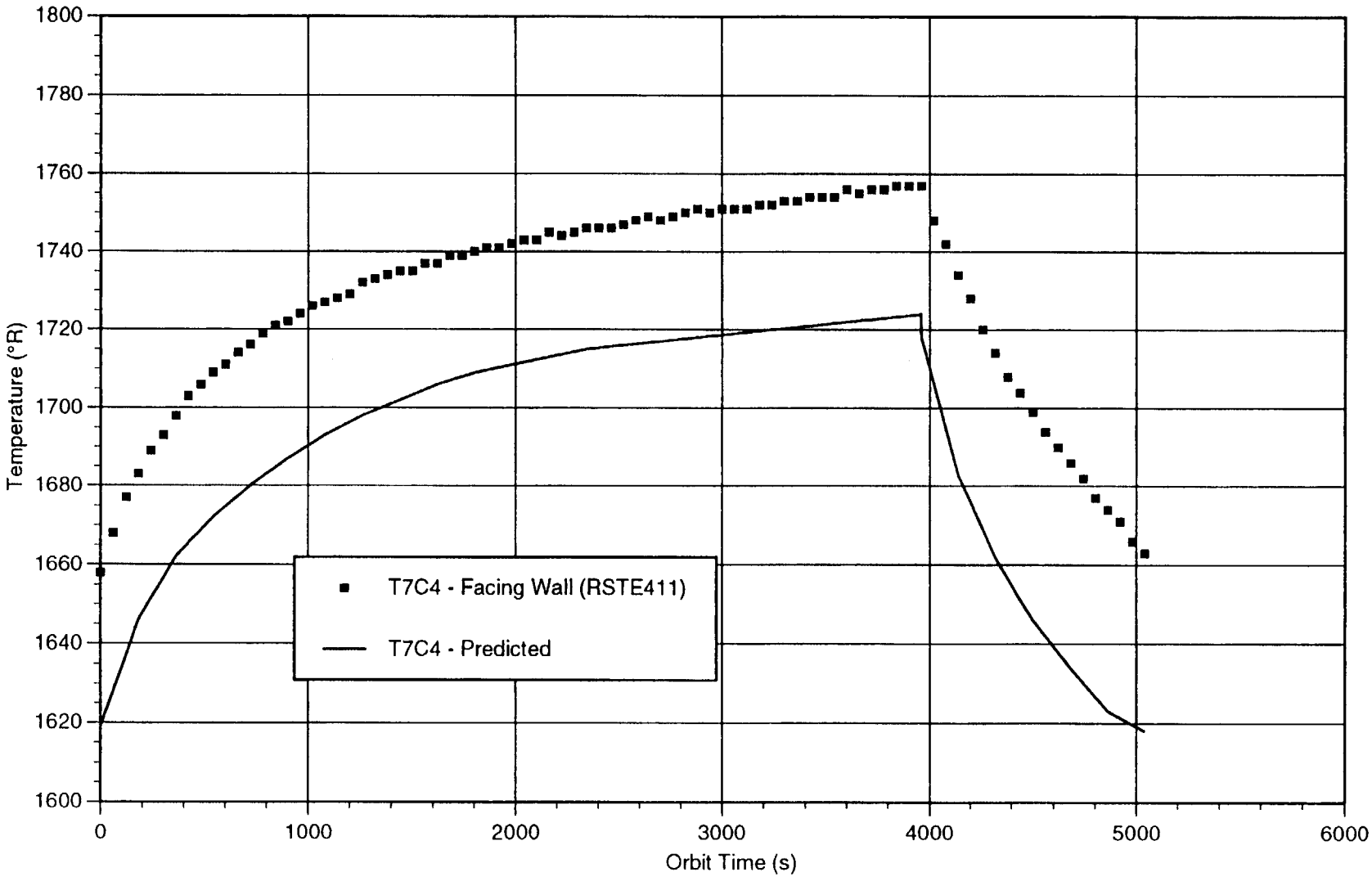

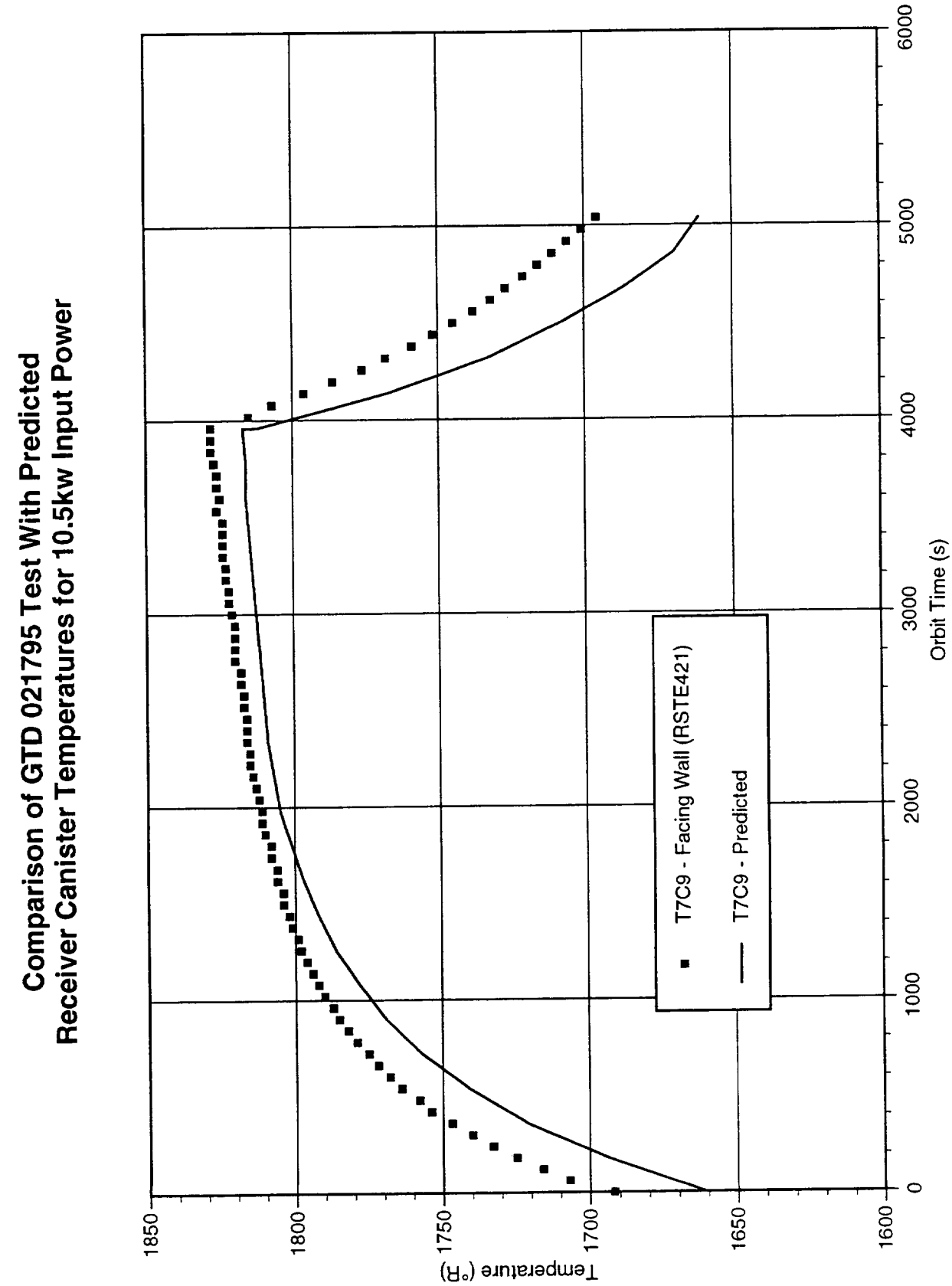
Comparison of GTD 021795 Test With Predicted
Receiver Canister Temperatures for 10.5kw Input Power
Temperature (°R)
1850
1800
1750
1700
1650
1600
0
1000
2000
3000
4000
5000
6000
Orbit Time (s)
T7C9 - Facing Wall (RSTE421)
T7C9 - Predicted

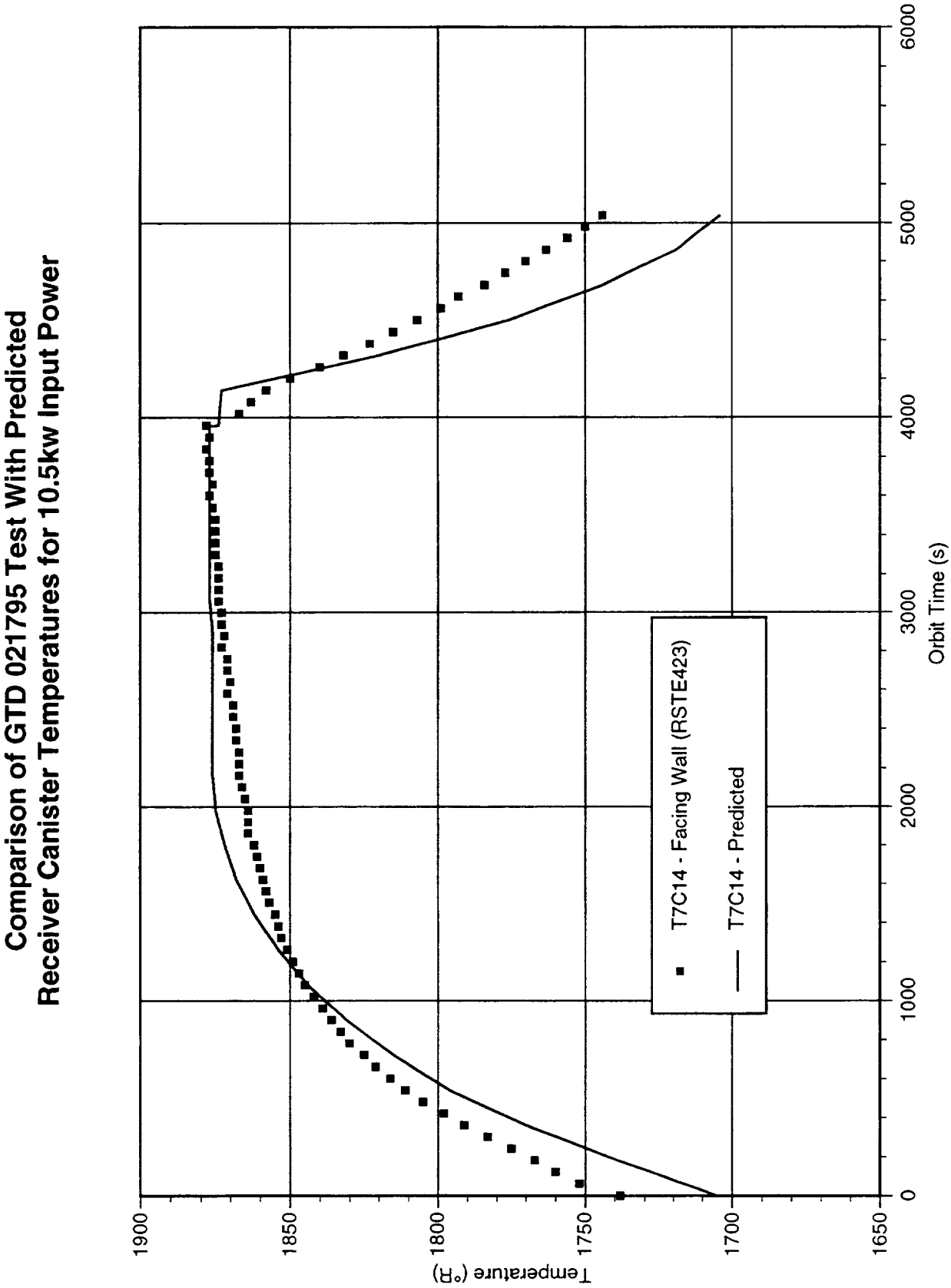
Comparison of GTD 021795 Test With Predicted
Receiver Canister Temperatures for 10.5kw Input Power
Temperature (°R)
1900
1850
1800
1750
1700
1650
0
1000
2000
3000
4000
5000
6000
Orbit Time (s)
T7C14 - Facing Wall (RSTE423)
T7C14 - Predicted

Comparison of GTD 021795 Test With Predicted Receiver Canister Temperatures for 10.5kw Input Power

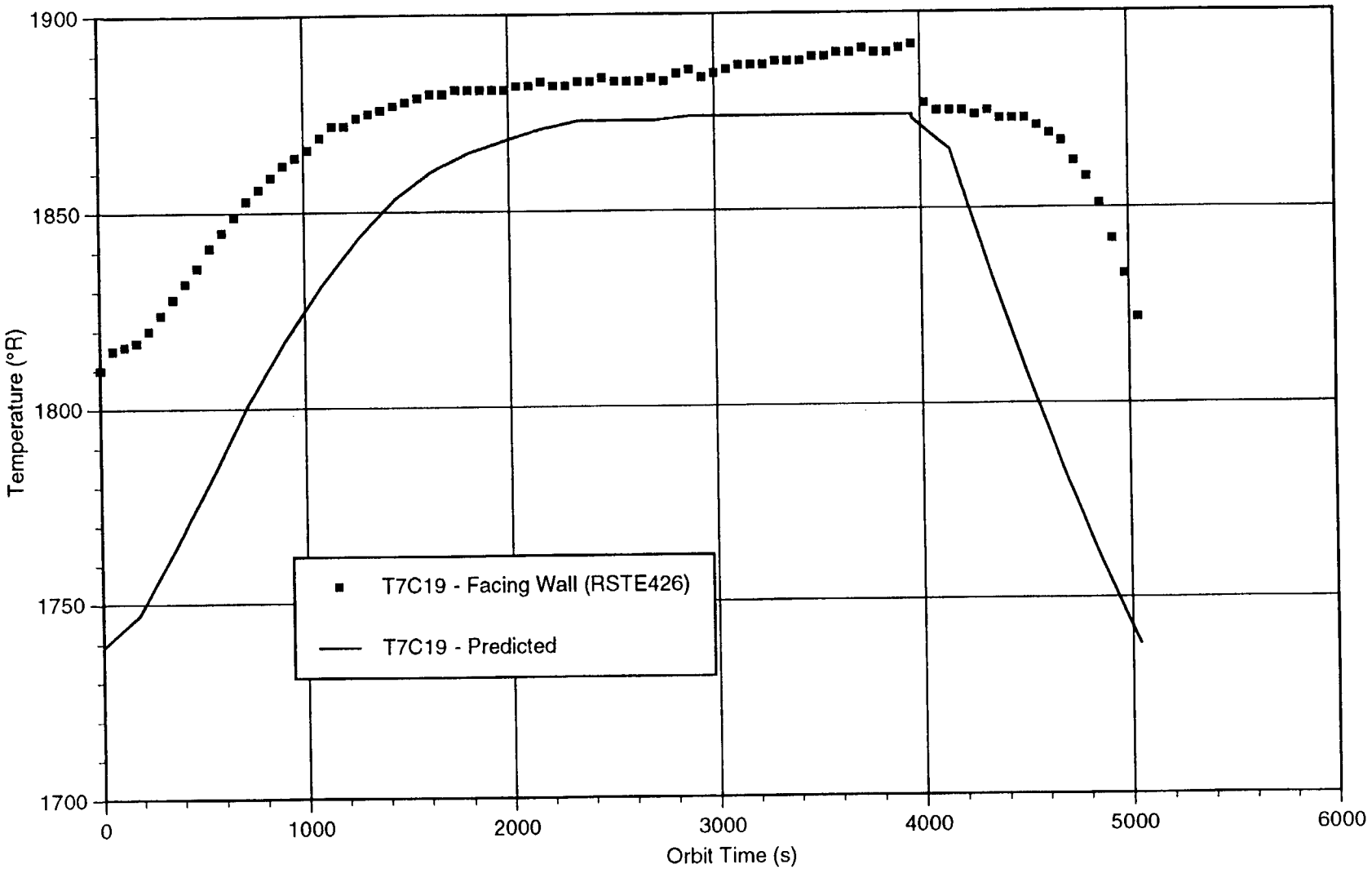

Comparison of GTD 021795 Test With Predicted Receiver Canister Temperatures for 10.5kw Input Power

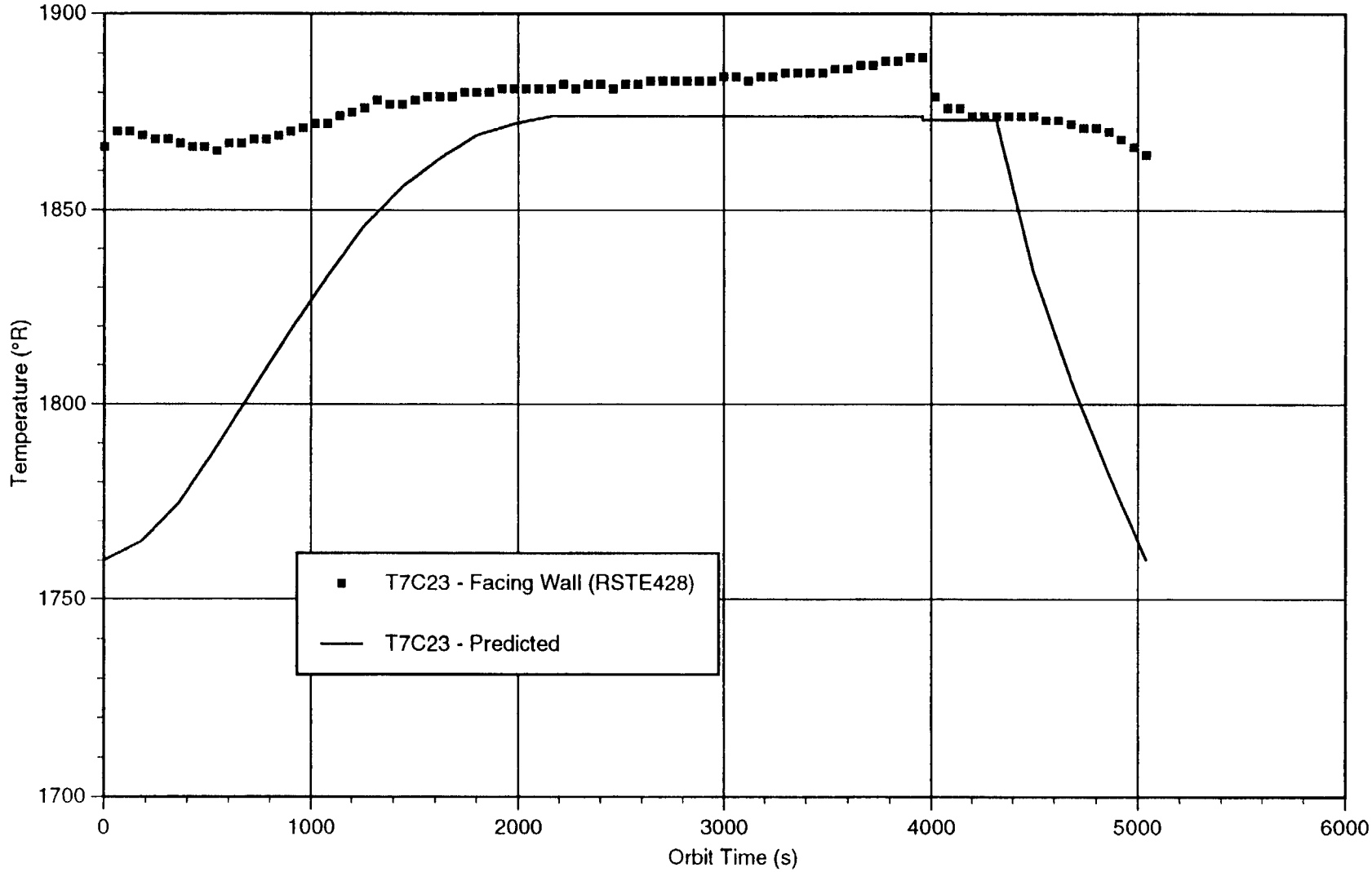

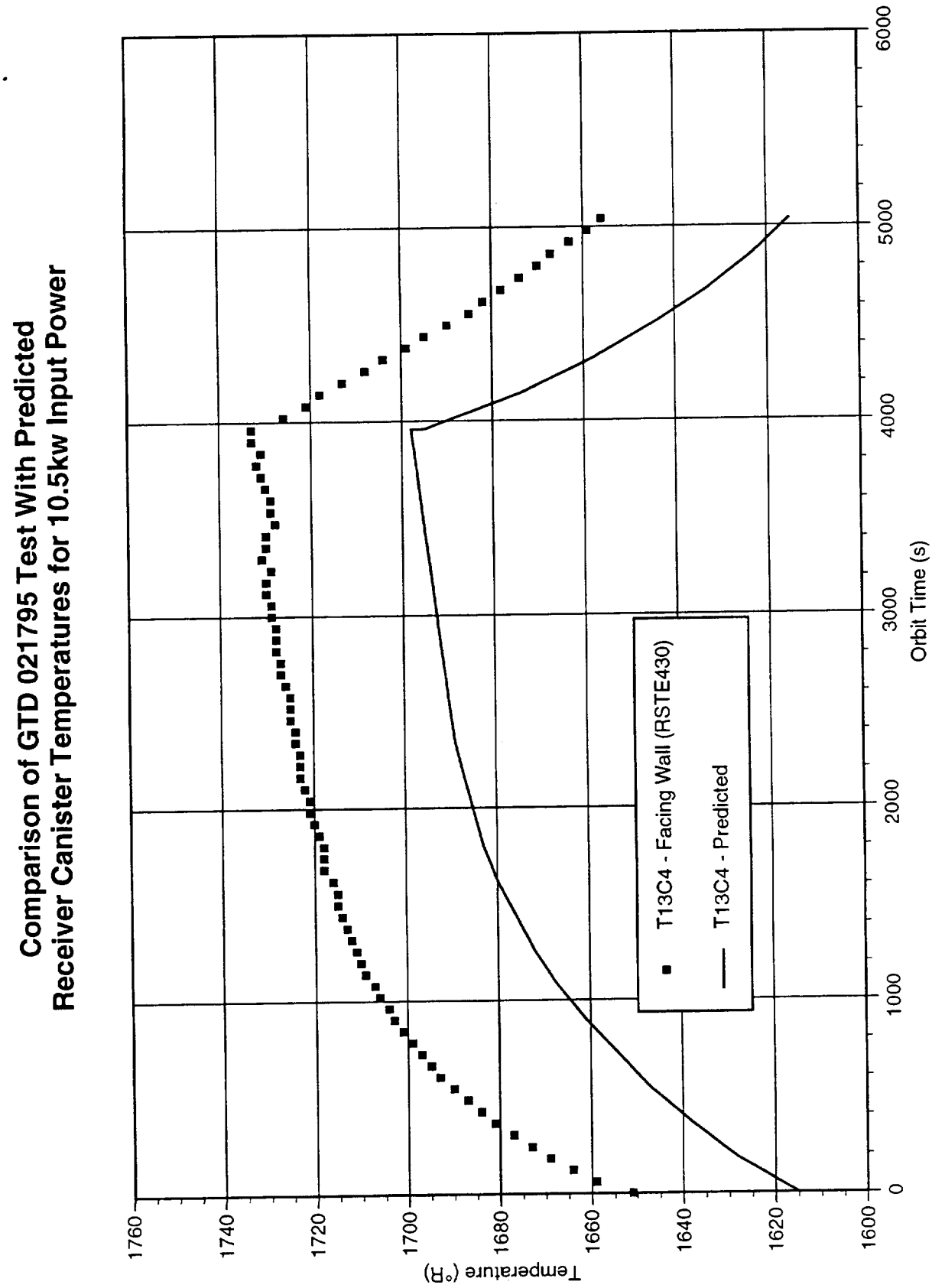
Comparison of GTD 021795 Test With Predicted
Receiver Canister Temperatures for 10.5kw Input Power
Temperature (°R)
1760
1740
1720
1700
1680
1660
1640
1620
1600
0
1000
2000
3000
4000
5000
6000
Orbit Time (s)
T13C4 - Facing Wall (RSTE430)
T13C4 - Predicted

Comparison of GTD 021795 Test With Predicted Receiver Canister Temperatures for 10.5kw Input Power

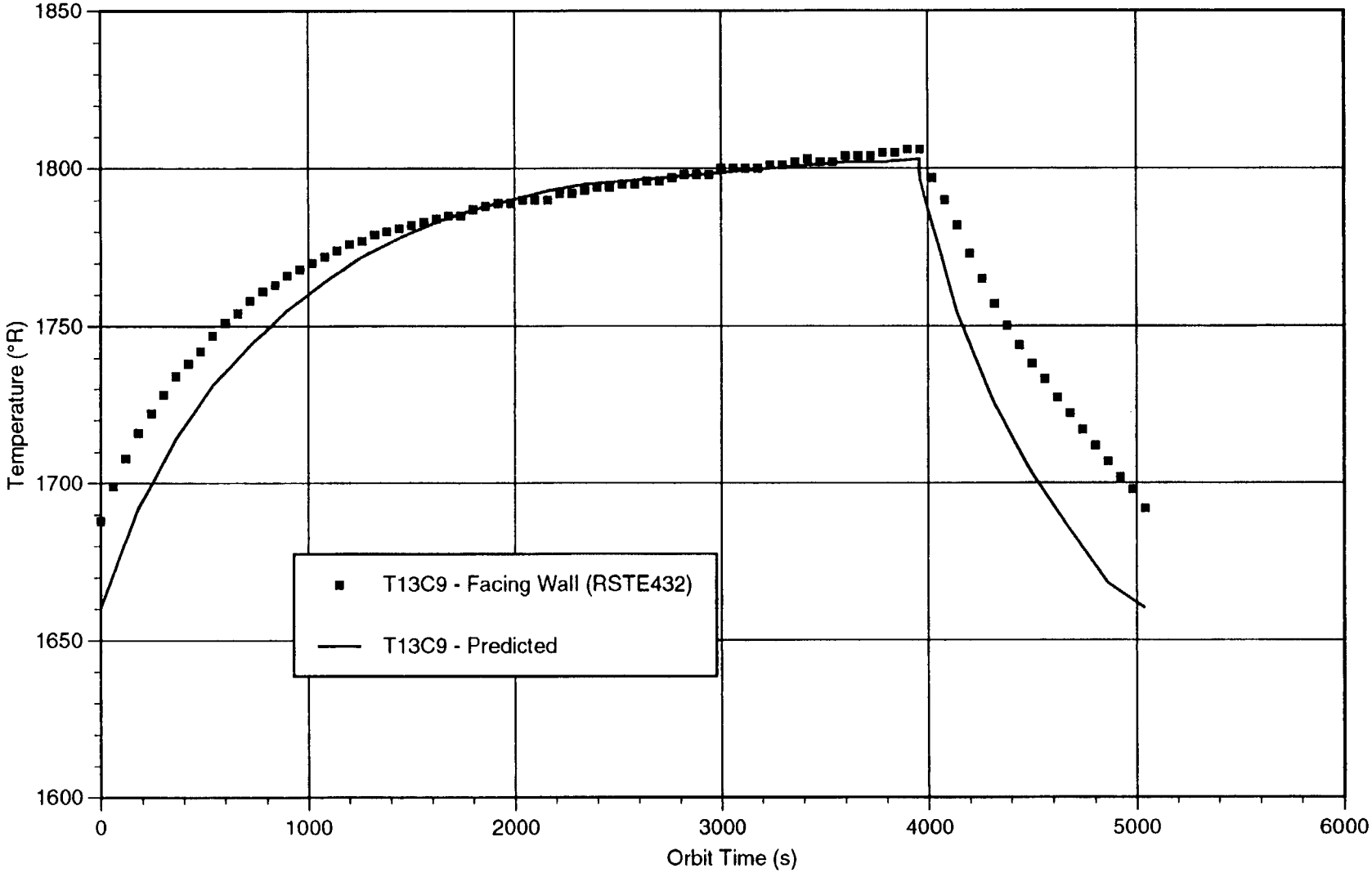

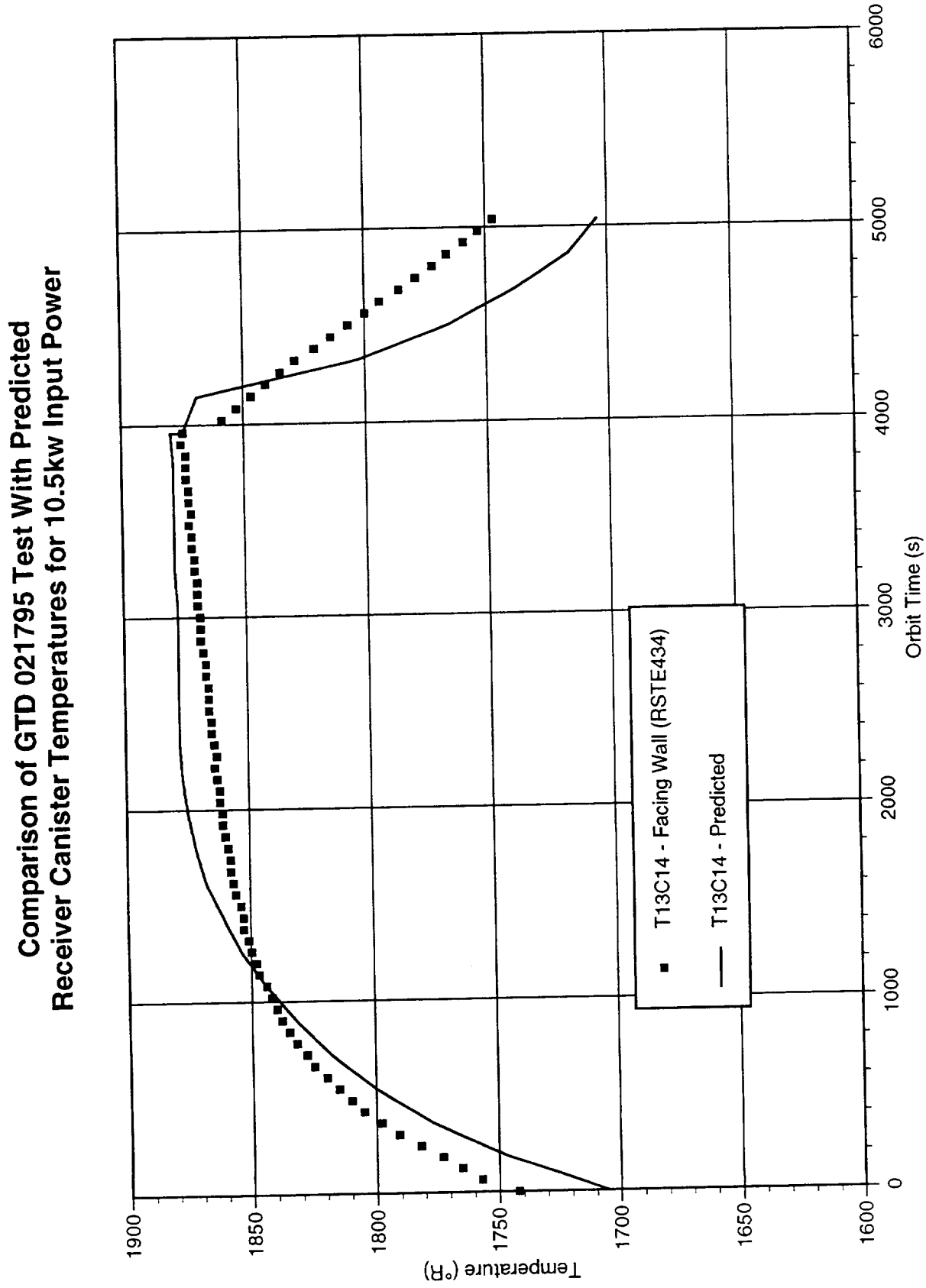
Comparison of GTD 021795 Test With Predicted
Receiver Canister Temperatures for 10.5kw Input Power
Temperature (°R)
1900
1850
1800
1750
1700
1650
1600
0
1000
2000
3000
4000
5000
6000
Orbit Time (s)
T13C14 - Facing Wall (RSTE434)
T13C14 - Predicted

Comparison of GTD 021795 Test With Predicted Receiver Canister Temperatures for 10.5kw Input Power

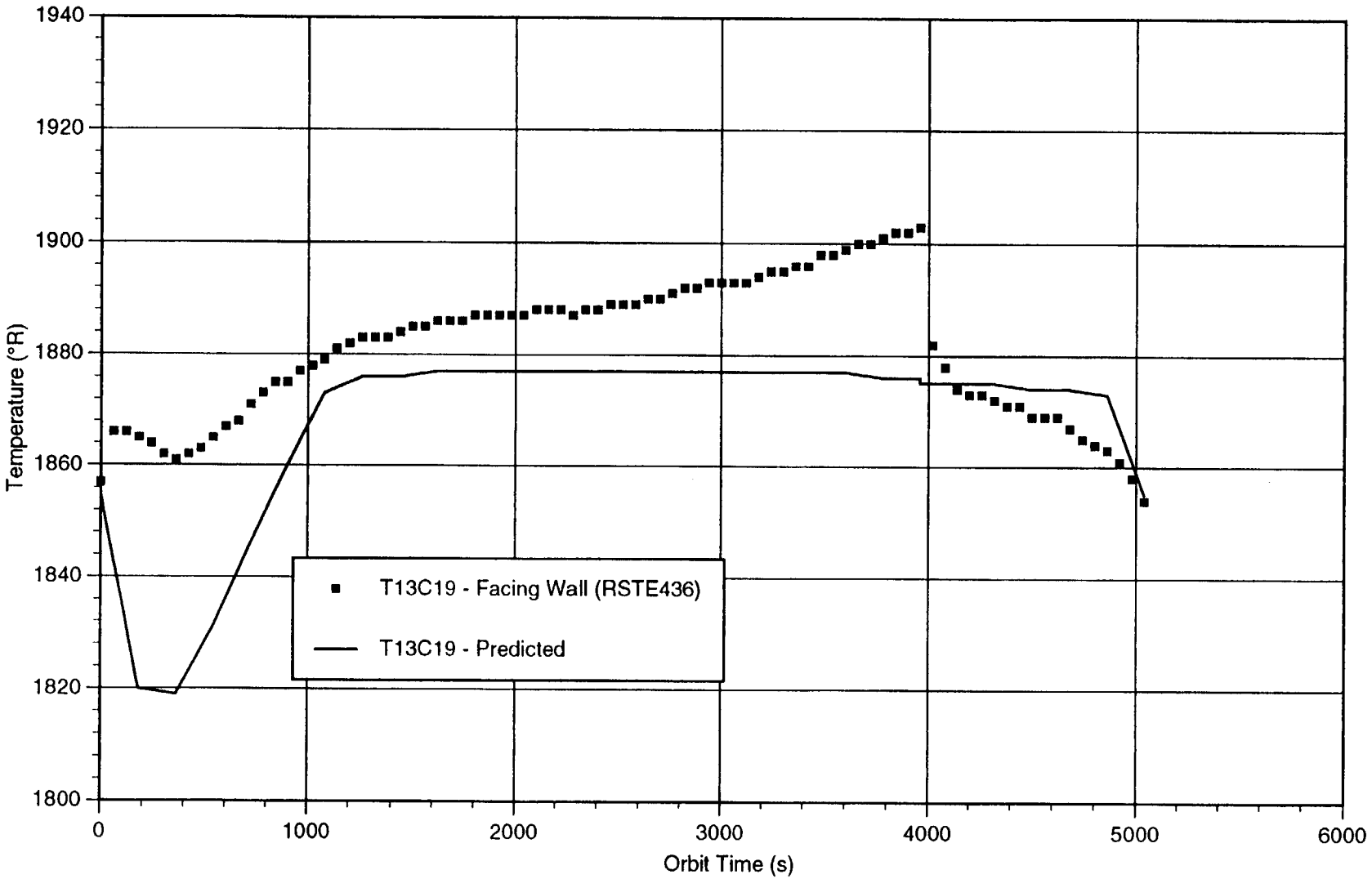

Comparison of GTD 021795 Test With Predicted Receiver Canister Temperatures for 10.5kw Input Power

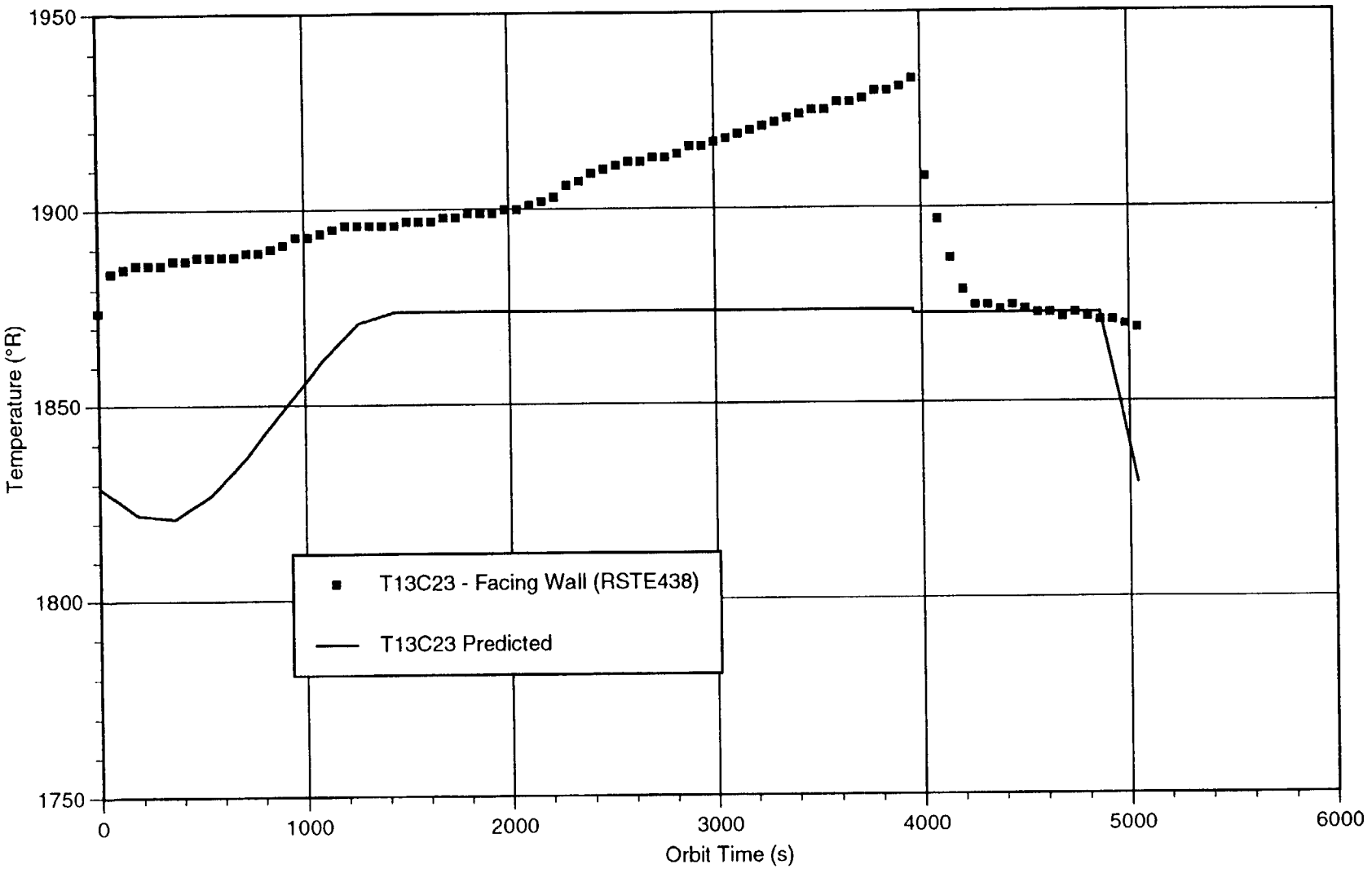

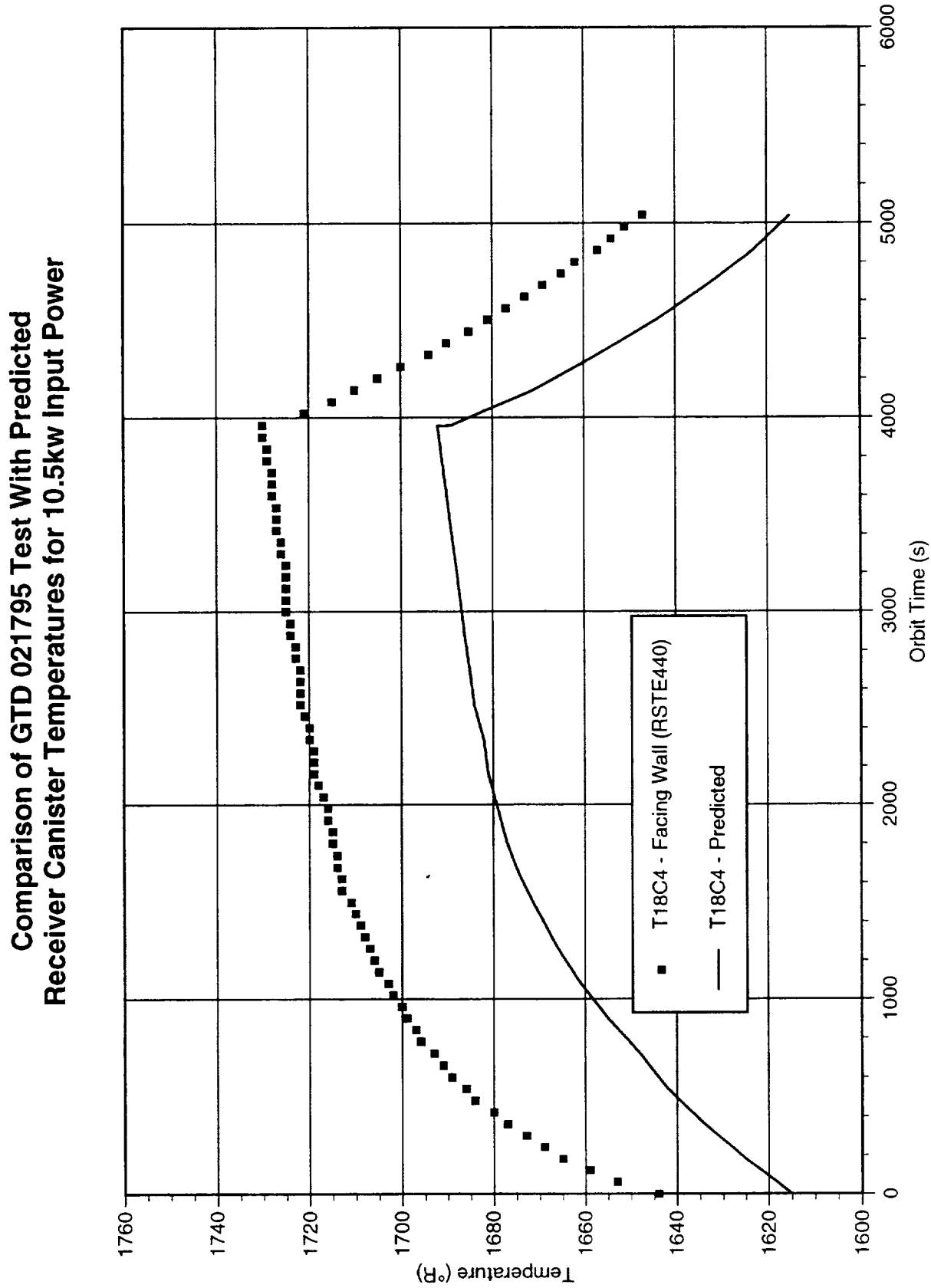
Comparison of GTD 021795 Test With Predicted
Receiver Canister Temperatures for 10.5kw Input Power
Temperature (°R)
1760
1740
1720
1700
1680
1660
1640
1620
1600
0
1000
2000
3000
4000
5000
6000
Orbit Time (s)
T18C4 - Facing Wall (RSTE440)
T18C4 - Predicted

Comparison of GTD 021795 Test With Predicted Receiver Canister Temperatures for 10.5kw Input Power

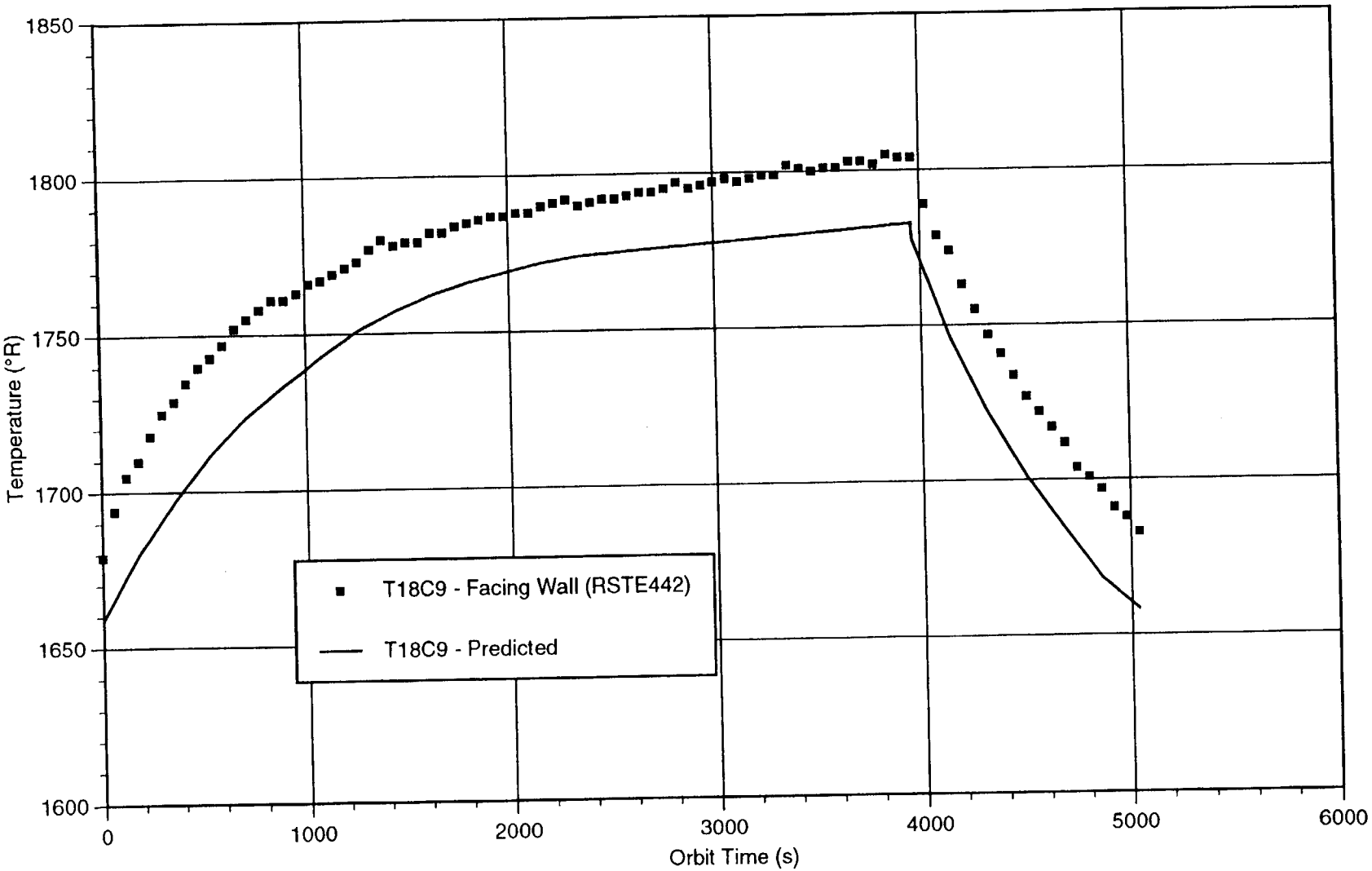

Comparison of GTD 021795 Test With Predicted Receiver Canister Temperatures for 10.5kw Input Power

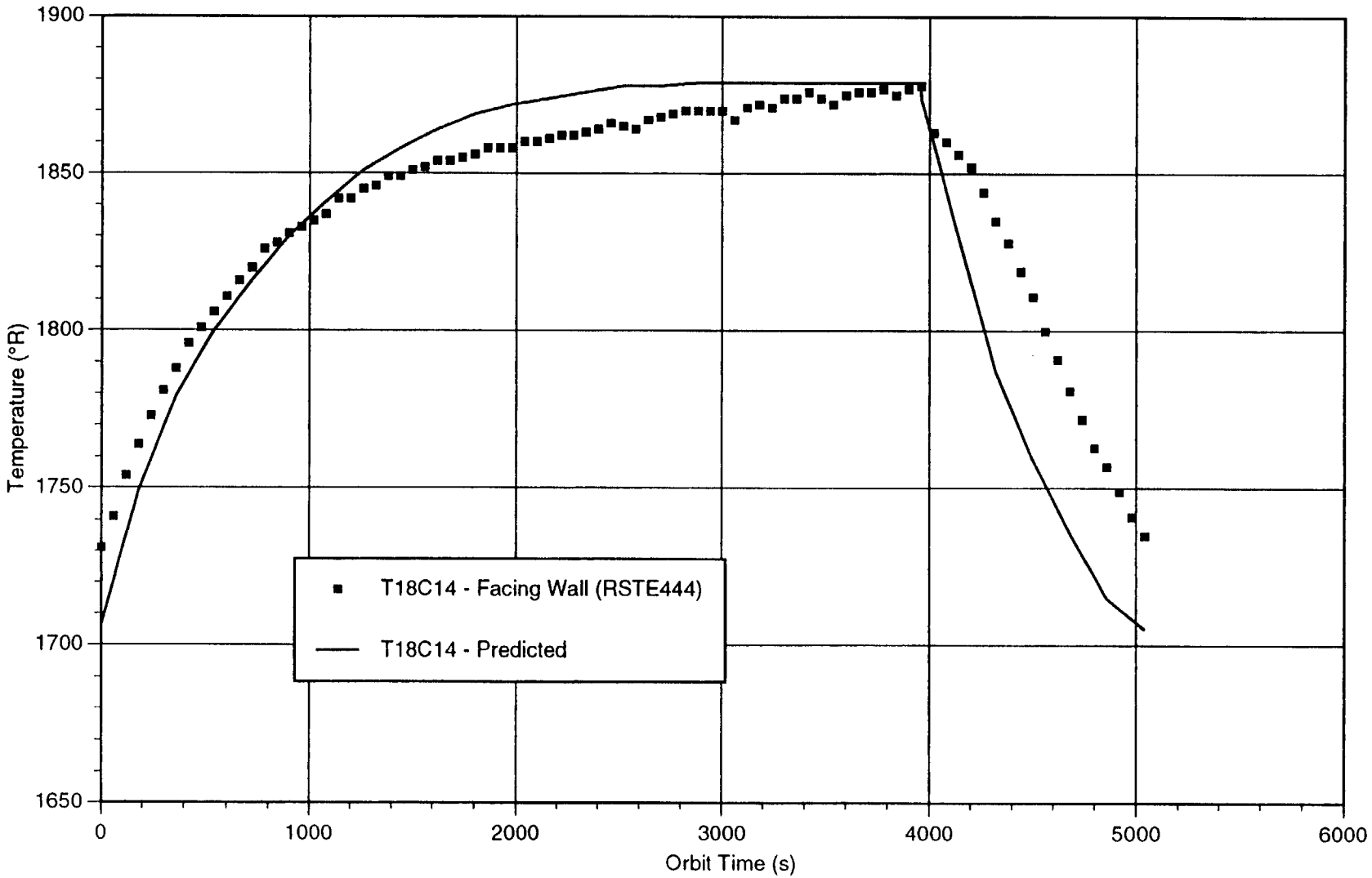

Comparison of GTD 021795 Test With Predicted Receiver Canister Temperatures for 10.5kw Input Power

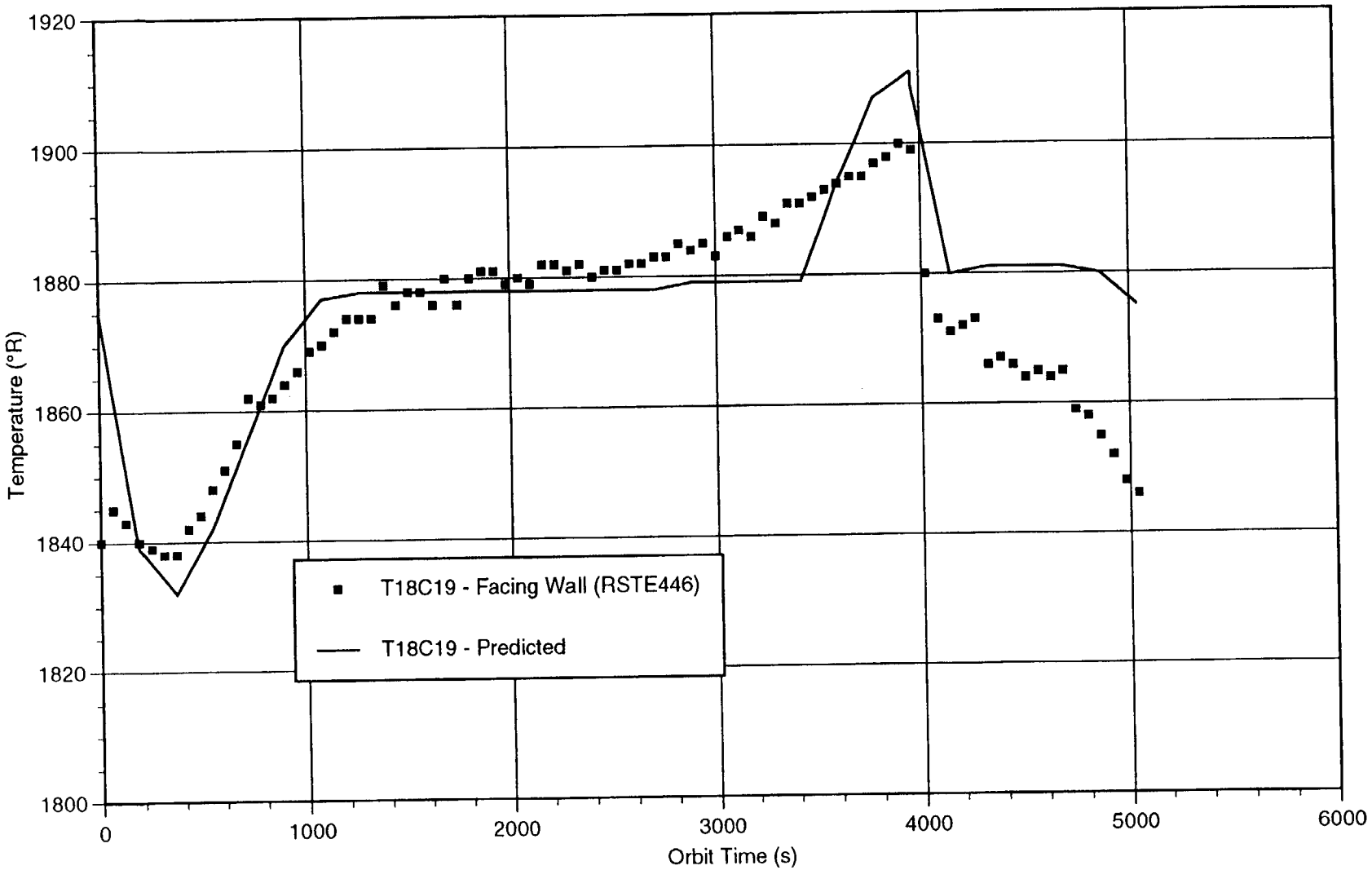

Comparison of GTD 021795 Test With Predicted Receiver Canister Temperatures for 10.5kw Input Power

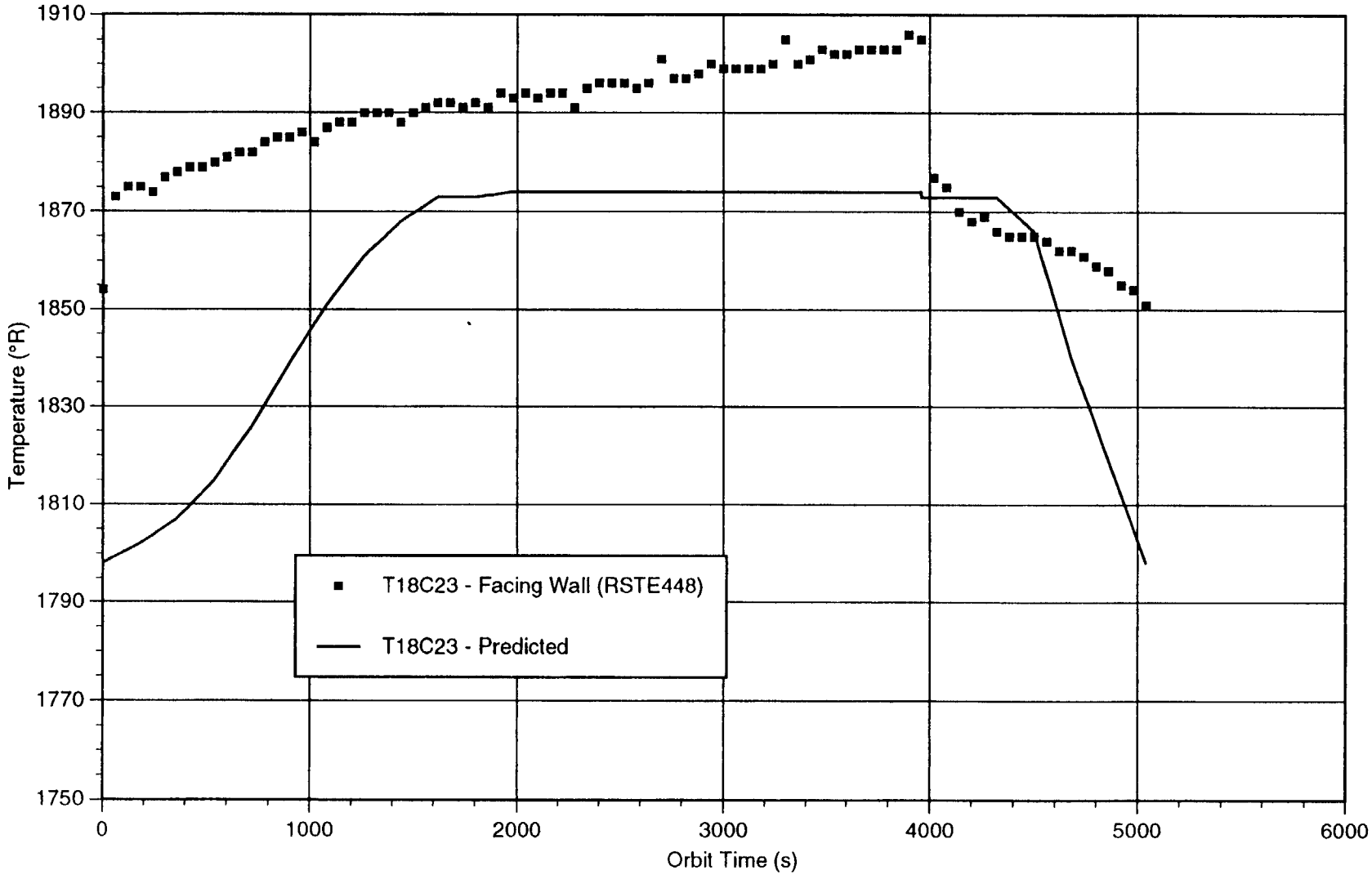

REPORT DOCUMENTATION PAGE

Form Approved
OMB No. 0704-0188

1. AGENCY USE ONLY (*Leave blank*)	2. REPORT DATE	3. REPORT TYPE AND DATES COVERED
	February 1997	Final Contractor Report

4. TITLE AND SUBTITLE

2 kWe Solar Dynamic Ground Test Demonstration Project
Volume III: Fabrication and Test Report

5. FUNDING NUMBERS

WU-233-03-0B
C-NAS3-26605

6. AUTHOR(S)

Dennis Alexander

7. PERFORMING ORGANIZATION NAME(S) AND ADDRESS(ES)

AlliedSignal Aerospace
Tempe, Arizona

8. PERFORMING ORGANIZATION REPORT NUMBER

E-10005

9. SPONSORING/MONITORING AGENCY NAME(S) AND ADDRESS(ES)

National Aeronautics and Space Administration
Lewis Research Center
Cleveland, Ohio 44135-3191

10. SPONSORING/MONITORING AGENCY REPORT NUMBER

NASA CR-198423, Vol. III

11. SUPPLEMENTARY NOTES

Project Manager, Richard K. Shaltens, Power Technology Division, NASA Lewis Research Center, organization code 5490, (216) 433-6138.

12a. DISTRIBUTION/AVAILABILITY STATEMENT

Unclassified - Unlimited
Subject Category 20

This publication is available from the NASA Center for AeroSpace Information, (301) 621-0390.

12b. DISTRIBUTION CODE

13. ABSTRACT ***(Maximum 200 words)***

The Solar Dynamic Ground Test Demonstration (SDGTD) project has successfully designed and fabricated a complete solar-powered closed Brayton electrical power generation system and tested it in a relevant thermal vacuum facility at NASA Lewis Research Center (LeRC). In addition to completing technical objectives, the project was completed 3-1/2 months early, and under budget.

14. SUBJECT TERMS

Space power; Solar dynamic; Brayton cycle; System testing

15. NUMBER OF PAGES

182

16. PRICE CODE

A09

17. SECURITY CLASSIFICATION OF REPORT	18. SECURITY CLASSIFICATION OF THIS PAGE	19. SECURITY CLASSIFICATION OF ABSTRACT	20. LIMITATION OF ABSTRACT
Unclassified	Unclassified	Unclassified	